BioMed Research International

Neurobiology of Hearing Loss and Ear Disease

Lead Guest Editor: Yong-Ho Park
Guest Editors: Sung K. Moon, Kenneth H. Lee, and Jeong-Han Lee

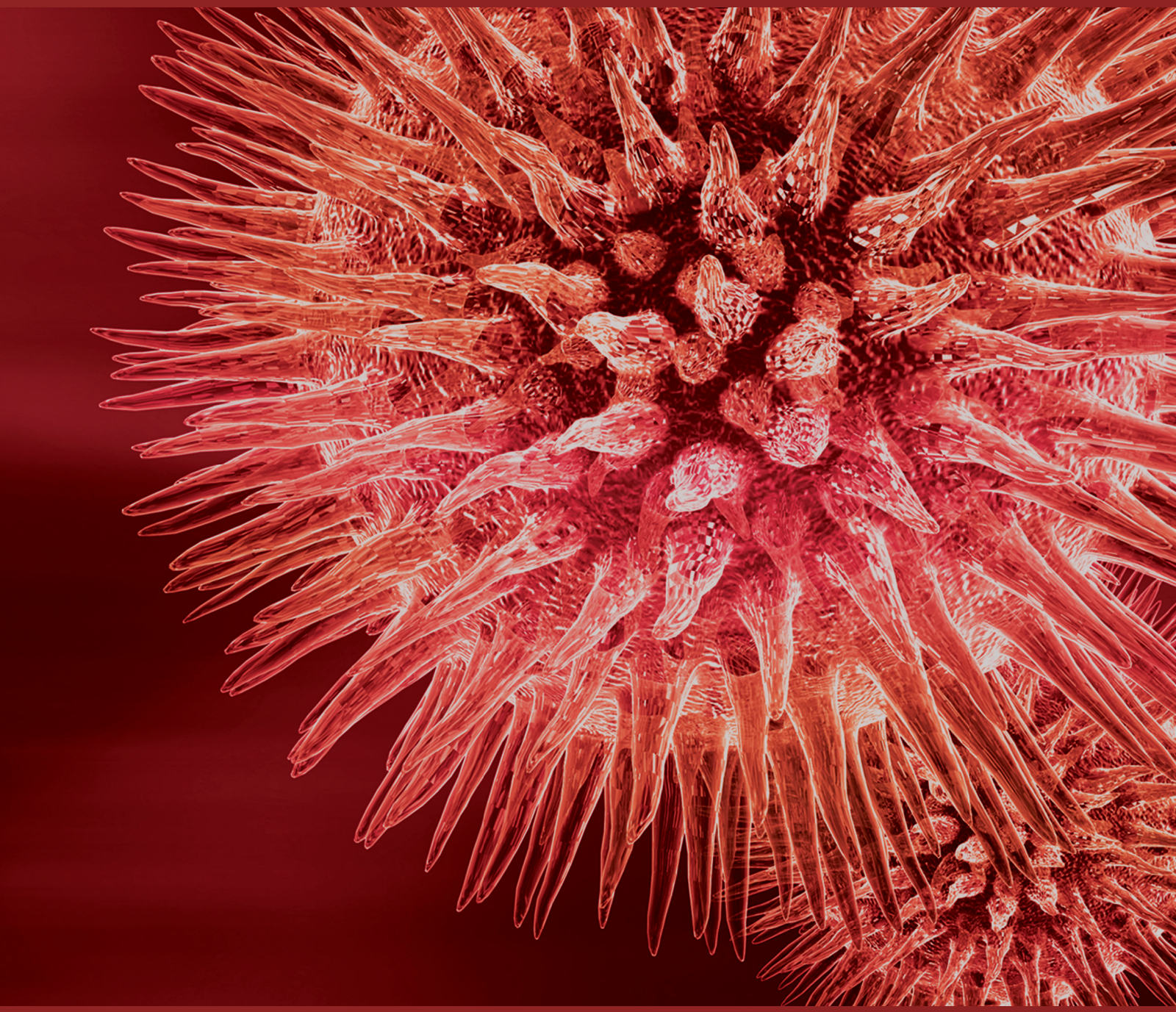

Neurobiology of Hearing Loss and Ear Disease

BioMed Research International

Neurobiology of Hearing Loss and Ear Disease

Lead Guest Editor: Yong-Ho Park
Guest Editors: Sung K. Moon, Kenneth H. Lee, and Jeong-Han Lee

Contents

Hindawi
BioMed Research International
Volume 2018, Article ID 2464251, 1 page
https://doi.org/10.1155/2018/2464251

Editorial

Neurobiology of Hearing Loss and Ear Disease

Yong-Ho Park,[1] **Sung K. Moon**,[2] **Kenneth H. Lee**,[3] **and Jeong-Han Lee**[4]

[1]*Department of Otolaryngology, College of Medicine, Chungnam National University, Daejeon, Republic of Korea*
[2]*Department of Head and Neck Surgery, David Geffen School of Medicine, University of California, Los Angeles, Los Angeles, CA, USA*
[3]*Department of Otolaryngology-Head and Neck Surgery, University of Texas Southwestern Medical Center, Dallas, TX, USA*
[4]*Department of Physiology and Cell Biology, School of Medicine, University of Nevada, Reno, Reno, NV, USA*

Correspondence should be addressed to Yong-Ho Park; parkyh@cnu.ac.kr

Received 15 March 2018; Accepted 15 March 2018; Published 19 April 2018

The interest towards research in hearing loss and ear disease has seen a great and progressive increase in the light of the continuous increase in the number of challenging research articles. Although hearing loss is a worldwide health problem and its socioeconomic burden is globally significant, nonregenerative hair cells in the cochlea and difficult drug delivery to the inner ear hindered progress in the field of hearing recovery [1]. However, with the advancement of molecular biology technologies and innovative imaging techniques, recent researches for hearing loss are focused on innovative approach such as gene therapy, stem cell therapy, and brain network analysis, heading one step forward to the new era of hearing research [2–4].

This special issue brings together 10 research articles and review article which nicely illustrate the wide spectrum of basic inner ear research and its related research about central auditory pathway. While some cutting-edge researches about neuroimaging study of central pathway including auditory cortex and higher cognitive function were illustrated, basic inner ear studies using many kinds of animal models were also described. In detail, diabetic mice, gerbil hearing loss model with aminoglycoside administration, and specifically devised early progressive hearing loss model were introduced. This special issue also includes deriving significant clinical implication, predicting the surgical outcomes from the data of cochlear implant recipients. Finally, the art of nanomedicine was thoroughly reviewed in the field of inner ear research.

The collection of papers published in this special issue nicely covers all the fields of hearing science including basic molecular study, imaging study, and clinical implication study and we hope that it will attract the interests of a large number of basic researchers as well as clinicians aiming at improving the treatment of hearing loss.

Yong-Ho Park
Sung K. Moon
Kenneth H. Lee
Jeong-Han Lee

References

[1] A. N. Salt and K. Hirose, "Communication pathways to and from the inner ear and their contributions to drug delivery," *Hearing Research*, 2017.

[2] A. Warnecke, A. J. Mellott, A. Römer, T. Lenarz, and H. Staecker, "Advances in translational inner ear stem cell research," *Hearing Research*, vol. 353, pp. 76–86, 2017.

[3] H. Ahmed, O. Shubina-Oleinik, and J. R. Holt, "Emerging Gene Therapies for Genetic Hearing Loss," *Journal of the Association for Research in Otolaryngology*, vol. 18, no. 5, pp. 649–670, 2017.

[4] A. Pannese, D. Grandjean, and S. Frühholz, "Subcortical processing in auditory communication," *Hearing Research*, vol. 328, pp. 67–77, 2015.

Hindawi
BioMed Research International
Volume 2018, Article ID 7807426, 10 pages
https://doi.org/10.1155/2018/7807426

Research Article

Effect of Long-Term Sodium Salicylate Administration on Learning, Memory, and Neurogenesis in the Rat Hippocampus

Haichen Niu,[1] Sheng Ding,[2] Haiying Li,[3] Jianfeng Wei,[4] Chao Ren,[5] Xiujuan Wu,[2] Tanzeel Huma ,[1,6] and Qiang Zhang [1]

[1]*Department of Genetics, Xuzhou Medical University, Xuzhou, Jiangsu 221006, China*
[2]*School of Public Health, Xuzhou Medical University, Xuzhou, Jiangsu 221006, China*
[3]*Department of Pathology, Xuzhou Medical University, Xuzhou, Jiangsu 221006, China*
[4]*Department of Histology and Embryology, School of Basic Medical Sciences, Xuzhou Medical University, Xuzhou, Jiangsu 221006, China*
[5]*Department of Neurology, The Affiliated Yantai Yuhuangding Hospital of Qingdao University, Yantai, Shandong 264000, China*
[6]*Institute of Molecular Biology and Biotechnology, University of Lahore, Lahore 54000, Pakistan*

Correspondence should be addressed to Tanzeel Huma; tanzeelhuma@gmail.com and Qiang Zhang; shoutian@163.com

Received 20 October 2017; Accepted 18 December 2017; Published 1 April 2018

Academic Editor: Kenneth H. Lee

Tinnitus is thought to be caused by damage to the auditory and nonauditory system due to exposure to loud noise, aging, or other etiologies. However, at present, the exact neurophysiological basis of chronic tinnitus remains unknown. To explore whether the function of the limbic system is disturbed in tinnitus, the hippocampus was selected, which plays a vital role in learning and memory. The hippocampal function was examined with a learning and memory procedure. For this purpose, sodium salicylate (NaSal) was used to create a rat animal model of tinnitus, evaluated with prepulse inhibition behavior (PPI). The acquisition and retrieval abilities of spatial memory were measured using the Morris water maze (MWM) in NaSal-treated and control animals, followed by observation of c-Fos and delta-FosB protein expression in the hippocampal field by immunohistochemistry. To further identify the neural substrate for memory change in tinnitus, neurogenesis in the subgranular zone of the dentate gyrus (DG) was compared between the NaSal group and the control group. The results showed that acquisition and retrieval of spatial memory were impaired by NaSal treatment. The expression of c-Fos and delta-FosB protein was also inhibited in NaSal-treated animals. Simultaneously, neurogenesis in the DG was also impaired in tinnitus animals. In general, our data suggest that the hippocampal system (limbic system) may play a key role in tinnitus pathology.

1. Introduction

Tinnitus is a conscious awareness of sound without an external source of the sound. It is described by a patient as a ringing or buzzing in one or both ears in the absence of an auditory stimulus. The prevalence rate of chronic tinnitus ranges from approximately 5% to 15% of the population [1]. Studies indicate that any level of the auditory pathway, including the cochlear nerve, acoustic nerve, or central auditory pathways, can induce tinnitus [2]. Tinnitus can induce many other symptoms including anxiety, emotional disorders, sleep disturbance, and work impairment [3]. Tinnitus affects the quality of life in general [4]. However, a number of neuroimaging studies in humans indicate that the limbic system may have functional and anatomical roles in the tinnitus-related field, outside of the central auditory pathways. In this disorder, limbic changes were the result of tinnitus, not the cause. It seems that central auditory dysfunction may not be the only target for understanding chronic tinnitus.

The hippocampus, which is a part of the limbic system, plays a vital role in learning and memory process. Sensory systems can transduce information of the external stimulus to neural representations in the central nervous system (CNS), which will help the memory system to establish a memory

trace [5]. Accurately, the auditory system can transfer external information to the memory system by transforming it into memory-related information. For long-term auditory memory, auditory information is first processed in the hippocampus to form a short-term memory. Later, the short-term memory is transformed into a long-term memory [6]. Preliminary studies in primates indicated that large medial temporal lobe lesions impair auditory recognition memory [7]. However, at present, there is no reference study indicating the effect on nonauditory memory. It is unclear whether the nonauditory memory of tinnitus is affected or not.

In the hippocampus, the subgranular zone of the dentate gyrus (DG) continually generates new neurons in adulthood. These new neurons synaptically integrate into hippocampal networks and provide potential substrates for learning. Continuous integration of new neurons affects the establishment of memories at the circuit level of the hippocampus. New neurons integrate into the hippocampus by competing with existing cells in the neural memory network, establishing new memory circuits that may coexist with or even replace first memory circuits. In addition, neurogenesis can be impaired by pathological changes or pharmacological treatments, resulting in disturbance of learning and memory.

Sodium salicylate (NaSal) is frequently used in clinical settings and has the potential to cause reversible tinnitus and sensorineural hearing loss [8]. NaSal-induced tinnitus in rats is a popular animal model for the study of tinnitus and has been used in many substantial pharmacological and pathological studies [8, 9].

Previous studies suggested that tinnitus originated at the cochlear level and developed in the CNS, resulting in neuroplasticity-related dysfunction. At the same time, many studies indicated that hippocampal plasticity promotes the learning and memory procedure in rodents and humans. But so far, it is unknown whether NaSal treatment will have effects on the learning and memory procedure. We designed this study to investigate whether tinnitus affects the hippocampal function or not. For this purpose, we developed a tinnitus rat model by inducing tinnitus in rats via long-term NaSal administration, and tinnitus-like behavior was confirmed using the prepulse inhibition (PPI) test. The Morris water maze (MWM) was used to examine the nonauditory learning ability in tinnitus rats, and neurogenesis of the DG was observed using an immunohistochemical tool. The results of this study will help to elucidate the contribution to learning and memory in the hippocampus during tinnitus induced by sodium salicylate.

2. Materials and Methods

2.1. Animals. In this study, male Sprague-Dawley rats were used (200–220 g). Rats were kept on a 12/12 h dark/light cycle with the light phase starting at 7 p.m., with ad libitum access to food and water. Experimental procedures were in accordance with the guidelines and regulations set out by Xuzhou Medical University. All experiments were approved by the Institutional Animal Care and Use of Xuzhou Medical University under the animal protocol number 2015A1204B07. Rats were subjected to intraperitoneal (i.p.) injection of sodium salicylate 300 mg/kg (Sigma, S3007, Shanghai, China) daily for 7 or 14 consecutive days. The control groups were treated with saline for 7 or 14 consecutive days. Behavior tests were performed 2 h after the last injection, as previously described [10].

2.2. Tinnitus Tests. To test the auditory stimulus-specific gap detection deficits, we developed a custom-made auditory setup to induce prepulse inhibition (PPI) in the animals. Tests were performed in a sound-attenuating chamber. The PPI procedure was done as previously described [11, 12]. For the gap detection tests that were used to evaluate tinnitus perception, all animals were located in a sound-attenuating room with a 60 dB ambient noise level. During every experiment, animals were habituated to the device fixed above a platform to a gravity accelerometer and were exposed to 65 dB of sound pressure level (SPL) white background noise. This signal was detected by a sensitive sensor and transferred to a computer in an adjacent room to collect the startle-response data. During the test session, the rats were first presented with ten trials of randomly delivered 115 dB SPL pulses. Then, animals were given 30 trials of randomly delivered acoustic stimuli delivered through a speaker. The acoustic stimuli consisted of 10 trials of a 115 dB SPL pulse stimulus, 10 trials without a delivered stimulus (NOSTIM), and 30 trials of a prepulse startle stimulus. The SPL pulse was a single 20 ms sound presentation. The prepulse startle stimuli were 100 ms of 20 ms white-noise pulses that contained nonstartling stimuli of 75, 80, or 85 dB SPL (PPI2, PPI4, and PPI8, resp.) followed by a single 20 ms 115 dB SPL pulse. Intertrial intervals (ITIs) of 27–32 s were used between the stimuli presentations. PPI was quantified as the percent decrease in the peak amplitude of the startle response (ASR) when a prepulse preceded the startling noise in comparison to the amplitude when no gap or prepulse was present $[(1 - \text{PPI/ASR}) \times 100]$.

2.3. Spatial Memory Tests. The MWM was used to evaluate the spatial memory abilities in rats [13], which consisted of a circular plastic pool filled with warm water with the addition of nontoxic yellow paint. A video camera was suspended above the pool to track the animals which were connected to a computer with a tracing system. Different visual cues were placed on the surrounding walls so that the rats could use them for spatial orientation and remained unchanged during the experimental period.

24 hours after tinnitus examination rats were trained for four days in a water maze by doing four trials per day. On the 4th day, the latency to find the hidden platform underwater was also recorded. A maximum time of 90 s was provided to each experimental rat. Each trial had a different starting point, and if they failed to find the platform in 90 s, the rats would be guided to the platform manually and kept on the platform for 10 s. The time taken by each rat to reach the platform (latency) was recorded. The spatial probe test was conducted on the fifth day. This test is used to evaluate reversal learning, revealing whether or not animals can extinguish their initial learning of the platform's position and acquire a direct path to the new goal position. The platform was removed, and each rat was released opposite the

target quadrant (the southeast quadrant), facing the wall of the pool. In the probe test, the time that the rats spent getting to the target quadrant was recorded to assess their spatial memory ability.

2.4. c-Fos and delta-FosB Immunohistochemistry (IHC). For c-Fos IHC experiments, animals were anesthetized with trichloroacetaldehyde monohydrate (chloral hydrate; 10%, 0.3 ml/100 g, Sinopharm Chemical Reagent Co., Ltd., Shanghai, China) 4 h after acquisition training on the 4th day, and for delta-FosB IHC experiment, animals were anesthetized with chloral hydrate 48 h after a second probe test (7th day). Animals were then immediately perfused transcardially with 100 ml of 0.9% saline in 0.01 M (pH = 7.2) phosphate-buffered saline (PBS), followed by 200 ml of 4% paraformaldehyde (PFA) in 0.01 M PBS (pH = 7.2). Brains were extracted followed by fixation in 4% PFA and stored overnight at 4°C. After 24 h, the brains were dehydrated by 10%, 20%, and 30% sugar in 0.01 M PBS (pH = 7.2) until the brains sunk to the bottom at 4°C. Then, consecutive coronal sections (thickness = 25 μm) of hippocampal fields were cut using Leica freezing microtome (Leica, CM1950).

For immunostaining in the hippocampus, three slices per animal per target brain field were selected. The selected brain slices were washed three times for 3 min in PBS and then washed in a buffer containing 5% normal goat serum and 0.5% Triton X-100 in PBS for 30 min. Later, these slices were incubated with polyclonal goat anti-c-Fos 1 : 200 (sc-52; Santa Cruz Biotechnology, Shanghai, China) or anti-ΔFosB (H-75, sc-48, Santa Cruz Biotechnology, Shanghai, China) overnight at 4°C. Sections were rinsed three times for 3 min in 0.01 M PBS and incubated for 1 h at room temperature with the appropriate secondary antibodies. After washing, sections were incubated with the avidin-biotin-peroxidase complex for 1 h (ABC kit, Beyotime Biotechnology, Beijing, China), and a DAB kit was used to process the immunoreaction results. Three slices per brain region were analyzed in all experiments with data (cell counts) averaged per animal across slices.

2.5. BrdU Injection for Neurogenesis. To observe the neurogenesis in the dentate gyrus of the hippocampus, 5-bromodeoxyuridine (BrdU, 10 mg/ml, Sigma-Aldrich) labeling dissolved in 0.9% saline was used in rats. After tinnitus examination, rats were injected with 50 mg/kg BrdU at 9:00 a.m. Brains were collected for BrdU immunohistochemistry 12 h after the last injection of BrdU. For quantification of BrdU+ cells, every fifth section (thickness = 25 μm) throughout the hippocampus was collected. The sections were washed with 0.01 M (pH = 7.2) PBS (3 min × 3) and 0.1% Triton X-100. The primary antibody was then added (Abcam, 1 : 500, mice anti-BrdU; Abcam 8955), and the tissue was incubated at 4°C overnight. Then, the secondary antibody (Goat Anti-Alexa Fluor 488, ab150113) was added at room temperature for 1 h. The sections were then washed with 0.01 M PBS (3 min × 3) and mounted on slides, coverslipped with Fluoromount G (Beckman Coulter), and stored at −20°C. Fluorescent images were captured using an Olympus confocal microscope. The total number of BrdU+ cells in the DG was extrapolated for the entire volume of the hippocampus.

3. Statistical Analysis

Statistical analysis was performed with SPSS (version 13.0). Results were expressed as the mean ± SEM. We used Fisher's exact test to examine the differences in latency between the groups and one-way analysis of variance (ANOVA) followed by the least significant difference (LSD) test to analyze histologically and MWM score differences. The ASR and PPI were calculated by the maximal amplitude of the spontaneous motor activity from the maximal amplitude of the startle response. Subsequently, the mean of the ASR and PPI response per stimulus and animal was calculated. PPI (%) = 1 − (ASR−PPI)/ASR ∗ 100%. Statistical analysis was carried out using the statistical software SPSS (Version 13.0). For each animal, ASR and PPI were analyzed in one- and/or two-way ANOVA with separate factors of test frequency, gap length, or bandwidth. Post hoc analysis was carried out using Tukey's HSD or independent contrasts corrected for multiple comparisons with the Bonferroni-Holm procedure. Significance levels are indicated in figures as $^{*}p < 0.05$, $^{**}p < 0.01$, and $^{***}p < 0.001$.

4. Results

4.1. Tinnitus Examination by PPI. After animals were treated for 7 consecutive days with NaSal or control injection (Figure 1(a)), PPI values for the different prepulse startle stimuli were measured and compared between groups: PPI2, −16.2 ± −35.4 in the control group and 12.3±16.3 in the NaSal group, $p < 0.05$; PPI4, −22.8 ± −30.9 in the control group and 4.1 ± 17 in the NaSal group, $p < 0.05$; PPI8: −25.4 ± −11.1 in the control group and 6.7±4.7 in the NaSal group, $p > 0.05$; furthermore, no significant difference in the ASR was found between groups ($p > 0.05$). On the 14th day of treatment with NaSal or control injection (Figure 1(b)), studies indicated that more significant differences were found between groups: PPI2, −12.6 ± −5.9 in the control group and 12.7 ± 5.4 in the NaSal group, $p < 0.05$; PPI4, −21 ± −10.2 in the control group and 14.1±6.8 in the NaSal group, $p < 0.05$; PPI8, −25.7 ± −9.1 in the control group and 8.5±7.9 in the NaSal group, $p < 0.05$; furthermore, no significant difference was found in the ASR between groups ($p > 0.05$). Because tinnitus occupied the gap space, rats treated with NaSal showed significantly lower PPI values than control rats.

4.2. NaSal Administration Inhibited the Learning and Memory of the Water Maze. Rats were trained in the MWM to test their spatial learning and memory abilities. After 7 consecutive days of NaSal treatment and the PPI test, the learning and memory abilities were tested in the water maze. During the learning phase, training was performed for 4 consecutive days. The results showed that the escape latency was progressively decreased during these 4 training days in all groups, but the rats treated with NaSal for 7 days (7 NaSal-treated rats) showed a decreased reduction in escape latency

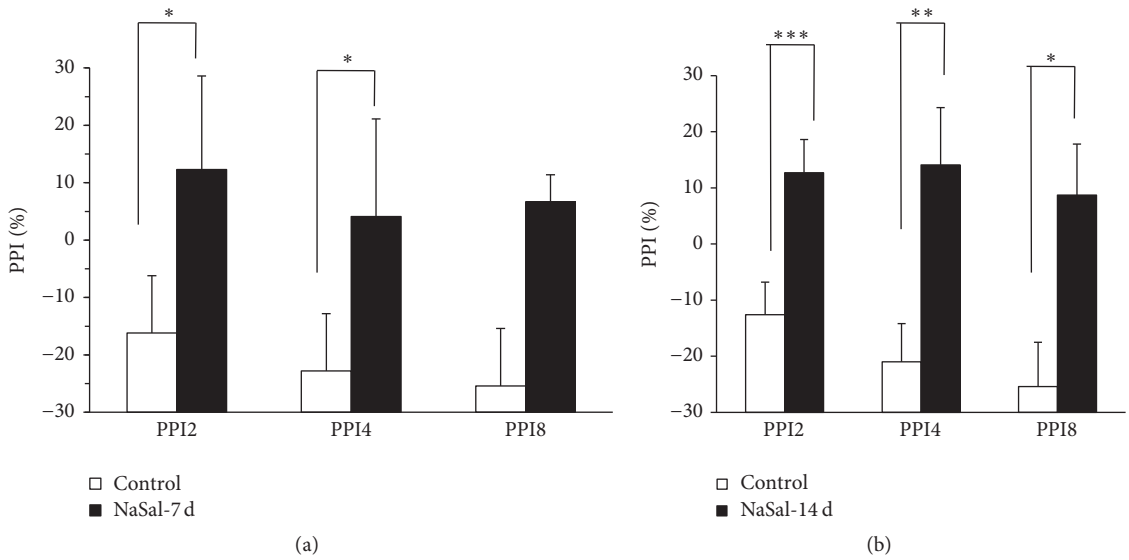

Figure 1: NaSal treatment induced tinnitus. (a) The PPI response measured in rats on the 7th day of NaSal treatment. (b) The PPI response measured in rats on the 14th day of NaSal treatment. n = 8–10; values are presented as mean ± SEM. Prepulse stimuli: PPI2, 75 dB SPL; PPI4, 80 dB SPL; and PPI8, 85 dB SPL ($^{***}p < 0.001$, $^{**}p < 0.01$, and $^{*}p < 0.05$, resp.).

on the 4th day compared to the control rats (control group: 6.3 ± 1.4; 7 NaSal group: 11.8 ± 4.7, $p < 0.05$).

During the probe test, the 7-day NaSal-treated rats spent more time getting to the target quadrant on the 5th day compared to the control rats (control group: 8.3 ± 3.3; 7 NaSal group: 13.6 ± 9.1, $p < 0.05$), indicating that memory extinction was slower in the NaSal-treated rats than in the control rats.

After chronic (14 days) NaSal treatment and the PPI test, training was performed across 4 consecutive days during the learning phase. The results showed that the escape latency of every group showed a progressive decrease in the 4 training days, but the 14 NaSal-treated rats showed a smaller reduction in escape latency on the 4th day than the control rats (control group: 6.3 ± 1.4; 14 NaSal group: 11.8 ± 4.7, $p < 0.05$). During the probe test, the 14 NaSal-treated rats spent more time getting to the target quadrant on the 5th day than the control rats (control group: 8.3 ± 3.3; 14 NaSal group: 13.6 ± 9.1, $p < 0.05$), indicating that the memory extinction of the NaSal-treated rats was slower than that observed in the control rats (Figures 2(a) and 2(b)).

4.3. NaSal Administration Impaired the Expression of c-Fos during the Acquisition of Spatial Memory. Spatial memory acquisition in the water maze is dependent on the activation of rapid gene expression (*fos* gene) in the hippocampus [14]. Therefore, we examined the expression of the c-Fos protein, which is dependent on neuronal activity [15]. The numbers of c-Fos-positive cells in the hippocampal CA1 region were compared between the treated and control groups after the water maze training on the 4th day using immunohistochemistry. Independent-samples t-tests revealed a significant decrease in the c-Fos expression on the 4th day after 7 days [t (17) = 2.334, $p < 0.05$] and 14 days of consistent NaSal administration [t (17) = 5.912, $p < 0.001$] (Figure 3(b)). The NaSal-treated animals (treated for 7 days and 14 days) showed a significant decrease in the c-Fos-positive cells compared with the control animals after MWM training. These results indicated that NaSal administration inhibited the induction of c-Fos expression in the CA1 of the hippocampus during acquisition of spatial memory in MWM training.

4.4. NaSal Administration Impaired the Expression of delta-FosB during Spatial Memory Retrieval. Memory retrieval requires hippocampal-dependent learning and memory, and ΔFosB plays a significant role [16]. However, to date, it is unknown whether ΔFosB expression is affected by NaSal exposure during memory retrieval in rats. As expected, water maze training induced an enhancement of ΔFosB protein in the CA1 of the hippocampus, and exposure to NaSal significantly inhibited expression of the ΔFosB protein in the CA1 of the hippocampus in the rats exposed to NaSal for 7 (t (15) = 3.521, $p < 0.05$) and 14 (t (15) = 5.859, $p < 0.01$) days. The NaSal-treated animals showed significantly decreased ΔFosB-positive cells compared with the control rats during retrieval (Figure 4). These results indicated that NaSal exposure inhibited the induction of ΔFosB in the CA1 of the hippocampus following training.

4.5. NaSal Administration Inhibited Neurogenesis in the DG of the Hippocampus. BrdU staining, a marker of neurogenesis, was used to assess cell proliferation in the DG of both control and NaSal-treated rats. Consistent with previous studies, we detected strong BrdU staining in the hippocampus [17]. The BrdU+ cells were detected mainly in the subgranular zone of the DG. After MWM training, 7 and 14 days of NaSal treatment resulted in significant inhibition of BrdU staining in the DG [7 days: t (14) = 2.374, $p < 0.05$; 14 days: t (14) = 4.876, $p < 0.01$] (Figure 5). These results suggest that chronic NaSal administration inhibited neurogenesis.

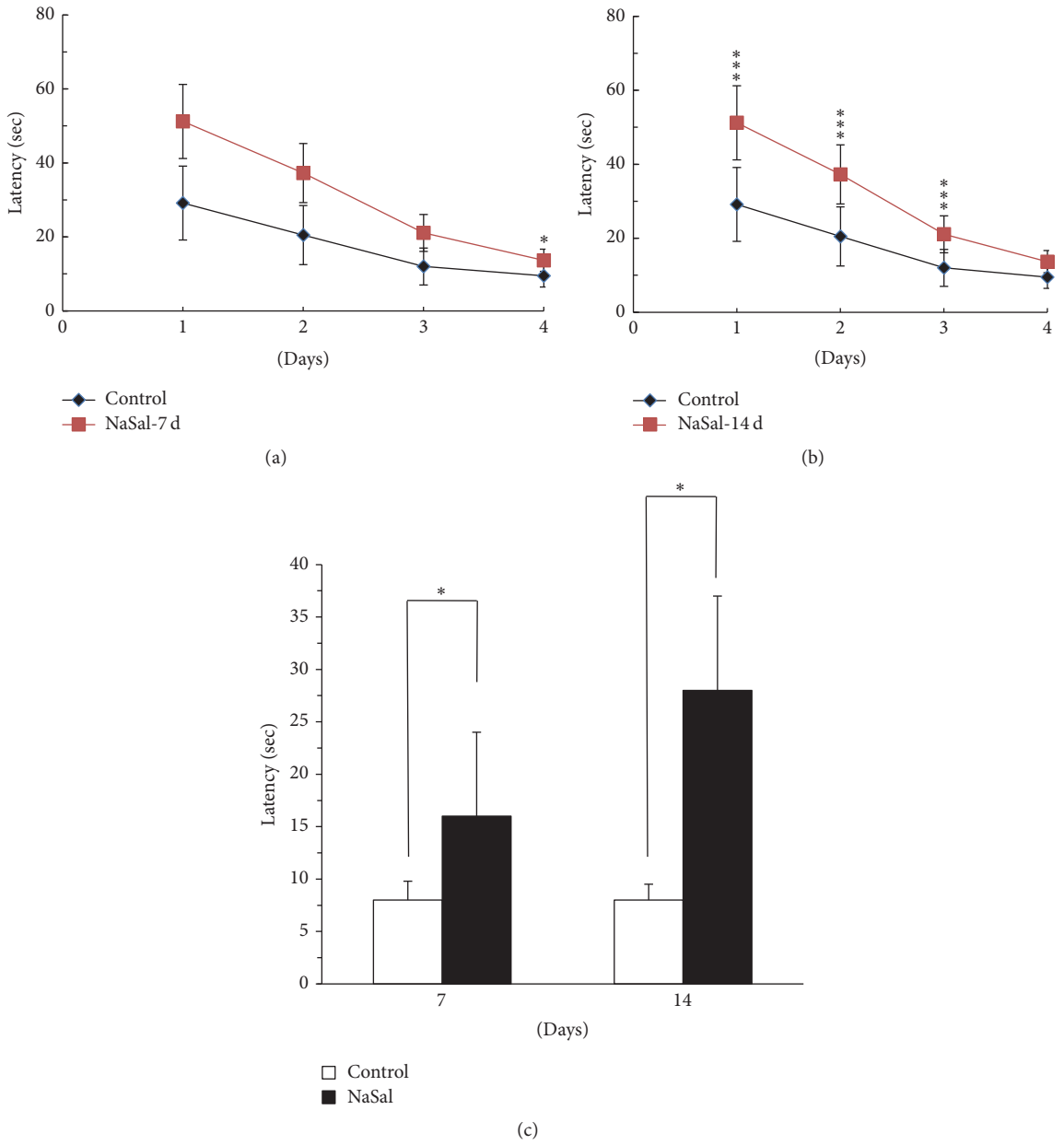

FIGURE 2: NaSal administration inhibits learning and memory of the water maze in rats. NaSal administration impaired the acquisition of spatial memory in the MWM as shown in (a) and (b) at 7 and 14 days, respectively. Also, the NaSal treatment for 7 and 14 days impaired the retrieval of the spatial memory in the MWM (c). $n = 8$–10, mean ± SEM ($^{*}p < 0.05$ and $^{***}p < 0.001$).

5. Discussion

Various studies have indicated that environmental factors, including auditory and nonauditory factors, could be encoded into memories for places and events by the hippocampus. In adulthood, hippocampal neurogenesis plays a vital role in modulating memory function [3]. In the present study, we examined learning and memory abilities in a tinnitus model induced by NaSal administration, using the MW test for acquisition and retrieval of spatial memory. The results indicated that the abilities of acquisition and retrieval of spatial memory were impaired in the NaSal-treated animals. Moreover, NaSal treatment resulted in inhibition of c-Fos protein expression in the CA1 of the hippocampus after memory acquisition and delta-FosB protein expression in the CA1 after memory retrieval. In parallel, neurogenesis in the DG of the hippocampus was decreased by NaSal treatment.

NaSal is a well-known clinical drug that can induce reversible tinnitus and hearing loss [18]. Therefore, in animal studies, NaSal has been used to produce an animal model of tinnitus. Now, we established a tinnitus rat model using the

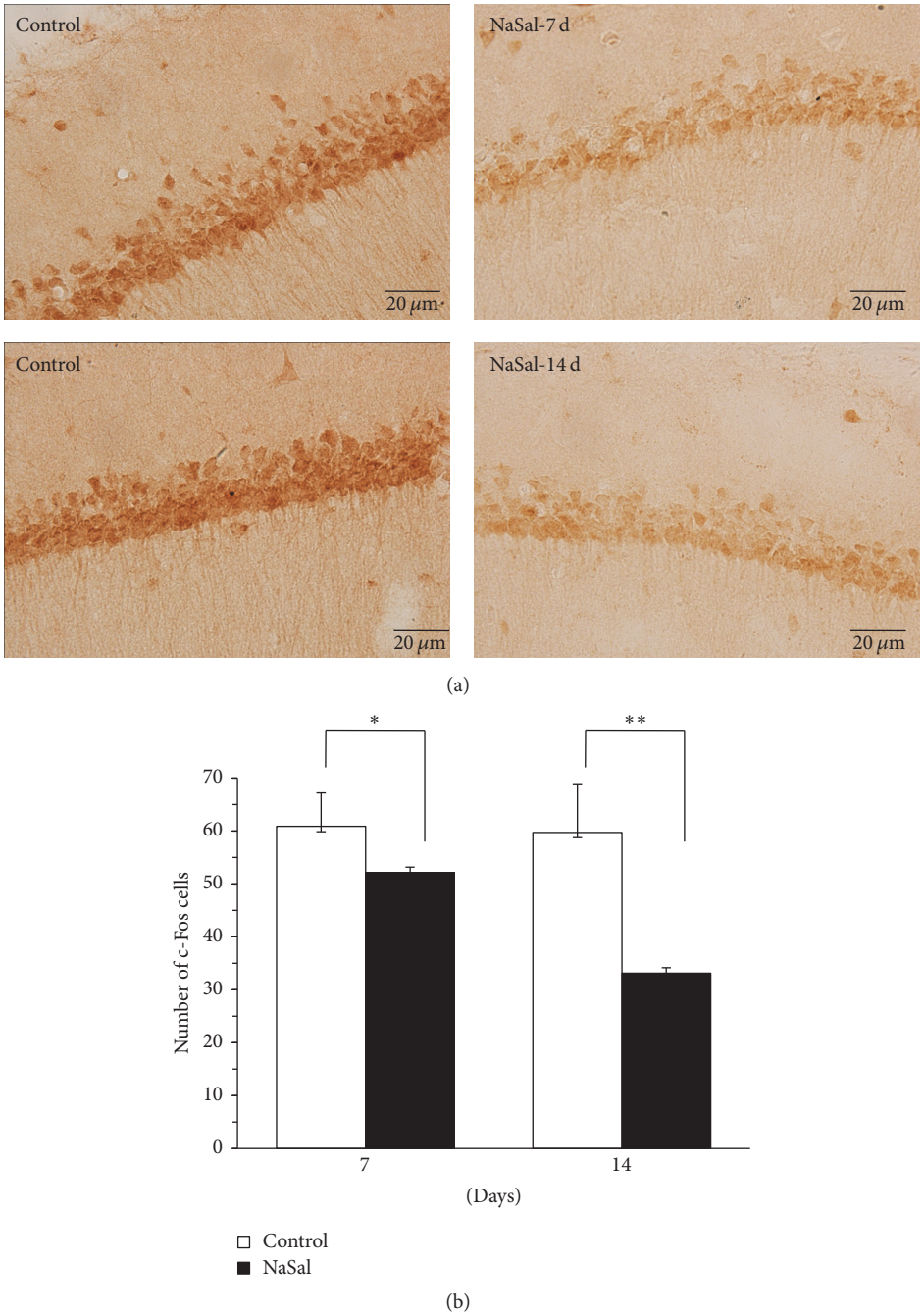

FIGURE 3: NaSal administration impaired the expression of c-Fos during the acquisition of spatial memory. (a) Representative immunohistochemical staining of c-Fos-positive cells in the hippocampal CA1 region from NaSal-treated and control rats. (b) Comparison of c-Fos expression during the acquisition of spatial memory in NaSal-treated and control rats. Independent-samples t-tests revealed significant effects on the 4th day of MWM training in rats given NaSal for 7 [t (17) = 2.334, $p < 0.05$] and 14 [t (17) = 5.912, $p < 0.001$] consecutive days. n = 8–10, mean ± SEM, $^{*}p < 0.05$, $^{**}p < 0.001$.

long-term administration of sodium salicylate (200 mg/kg) twice daily for 7 or 14 consecutive days. Tinnitus behavior was confirmed by the PPI response, which was consistent with previous studies [19, 20]. Maladaptation of central system processing was thought to be responsible for tinnitus perception and generation. Previous fMRI and neurophysiological studies have indicated that the functions of the central auditory system and the prefrontal cortex, hippocampus, and emotional centers are disturbed in tinnitus, which are all brain regions considered to take part in mediating learning and memory. It has also been reported that structural abnormalities in the subgenual anterior cingulate cortex and the hippocampus are detected following salicylate administration [19, 20].

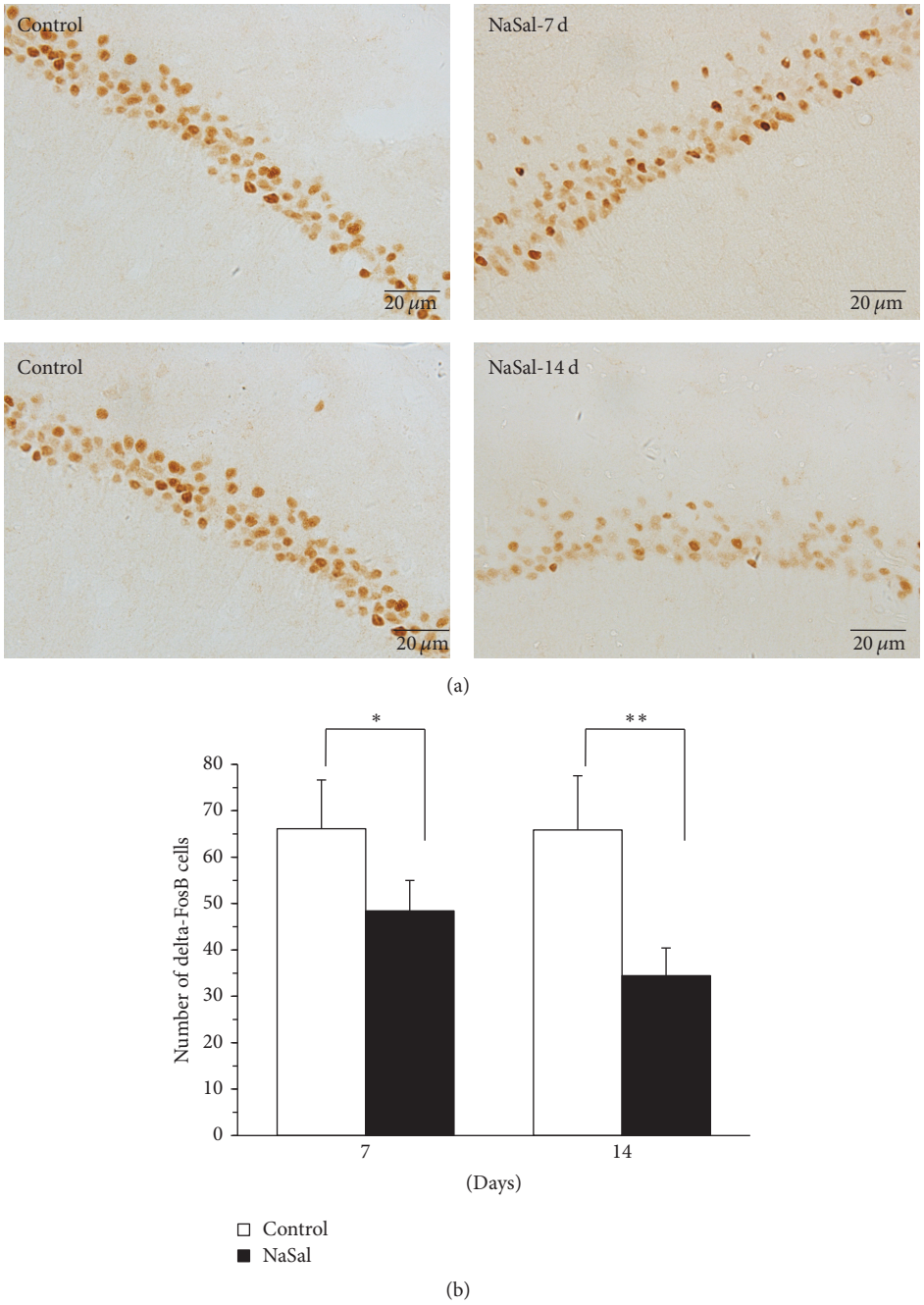

Figure 4: NaSal administration impaired the expression of delta-FosB during spatial memory retrieval. (a) Representative immunohistochemical staining of delta-FosB-positive cells in the hippocampal CA1 region from NaSal-treated and control rats. (b) Contrasting expression of delta-FosB during the retrieval of the spatial memory in NaSal-treated and control rats. Independent-samples t-tests revealed that NaSal treatment showed a significant decrease on the day of the probe test in the rats treated for 7 [t (15) = 3.521, $p < 0.05$] and 14 [t (15) = 5.859, $p < 0.01$] days. n = 8–10, mean ± SEM, $^{*}p < 0.05$, $^{**}p < 0.001$.

For the functional test, we examined the activation of gene expression in hippocampal neurons including the induction of c-Fos expression required for memory acquisition [14, 21]. The numbers of c-Fos-positive cells in the hippocampal CA1 region were decreased after consistent NaSal administration, indicating that NaSal administration inhibited the induction of c-Fos expression in the CA1 of the hippocampus during acquisition of spatial memory. As the expression of the c-Fos protein is tightly correlated to neuronal activity, our data suggest that, at least partially, the tinnitus may result in depressed neuronal activity in the CA1, leading to impairments of memory acquisition in the NaSal group. delta-FosB is a transcription factor within the Fos family that has been known to regulate synaptic plasticity in

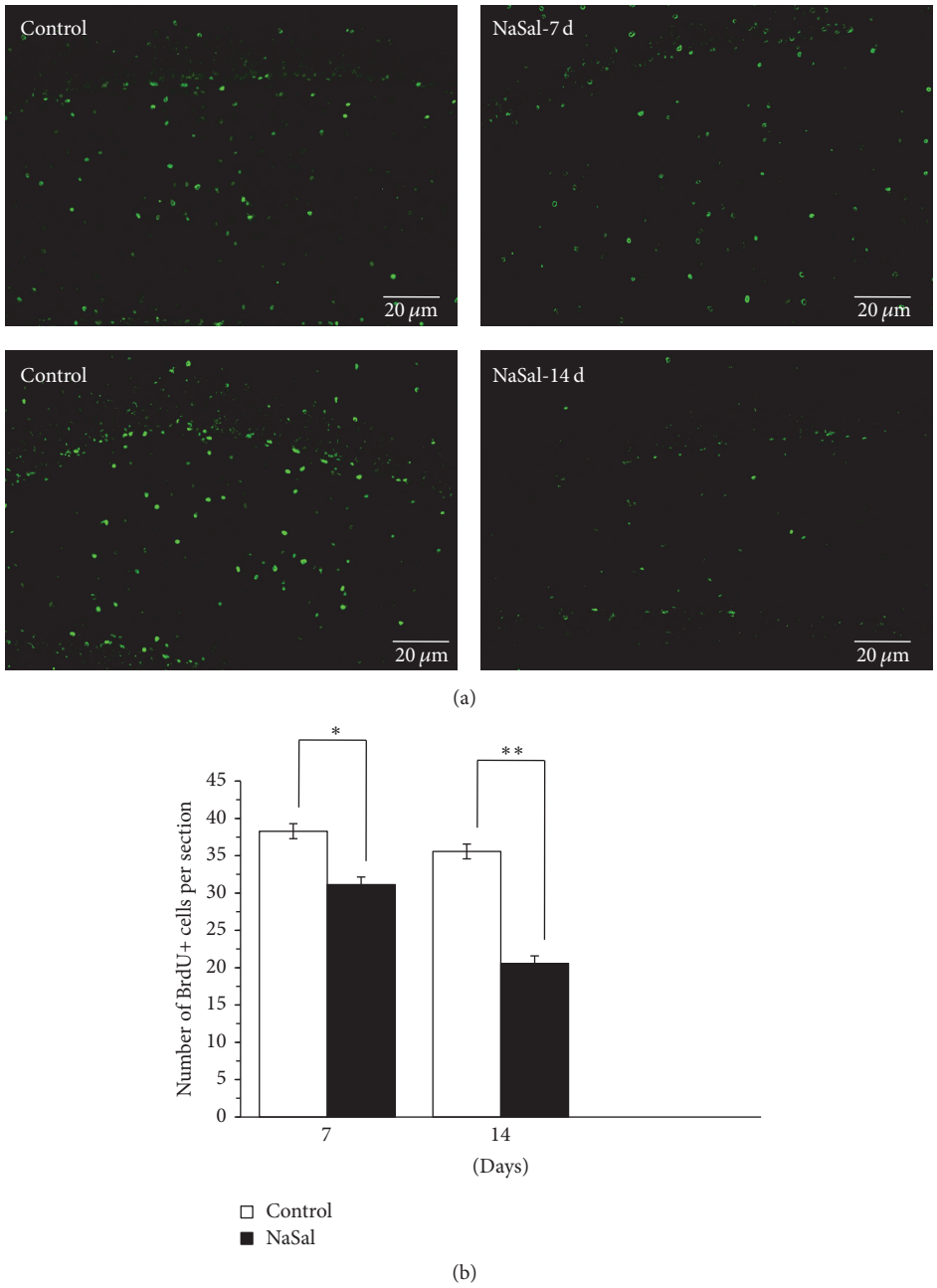

Figure 5: NaSal administration inhibited neurogenesis in the DG of the hippocampus. (a) Representative immunohistochemical staining of BrdU-positive cells in DG of the hippocampus in NaSal-treated and control rats. (b) Statistical analysis showed that consistent (7 days or 14 days) NaSal administration inhibited neurogenesis in DG of the hippocampus [7 days: t (14) = 2.374, $p < 0.05$; 14 days: (t (14) = 4.876, $p < 0.01$)]. n = 8–10, mean ± SEM, $^{**}p < 0.001$.

brain reward regions, such as the nucleus accumbens (NAc), prefrontal cortex, and ventral tegmental area [22, 23], and has a long half-life of 8 days in vivo after chronic stimuli [24]. Previous studies indicated that silencing the transcriptional activity of hippocampal delta-FosB impaired learning and memory across a battery of hippocampal-dependent memory tasks [16]. During our memory retrieval, the number of delta-FosB$^+$ cells in the CA1 of the hippocampus was smaller in NaSal-treated rats than that observed in control rats. Considering that memory retrieval requires hippocampal-dependent learning and memory in which delta-FosB plays a significant role, we think that decreased delta-FosB level following tinnitus obviously contributes to the deteriorated memory retrieval. In general, the learning and memory abilities of NaSal-treated rats were shown to be impaired in MWM test compared to the control group, indicating that

the network was disturbed with the NaSal administration. Taken together, these findings indicate that salicylate affects nonauditory regions of the CNS.

Additionally, neurogenesis has been implicated in learning and memory. Recently, it has been shown that neurogenesis in the adult hippocampus regulates hippocampus-dependent memories [25]. Previous studies have suggested that increasing hippocampal neurogenesis could accelerate forgetting, whereas inhibiting hippocampal neurogenesis could enhance the existing hippocampus-dependent memories [26]. In our studies, we first showed that neurogenesis of the DG field was impaired in NaSal-treated rats following water maze training during retrieval of the memory. It was previously reported that newborn neurons expressing c-Fos exert a long-term effect on DG function related to learning and memory [1]. Studies have indicated that tinnitus could arise from damage at any level of the auditory and nonauditory pathways, which could be induced by different factors leading to alterations in neuroplasticity in the auditory and nonauditory systems [27].

In conclusion, the results of this study support the hypothesis that tinnitus induced by NaSal affected the hippocampal system leading to memory dysfunction.

Conflicts of Interest

The authors declare that there are no conflicts of interest regarding the publication of this paper.

Authors' Contributions

Haichen Niu and Sheng Ding contributed equally to this work.

Acknowledgments

This work is supported by the National Natural Science Foundation of China (81471330, 81601198, and 81501185), the Xuzhou Science & Technology Foundation (KC15SM048, KC16SG252), Xuzhou Medical University Foundation (D2014004), Shandong Provincial Key Research and Development Project (2017GSF218043), Education Department Nature Science Foundation of Jiangsu Province (no. 14KJB310021), and Qing Lan Project.

References

[1] H. Inaba, D. Kai, and S. Kida, "N-glycosylation in the hippocampus is required for the consolidation and reconsolidation of contextual fear memory," *Neurobiology of Learning and Memory*, vol. 135, pp. 57–65, 2016.

[2] B. Langguth, P. M. Kreuzer, T. Kleinjung, and D. De Ridder, "Tinnitus: causes and clinical management," *The Lancet Neurology*, vol. 12, no. 9, pp. 920–930, 2013.

[3] J. T. Gonçalves, S. T. Schafer, and F. H. Gage, "Adult Neurogenesis in the Hippocampus: From Stem Cells to Behavior," *Cell*, vol. 167, no. 4, pp. 897–914, 2016.

[4] G. Andersson and L. McKenna, "The role of cognition in tinnitus," *Acta Oto-Laryngologica*, vol. 126, no. 556, pp. 39–43, 2006.

[5] X. Liu, K. K. Lauer, B. D. Ward, S. M. Rao, S.-J. Li, and A. G. Hudetz, "Propofol disrupts functional interactions between sensory and high-order processing of auditory verbal memory," *Human Brain Mapping*, vol. 33, no. 10, pp. 2487–2498, 2012.

[6] T. Tzounopoulos and N. Kraus, "Learning to Encode Timing: Mechanisms of Plasticity in the Auditory Brainstem," *Neuron*, vol. 62, no. 4, pp. 463–469, 2009.

[7] L. R. Squire, H. Schmolck, and S. M. Stark, "Impaired auditory recognition memory in amnesic patients with medial temporal lobe lesions," *Learning & Memory*, vol. 8, no. 5, pp. 252–256, 2001.

[8] Y.-C. Chen, X. Li, L. Liu et al., "Tinnitus and hyperacusis involve hyperactivity and enhanced connectivity in auditory-limbic-arousal-cerebellar network," *eLife*, vol. 4, no. MAY, Article ID e06576, 2015.

[9] D. Bing, S. C. Lee, D. Campanelli et al., "Cochlear NMDA receptors as a therapeutic target of noise-induced tinnitus," *Cellular Physiology and Biochemistry*, vol. 35, no. 5, pp. 1905–1923, 2015.

[10] N. Steube, M. Nowotny, P. K. D. Pilz, and B. H. Gaese, "Dependence of the startle response on temporal and spectral characteristics of acoustic modulatory influences in rats and gerbils," *Frontiers in Behavioral Neuroscience*, vol. 10, article no. 133, 2016.

[11] H. Niu, X. He, T. Zhou et al., "Neural circuits containing olfactory neurons are involved in the prepulse inhibition of the startle reflex in rats," *Frontiers in Behavioral Neuroscience*, vol. 9, article no. 74, 2015.

[12] Z. Q. Meng, D. M. Zhou, J. H. Wang, and Y. Y. Ma, "Chronic morphine treatment decreases acoustic startle response and prepulse inhibition in rats," *SCIENCE CHINA Life Sciences*, vol. 53, no. 11, pp. 1356–1360, 2010.

[13] D. L. Haus, L. López-Velázquez, E. M. Gold et al., "Transplantation of human neural stem cells restores cognition in an immunodeficient rodent model of traumatic brain injury," *Experimental Neurology*, vol. 281, pp. 1–16, 2016.

[14] H. Niu, Y. Zheng, J. D. Rizak et al., "The effects of lesion of the olfactory epithelium on morphine-induced sensitization and conditioned place preference in mice," *Behavioural Brain Research*, vol. 233, no. 1, pp. 71–78, 2012.

[15] P. W. Frankland, B. Bontempi, L. E. Talton, L. Kaczmarek, and A. J. Silva, "The involvement of the anterior cingulate cortex in remote contextual fear memory," *Science*, vol. 304, no. 5672, pp. 881–883, 2004.

[16] A. L. Eagle, P. A. Gajewski, M. Yang et al., "Experience-dependent induction of hippocampal ΔFosB controls learning," *The Journal of Neuroscience*, vol. 35, no. 40, pp. 13773–13783, 2015.

[17] M. S. Nokia, S. Lensu, J. P. Ahtiainen et al., "Physical exercise increases adult hippocampal neurogenesis in male rats provided it is aerobic and sustained," *The Journal of Physiology*, vol. 594, no. 7, pp. 1855–1873, 2016.

[18] E. F. Evans, J. P. Wilson, and T. A. Borerwe, "Animal Models of Tinnitus," *Ciba Foundation Symposium 85 - Tinnitus*, vol. 85, pp. 108–138, 1981.

[19] H. Yu, K. V. Patil, C. Han et al., "GLAST deficiency in mice exacerbates gap detection deficits in a model of salicylate-induced tinnitus," *Frontiers in Behavioral Neuroscience*, vol. 10, article no. 158, 2016.

[20] A. S. Lowe and J. P. Walton, "Alterations in peripheral and central components of the auditory brainstem response: A neural assay of tinnitus," *PLoS ONE*, vol. 10, no. 2, Article ID e0117228, 2015.

[21] A. Seoane, C. J. Tinsley, and M. W. Brown, "Interfering with Fos expression in rat perirhinal cortex impairs recognition memory," *Hippocampus*, vol. 22, no. 11, pp. 2101–2113, 2012.

[22] Q. Zhang, Q. Liu, T. Li et al., "Expression and colocalization of NMDA receptor and FosB/δFosB in sensitive brain regions in rats after chronic morphine exposure," *Neuroscience Letters*, vol. 614, pp. 70–76, 2016.

[23] B. N. Greenwood, T. E. Foley, T. V. Le et al., "Long-term voluntary wheel running is rewarding and produces plasticity in the mesolimbic reward pathway," *Behavioural Brain Research*, vol. 217, no. 2, pp. 354–362, 2011.

[24] P. G. Ulery-Reynolds, M. A. Castillo, V. Vialou, S. J. Russo, and E. J. Nestler, "Phosphorylation of ΔFosB mediates its stability in vivo," *Neuroscience*, vol. 158, no. 2, pp. 369–372, 2009.

[25] K. G. Akers, A. Martinez-Canabal, L. Restivo et al., "Hippocampal neurogenesis regulates forgetting during adulthood and infancy," *Science*, vol. 344, no. 6184, pp. 598–602, 2014.

[26] J. R. Epp, R. S. Mera, S. Köhler, S. A. Josselyn, and P. W. Frankland, "Neurogenesis-mediated forgetting minimizes proactive interference," *Nature Communications*, vol. 7, Article ID 10838, 2016.

[27] M. Regensburger, I. Prots, and B. Winner, "Adult hippocampal neurogenesis in Parkinson's disease: impact on neuronal survival and plasticity," *Neural Plasticity*, vol. 2014, Article ID 454696, 12 pages, 2014.

Hindawi
BioMed Research International
Volume 2018, Article ID 6387983, 8 pages
https://doi.org/10.1155/2018/6387983

Research Article

Effect of Formaldehyde on Human Middle Ear Epithelial Cells

Shin Hye Kim,[1,2] Ji-Woong Choi,[3] Myung-Whan Suh,[4,5] Jun Ho Lee,[4,5] Seung-Ha Oh,[4,5] Jae-Jun Song,[1] and Moo Kyun Park[4,5]

[1]*Department of Otorhinolaryngology-Head and Neck Surgery, Korea University Medical Center, Korea University College of Medicine, Seoul, Republic of Korea*
[2]*Department of Otorhinolaryngology-Head and Neck Surgery, Haeundae Paik Hospital, Inje University College of Medicine, Busan, Republic of Korea*
[3]*Wide River Institute of Immunology, Seoul National University College of Medicine, Gangwon, Republic of Korea*
[4]*Department of Otorhinolaryngology-Head and Neck Surgery, Seoul National University Hospital, Seoul National University College of Medicine, Seoul, Republic of Korea*
[5]*Sensory Organ Research Institute, Seoul National University Medical Research Center, Seoul, Republic of Korea*

Correspondence should be addressed to Moo Kyun Park; aseptic@snu.ac.kr

Received 13 October 2017; Revised 29 January 2018; Accepted 20 February 2018; Published 26 March 2018

Academic Editor: Jeong-Han Lee

Formaldehyde (FA) is a familiar indoor air pollutant found in everything from cosmetics to clothing, but its impact on the middle ear is unknown. This study investigated whether FA causes cytotoxicity, inflammation, or induction of apoptosis in human middle ear epithelial cells (HMEECs). Cell viability was investigated using the trypan blue assay and a cell counting kit (CCK-8) in HMEECs treated with FA for 4 or 24 h. The expression of genes encoding the inflammatory cytokine tumor necrosis factor alpha (TNF-α) and mucin (MUC5AC) was analyzed using RT-PCR. Activation of the apoptosis pathway was determined by measuring mitochondrial membrane potential (MMP), cytochrome oxidase, caspase-9/Mch6/Apaf 3, and Caspase-Glo® 3/7 activities. The CCK-8 assay and trypan blue assay results showed a reduction in cell viability in FA-treated HMEECs. FA also increased the cellular expression of TNF-α and MUC5AC and reduced the activities of MMP and cytochrome oxidase. Caspase-9 activity increased in cells stimulated for 4 h, as well as caspase-3/7 activity in cells stimulated for 24 h. The decreased cell viability, the induction of inflammation and mucin gene expression, and the activation of the apoptosis pathway together indicate a link between environmental FA exposure and the development of otitis media.

1. Introduction

Otitis media (OM), or infection of the middle ear, is a common inflammatory disease among children. More than 80% of children will have one or more episodes of OM by the age of three [1]. OM leads to conductive hearing loss and may induce delays in the development of speech, language, balance, and learning [2]. Approximately 2.2 million children are diagnosed with OM each year, with the cost estimated at 3–5 billion USD in the USA alone [3, 4]. Therefore, identification and control of risk factors for OM will have a significant impact on healthcare costs.

Formaldehyde (FA) is a colorless, reactive, flammable gas with a strong odor. It is widely used in various household and industrial products and is both an indoor air pollutant and a byproduct of vehicle emissions and cigarette smoke [5]. Small amounts (<4 μM) of FA are also produced endogenously by tumor cells [6]. FA causes adverse health effects in exposed humans and animals and since 2012 it has been classified as a Group 1 carcinogen (carcinogenic to humans) by the International Agency for Research on Cancer [7]. Acute exposure to FA can cause eye, nose, throat, and skin irritation, in addition to Alzheimer's disease-like changes in the brain [8]; long-term exposure has been associated with various cancers [7, 9].

FA also irritates the upper and lower respiratory tracts [10]. Several mechanisms by which FA might cause airway disease have been proposed. For example, FA may associate with protein molecules, such as albumin, to create new antigenic moieties [11]. This may in turn lead to the formation

of specific IgE antibodies that bind to mast cells, followed by degranulation of such cells, and the release of mediators of inflammation [12, 13]. In addition, FA inhalation nonspecifically provokes airway mucosal inflammation [14, 15].

Middle ear disease may develop as an extension of upper airway disease, with the two anatomic sites linked through the Eustachian tube. This situation is more common in children because of their wider and more horizontal Eustachian tubes [16]. Consequently, a toxic substance in the upper airway can trigger middle ear disease, especially in children. The aim of this study was to investigate the effect of FA on cell viability and induction of inflammation in human middle ear epithelial cells (HMEECs). We also examined FA-induced activation of apoptosis.

2. Materials and Methods

2.1. Cell Culture. HMEECs were kindly provided by Dr. David J. Lim [17] and grown as described previously [18]. Briefly, Dulbecco's modified Eagle's medium (DMEM) and bronchial epithelial basal medium (BEBM) (1 : 1) mixed with supplements served as the growth medium. The cells were incubated at 37°C in a humidified atmosphere containing 95% air with 5% CO_2. The growth medium was changed every third or fourth day. After 1 week, the cells were stimulated with different concentrations of FA (Sigma, St Louis, MO, USA) suspended in phosphate-buffered saline (PBS). As a control group, HMEECs were not treated with FA. This study was approved by the institutional review board of Seoul National University Hospital [H-1607-127-777].

2.2. Cell Viability

2.2.1. Trypan Blue Assay. Trypan blue stains dead cells. Live cells possess intact membranes that exclude the dye, whereas dead cells do not. HMEECs were seeded in 96-well plates at 1×10^5 cells/well and then incubated with 0, 0.5, 1, or 2 mM FA for 4 or 24 h. After three washes with PBS, 0.2% trypan blue solution (Gibco, Waltham, MA, USA) was added to each well. After incubation for 1 min at room temperature, the trypan blue solution was removed and 4% paraformaldehyde (PFA) was added to each well for 10 min. The cells were then washed three times with PBS. Viable cells were observed by microscopy with or without a green filter. The results were obtained from two repeated experiments using triplicate samples.

2.2.2. CCK-8 Assay. We used a cell counting kit (CCK-8; Dojindo Laboratories, Kumamoto, Japan) to analyze cell viability and establish experimental conditions for the HMEEC assays. HMEECs were seeded into 96-well plates at 1.7×10^4 cells/well. After 24 h, the cells were incubated with various concentrations of FA (0, 0.025, 0.05, 0.1, 0.2, 0.4, 0.6, 0.8, 1, 1.25, 1.5, or 2 mM) for 4 or 24 h. The cells were then washed three times with PBS, and the CCK-8 solution [10% (v/v)] was added to each well. The plates were incubated in the dark for 1 h at 37°C and then placed on a shaker at room temperature for 5 min. Optical densities were measured at 450 nm using a microplate reader (Cytation 5; BioTek, Winooski, VT, USA). The results are the means of three experiments, each performed in triplicate.

2.3. Expression of Genes Encoding the Inflammatory Cytokine (TNF-α) and Mucin (MUC5AC). HMEECs were seeded in 96-well plates at 1.7×10^4 cells/well. After 24 h, they were incubated with 0, 1.5, and 2 mM FA for 4 h and 0, 0.1, and 0.2 mM FA for 24 h. Total RNA was extracted from the HMEECs using an RNeasy® mini kit (Qiagen GmbH, Hilden, Germany). RNA (3 μg) was reverse-transcribed at 55°C for 30 min and the resulting cDNAs were then amplified using a PCR kit (Qiagen, Valencia, CA, USA). The sequences of the oligonucleotide primers used in the PCRs were as follows: *TNF*, 5′-GGAGAAGGGTGACCGACTCA-3′; *MUC5AC*, 5′-CAGCACAACCCCTGTTTCAAA-3′; and *GAPDH*, 5′-ATGGCACCGTCAAGGCTGAG-3′. PCR amplification was performed under the following conditions: a holding stage at 95°C for 20 s followed by 45 cycles of 95°C for 1 s and 60°C for 20 s and then a melting stage at 95°C for 15 s and 60°C for 60 s. The results were obtained from three repeated experiments using triplicate samples. The data were analyzed using QuantStudio 6 Flex software (Applied Biosystems, Foster City, CA, USA).

2.4. Cell Apoptosis

2.4.1. Measurement of Mitochondrial Membrane Potential (MMP). HMEECs were incubated with 0, 1.5, or 2 mM FA for 4 h and 0, 0.1, or 0.2 μM FA for 24 h and then mixed with 2 μM 5′,6,6′-tetrachloro-1,1′,3,3′-tetraethylbenzimidazolylcarbocyanine iodide (JC-1) reagent. The stained cells were counted. To confirm a change in the JC-1 reaction due to a change in the MMP, a reference reaction with 50 μM CCCP (carbonyl cyanide 3-chlorophenylhydrazone) was established. The stained HMEECs were analyzed using a flow cytometer with an excitation wavelength of 530/30 nm and 585/42 nm bandpass emission filters. Normal membrane potential was indicated by JC-1 red fluorescence and a loss of membrane potential by JC-1 green fluorescence. The loss of membrane potential (%) was calculated based on measurements from six samples.

2.4.2. Cytochrome Oxidase Activity Colorimetric Assay. HMEECs were incubated with 0, 1.5, and 2 mM FA for 4 h and 0, 0.1, and 0.2 μM FA for 24 h. Apoptosis was then analyzed using a cytochrome oxidase activity colorimetric assay kit (BioVision, Milpitas, CA, USA) after cell lysis. The change in absorbance at 550 nm via the oxidation of reduced cytochrome c, measured in six replicate samples, served as an indicator of cytochrome oxidase activity.

2.4.3. Caspase-9/Mch6/Apaf-3 Colorimetric Protease Assay. HMEECs were incubated with 0, 1.5, and 2 mM FA for 4 h and 0, 0.1, and 0.2 μM FA for 24 h. Apoptotic cells were quantified using an ADAM cell counter (ADAM MC; Digital Bio, Seoul, Korea), and the amount of cell protein was quantified in a bicinchoninic acid assay after cell lysis. Apoptosis markers

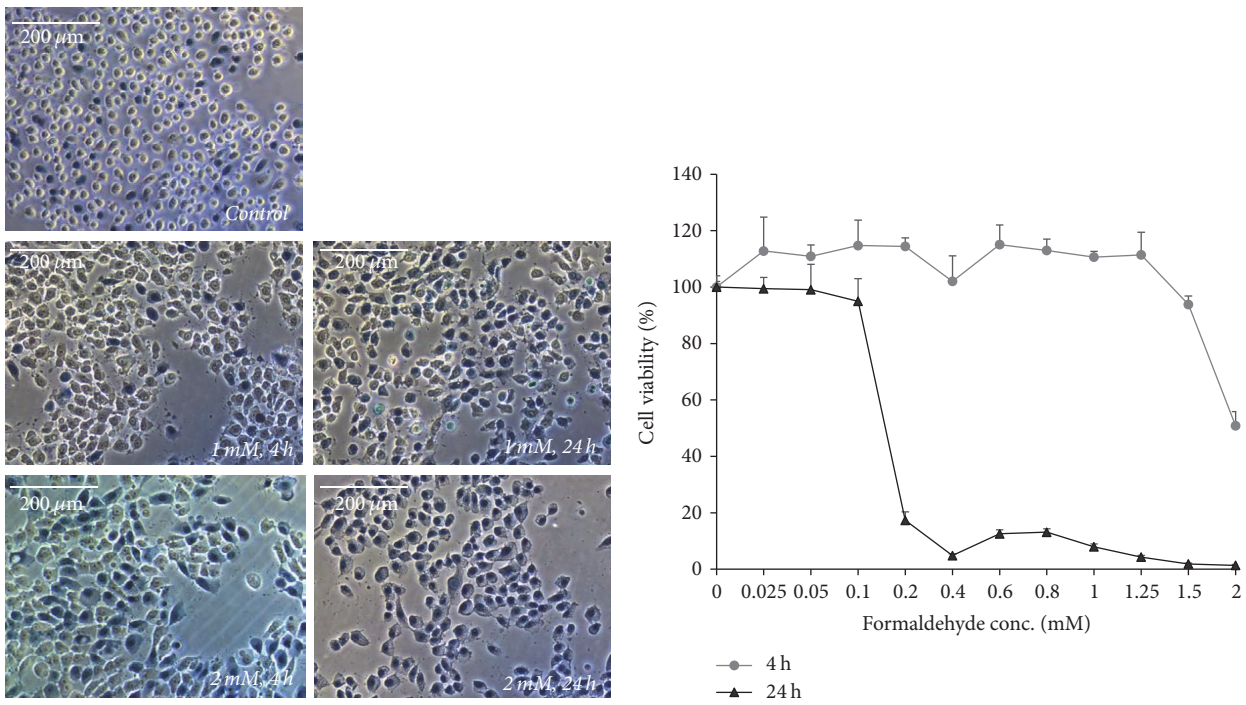

Figure 1: *Viability of human middle ear epithelial cells (HMEECs) following formaldehyde (FA) exposure.* (a) Nonviable cells take up trypan blue and their numbers increase to greater extents in cultures exposed to FA for 24 h versus 4 h and to 2 mM versus 1 mM FA (×200, trypan blue assay without green filter). (b) The cell counting kit- (CCK-) 8 assay revealed that cell viability decreased after cells were exposed to 1.5 mM FA for 4 h and 0.2 mM FA for 24 h. Error bars represent standard deviation (SD) of the mean.

were detected in real time using a caspase-9/Mch6/Apaf-3 colorimetric protease assay kit (Invitrogen, Carlsbad, CA, USA). Cells seeded in 96-well plates were scanned and their optical density (OD) at 405 nm was measured using a microreader (Cytation 3; BioTek, Winooski, VT, USA). The relative absorbance of six FA-treated versus untreated samples was determined.

2.4.4. Caspase-Glo 3/7 Assay. HMEECs were incubated with 0, 1.5, and 2 mM FA for 4 h and 0, 0.1, and 0.2 μM FA for 24 h. Apoptosis activity was analyzed using a Caspase-Glo 3/7 assay kit (Promega, Madison, WI, USA). Following caspase cleavage, a substrate that reacts with luciferase (aminoluciferin) is released and the light produced in the reaction is then measured. In this study, the luminescence of six FA-treated and untreated samples was measured at 0.5, 1.0, 1.5, 2.0, 2.5, and 3.0 h using a microplate reader.

2.5. Statistical Analysis. Statistical significance was determined with the aid of the one-tailed paired-sample *t-test*. A P value < 0.05 for the null hypothesis was considered to indicate a statistically significant difference. SPSS software (ver. 11.0; SPSS Inc., Chicago, IL, USA) was used for the statistical analysis.

3. Results

3.1. FA Reduces the Viability of HMEECs. In the trypan blue assay, dead cells were stained with trypan blue. The number of viable cells decreased with increasing FA concentrations and longer FA exposure time compared to untreated control cells (Figure 1(a)). Moreover, there were fewer viable cells in cultures subjected to 2 mM FA for 24 h than in cultures incubated with 1 mM FA for 4 h.

The CCK-8 assay of HMEECs treated with 0.025–1.25 mM FA for 4 h showed that cell viability was maintained at almost 100% but decreased to 50.9% in cells exposed to 2 mM FA (Figure 1(b)). In HMEECs treated with 0.2 mM FA for 24 h, viability rapidly decreased to <20%. Thus, in the following experiments, these concentrations were considered appropriate when performing the 4 and 24 h exposure experiments. The 50% lethal concentration (LC_{50}) of FA was 2.038 mM over 4 h and 0.154 mM over 24 h.

3.2. FA Increases Inflammatory Cytokine and Mucin Gene Expression in HMEECs. Significant increases in *TNF-α* gene expression in HMEECs exposed to 2 mM FA for 4 h and to 0.2 mM FA for 24 h were determined (Figure 2(a)). The expression of the *MUC5AC* gene in HMEECs increased significantly as well as when exposed to 0.2 mM FA for 24 h (Figure 2(b)).

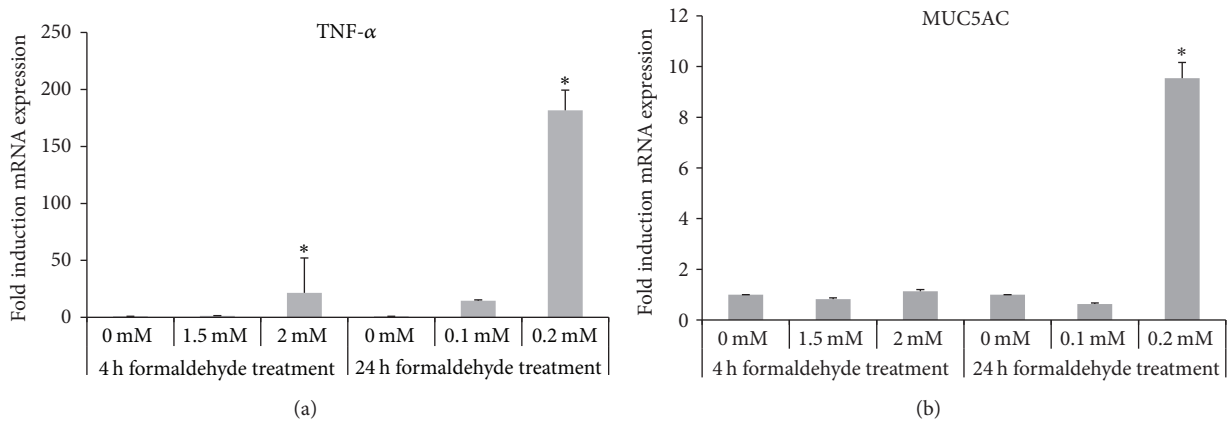

Figure 2: *Upregulation of the inflammatory cytokine tumor necrosis factor alpha (TNF-α) and mucin gene (MUC5AC) expression in HMEECs exposed to FA*. (a) The expression of mRNA encoding TNF-α was upregulated in cells treated with 2 mM FA for 4 h and 0.2 mM FA for 24 h. (b) The expression of mRNA encoding MUC5AC was upregulated in cells treated with 0.2 mM FA for 24 h. Error bars represent SD of the mean. Data represent the means ± SD from three repeated experiments with triplicate samples. $^*P < 0.05$ compared with the control values.

3.3. FA Increases the Loss of MMP in HMEECs. When exploring MMP- and apoptosis-related activity, cells were exposed to 0.1 and 0.2 μM FA (rather than 0.1 and 0.2 mM FA) for 24 h, because exposure to 0.1 or 0.2 mM FA for 24 h induced cell fixation. JC-1 red (normal membrane potential) and JC-1 green (loss membrane potential) fluorescence were analyzed using flow cytometry (Figures 3(a) and 3(b)). The loss of MMP was significant in cells stimulated with 1.5 and 2 mM FA for 4 h (9.9% and 8.9%, resp.); smaller losses occurred in response to 0.1 and 0.2 μM FA for 24 h (4.9% and 5.4%, resp.) (Figure 3(c)).

3.4. FA Increases Apoptosis in HMEECs. Cytochrome oxidase activity was measured in HMEECs exposed to 0, 1.5, and 2 mM FA for 4 h and to 0, 0.1, and 0.2 μM FA for 24 h (Figures 4(a) and 4(b)). After the 4 h of FA treatment, the luminescence levels were lower than those of controls at the higher FA concentrations. After 24 h of FA treatment, the luminescence was greater at the higher FA concentration compared to that of the control. To determine whether FA exposure activates the caspase cascade in HMEECs, the functional activities of the apoptosis initiator caspase-9 and the apoptosis effector caspase-3/7 were measured in HMEECs exposed to 0, 1.5, or 2 mM FA for 4 h or to 0, 0.1, or 0.2 μM FA for 24 h. In the caspase-9 assay, the relative absorbance after 4 h of exposure to FA was greater at the higher FA concentration (Figure 4(c)). In the caspase-3/7 assay, the extent of luminescence after 24 h of exposure to FA was greater at the higher FA concentration (Figure 4(d)). Although the FA concentration during the 24 h treatment was 1/1,000-fold of that during the 4 h FA treatment, the luminescence levels indicated that caspase-3/7 activity levels were higher.

4. Discussion

In this study, we demonstrated that FA affects the viability of HMEECs even at low-dose FA (0.2 mM) during a long exposure (24 h). Under those conditions, cytotoxicity was greater than after a short exposure (4 h) to high-dose FA (2 mM). The endogenous concentration of FA in human blood is 80–100 μM [19]. Thus, a prolonged exposure to a small additional amount of FA could lead to cytotoxicity in humans. FA affects cell morphology, causing cell shrinkage and decreasing the colony size of human NK cells within 1 h [20]. FA at concentrations of 0.1–0.2 mM also induces nuclear fragmentation and chromatin condensation, as hallmarks of apoptosis, in neuroblastoma cells [21]. Endogenous FA reacts with proteins to form immunogenic and atherogenic adducts (epitopes) [13]. FA cytotoxicity is explained in part by the fact that FA forms adducts with DNA and proteins [9, 22].

Our study further demonstrated that FA induces inflammatory cytokine *(TNF-α)* and mucin *(MUC5AC)* gene expression in HMEECs. Inflammatory cytokines including TNF-α, cyclooxygenase-2 (COX-2), nuclear factor- (NF-) κB, interleukin- (IL-) 1, IL-6, and IL-8 play important roles in the initiation of mucosal changes, stimulation of mucin secretion, and immune regulation seen in OM [23–25]. We previously reported increased inflammatory cytokine and mucin gene expression in HMEECs exposed to environmental pollutants [18, 25, 26]. Some materials toxic to lung epithelium are also toxic to the middle ear mucosa because of the similar composition of these two tissues. For example, acrolein induces an inflammatory response and increases mucin gene expression in both human lung epithelial cells and HMEECs [26]. In murine alveolar macrophages immediately after FA exposure, several cytokines (IL-4, IL-10, IFN-γ, and TNF-α) became detectable by ELISA of cell supernatants [27]. FA aggravates asthma, at least in part by increasing the T helper-2 dominant response, which is related to levels of the cytokine mediators of asthma (IL-4, IL-5, IL-9, and IL-13) [12]. In addition, FA interferes with thiols, leading to accelerated reduction of the endogenous bronchodilator S-nitrosoglutathione [14]. Also, the Rho kinase-dependent Ca^{2+} sensitization pathway plays a role in the airway hyperresponsiveness induced by FA [28].

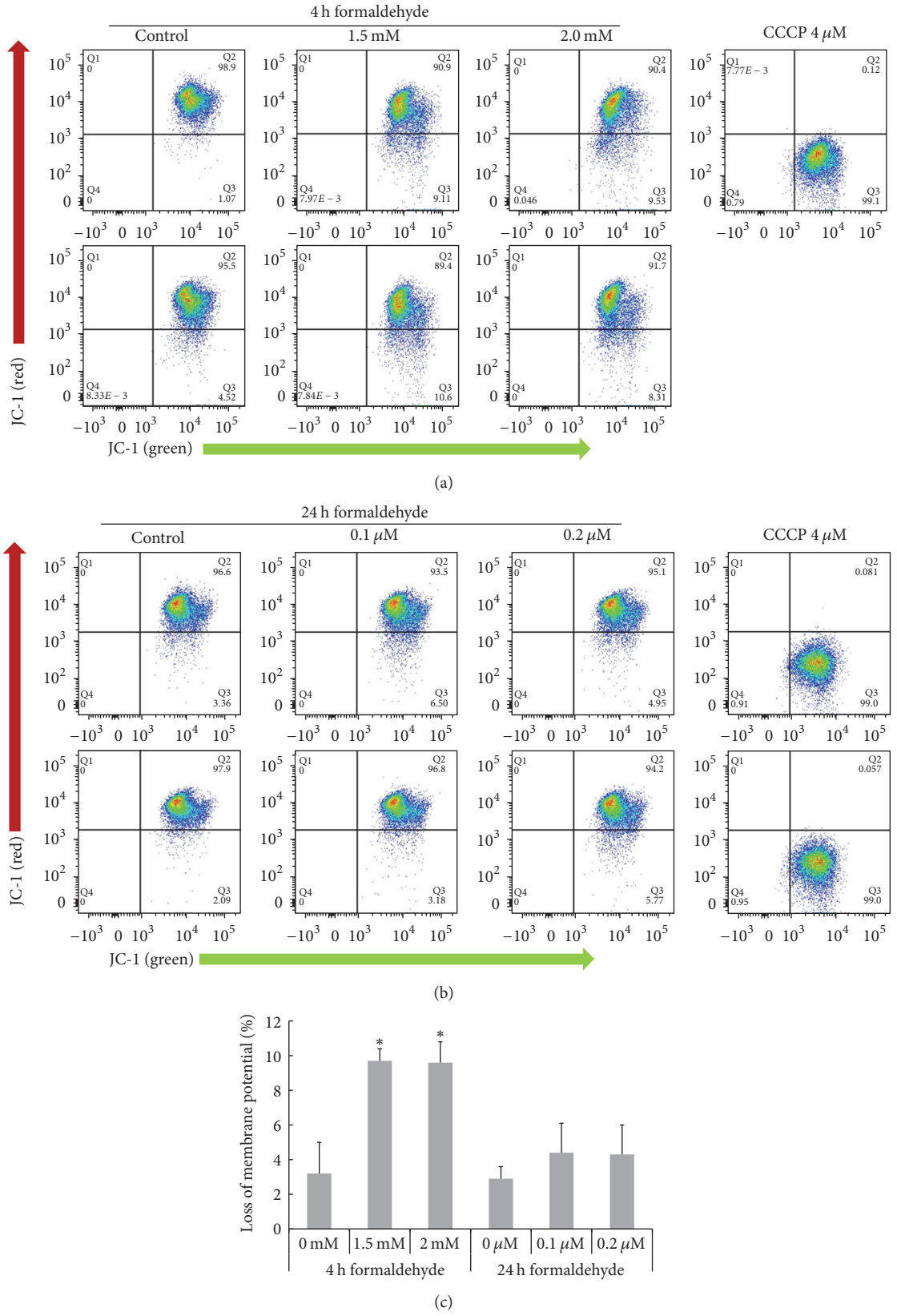

FIGURE 3: *Loss of mitochondrial membrane potential (MMP) in HMEECs following FA exposure.* (a, b) Histogram of a MitoProbe[6] JC-1 assay shows the decreased red/green fluorescence intensity ratios following cell exposure to FA for 4 h or 24 h. (c) HMEECs exhibited reductions in MMP levels after 4 or 24 h of FA treatment. After 4 h of FA treatment, the reduction in MMP level was statistically significant. Error bars represent SD of the mean. The data represent the means ± SD of three repeated experiments with six samples. $^{*}P < 0.05$ compared with control.

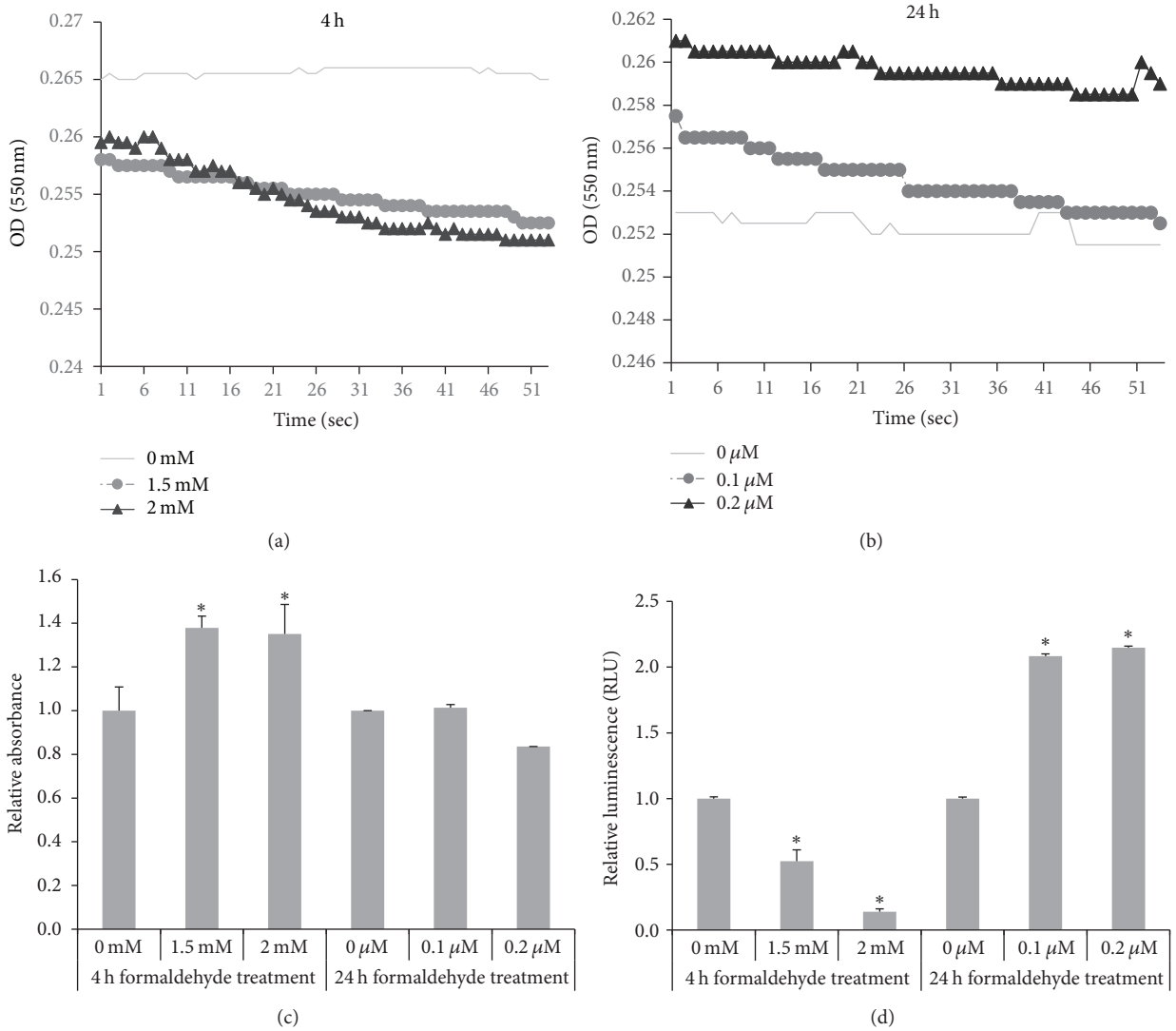

Figure 4: *Apoptosis pathway activity in HMEECs exposed to FA*. (a, b) Cytochrome oxidase activity decreased after 4 h of FA exposure and increased after 24 h of FA exposure in a dose-dependent manner. (c) Caspase-9/Mch6/Apaf-3 activity, measured as the relative absorbance, increased in cells stimulated for 4 h with 1.5 and 2 mM FA. (d) Caspase-Glo 3/7 activity, measured as relative luminescence, decreased after 4 h of FA exposure but increased after 24 h of exposure to FA. Error bars represent the SDs of the mean. The data represent the averages (a, b) or means ± SD (c, d) of three experiments, each with six replicates. $^{*}P < 0.05$ compared with control.

In this study, MMP decreased and apoptosis-related activity increased in FA-treated HMEECs. That the cytotoxicity of FA is related to the induction of apoptosis has previously been demonstrated in tumor cells, endothelial cell cultures, neural cells, and NK cells [20–22]. In a previous experiment, we showed that FA increases apoptosis (data not shown), but very high doses of FA result in necrotic cell death, especially coagulation necrosis, but also lytic cell death [22]. FA-mediated apoptosis is characterized by a marked decrease in MMP, inhibition of mitochondrial respiration, and formation of reactive oxygen species [29]. A decrease in MMP occurs in response to many apoptotic stimuli and is linked to the release of cytochrome c during apoptosis [30]. In this study, MMP loss was higher in cells treated with 1.5 or 2 mM FA for 4 h than in those treated with 0.1 or 0.2 μM FA for 24 h.

In the HMEECs examined in our study, low-dose (0.1–0.2 μM) FA increased cytochrome oxidase and caspase-7/3 activity in cells exposed for 24 h. However, after 4 h of exposure to 1.5 and 2 mM FA, reduced levels of both cytochrome oxidase and caspase-7/3 activity were measured. Cytochrome c interacts with apoptotic protease activating factor 1 (APAF1), which activates caspase-9. Active caspase-9, in turn, activates caspase-3 and caspase-7, eventually leading to apoptosis [31]. Accordingly, low cytochrome oxidase activity in cells exposed to FA for 4 h may diminish caspase-7/3 activity, although the relationship between cytochrome oxidase and the loss of MMP is not understood. A previous study showed that FA inhibits NADH dehydrogenase (complex I) and cytochrome c oxidase (complex IV) [21]. FA is commonly used for histological fixation of tissues

and cultured cells; the effects of FA increase over time [32]. We found that some cells were fixed after exposure to 0.1–0.2 mM FA for 24 h. To minimize cell fixation caused by high concentrations of FA and to accurately measure the extent of apoptosis, we exposed cells to 0.1–0.2 μM FA (rather than 0.1–0.2 mM FA) in the 24 h experiments, evaluating MMP status and apoptosis-related activity.

FA is highly water-soluble, existing in tissues as a reversibly hydrated form (methanediol) [33]. Most FA exposures occur by inhalation or skin/eye contact [33]. For the same level of FA, children may experience a larger exposure than adults because of the greater surface area of the pediatric lung [11]. Furthermore, because higher levels of FA occur nearer to the ground (lower specific gravity than air), short stature children may be exposed to higher levels than adults in the same location [11]. FA is highly reactive at the site of entry and reacts readily with macromolecules, including DNA, to form DNA-protein and DNA-DNA cross-links [34]. Inhaled FA is absorbed primarily in the upper airways because of its high water solubility, metabolism, and reactivity [35]. Diffusion through the mucus layer is the dominant transport mechanism for FA. Once in the mucus layer, FA undergoes a reversible reaction with water to form methanediol [33]. A proportion of inhaled FA passes through the mucus layer to reach the epithelium, wherein FA undergoes enzymatic transformation and removal in nasal tissue, and engages in nonenzymatic reactions with glutathione and macromolecules, including proteins and DNA [33]. The Rho kinase-dependent Ca^{2+} sensitization pathway plays a role in airway hyperresponsiveness to FA [28].

Environmental exposure to FA is a frequent occurrence but treatment is limited to supportive care, including decontamination (flushing of skin and eyes with water, gastric lavage, and administration of activated charcoal), administration of supplemental oxygen, intravenous sodium bicarbonate and/or isotonic fluid, and hemodialysis [36]. Therefore, greater efforts should be made to prevent exposure to FA, based on an awareness of its toxicity.

5. Conclusions

Our study proposes a link between environmental FA exposure and OM development. FA increases *TNF-α* and *MUC5AC* mRNA expression in HMEECs. Both mediators are increased in OM. FA decreases cell viability, increases the activity of the apoptosis pathway, causes a significant loss of MMP, and increases cytochrome oxidase, caspase-9, and caspase-3/7 activities.

Additional Points

The English language in this document has been checked by at least two professional editors, both native speakers of English. For a certificate, please see http://www.textcheck.com/certificate/6VvQB2.

Conflicts of Interest

The authors have no conflicts of interest to declare regarding the publication of this paper.

Acknowledgments

This research was supported by the Korean Ministry of Environment (MOE) as the Environmental Health Action Program (Grant no. 2016001360009).

References

[1] L. Monasta, L. Ronfani, F. Marchetti et al., "Burden of disease caused by otitis media: systematic review and global estimates," *PLoS ONE*, vol. 7, no. 4, Article ID e36226, 2012.

[2] M. M. Rovers, "The burden of otitis media," *Vaccine*, vol. 26, no. 7, pp. G2–G4, 2008.

[3] A. M. Capra, T. A. Lieu, S. B. Black, H. R. Shinefield, K. E. Martin, and J. O. Klein, "Costs of otitis media in a managed care population," *The Pediatric Infectious Disease Journal*, vol. 19, no. 4, pp. 354-355, 2000.

[4] P. Shekelle, G. Takata, L. S. Chan et al., "Diagnosis, natural history, and late effects of otitis media with effusion.," *Evidence report/technology assessment (Summary).*, no. 55, pp. 1–5, 2002.

[5] U. S. E. P. Agency, Facts about formaldehyde, in facts about formaldehyde, 2017.

[6] S. Kato, P. J. Burke, T. H. Koch, and V. M. Bierbaum, "Formaldehyde in human cancer cells: detection by preconcentration-chemical ionization mass spectrometry," *Analytical Chemistry*, vol. 73, no. 13, pp. 2992–2997, 2001.

[7] I. A. f. R. o. C. IARC, Monographs on the evaluation of carcinogenic risks to humans, 2017.

[8] X. Liu, Y. Zhang, R. Wu et al., "Acute formaldehyde exposure induced early Alzheimer-like changes in mouse brain," *Toxicology Mechanisms and Methods*, pp. 1–10, 2017.

[9] S. L. W. Tan, S. Chadha, Y. Liu et al., "A Class of Environmental and Endogenous Toxins Induces BRCA2 Haploinsufficiency and Genome Instability," *Cell*, vol. 169, no. 6, pp. 1105–1118.e15, 2017.

[10] P. Wolkoff and G. D. Nielsen, "Non-cancer effects of formaldehyde and relevance for setting an indoor air guideline," *Environment International*, vol. 36, no. 7, pp. 788–799, 2010.

[11] G. McGwin Jr., J. Lienert, and J. I. Kennedy Jr., "Formaldehyde exposure and asthma in children: A systematic review," *Environmental Health Perspectives*, vol. 118, no. 3, pp. 313–317, 2010.

[12] J. A. Elias, C. G. Lee, T. Zheng, B. Ma, R. J. Homer, and Z. Zhu, "New insights into the pathogenesis of asthma," *The Journal of Clinical Investigation*, vol. 111, no. 3, pp. 291–297, 2003.

[13] J. Nakamura, T. Shimomoto, L. B. Collins et al., "Evidence that endogenous formaldehyde produces immunogenic and atherogenic adduct epitopes," *Scientific Reports*, vol. 7, no. 1, Article ID 10787, 2017.

[14] C. M. Thompson, R. P. Subramaniam, and R. C. Grafström, "Mechanistic and dose considerations for supporting adverse pulmonary physiology in response to formaldehyde," *Toxicology and Applied Pharmacology*, vol. 233, no. 3, pp. 355–359, 2008.

[15] L. Li, L. Hua, Y. He, and Y. Bao, "Differential effects of formaldehyde exposure on airway inflammation and bronchial hyperresponsiveness in BALB/c and C57BL/6 mice," *PLoS ONE*, vol. 12, no. 6, Article ID e0179231, 2017.

[16] C. D. Bluestone and M. B. Bluestone, *Eustachian tube: structure, function, role in otitis media*, BC Decker, Hamilton, Lewiston, NY, USA, 2005.

[17] Y.-M. Chun, S.-K. Moon, D. E. Brackmann et al., "Immortalization of normal adult human middle ear epithelial cells using a

retrovirus containing the E6/E7 genes of human papillomavirus type 16," *Annals of Otology, Rhinology & Laryngology*, vol. 111, no. 6, pp. 507–517, 2002.

[18] J.-J. Song, J. D. Lee, B. D. Lee, S. W. Chae, and M. K. Park, "Effect of diesel exhaust particles on human middle ear epithelial cells," *International Journal of Pediatric Otorhinolaryngology*, vol. 76, no. 3, pp. 334–338, 2012.

[19] H. D. Heck, M. Casanova-schmitz, and P. B. Dodd, "Formaldehyde (CH2O) Concentrations in the Blood ofHumans and Fischer-344 Rats Exposed to CH2O Under Controlled Conditions," *American Industrial Hygiene Association Journal*, vol. 46, no. 1, pp. 1–3, 1985.

[20] Q. Li, Q. Mei, T. Huyan et al., "Effects of formaldehyde exposure on human NK cells in vitro," *Environmental Toxicology and Pharmacology*, vol. 36, no. 3, pp. 948–955, 2013.

[21] T. Zerin, J.-S. Kim, H.-W. Gil, H.-Y. Song, and S.-Y. Hong, "Effects of formaldehyde on mitochondrial dysfunction and apoptosis in SK-N-SH neuroblastoma cells," *Cell Biology and Toxicology*, vol. 31, no. 6, pp. 261–272, 2015.

[22] B. Szende and E. Tyihák, "Effect of formaldehyde on cell proliferation and death.," *Cell Biology International*, vol. 34, no. 12, pp. 1273–1282, 2010.

[23] H. Y. Lee, Y. I. Kim, J. W. Lee, J. Y. Byun, M. S. Park, and S. G. Yeo, "Decreased expression of TLR-9 and cytokines in the presence of bacteria in patients with otitis media with effusion," *Clinical and Experimental Otorhinolaryngology*, vol. 6, no. 4, pp. 195–200, 2013.

[24] J. E. Kerschner, "Mucin gene expression in human middle ear epithelium," *The Laryngoscope*, vol. 117, no. 9, pp. 1666–1676, 2007.

[25] J. J. Song, J. Y. Kim, A. S. Jang et al., "Effect of cadmium on human middle ear epithelial cells," *The Journal of International Advanced Otology*, vol. 11, no. 3, pp. 183–187, 2015.

[26] J.-J. Song, J. D. Lee, B. D. Lee, S. W. Chae, and M. K. Park, "Effect of acrolein, a hazardous air pollutant in smoke, on human middle ear epithelial cells," *International Journal of Pediatric Otorhinolaryngology*, vol. 77, no. 10, pp. 1659–1664, 2013.

[27] K. Nandate, T. Ishidao, H. Hori, Y. Morimoto, and M. Ogata, "The effect of formaldehyde exposure on cytokine production in murine alveolar macrophages," *Journal of UOEH*, vol. 25, no. 2, pp. 197–205, 2003.

[28] J. Jude, C. Koziol-White, J. Scala et al., "Formaldehyde induces rho-associated kinase activity to evoke airway hyperresponsiveness," *American Journal of Respiratory Cell and Molecular Biology*, vol. 55, no. 4, pp. 542–553, 2016.

[29] S. Teng, K. Beard, J. Pourahmad et al., "The formaldehyde metabolic detoxification enzyme systems and molecular cytotoxic mechanism in isolated rat hepatocytes," *Chemico-Biological Interactions*, vol. 130-132, pp. 285–296, 2001.

[30] E. Gottlieb, S. M. Armour, M. H. Harris, and C. B. Thompson, "Mitochondrial membrane potential regulates matrix configuration and cytochrome c release during apoptosis," *Cell Death & Differentiation*, vol. 10, no. 6, pp. 709–717, 2003.

[31] G. Ichim and S. W. G. Tait, "A fate worse than death: Apoptosis as an oncogenic process," *Nature Reviews Cancer*, vol. 16, no. 8, pp. 539–548, 2016.

[32] C. H. Fox, F. B. Johnson, J. Whiting, and P. P. Roller, "Formaldehyde fixation," *Journal of Histochemistry & Cytochemistry*, vol. 33, no. 8, pp. 845–853, 1985.

[33] National Research Council (U.S.), *Committee to Review EPA's Draft IRIS Assessment of Formaldehyde, "Review of the Environmental Protection Agency's draft IRIS assessment of formaldehyde,"*, National Academies Press, Washington, DC, USA, 2011.

[34] H. M. Bolt, "Experimental toxicology of formaldehyde," *Journal of Cancer Research and Clinical Oncology*, vol. 113, no. 4, pp. 305–309, 1987.

[35] S. T. Larsen, P. Wolkoff, M. Hammer, V. Kofoed-Sørensen, P. A. Clausen, and G. D. Nielsen, "Acute airway effects of airborne formaldehyde in sensitized and non-sensitized mice housed in a dry or humid environment," *Toxicology and Applied Pharmacology*, vol. 268, no. 3, pp. 294–299, 2013.

[36] "Medical Management Guidelines for Formaldehyde," 2016.

Hindawi
BioMed Research International
Volume 2018, Article ID 5675848, 9 pages
https://doi.org/10.1155/2018/5675848

Research Article

Does the Width of the Bony Cochlear Nerve Canal Predict the Outcomes of Cochlear Implantation?

Juyong Chung,[1] **Jeong Hun Jang**,[2] **Sun O Chang**,[3] **Jae-Jin Song**,[4] **Sung-Woo Cho**,[5] **So Young Kim**,[6] **Jun Ho Lee**,[5,7] **and Seung-Ha Oh**[5,7]

[1]*Department of Otorhinolaryngology-Head and Neck Surgery, Wonkwang University College of Medicine, Iksan, Republic of Korea*
[2]*Department of Otolaryngology, Ajou University School of Medicine, Suwon, Republic of Korea*
[3]*Department of Otolaryngology-Head and Neck Surgery, Kangbuk Samsung Hospital, Sungkyunkwan University School of Medicine, Seoul, Republic of Korea*
[4]*Department of Otorhinolaryngology, Seoul National University Bundang Hospital, Seoul National University College of Medicine, Seongnam, Republic of Korea*
[5]*Department of Otorhinolaryngology, Seoul National University College of Medicine, Seoul, Republic of Korea*
[6]*Department of Otorhinolaryngology, CHA Bundang Medical Center, CHA University, Seongnam, Republic of Korea*
[7]*Sensory Organ Research Institute, Seoul National University Medical Research Center, Seoul, Republic of Korea*

Correspondence should be addressed to Sun O Chang; suno@snu.ac.kr

Received 16 November 2017; Accepted 22 January 2018; Published 21 March 2018

Academic Editor: Kenneth H. Lee

A narrow bony cochlear nerve canal (BCNC) is associated with sensorineural hearing loss necessitating cochlear implantation (CI). This study evaluated the implications of BCNC width for post-CI outcomes. A total of 56 children who had received CIs were included. The patients were divided into three groups according to the width of the BCNC (Group 1: diameter < 1.4 mm, $n = 17$; Group 2: diameter 1.4–2.0 mm, $n = 14$; Group 3: diameter > 2.0 mm, $n = 25$). The post-CI speech performances were compared among the three groups according to BCNC width. The correlation between BCNC width and post-CI speech performance was evaluated. Logistic regression analysis was also performed to investigate factors that can impact post-CI speech performance. Cochlear nerve deficiency (CND) occurred more frequently in Group 1. Groups 1 and 2 had significantly worse post-CI outcomes. Patients with intact cochlear nerves had significantly better post-CI outcomes than those with CND. When the cochlear nerve was intact, patients with a narrower BCNC showed less favorable results. Therefore, patients with either a narrow BCNC or CND seemed to have poorer outcomes. A narrow BCNC is associated with higher CND rates and poor outcomes. Measurement of BCNC diameter may help predict CI outcomes.

1. Introduction

The cochlear implant (CI) is an innovative device that is used to treat patients with bilateral, severe, or profound sensorineural hearing loss. It converts the auditory signal into an electrical signal, which in turn stimulates spiral ganglion neurons (SGNs), thus transmitting the signal to the auditory brainstem via the cochlear nerve. Therefore, the integrity of the cochlear nerve is the main factor affecting improvement in speech performance after CIs. This can be evaluated before surgery using magnetic resonance imaging (MRI) or the promontory stimulation test (PST).

The bony cochlear nerve canal (BCNC) lies between the fundus of the internal auditory canal (IAC) and the base of the cochlea. It encases the cochlear nerve fibers from the spiral ganglion to the cochlear nerve [1] (Figure 1). Therefore, a narrow BCNC likely indicates anatomic or functional deficiency in the cochlear nerve. Specifically, if the width of the BCNC—the distance between the inner margins of the bony walls at the midportion—is less than 1.4 mm, then the cochlear nerve may be abnormal [2]. One study found such a narrow BCNC in approximately 60% of patients with unilateral sensorineural hearing loss (SNHL) [3]. Furthermore, BCNC stenosis may be related

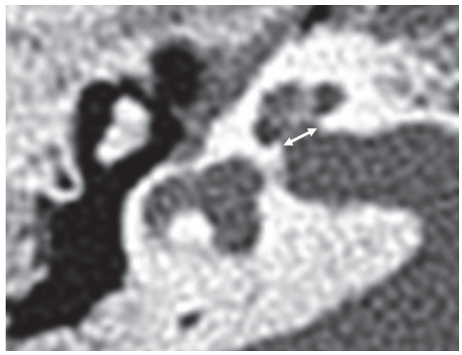

Figure 1: Axial slices of temporal bone computed tomography for the measurement of bony cochlear nerve canal (BCNC) in normal bony cochlear nerve canal. The width was measured by the distance between the inner margins of bony walls at midportion, at the fundus level of cochlear nerve in internal auditory canal.

to cochlear nerve hypoplasia [3–5]. It follows that patients with BCNC stenosis may not benefit from CI and that the condition may be a predictor of poor post-CI outcome [2]. However, the relationship between BCNC diameter and post-CI outcome has not been characterized in previous studies.

In the present study, we aimed to evaluate the width distribution of the BCNC in ears that had received CIs, to evaluate the association between BCNC width and cochlear nerve deficiency (CND), and to analyze the correlation between BCNC width and speech performance after CI. This information may be helpful in predicting improvements in speech performance after CI.

2. Materials and Methods

2.1. Subjects. This retrospective study was approved by the Institutional Review Board of the Clinical Research Institute (SNUH IRB number 1006-099-322). The need for informed consent was waived. A total of 452 children who had received a CI between January 2005 and April 2012 were enrolled. Their medical records were reviewed retrospectively for data regarding otorhinolaryngological examinations, evaluation of preoperative hearing status, pre- and postoperative speech performance, temporal bone computed tomography (TBCT), and magnetic resonance imaging (MRI) of the IAC. Among these 452 patients, children satisfying one of following criteria were excluded: (1) follow-up less than 3 years, (2) insufficient medical records, (3) either MRI or TBCT unavailable, (4) device failure or incomplete electrode insertion, and (5) children with inner ear anomaly, as classified by the system published by Sennaroglu et al. [6]. The CT findings of all ears included in this study were normal except for differences in the BCNC width. After all exclusions, our cohort was comprised of 56 children who were followed up for more than 3 years, had both available TBCT and MRI of the IAC, and had no inner ear anomaly except for differences in the BCNC width.

Ultimately, 56 children were classified into three groups according to the BCNC width. BCNC stenosis was defined as a BCNC width less than 1.4 mm, as reported in a previous study [2]. When the BCNC was greater than 2.0 mm in diameter, it was defined as having a normal size, as described in previous research [1]. Children in this study were divided into three groups based on the BCNC width: Group 1 (<1.4 mm, $n = 17$), Group 2 (1.4–2.0 mm, $n = 14$), and Group 3 (>2.0 mm, $n = 25$). The mean ages at the time of CI in the three groups were 27.92 ± 15.92 months, 29.32 ± 9.84 months, and 33.43 ± 15.7 months, respectively. The mean follow-up periods were 27.17 ± 13.66 months, 47.20 ± 16.69 months, and 49.64 ± 21.91 months, respectively.

2.2. Measurements. In this study, two parameters were used to analyze the correlation between the BCNC and the post-CI outcome: BCNC width and the status of cochlear nerve. The BCNC width was estimated using the axial plane of the TBCT. The axial plane runs parallel to the infraorbitomeatal line. As reported in a previous study, the width of the BCNC was measured at its midportion and was defined as the distance between the inner margins of the bony walls (Figure 1) [3, 7]. We evaluated the status of the cochlear nerve at the lateral part of the IAC using the MRI images. At this site, the facial and cochlear nerves are of similar size and larger than the vestibular nerve [8, 9]. Therefore, CND was defined when the cochlear nerve at the lateral aspect of IAC was smaller than (1) the superior or inferior vestibular nerve and (2) the facial nerve at the same point. All measurements were performed separately by two otologists—J. H. J., who had 9 years' experience, and J. C., who had 8 years' experience in otorhinolaryngology. They estimated the BCNC width and the status of the cochlear nerve using a computer-based caliper in the PACS system; they were blinded to the medical history of all the children. To evaluate post-CI speech performance, we reviewed (1) the preoperative categories of auditory performance (CAP) score, (2) the CAP score at 6, 12, 24, and 36 months postoperatively, (3) open-set test results (word/sentence), and (4) the Korean picture vocabulary test (K-PVT) percentage. The K-PVT is similar to the Peabody PVT-revised edition; it evaluates the receptive vocabulary of Korean children, with reference to their age and to the population with normal hearing. The examiner speaks one word that describes one of four pictures and asks the individual to say the number of picture or point to it. The result is expressed as a percentile score, which is then compared with the scores of children of the same age who have normal hearing.

2.3. Data Analysis. The post-CI speech performances were compared among the three groups using the Mann–Whitney–Wilcoxon test. The correlation between BCNC width and post-CI speech performance was evaluated using Pearson correlation analysis. The association between the BCNC width and speech performance was assessed using multiple logistic regression. All analyses was performed using SPSS version 17.0 (SPSS Inc., Chicago, Illinois), and the 95% confidence intervals were also assessed. In all analyses, p values < 0.05 were considered statistically significant.

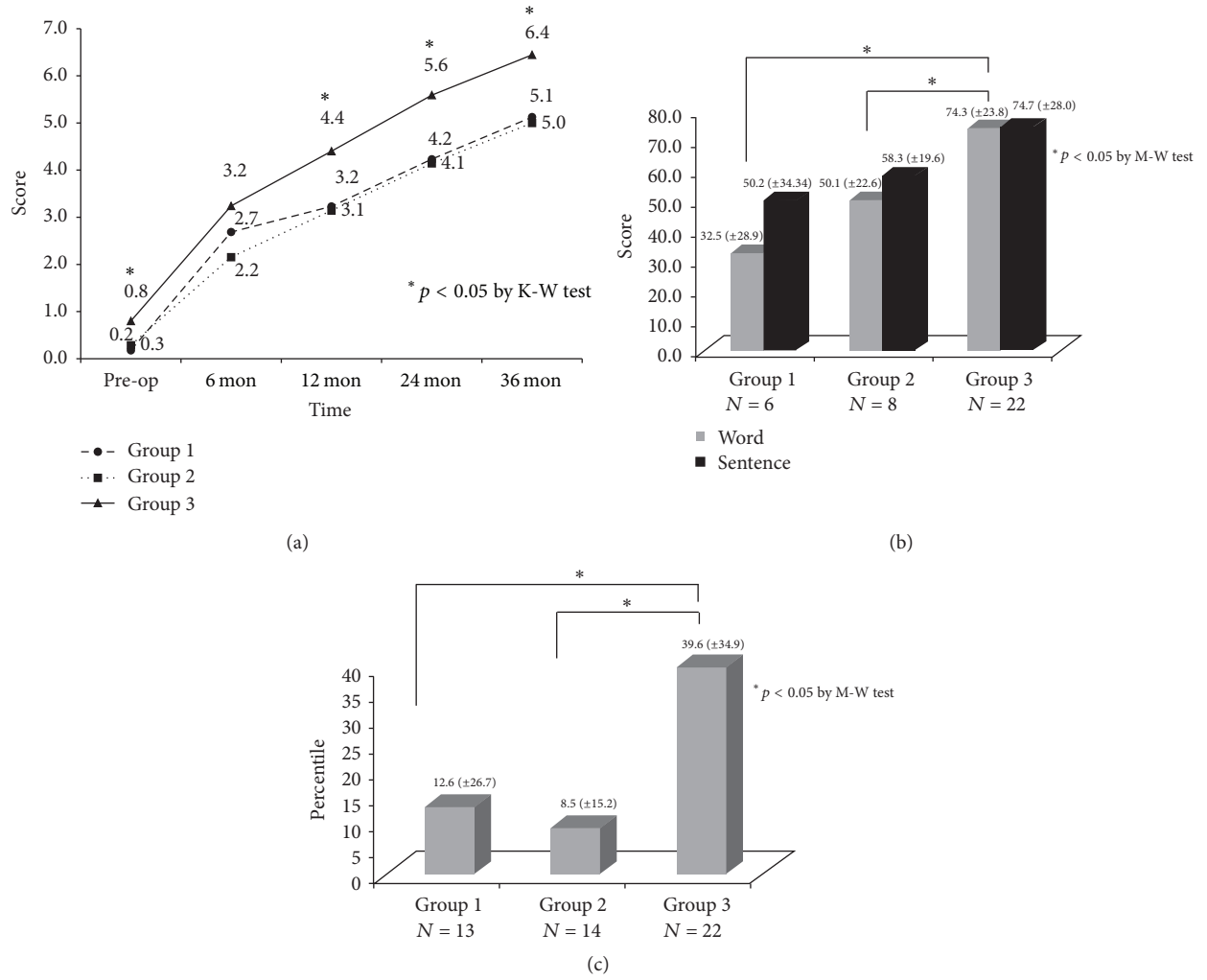

FIGURE 2: Comparisons of post-CI speech performance between three groups. ∗ means statistically significant. (a) CAP score. Since 12 months after CI, Group 3 showed significantly better outcomes than Groups 1 and 2. (b) Open-set score. Groups 1 and 2 showed less favorable results. (c) Picture vocabulary tests.

3. Results

3.1. Factors Influencing the Outcomes of CI in the Three Groups. There were no significant differences among the groups in age at the time of CI, duration of hearing aid use, or residual hearing. The mean BCNC width in Group 1 was 0.91 ± 0.32 mm, that in Group 2 was 1.89 ± 0.17 mm, and that in Group 3 was 2.34 ± 0.14 mm. Most differences among the groups were not statistically significant; however Group 1 had a higher rate of CND (13/17; 76%) than Group 2 (3/14; 21%) and Group 3 (0/25; 0%; Table 1).

3.2. Post-CI Speech Performance according to BCNC Width. We compared the speech performance among the groups. In Groups 1 and 2, the CAP score 36 months after CI was lower than that in Group 3 (Figure 2(a)). With regard to the open-set score 24 months after CI, Groups 1 and 2 scored worse than Group 3 (Figure 2(b)). We saw a similar trend in the K-PVT 24 months after CI, in which Groups 1 and 2 continued to underperform (Figure 2(c)).

3.3. Postoperative Speech Performance—according to BCNC Width—of CI Patients with an Intact Cochlear Nerve. To rule out confounding factors related to CND, we investigated the post-CI speech performance according to BCNC width when the cochlear nerve was present. To do so, we referred to the parasagittal constructive interference in the steady state MRI images of the IAC. There were no significant differences in CAP score between the groups. However, the open-set sentence score of Group 2 was lower than that of Group 3. Group 1 contained only one patient and therefore had few statistical power. The trend continued in the K-PVT (Figure 3).

3.4. Correlation between BCNC Width and Post-CI Speech Performance. We analyzed the implications of BCNC width for post-CI speech performance using Pearson correlation analysis. The Pearson correlation coefficients were calculated between BCNC width and various measures of post-CI speech performance such as CAP score, open-set word or sentence score, and K-PVT results. The CAP score 24 and

Table 1: Influencing factors on outcome of CI between 3 groups.

	Group 1 (n = 17)	Group 2 (n = 14)	Group 3 (n = 25)	p value
Age at CI (months)	27.92 (±15.92)	29.32 (±9.84)	33.43 (±15.7)	0.450
Hearing aids applied (months)	13.47 (±11.8)	12.47 (±9.05)	12.75 (±14.01)	0.972
PTA at CI side (dB)	94.00 (±9.98)	100.35 (±11.05)	93.40 (±9.37)	0.102
PTA at contralateral side (dB)	96.23 (±11.78)	97.92 (±12.31)	92.52 (±10.16)	0.322
BCNC width (mm)	0.91 (±0.32)	1.89 (±0.17)	2.34 (±0.14)	<0.05
CND	13/17	3/14	0/25	<0.05

CI: cochlear implantation; PTA: pure tone average; BCNC: bony cochlear nerve canal; CND: cochlear nerve deficiency. Statistical analyses by Wilcoxon rank-sum test.

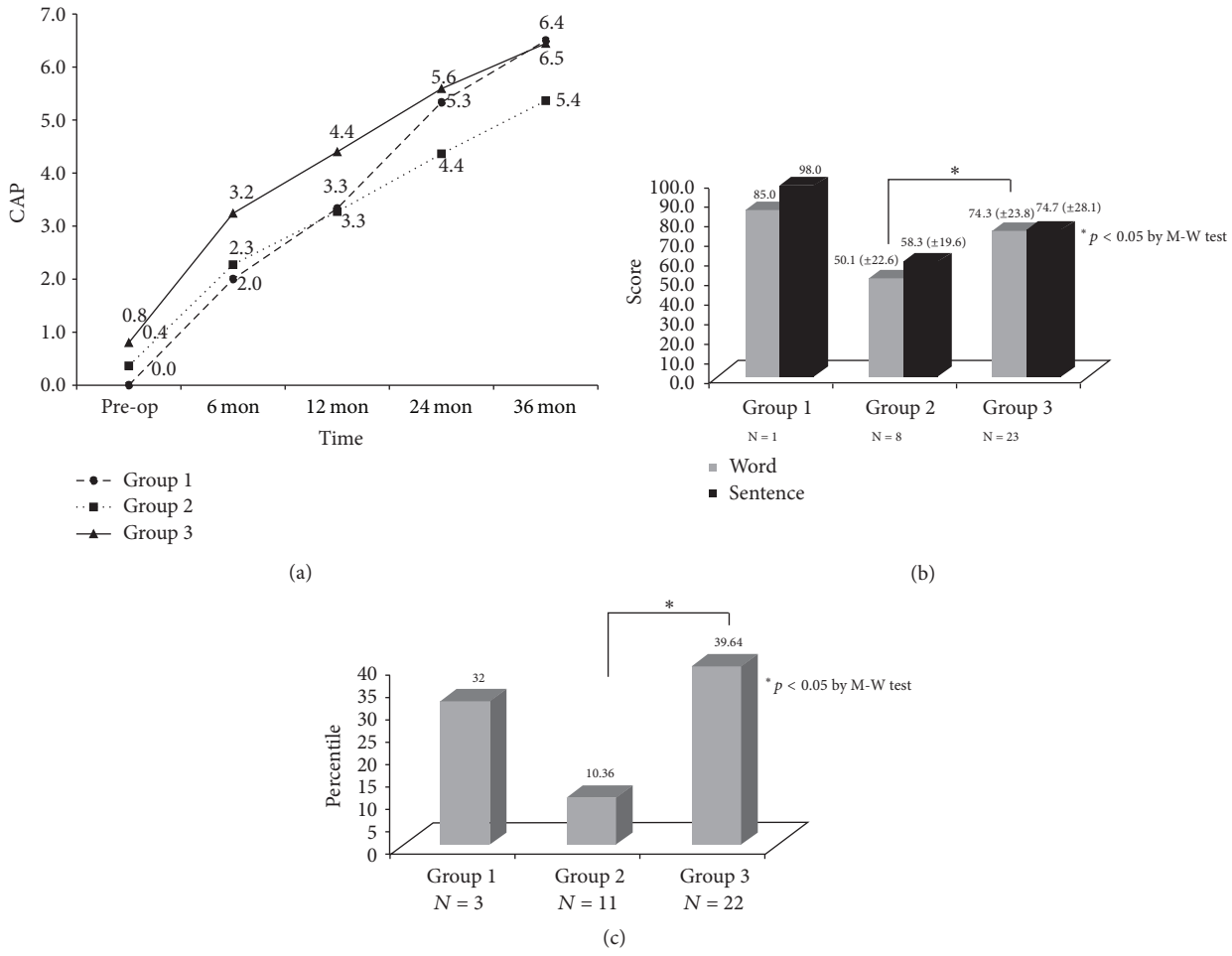

Figure 3: Comparisons of post-CI speech performance between three groups when the CN is present. ∗ means statistically significant. (a) CAP score. (b) Open-set score. (c) Picture vocabulary test.

36 months after CI was correlated linearly with BCNC width (Figure 4(a)). In CAP score at 24 months and 36 months post-CI, the correlation coefficient of 0.377, 0.395 demonstrates a linear relationship between the two variables ($p < 0.05$). Furthermore, BCNC width and open-set word score 24 months after CI showed a positive correlation (correlation coefficient = 0.533, $p < 0.05$), and BCNC width was positively correlated with K-PVT 24 months after CI (correlation coefficient = 0.342, $p < 0.05$) (Figures 4(b) and 4(c)). These findings suggest that preoperative measurement of the BCNC width using CT images might be related to post-CI outcomes and that such measurement provides clinicians with useful information for counseling parents and patients.

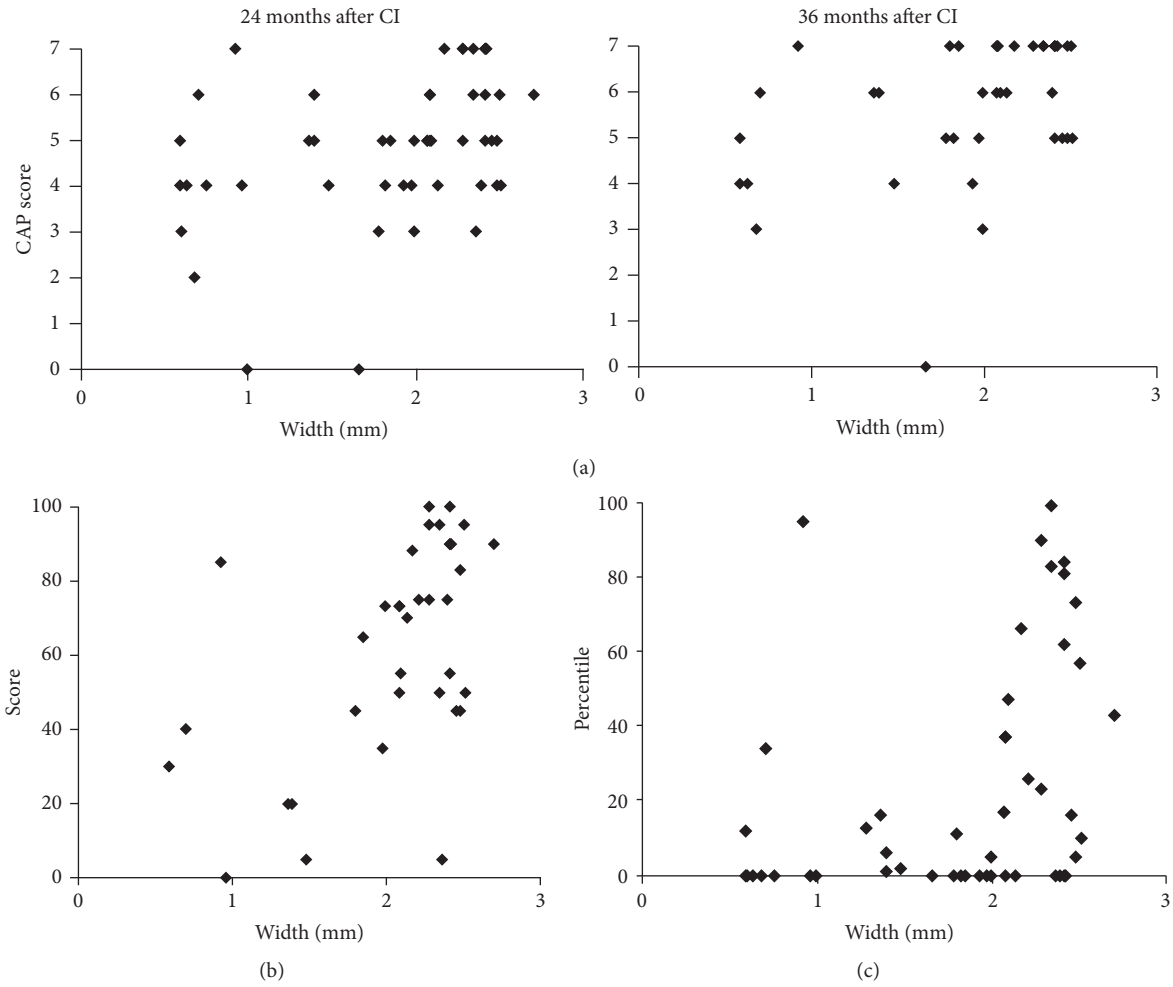

Figure 4: Correlation of width of BCNC with post-CI speech performances was shown. (a) The CAP score 24 and 36 months after CI was correlated linearly with BCNC width. (b) Positive correlation between the width of BCNC and open-set word score at 24 months after CI. (c) Positive correlation between width of BCNC and Picture vocabulary test at 24 months after CI.

3.5. Factors Determining the Auditory Performance after CI. We used multiple regression analysis to ascertain which factors influence post-CI speech performance in Group 1, Group 2, and Group 3. We analyzed five potential influencing factors: (1) age at the time of CI, (2) BCNC width, (3) presence of CND, (4) duration of hearing aids used before CI, and (5) residual hearing. The results of the analysis varied depending on the specific test used to evaluate speech performance; nonetheless, BCNC width was significantly associated with open-set sentence score after CI (Table 2). In addition, the presence of CND was statistically associated with K-PVT results, and the duration of hearing aids used before CI was significantly related to CAP score (Table 2). However, age at the time of CI and residual hearing were not statistically associated with CI outcomes.

4. Discussion

In a previous study, we evaluated the BCNC length and width in normal inner ears: 1.07 mm and 2.38 mm, respectively. In cases of congenital unilateral sensorineural hearing loss, the BCNC length and width in affected inner ears were significantly smaller than those in normal inner ears [1]. The mean width in the affected inner ears in our previous study was 1.58 mm; other investigators have reported mean widths of 1.12 mm and 1.0 mm [10, 11]. Many authors have reported that the BCNC length in normal hearing inner ears ranges from 0.93 mm to 1.17 mm and that the width ranges from 1.88 mm to 2.13 mm (Table 3) [2, 11, 14]. In 2000, Fatterpekar et al. [3] reported that the width of the BCNC was significantly smaller in patients with SNHL than in a control group. One year later, Nelson and Hinojosa [14] recounted histological evidence of cochlear nerve aplasia in the normal inner ear and IAC. In 2006, Adunka et al. [15] stated that cochlear nerve aplasia is not always associated with IAC hypoplasia and that both high-resolution MRI and CT must be performed in patients with profound SNHL. Komatsubara et al. [10] reported that cochlear nerve aplasia may be present when the canals are narrower than 1.5 mm on TBCT; such aplasia can definitively be seen using MRI. In all these efforts to ascertain the significance of BCNC width, clinicians took note of the clinical implications of BCNC width in CI candidates.

Table 2: Results of multiple regression analysis regarding contributions of factors to the speech performance of CI.

Variable	CAP score at 24 months after CI		CAP score at 36 months after CI		Open-set word score at 24 months after CI		Picture vocabulary test (percentile) at 24 months after CI	
	β	*p value*	β	*p value*	β	*p value*	β	*p value*
Age at CI		ns		ns		ns		ns
BCNC Width		ns		ns	0.533	0.001		ns
CND		ns		ns		ns	0.346	0.015
Duration of hearing aids use		ns	−0.244	0.048		ns		ns
Residual hearing		ns		ns		ns		ns

CI: cochlear implantation; CAP: categories of auditory performance; CND: cochlear nerve deficiency; ns: nonsignificant.

Table 3: Technical differences and measured width of BCNC in the previous studies in normal hearing and bilateral SNHL.

	Imaging protocol	Slice chosen	Measurement	Width (mm) in control	Width (mm) in bilateral SNHL
Fatterpekar et al. [3]	Parallel to the infraorbitomeatal line	Slice at oval window	Manual measurement along the inner margin of its bony walls at its midportion	2.13 ± 0.44 (N = 50 ears)	1.82 ± 0.24 in profound bilateral SNHL (N = 33 ears)
Komatsubara et al. [10]	30° downward to the orbitomeatal line	Slice with maximum width	Digital measurement at midline between two straight lines drawn on the fundus of the IAC and the base of the modiolus	1.91 ± 0.27 (N = 100 ears)	0.99 ± 0.37 (with CND) 1.73 ± 0.32 (with developed cochlear nerve)
Kono [11]	Parallel to the infraorbitomeatal line	n.a	Measurement at the base of the modiolus	2.1 ± 0.2 (N = 118 ears)	n.a
Stjernholm et al. [2]	Temporal bone cast using silicone rubber	n.a	Measurement in axiopetrosal plane	2.58 ± 0.31 (N = 117 ears)	n.a
	Parallel to the infraorbitomeatal line	Slice at posterior semicircular canal	Measurement along the inner margin of its bony walls at its midportion	1.91 ± 0.24 (N = 100 ears)	n.a
Pagarkar et al. [12]	Direct scanning in axial plane spiral with a pitch of 1	Slice with maximum width	Maximum width was measured to the nearest 0.1 mm	1.9 ± 0.7 (N = 19 ears)	1.0 ± 0.2 (N = 8 ears)
Teissier et al. [13]	Parallel to the lateral semicircular canal	Slice containing the cochlear modiolus, the oval window	Measurement at the entry of the cochlea	2.16 ± 0.24 (N = 174 ears)	2.12 ± 0.55 (N = 120 ears)

BCNC: bony cochlear nerve canal; SNHL: sensorineural hearing loss; n.a: not available.

Previous research has suggested that the lower limit of normal BCNC width is 2.10 mm; this was obtained by subtraction of the standard deviation from the mean value in normal hearing inner ears [1]. Thus, the mean BCNC width in normal patients is higher than 2.0 mm. When we divided the patients of the present study into three groups based on the BCNC width, Group 3 (normal BCNC width) comprised all patients whose BCNC was wider than 2.0 mm.

Recently, there have been more requests for imaging to evaluate inner ear anomalies and predict post-CI outcomes. High-resolution CT (HRCT) of the temporal bone provides additional information regarding temporal bone pathology, facial nerve position, and inner ear malformations [4]. Furthermore, MRI is better able to show the labyrinth and eighth cranial nerve [4]. Thus, MRI is the best tool to evaluate the status of the cochlear nerve in cases of aplasia or hypoplasia and to predict negative outcomes in CI candidates [15, 16].

Imaging studies provide useful information regarding inner ear anomalies. Sennaroglu [6] classified inner ear malformations to investigate their etiology. However a classification of this kind may not be sufficient to predict CI outcomes, because it does not include IAC malformations, such as narrow IAC and BCNC hypoplasia, which have a negative impact on CI outcomes because they indicate CND [4, 17]. Recently, some authors have reported a relationship

between BCNC stenosis and cochlear nerve hypoplasia [3, 10, 11, 18]. In fact, BCNC stenosis may be secondary to cochlear nerve hypoplasia [11]. Stjernholm and Muren [2] stipulated that a cochlear nerve abnormality was a possibility when the BCNC was less than 1.4 mm in diameter. In a report by Komatsubara et al. [10], patients with a narrow BCNC on CT were diagnosed as having cochlear nerve hypoplasia, which was confirmed using MRI, with 88.9% sensitivity and 88.9% specificity. The same authors stated that when the BCNC was less than 1.5 mm on CT, cochlear nerve hypoplasia could be seen on MRI. In a report by Kono [11], a BCNC diameter less than 1.7 mm suggested cochlear nerve hypoplasia, even when no cochlear abnormality could be found on CT. BCNC stenosis with a diameter of 1.5 mm or less suggests cochlear nerve hypoplasia or aplasia. On the other hand, cochlear nerve hypoplasia was not seen in children who had BCNC stenosis with a diameter greater than 1.5 mm. A previous study indicated that children who had BCNC stenosis with a diameter of 1.5 mm or less and those who had severe inner ear malformations on HRCT require MRI of the cochlear nerve [4]. Therefore, noting the presence of BCNC stenosis confirms a diagnosis of cochlear nerve hypoplasia or aplasia [18]. Moreover, BCNC stenosis with a diameter of 1.5 mm or less further confirms such a diagnosis [10].

In the present study, CND was frequently associated with a narrow BCNC, especially one less than 1.4 mm in diameter; therefore, measurements of the BCNC may help in predicting the outcomes of CI. In addition, if BCNC stenosis or cochlear malformation is revealed on HRCT, additional MRI may show cochlear nerve aplasia or hypoplasia. Thus, MRI can confirm the status of the cochlear nerve, whether aplastic or hypoplastic, and help predict improvements in hearing performance after CI. In turn, BCNC stenosis could be used to select children who should undergo further evaluation using MRI. These findings have important implications for clinicians who evaluate children with SNHL.

Several case reports have included information on the speech performance of patients with CND. Recent reports of CI among children with CND have been reported with generally poor results. Buchman et al. reported post-CI speech performance among 22 children with CND [19]. Children with CND had higher pure tone averages and required greater charge for CI stimulation than other inner ear malformation types [19]. In addition, open-set speech perception after CI was achieved in only 19% of CND cases and participating in mainstream education is more limited [19]. Zanetti et al. reported one case of CND after CI. In this report, although the child scored poorly in every perceptive category when using the CI alone, the device greatly enhanced his speech understanding when he also used a hearing aid in his opposite ear [20].

The present article is the first to report a correlation between BCNC width and post-CI speech performance. In addition, we performed multivariate logistic regression analysis to evaluate influencing factors. The speech performance after CI may be influenced by several factors [21]. The comprehensive evaluation of prognostic factors enables CI team to counsel the CI candidates for the post-CI outcome accurately. It was known that the physiologic factors (age at CI, duration of deafness, meningitis, genetic mutation), the anatomical factors (inner ear anomaly, BCNC, CND), functional factors (residual hearing level, preoperative use of hearing aid), device factors (coding strategy, brand of CI, the percentage of active electrode), and education/rehabilitation factors (mode of communication, socioeconomic status, post-CI rehabilitation service, family support) could be related to the CI outcome [22]. In this current study, BCNC, CND, and the duration of hearing aids use were related to post-CI outcome. On the other hand, the age at CI did not have an effect on speech performance after CI because most children were implanted at the age less than 2 years (age at CI < 2 years, 73%), which is consistent with previous studies [23, 24]. This study was mainly focused on the relationship between the BCNC and CI outcome, so several factors such as meningitis, genetic mutation, device factors, and education/rehabilitation factors were not analyzed.

Besides age at the time of CI and preoperative residual hearing, which were already known as prognostic factors for CI outcome, BCNC width was correlated with speech performance in a 3-year postoperative follow-up. The present study showed a positive correlation between post-CI long-term speech performance and BCNC width. These data suggest that BCNC width indirectly reflects the residual capability of the cochlear nerve. Hence, along with MRI of the IAC MRI, TBCT may contribute to preoperative evaluation of cochlear nerve residual capabilities, and it may be helpful in patient counseling.

The fundamental goal of preoperative imaging is the prediction of CI outcomes. In this regard, the results of the present study provide indirect evidence that TBCT is useful in CI candidates. Generally, MRI is recommended in the evaluation of cochlear nerve integrity in patients with profound SNHL; however, the estimation of BCNC using TBCT may play a supportive role. That is, narrow BCNC may indicate higher rates of CND and poor post-CI outcomes. Therefore, preoperative measurement of the BCNC on CT images may help to predict CI outcomes.

In the present study, we found that the frequency of CND was much higher in CI patients with BCNC hypoplasia (76%) than in CI patients with a normal BCNC (21%). Moreover, the width of the BCNC was significantly smaller in CI patients with CND (1.11 mm) than in CI patients with a normal cochlear nerve (2.08 mm). These correlations may be partially due to developmental abnormalities. We also tried to ascertain the relationship between BCNC width and post-CI speech performance. To understand the significance of BCNC width in this regard, we must understand the embryology of the inner ear and IAC. The exact cause of the narrow BCNC in patients with SNHL is not known. We assume that deficiencies in the development of the otic vesicle inhibit normal nerve growth factor production. This may in turn result in excessive neuronal degradation and prevent normal growth of the cochlear nerve. Furthermore, because most patients with profound SNHL are thought to have anomalies of the membranous labyrinth [1], this inner ear malformation may inhibit the normal trophic effects of nerve growth factor, causing a small cochlear nerve and hypoplasia of the BCNC. As the IAC develops—at 9 weeks'

gestation—the mesenchyme surrounding the otic vesicle begins to chondrify, finally forming the otic capsule by means of ossification. Therefore, the IAC is formed through the inhibition of cartilage formation at the medial aspect of the otic vesicle; the vestibulocochlear nerve mediates this inhibition by inducing nerve growth factor. In the absence of the nerve, a canal will not be formed [24, 25]. However, Casselman et al. [8] found that cochlear nerve hypoplasia and aplasia can occur with or without labyrinth anomalies. Several other authors have reported cases of cochlear nerve aplasia with normal IAC dimensions [18, 26]. Therefore, the etiology of acquired CND may be complex.

CND can result from degeneration of the nerve fibers in the IAC after cochlear injury (vascular, traumatic, compressive, or inflammatory injury). In the case of CND with a normal BCNC, it may be that the vestibulocochlear nerve is injured in one of the ways mentioned—that is, long after BCNC formation. The destruction of the cochlear neuroepithelium may lead to retrograde destruction of the spiral ganglia in the modiolus [27]. On the other hand, when the cochlear nerve is injured microscopically during the late stages of IAC formation (approximately 5 months' gestation) or when it has abnormalities related to growth factors, hypoplasia of the BCNC may result, even in cases of relatively intact cochlear nerve development.

In the present retrospective review, we found that the frequency of BCNC hypoplasia in CI patients without inner ear anomalies was 3.8% (17/452) and that the BCNC width was correlated with long-term speech performance (more than 24 months) after CI. Furthermore, the frequency of CND was 3.5% (16/452), and the probability of CND diagnosis by MRI is significantly increased when BCNC hypoplasia is diagnosed by TBCT. Patients who had both BCNC hypoplasia and CND tended to have poor speech performance after CI, and CND was frequently associated with a narrow BCNC. Therefore, a narrow BCNC may indicate higher rates of CND and poor outcomes. According to a recent study, BCNC stenosis is significantly associated with impaired speech discrimination; this would be expected if BCNC abnormalities indicated cochlear nerve dysfunction. Therefore, BCNC stenosis predicts poor outcomes for auditory rehabilitation, and BCNC measurement may help to predict CI outcomes.

The cochlear nerve size is thought to be associated with the population of spiral ganglion cells. Therefore, determining the caliber of the nerve may be helpful in predicting the outcome of CI [28]. In one previous study, even when the cochlear nerve was thin, it still effectively transmitted impulses to allow hearing; therefore, MRI depiction of CND is considered a relative contraindication for CI [29]. However, because CT and MRI are limited, patients with CND in the present study were further assessed by electrical auditory brainstem response testing and behavioral audiometry to check for residual hearing. Patients with a response received a CI. Thus, electrophysiological testing, such as the PST or intracochlear, electrically evoked auditory brainstem response, might have prognostic value in predicting the outcome of CI in patients with a narrow BCNC. Therefore, clinicians need to determine the anatomical status of the cochlear nerve by evaluating the BCNC width using TBCT or MRI. They must also (1) accurately analyze the implications of preoperative electrophysiological evaluation in patients with narrow IACs or BCNC and (2) correlate these findings with the actual anatomical status of the cochlear nerve.

5. Conclusions

In CI patients, a narrow BCNC on TBCT is strongly correlated with CND and poor CI outcomes of CI. Therefore, ear, nose, and throat doctors should determine the BCNC width on preoperative CT, keeping in mind its clinical significance. Because the width of the bony cochlear nerve canal is positively correlated with long-term, post-CI speech performance, we can predict the hearing outcomes of CI by preoperatively evaluating the BCNC width.

Conflicts of Interest

The authors declare that there are no conflicts of interest regarding the publication of this article.

Authors' Contributions

Juyong Chung and Jeong Hun Jang contributed equally to this work.

Acknowledgments

This research was supported by Basic Science Research Program through the National Research Foundation of Korea (NRF) funded by the Ministry of Education (Grant no. NRF-2017R1D1A3B03034486 to Juyong Chung).

References

[1] J. H. Jang, J. H. Kim, J. C. Yoo et al., "Implication of bony cochlear nerve canal on hearing in patients with congenital unilateral sensorineural hearing loss," *Audiology & Neuro-Otology*, vol. 17, no. 5, pp. 282–289, 2012.

[2] C. Stjernholm and C. Muren, "Dimensions of the cochlear nerve canal: A radioanatomic investigation," *Acta Oto-Laryngologica*, vol. 122, no. 1, pp. 43–48, 2002.

[3] G. M. Fatterpekar, S. K. Mukherji, J. Alley, Y. Lin, and M. Castillo, "Hypoplasia of the bony canal for the cochlear nerve in patients with congenital sensorineural hearing loss: Initial observations," *Radiology*, vol. 215, no. 1, pp. 243–246, 2000.

[4] M. Miyasaka, S. Nosaka, N. Morimoto, H. Taiji, and H. Masaki, "CT and MR imaging for pediatric cochlear implantation: emphasis on the relationship between the cochlear nerve canal and the cochlear nerve," *Pediatric Radiology*, vol. 40, no. 9, pp. 1509–1516, 2010.

[5] J. P. Simons, D. L. Mandell, and E. M. Arjmand, "Computed tomography and magnetic resonance imaging in pediatric unilateral and asymmetric sensorineural hearing loss," *Archives of Otolaryngology—Head and Neck Surgery*, vol. 132, no. 2, pp. 186–192, 2006.

[6] L. Sennaroglu, "Cochlear implantation in inner ear malformations—a review article," *Cochlear Implants International*, vol. 11, no. 1, pp. 4–41, 2010.

[7] G. M. Fatterpekar, S. K. Mukherji, Y. Lin, J. G. Alley, J. A. Stone, and M. Castillo, "Normal canals at the fundus of the internal auditory canal: CT evaluation," *Journal of Computer Assisted Tomography*, vol. 23, no. 5, pp. 776–780, 1999.

[8] J. W. Casselman, F. E. Offeciers, P. J. Govaerts et al., "Aplasia and hypoplasia of the vestibulocochlear nerve: diagnosis with MR imaging," *Radiology*, vol. 202, no. 3, pp. 773–781, 1997.

[9] H.-S. Kim, D.-I. Kim, I.-H. Chung, W.-S. Lee, and K.-Y. Kim, "Topographical relationship of the facial and vestibulocochlear nerves in the subarachnoid space and internal auditory canal," *American Journal of Neuroradiology*, vol. 19, no. 6, pp. 1155–1161, 1998.

[10] S. Komatsubara, A. Haruta, Y. Nagano, and T. Kodama, "Evaluation of cochlear nerve imaging in severe congenital sensorineural hearing loss," *ORL*, vol. 69, no. 3, pp. 198–202, 2007.

[11] T. Kono, "Computed tomographic features of the bony canal of the cochlear nerve in pediatric patients with unilateral sensorineural hearing loss," *Radiation Medicine - Medical Imaging and Radiation Oncology*, vol. 26, no. 3, pp. 115–119, 2008.

[12] W. Pagarkar, R. Gunny, D. E. Saunders, W. Yung, and K. Rajput, "The bony cochlear nerve canal in children with absent or hypoplastic cochlear nerves," *International Journal of Pediatric Otorhinolaryngology*, vol. 75, no. 6, pp. 764–773, 2011.

[13] N. Teissier, T. Van Den Abbeele, G. Sebag, and M. Elmaleh-Berges, "Computed tomography measurements of the normal and the pathologic cochlea in children," *Pediatric Radiology*, vol. 40, no. 3, pp. 275–283, 2010.

[14] E. G. Nelson and R. Hinojosa, "Aplasia of the cochlear nerve: A temporal bone study," *Otology & Neurotology*, vol. 22, no. 6, pp. 790–795, 2001.

[15] O. F. Adunka, P. A. Roush, H. F. B. Teagle et al., "Internal auditory canal morphology in children with cochlear nerve deficiency," *Otology & Neurotology*, vol. 27, no. 6, pp. 793–801, 2006.

[16] E. E. Russo and S. Manolidis, "Cochlear nerve size evaluation in children with sensorineural hearing loss by high-resolution magnetic resonance imaging," *American Journal of Otolaryngology - Head and Neck Medicine and Surgery*, vol. 27, no. 3, pp. 166–172, 2006.

[17] B. C. Papsin, "Cochlear implantation in children with anomalous cochleovestibular anatomy," *The Laryngoscope*, vol. 115, suppl. 106, no. 1, pp. 1–26, 2005.

[18] O. F. Adunka, V. Jewells, and C. A. Buchman, "Value of computed tomography in the evaluation of children with cochlear nerve deficiency," *Otology & Neurotology*, vol. 28, no. 5, pp. 597–604, 2007.

[19] C. A. Buchman, H. F. B. Teagle, P. A. Roush et al., "Cochlear implantation in children with labyrinthine anomalies and cochlear nerve deficiency: Implications for auditory brainstem implantation," *The Laryngoscope*, vol. 121, no. 9, pp. 1979–1988, 2011.

[20] D. Zanetti, M. Guida, M. G. Barezzani et al., "Favorable outcome of cochlear implant in VIIIth nerve deficiency," *Otology & Neurotology*, vol. 27, no. 6, pp. 815–823, 2006.

[21] J. Black, L. Hickson, B. Black, and C. Perry, "Prognostic indicators in paediatric cochlear implant surgery: A systematic literature review," *Cochlear Implants International*, vol. 12, no. 2, pp. 62–77, 2014.

[22] D. H. Kang, M. Lee, K.-Y. Lee, S. H. Lee, and J. H. Jang, "Prediction of cochlear implant outcomes in patients with prelingual deafness," *Clinical and Experimental Otorhinolaryngology*, vol. 9, no. 3, pp. 220–225, 2016.

[23] J. Phan, D. M. Houston, C. Ruffin, J. Ting, and R. F. Holt, "Factors affecting speech discrimination in children with cochlear implants: Evidence from early-implanted infants," *Journal of the American Academy of Audiology*, vol. 27, no. 6, pp. 480–488, 2016.

[24] J. R. McPhee and T. R. Van de Water, "Epithelial-mesenchymal tissue interactions guiding otic capsule formation: The role of the otocyst," *Journal of Embryology and Experimental Morphology (JEEM)*, vol. 97, pp. 1–24, 1986.

[25] P. P. Lefebvre, P. Leprince, T. Weber, J.-M. Rigo, P. Delree, and G. Moonen, "Neuronotrophic effect of developing otic vesicle on cochleo-vestibular neurons: evidence for nerve growth factor involvement," *Brain Research*, vol. 507, no. 2, pp. 254–260, 1990.

[26] L. Sennaroglu, I. Saatci, A. Aralasmak, B. Gursel, and E. Turan, "Magnetic resonance imaging versus computed tomography in pre-operative evaluation of cochlear implant candidates with congenital hearing loss," *The Journal of Laryngology & Otology*, vol. 116, no. 10, pp. 804–810, 2002.

[27] H. Spoendlin, "Retrograde degeneration of the cochlear nerve," *Acta Oto-Laryngologica*, vol. 79, no. 3–6, pp. 266–275, 1975.

[28] J. B. Nadol Jr. and W.-Z. Xu, "Diameter of the cochlear nerve in deaf humans: Implications for cochlear implantation," *Annals of Otology, Rhinology & Laryngology*, vol. 101, no. 12, pp. 988–993, 1992.

[29] S. Gupta, S. Maheshwari, M. Kirtane, and N. Shrivastav, "Pictorial review of MRI/CT Scan in congenital temporal bone anomalies, in patients for cochlear implant," *Indian Journal of Radiology and Imaging*, vol. 19, no. 2, pp. 99–106, 2009.

Hindawi
BioMed Research International
Volume 2018, Article ID 5058729, 11 pages
https://doi.org/10.1155/2018/5058729

Research Article

Effect of Lead on Human Middle Ear Epithelial Cells

Shin Hye Kim, Sun Hwa Shin, Yoon Young Go, Sung-Won Chae, and Jae-Jun Song

Department of Otorhinolaryngology-Head and Neck Surgery, Korea University Medical Center, Korea University College of Medicine, Seoul, Republic of Korea

Correspondence should be addressed to Jae-Jun Song; jjsong23@gmail.com

Received 28 August 2017; Revised 19 December 2017; Accepted 8 January 2018; Published 6 March 2018

Academic Editor: Jeong-Han Lee

Lead is a ubiquitous metal in the environment, but no studies have examined lead toxicity on the middle ear. Here, we investigated lead toxicity and its mechanism in human middle ear epithelial cells (HMEECs). Moreover, we investigated the protective effects of amniotic membrane extract (AME) and chorionic membrane extract (CME) against lead toxicity in HMEECs. Cell viability was analyzed using the cell counting kit, and reactive oxygen species (ROS) activity was measured using a cellular ROS detection kit. After lead(II) acetate trihydrate treatment, mRNA levels of various genes were assessed by semiquantitative real-time polymerase chain reaction. Following treatment with AME or CME after lead exposure, the changes in cell viability, ROS activity, and gene expression were analyzed. Exposure to >100 μg/mL of lead(II) acetate trihydrate caused a significant decrease in cell viability and increased ROS production in HMEECs. Lead exposure significantly increased the mRNA expression of genes encoding inflammatory cytokines and mucins. Administration of AME or CME restored cell viability, reduced ROS activity, and ameliorated mRNA levels. Our findings suggest that environmental lead exposure is related to the development of otitis media, and AME and CME may have antioxidative and anti-inflammatory effects against lead toxicity.

1. Introduction

Otitis media (OM) is a group of inflammatory diseases of the middle ear. The presence of inflammatory cytokines in middle ear fluid samples obtained from children with OM has been reported [1, 2]. OM is a common inflammatory disease among children, and more than 50% of children experience one or more episodes of OM by the age of three years [3]. Fluid and mucus trapped in the middle ear by OM may lead to conductive hearing loss and delays in speech development and cognitive abilities [4]. Thus, the identification and control of potentially preventable risk factors for OM, such as air pollution exposure, have significant implications for children's healthcare.

Lead is a common and versatile metal that is widely distributed in the environment, leading to human exposure. However, lead exposure through environmental (canned food, water pipes, soil, paint, plastics, household dust, air, etc.) or occupational routes can cause lead poisoning [5]. Particularly, in developing countries, lead is present in particulate form in the air and can be inhaled along with other heavy metals [6].

The major mechanism of lead toxicity is thought to be increased oxidative stress [7]. Lead induces an imbalance between the production of free radicals and detoxification of reactive intermediates or repair of the resulting damage. Oxidative stress occurs through two simultaneous pathways: generation of reactive oxygen species (ROS) and depletion of antioxidant reserves [8]. Ionic mechanisms and apoptosis have also been suggested as mechanisms of lead toxicity [9]. Lead can be substituted for other bivalent cations such as Ca^{2+}, Mg^{2+}, and Fe^{2+} as well as monovalent cations such as Na^{+}, affecting various fundamental physiological processes [9]. Although lead toxicity does not occur through a single unifying mechanism, its ability to substitute for Ca^{2+} is a common factor in its toxicity [10]. Lead has been reported to induce activation of several cellular and molecular processes, such as apoptosis in cancer cell models and rats [11, 12].

Lead toxicity via ROS generation, ionic mechanism, and apoptosis has been demonstrated using *in vitro* and *in vivo* experimental models. However, no studies have examined the effects of this heavy metal on the middle ear. Therefore, this study evaluated the effects and mechanism of lead

toxicity on human middle ear epithelial cells (HMEECs). In a previous study, we showed that amniotic membrane extract (AME) and chorionic membrane extract (CME) have anti-inflammatory effects on HMEECs; therefore, we evaluated the protective effect of AME and CME on lead toxicity [13].

2. Materials and Methods

2.1. Cell Culture. HMEECs (kindly provided by Dr. David J. Lim, House Ear Institutes, Los Angeles, CA, USA) established using human papillomavirus E6/E7 genes for the study of normal cell biology and pathological processes associated with development of OM were used. HMEECs were maintained in a mixture of Dulbecco's modified Eagle's medium (Invitrogen, Carlsbad, CA, USA) and bronchial epithelial basal medium (Lonza, Basel, Switzerland) (1 : 1) [14] and kept in an incubator with a humidified atmosphere at 37°C containing 95% air and 5% CO_2. The growth medium was changed every third or fourth day. The doubling time of HMEECs is approximately 3 days, and cells were used for subsequent studies after 6 days. After approximately 1 week, the cells were stimulated with 10, 50, or 100 μg/mL lead(II) acetate trihydrate (Sigma, St. Louis, MO, USA) suspended in phosphate-buffered saline (PBS) for 24 h. As a control group, HMEECs were treated with only PBS without lead(II) acetate trihydrate.

2.2. Cell Viability Assay. To analyze the viability of HMEECs, a cell viability assay was performed using a cell counting kit (CCK-8, Dojindo Laboratories, Kumamoto, Japan). HMEECs were seeded in 96-well plates, with each well containing 1×10^4 cells. The cells were treated with 0, 6.25, 12.5, 25, 50, 100, 200, 300, 400, 500, 600, 700, or 800 μg/mL of lead(II) acetate trihydrate on the following day. The cells were washed twice with PBS, and 10% CCK-8 solution was added to each well after 24 h. The plates were incubated for 2 h at 37°C, and the contents of the plates were mixed at room temperature (20–25°C) for 5 min using a shaker. The optical density was measured at 450 nm using a microplate reader (Spectra Max plus 384, Molecular Devices, Sunnyvale, CA, USA). The results were obtained from three repeated experiments using triplicate samples.

2.3. Cell Apoptosis Assay. After exposure to lead(II) acetate trihydrate for 24 h, apoptotic cells were detected in real-time using a caspase-3 detection kit (NucView™ 488 Caspase-3, Cat Number 4440, Biotium, Inc., Fremont, CA, USA). Following cell seeding, plates were warmed to 37°C for 30 min and then scanned using an IncuCyte Zoom system (Essen BioScience, Ann Arbor, MI, USA).

2.4. ROS Activity Assays. HMEECs (1.5×10^4) were treated with lead(II) acetate trihydrate for 24 h. ROS activity in the cells was quantified using a 2′,7′-dichlorofluorescin diacetate (DCFDA) cellular ROS detection assay kit (Abcam, Cambridge, UK). Briefly, the cells were washed twice with PBS and then incubated with 100 μL DCFDA in culture medium at 37°C for 30 min. The cells were washed twice with PBS and analyzed using an IncuCyte Zoom system (Essen Bioscience). As a positive control to assess the ROS activity, 50 μg/mL tert-butyl hydrogen peroxide (TBHP) was used.

2.5. Real-Time Reverse Transcriptase Polymerase Chain Reaction. *TNF-α* and *COX-2* are inflammatory cytokines genes related to the OM [15]. *MUC5AC* and *MUC5B* are mucins genes, and they reflect the mucins production and OM induction [16]. *ENaC-α*, *ENaC-β*, and *ENaC-γ* are genes encoding epithelial sodium channels and they reflect the mucociliary transport in the middle ear mucosa [17]. *AQP-4* is gene of aquaporin in middle ear mucosa and it reflects the homeostasis of the middle ear cavity [18]. To quantify the expression of *TNF-α*, *COX-2*, *MUC5AC*, *MUC5B*, *ENaC-α*, *ENaC-β*, *ENaC-γ*, and *AQP-4* in HMEECs, real-time polymerase chain reaction (RT-PCR) was performed. After exposure to lead, RNA was extracted from HMEECs using TRIzol, and reverse transcription was performed using a cDNA synthesis kit (Takara Bio, Inc., Shiga, Japan).

RT-PCR was performed using an ABI Prism 7300 real-time PCR system (Applied Biosystems, Foster City, CA, USA). Each reaction mixture contained 10 μL of LightCycler 480SYBR Green I Master (Roche, Mannheim, Germany), 1 μL of cDNA, and 5 pmol each of sense and antisense primer in a final volume of 20 μL. Reaction mixtures were incubated at 95°C for 5 min to activate the FastStart Taq DNA Polymerase. This was followed by amplification for 45 cycles (one cycle: 15 s at 95°C, 30 s at 60°C, and 30 s at 72°C). The data were analyzed using LightCycler 480 software 1.5 (Roche). Results were obtained from three repeated experiments using triplicate samples.

2.6. Effect of Amniotic Membrane Extract and Chorionic Membrane Extract on Lead Exposure. Human amniotic and chorionic membranes are known to have anti-inflammatory effects [19]. Amniotic and chorionic membranes were obtained from the placenta of a pregnant woman who delivered at our tertiary center. The study was approved by the institutional review board of Korea University Guro Hospital (KUGH14239-002), and all participants provided written informed consent. The amniotic and chorionic membranes were washed with PBS. After homogenization and sonication of the membranes, AME and CME were obtained from the supernatant via three rounds of centrifugation at 13000 rpm for 30 min. To examine the protective effect of AME and CME on lead toxicity, the changes in cell viability, ROS activity, and gene expression after simultaneous treatment with AME and CME in lead-treated HMEECs were analyzed.

2.7. Statistical Analysis. All data are expressed as means ± standard deviations. Statistical analyses were performed using SPSS ver. 12.0 (SPSS, Inc., Chicago, IL, USA). One-way analysis of variance (ANOVA) was used to determine significant differences between the control and experimental groups at each time or dose point. When significant differences were identified by ANOVA, Scheffe's F-test was used to correct for multiple comparisons. A p value < 0.05 was considered to indicate a statistically significant difference.

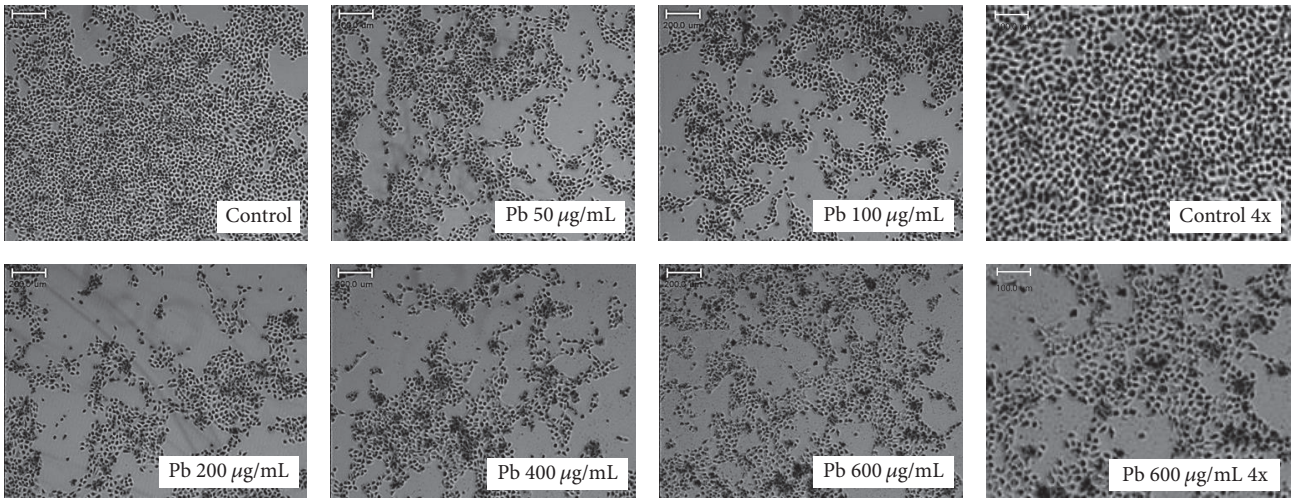

Figure 1: Cell morphology of human middle ear epithelial cells (HMEECs) following exposure to lead for 24 h. As a control group, HMEECs were treated with only PBS without lead(II) acetate trihydrate: administration of lead(II) acetate trihydrate resulted in reduced cell size and cell detachment from the Petri dishes.

3. Results

3.1. Lead Altered the Morphology and Induced Apoptosis of HMEECs. The morphology of HMEECs was altered following exposure to lead(II) acetate trihydrate (Figure 1). The nuclei of control cells were round and homogeneously stained. Addition of lead(II) acetate trihydrate resulted in reduced cell size and cell detachment from the Petri dishes. Apoptotic cells were detected by fluorescence, and the numbers of apoptotic cells increased with increasing concentrations of the lead(II) acetate trihydrate (Figure 2).

3.2. Lead Reduced the Cell Viability of HMEECs. Cell viability assays (CCK-8) showed that exposure to more than 100 μM of lead(II) acetate trihydrate for 24 h significantly decreased HMEECs viability compared to control cells (Figure 3).

3.3. Lead Increased ROS Production in HMEECs. Increased ROS activity was detected in cells exposed to 50–300 μg/mL of lead(II) acetate trihydrate compared to control cells (Figure 4). However, ROS activity was decreased in cells exposed to >400 μg/mL lead(II) acetate trihydrate compared to control cells, perhaps because of cell death caused by the high concentration of lead.

3.4. Lead Altered Gene Expression in HMEECs. When cells were stimulated with >50 and >100 μg/mL lead(II) acetate trihydrate for 24 h, gene expression of *TNF-α* and *COX-2* was significantly increased in HMEECs, respectively ($p < 0.05$, Figure 5(a)). Gene expression of *MUC5AC* and *MUC5B* in HMEECs significantly increased following stimulation with >100 and >200 μg/mL of lead(II) acetate trihydrate for 24 h, respectively ($p < 0.05$, Figure 5(b)). Gene expression of *ENaC-α*, *ENaC-β*, and *ENaC-γ* significantly decreased when cells were stimulated with >200, >50, and >50 μg/mL of lead(II) acetate trihydrate for 24 h, respectively ($p < 0.05$, Figure 5(c)). Gene expression of *AQP-4* significantly increased when cells were stimulated with 400 μg/mL lead(II) acetate trihydrate for 24 h ($p < 0.05$, Figure 5(d)).

3.5. Amniotic and Chorionic Membrane Extracts Reduced Lead Toxicity. HMEECs were decreased in size, and nuclei were condensed following exposure to 600 μg/mL lead(II) acetate trihydrate; however, the morphology was recovered by treatment with AME or CME (Figure 6). Addition of AME or CME to 600 μg/mL lead(II) acetate trihydrate also decreased the number of apoptotic cells (Figure 7). The number of HMEECs was significantly reduced by 600 μg/mL lead(II) acetate trihydrate; however, the negative effect of lead on the cell viability of HMEECs was significantly reduced by administration of 100 and 200 μg/mL AME or CME (Figure 8). ROS activity was increased by administration of 600 μg/mL lead(II) acetate trihydrate; however, administration of 100 and 200 μg/mL AME or CME decreased ROS activity (Figure 9).

3.6. Amniotic and Chorionic Membrane Extracts Recovered Normal Gene Expression in HMEECs following Exposure to Lead. The increased expression of *TNF-α* and *COX-2* following administration of 600 μg/mL lead(II) acetate trihydrate was decreased following administration of AME and CME (Figure 10(a)). The increased expression of *MUC5AC* and *MUC5B* following exposure to 600 μg/mL lead(II) acetate trihydrate was also decreased following administration of AME and CME (Figure 10(b)). The decreased expression of *ENaC-α*, *ENaC-β*, and *ENaC-γ* following 600 μg/mL lead(II) acetate trihydrate administration was also recovered by AME

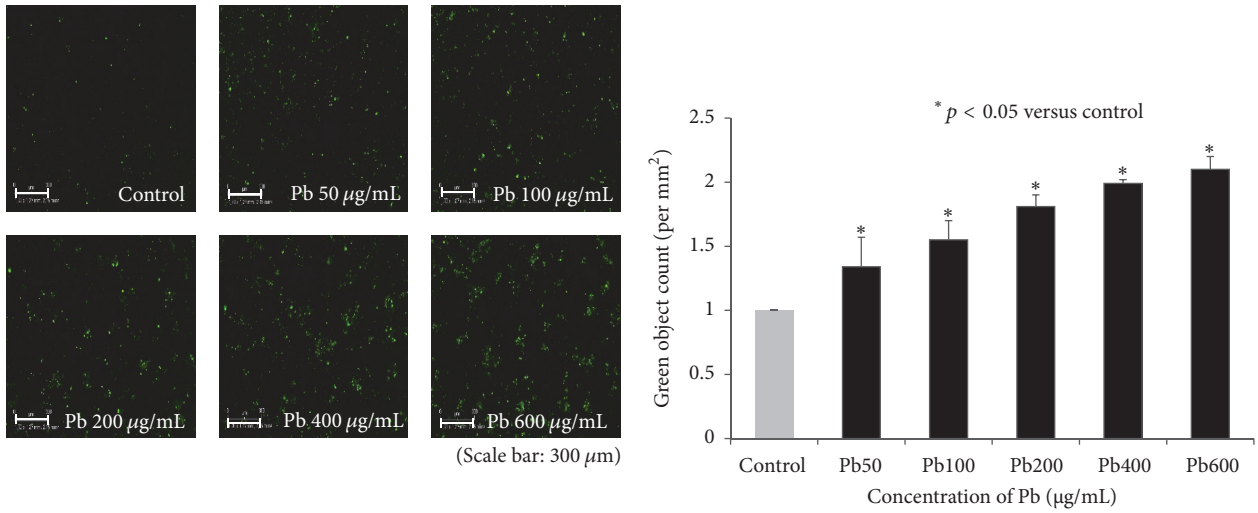

Figure 2: Apoptosis of human middle ear epithelial cells (HMEECs) following exposure to lead for 24 h. Apoptotic cells were detected by fluorescence using an IncuCyte Zoom system: the numbers of apoptotic cells increased with increasing concentration of lead(II) acetate trihydrate. Error bars indicate the standard error of the mean (SEM).

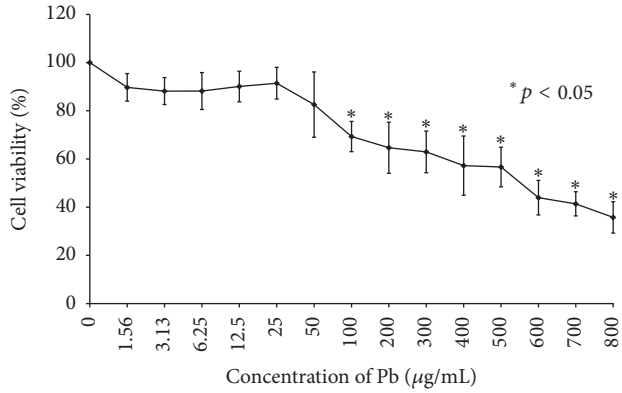

Figure 3: Cell viability of human middle ear epithelial cells (HMEECs) following exposure to lead: exposure to more than 100 μg/mL of lead(II) acetate trihydrate for 24 h significantly decreased HMEECs viability as compared to control cells. Error bars indicate the standard error of the mean (SEM).

and CME (Figure 10(c)). The increased expression of *AQP-4* following 600 μg/mL lead(II) acetate trihydrate administration was decreased following administration of AME and CME (Figure 10(d)).

4. Discussion

Lead is an insidiously hazardous material that has the potential to cause irreversible negative health effects. Lead is known to interfere with numerous physiological functions, primarily affecting the central nervous, hematopoietic, hepatic, and renal systems [7, 20]. Lead is present in the form of airborne particulate matter, along with other heavy metals. We predicted that lead, similar to other air pollutants or smoke, can enter the middle ear space through the Eustachian tubes or via the systemic circulation. The potential for lead exposure to have adverse effects is heightened in children for three reasons: young children often place objects in their mouths, resulting in ingestion of dust and soil; intake of lead per unit of body weight is higher for children than for adults; and young children are undergoing rapid development and are consequently more vulnerable than adults to lead toxicity [21–23].

Lead persists in the environment as it is a nonbiodegradable material. Environmental exposure to lead became relatively high in the latter part of the 20th century, and concerted efforts were required to reduce lead exposure. In the late 1970s, the median blood lead level of US preschool children was 15 μg/dL, and 88% of children had a level exceeding 10 μg/dL [24]. Based on the National Health and Nutrition Examination Survey (NHANES) (1991–1994, USA), the mean blood lead level among American children aged 1–5 years was 2.7 μg/dL, and 4.4% of these children (890,000

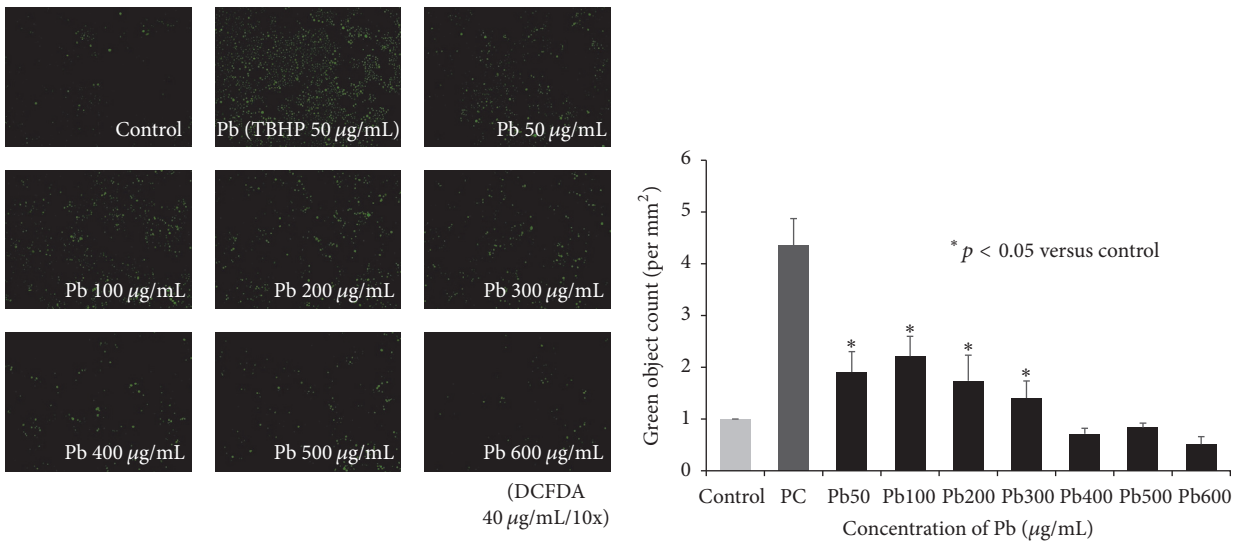

Figure 4: Reactive oxygen species (ROS) activity of human middle ear epithelial cells (HMEECs) following exposure to lead. As a positive control, 50 μg/mL tert-butyl hydrogen peroxide (TBHP) was used: ROS activity was increased in cells exposed to 50–300 μg/mL of lead(II) acetate trihydrate compared to control cells, but the ROS activity was decreased in cells exposed to >400 μg/mL lead(II) acetate trihydrate compared to control cells. Error bars indicate the standard error of the mean (SEM).

in the USA population) had elevated blood lead levels [25]. In humans with chronic exposure of lead containing substances, immune, reproductive, and cardiovascular systems are adversely affected at blood levels of 10 μg/dL and even lower [26]. Children stratified into the low-lead group (lead < 10 μg/dL) were reported to have a lower relative risk of respiratory illnesses and OM than those with lead ≥ 10 μg/dL [27].

Studies on lead toxicity have reported that the presence of lead in the body induces toxicological manifestations through various cellular, intracellular, and molecular mechanisms. Oxidative stress has been reported as a major mechanism of lead toxicity. Under the influence of lead, the onset of oxidative stress occurs via two distinct but simultaneously operating pathways: generation of ROS, such as hydroperoxides ($HO2^{\bullet}$) and singlet oxygen and hydrogen peroxide (H_2O_2), and depletion of antioxidant reserves [14]. The ionic mechanism of lead toxicity mainly operates because lead can substitute for other bivalent cations such as Ca^{2+}, Mg^{2+}, and Fe^{2+} as well as monovalent cations such as Na^{+} (although bivalent cations are more readily substituted), affecting various fundamental physiological processes [19].

To investigate the mechanism of lead toxicity, considering the HMEECs with short-term (24 h) exposure of lead(II) acetate trihydrate, this *in vitro* study used higher concentration of lead (e.g., 100 μg/mL: 1000 times for 10 μg/dL, *in vivo* criteria). We demonstrated that lead decreased the cell viability of HMEECs and increased ROS production. Lead also induced inflammatory mucins production. Inflammatory cytokines and mucins secretion play important roles in the development of OM. Inflammatory cytokines, including COX-2, TNF-α, NF-κB, IL-1, IL-6, and IL-8, play a critical role in the initiation of mucosal changes, inflammatory response in the middle ear, and mucins secretion [15, 16]. Increased expression of genes encoding inflammatory cytokines and mucins has been detected in cigarette smoke-, diesel-, cadmium-, and Asian sand dust-induced OM [28–31]. In the present study, lead caused increased gene expression of inflammatory cytokines (*TNF-α* and *COX-2*) and mucins (*MUC5AC* and *MUC5B*). Lead reduced the expression of genes encoding for epithelial sodium channels (*ENaC-α*, *ENaC-β*, and *ENaC-γ*) and consequently deteriorated mucociliary transport in the middle ear mucosa. Lead also induced gene expression of aquaporin *(AQP-4)* in the middle ear mucosa and consequently dysregulated the homeostasis of the middle ear cavity. Later, *in vivo* study confirming the concentration of lead inducing the toxicity will be needed.

The amniotic and chorionic membranes, located in the inner side of the placenta and formed by cubical cells and an inner mesodermal tissue, have been shown to have antiapoptotic, antiangiogenic, and anti-inflammatory effects on epithelial cells [32, 33]. The mesenchymal stem cells obtained from mesoderm of human amniotic membrane possess immunosuppressive functions through soluble factors such as prostanoids and proteins [34]. AME, an extract of the human amniotic membrane, has also been shown to have anti-inflammatory effects. From the experiment using human corneal epithelial cells, homogenized human AME less than 3 kDa had a greater capacity to decrease the inflammation and secretion of IL-6 and IL-8 [35]. Human AME has been proven to contain human neutrophil peptides, lysozyme, LL-37 (C-terminal part of the only human cathelicidin), bactericidal/permeability-increasing protein, calprotectin, and ubiquitin, and to show anti-inflammatory effects [36, 37]. In the present study, both AME and CME showed

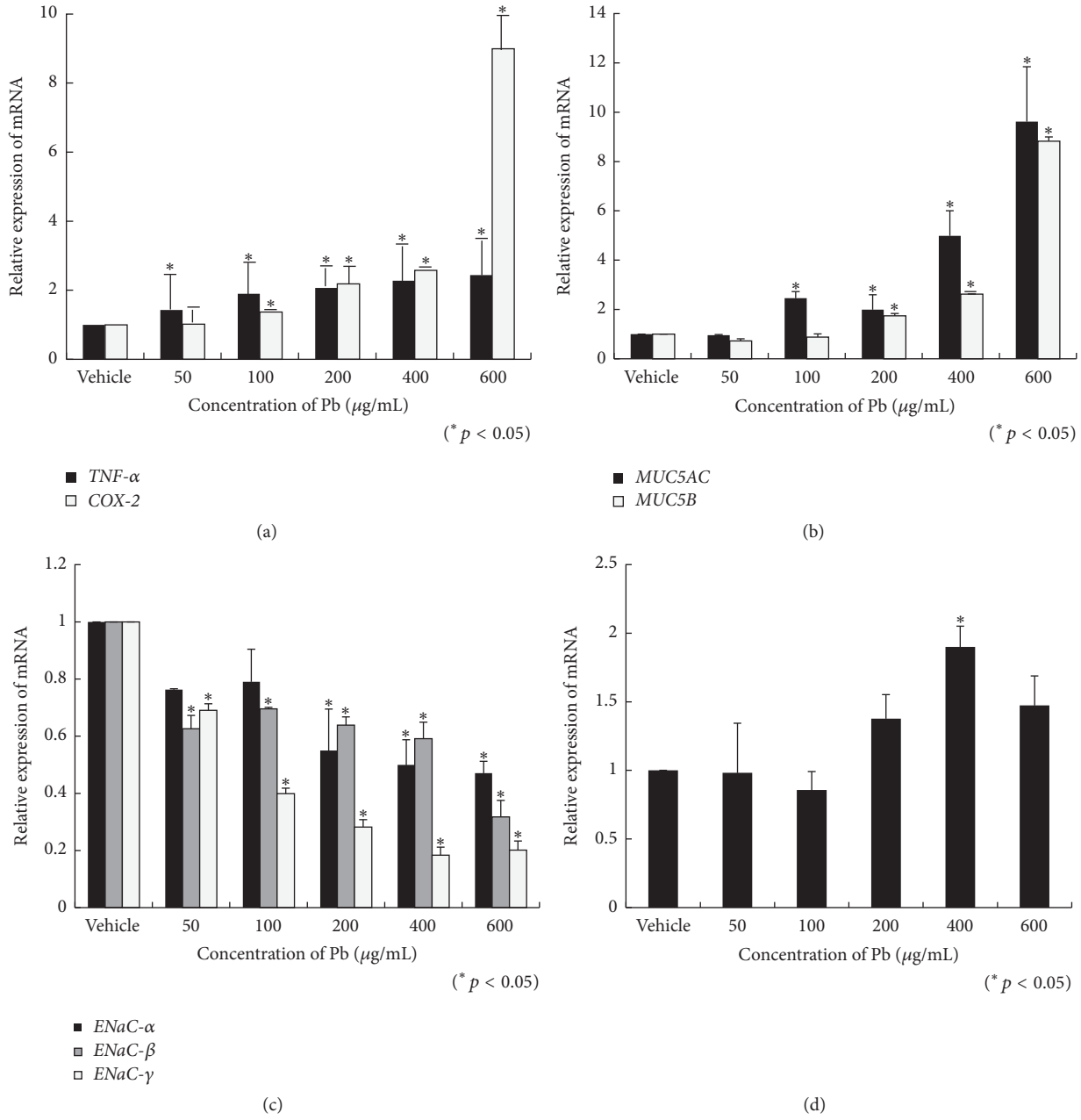

Figure 5: Alteration of gene expression in human middle ear epithelial cells (HMEECs) following exposure to lead: lead(II) acetate trihydrate concentrations of >50 and >100 μg/mL for 24 h significantly increased gene expression of *TNF-α* and *COX-2* HMEECs, respectively (a). Lead(II) acetate trihydrate at >100 and >200 μg/mL for 24 h significantly increased gene expression of *MUC5AC* and *MUC5B* in HMEECs, respectively (b). Lead(II) acetate trihydrate at >200, >50, and >50 μg/mL for 24 h significantly decreased gene expression of *ENaC-α*, *ENaC-β*, and *ENaC-γ*, respectively (c). Lead(II) acetate trihydrate at 400 μg/mL for 24 h significantly increased gene expression of *AQP-4* (d). Error bars indicate the standard error of the mean (SEM).

antiapoptotic and anti-inflammatory effects on HMEECs following exposure to lead. The first clinical use of AME was to treat epithelial defects of the cornea [38], and it is used for the treatment of ocular and dermatologic injuries and diseases. Despite the fact that therapies with AME have been used to ameliorate acute and chronic inflammatory diseases of eye and skin, the precise mechanisms by which these cells or soluble factors exert their function are yet poorly understood. Additional experiments to confirm what components of AME and CME show antiapoptotic and anti-inflammatory effects will be needed.

5. Conclusions

Our study revealed a causal relationship between environmental lead exposure and OM. One limitation of this *in vitro*

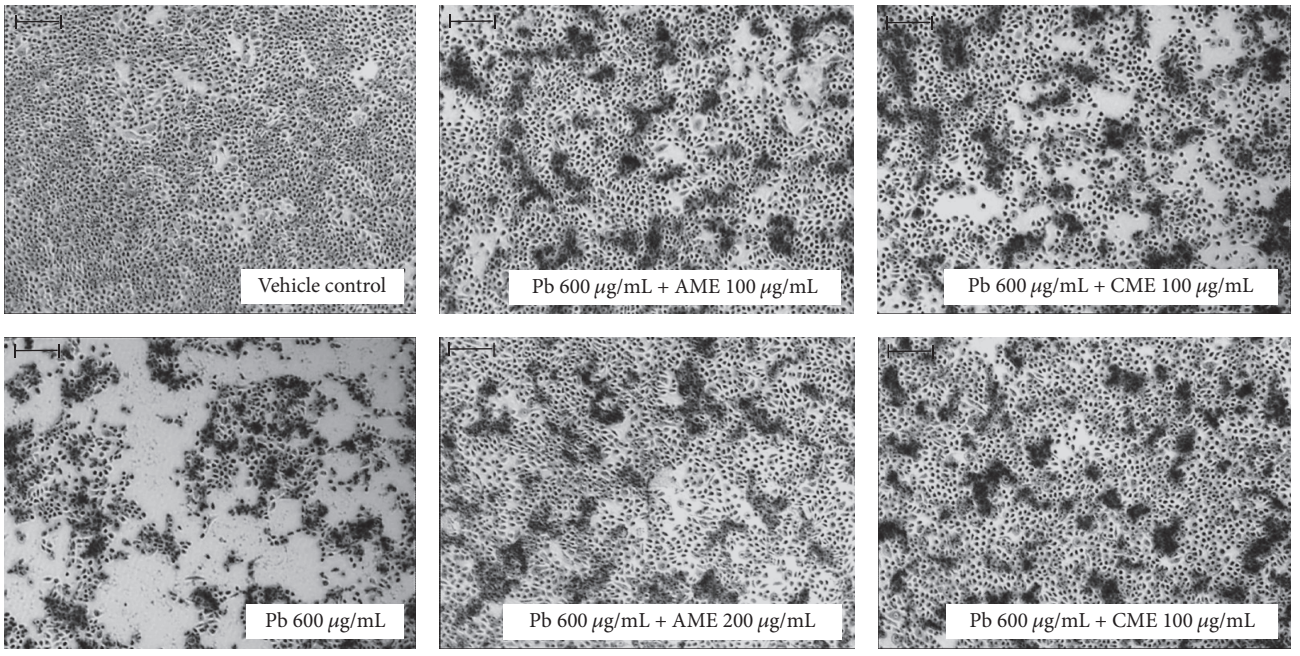

Figure 6: Effect of amniotic membrane extract (AME) and chorionic membrane extract (CME) on cell morphology in human middle ear epithelial cells (HMEECs) following exposure to lead for 24 h: reduced cell size and condensed nuclei by exposure to 600 μg/mL lead(II) acetate trihydrate was recovered by treatment with AME or CME.

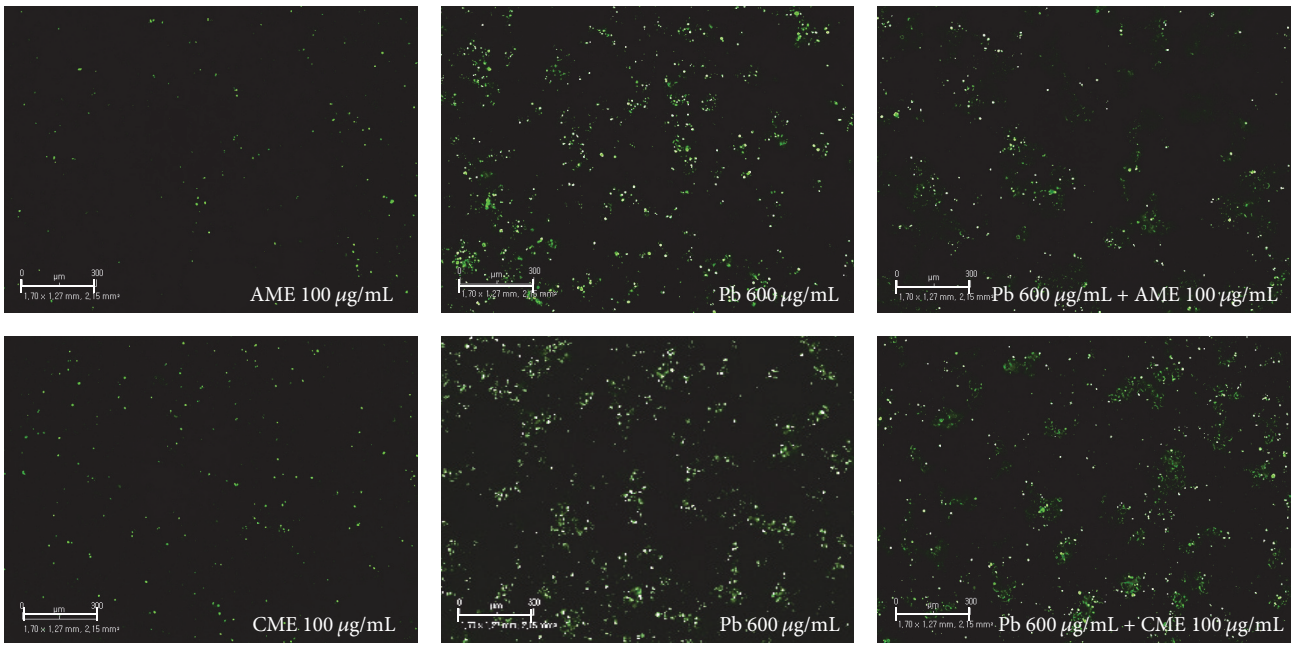

Figure 7: Effect of amniotic membrane extract (AME) and chorionic membrane extract (CME) on apoptosis in human middle ear epithelial cells (HMEECs) following exposure to lead for 24 h: addition of 100 μg/mL AME or CME to cells treated with 600 μg/mL lead(II) acetate trihydrate decreased the number of apoptotic cells.

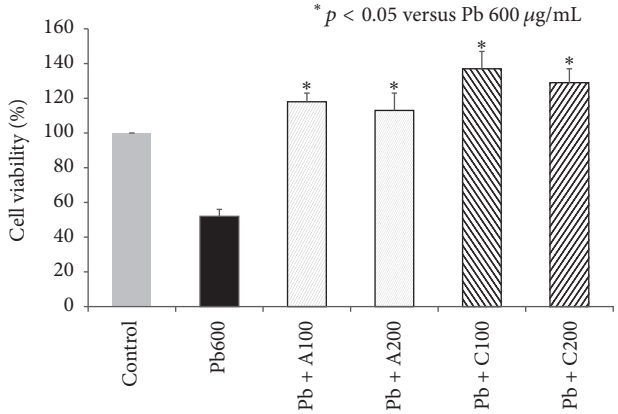

Figure 8: Effect of amniotic membrane extract (AME) and chorionic membrane extract (CME) on cell viability of human middle ear epithelial cells (HMEECs) following exposure to lead for 24 h: administration of 100 and 200 μg/mL AME or CME significantly increased cell viability of HMEECs exposed to 600 μg/mL lead(II) acetate trihydrate. Error bars indicate the standard error of the mean (SEM).

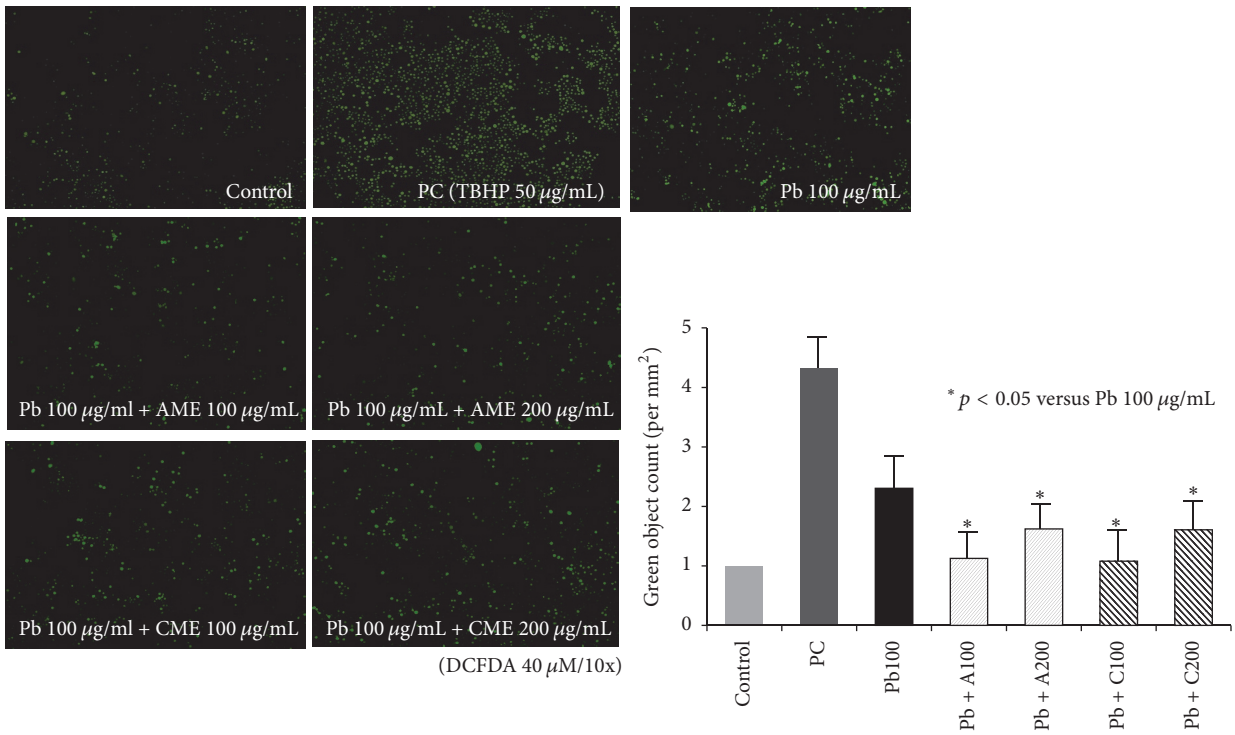

Figure 9: Effect of amniotic membrane extract (AME) and chorionic membrane extract (CME) on reactive oxygen species (ROS) activity of human middle ear epithelial cells (HMEECs) following exposure to lead. As a positive control, 50 μg/mL tert-butyl hydrogen peroxide (TBHP) was used: administration of 100 and 200 μg/mL AME or CME significantly decreased ROS activity in HMEECs exposed to 100 μg/mL lead(II) acetate trihydrate. Error bars indicate the standard error of the mean (SEM).

study is that we evaluated lead toxicity in the cell model of the human middle ear. In the future, *in vivo* studies and clinical trials are needed to confirm the toxicity of lead and protective effects of AME and CME in the middle ear.

Disclosure

An earlier version of this experiment was presented as a poster at 2017 Korean Society of Otorhinolaryngology-Head and Neck Surgery (KORL-HNS) meeting.

The funders had no role in study design, data collection and analysis, decision to publish, or preparation of the manuscript.

Conflicts of Interest

The authors declare that the research was conducted in the absence of any commercial or financial relationships that could be construed as potential conflicts of interest.

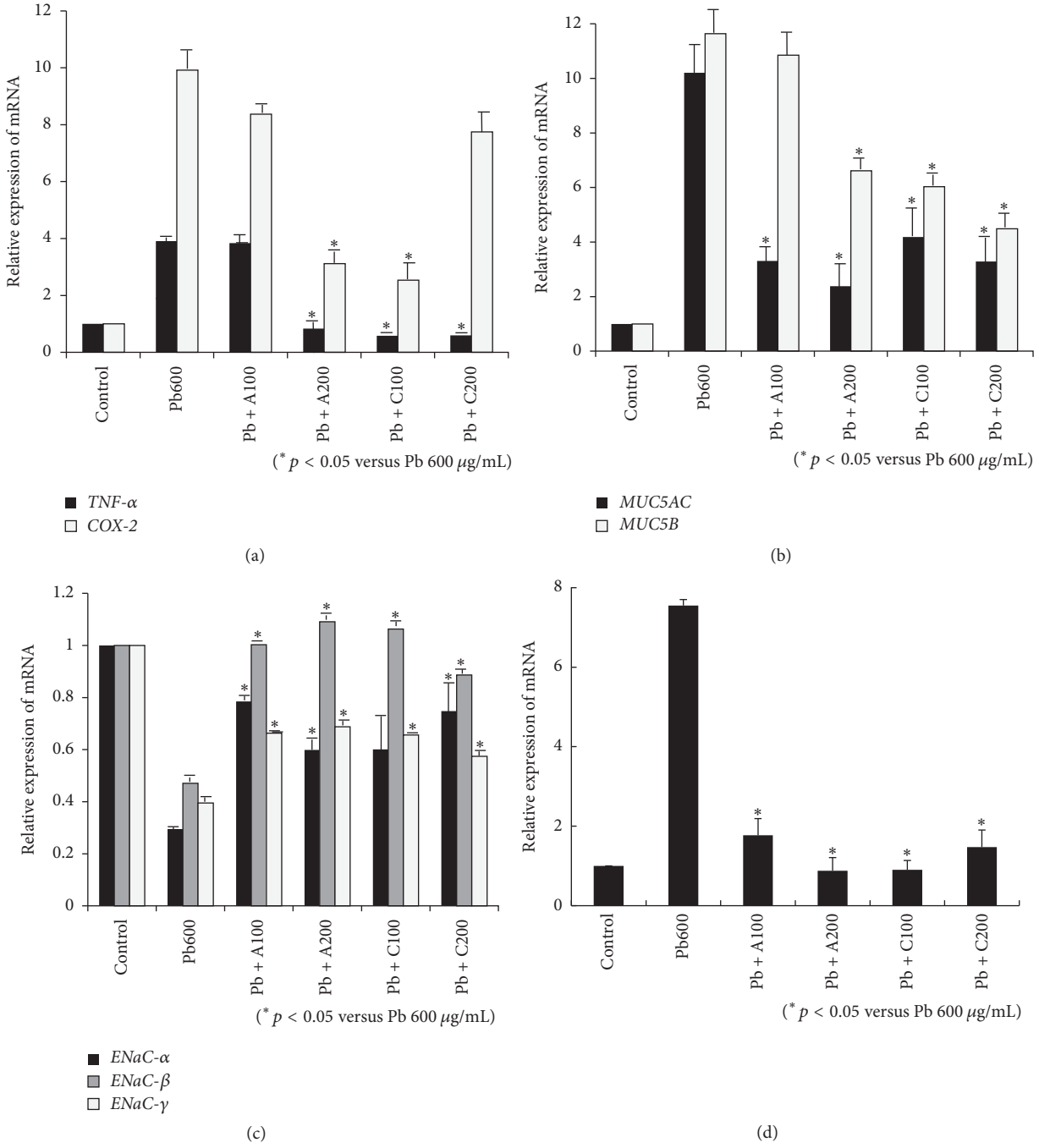

Figure 10: Effect of amniotic membrane extract (AME) and chorionic membrane extract (CME) on alterations of gene expression in human middle ear epithelial cells (HMEECs) following exposure to lead: administration of AME and CME decreased gene expression of *TNF-α* and *COX-2* (a), *MUC5AC*, *MUC5B* (b), and *AQP-4* (d) in HMEECs exposed to 600 μg/mL lead(II) acetate trihydrate. Administration of AME and CME increased gene expression of *ENaC-α*, *ENaC-β*, and *ENaC-γ* (c) in HMEECs exposed to 600 μg/mL lead(II) acetate trihydrate. Error bars indicate the standard error of the mean (SEM).

Authors' Contributions

Shin Hye Kim analyzed the results and wrote the manuscript. Sun Hwa Shin and Yoon Young Go performed the experiment. Jae-Jun Song designed this study and revised the manuscript with Sung-Won Chae. All authors read and approved the final manuscript.

Acknowledgments

This work was supported by a grant from the Korea Health Technology R&D Project through the Korea Health Industry Development Institute (KHIDI), funded by the Ministry of Health & Welfare, Republic of Korea (Grant no. HI15C2809).

References

[1] S. K. Juhn, W. J. Garvis, C. T. Le, C. J. Lees, and C. S. Kim, "Determining otitis media severity from middle ear fluid analysis," *Annals of Otology, Rhinology & Laryngology*, vol. 103, no. 5, pp. 43–45, 1994.

[2] R. F. Yellon, W. J. Doyle, T. L. Whiteside, W. F. Diven, A. R. March, and P. Fireman, "Cytokines, Immunoglobulins, and Bacterial Pathogens in Middle Ear Effusions," *Archives of Otolaryngology–Head and Neck Surgery*, vol. 121, no. 8, pp. 865–869, 1995.

[3] H. J. Hoffman, K. A. Daly, K. E. Bainbridge et al., "Panel I: Epidemiology, natural history, and risk factors," *Otolaryngology - Head and Neck Surgery (United States)*, vol. 148, no. 4, pp. E1–E25, 2013.

[4] J. O. Klein, "The burden of otitis media," *Vaccine*, vol. 19, no. 1, pp. S2–S8, 2000.

[5] M. A. Smith, "Lead in history," in *The Environmental Toxicology and Child Health*, R. Lansdown and W. Yule, Eds., pp. 7–24, Croom Helm, London, UK, 1984.

[6] X. LI, Y. ZHANG, M. TAN et al., "Atmospheric lead pollution in fine particulate matter in Shanghai, China," *Journal of Environmental Sciences*, vol. 21, no. 8, pp. 1118–1124, 2009.

[7] G. Flora, D. Gupta, and A. Tiwari, "Toxicity of lead: a review with recent updates," *Interdisciplinary Toxicology*, vol. 5, no. 2, pp. 47–58, 2012.

[8] S. J. S. Flora, "Nutritional components modify metal absorption, toxic response and chelation therapy," *Journal of Nutritional and Environmental Medicine*, vol. 12, no. 1, pp. 53–67, 2002.

[9] T. I. Lidsky and J. S. Schneider, "Lead neurotoxicity in children: basic mechanisms and clinical correlates," *Brain*, vol. 126, part 1, pp. 5–19, 2003.

[10] J. P. Bressler and G. W. Goldstein, "Mechanisms of lead neurotoxicity," *Biochemical Pharmacology*, vol. 41, no. 4, pp. 479–484, 1991.

[11] C. G. Yedjou, J. N. Milner, C. B. Howard, and P. B. Tchounwou, "Basic apoptotic mechanisms of lead toxicity in human leukemia (Hl-60) cells," *International Journal of Environmental Research and Public Health*, vol. 7, no. 5, pp. 2008–2017, 2010.

[12] L.-H. Xu, F.-F. Mu, J.-H. Zhao et al., "Lead induces apoptosis and histone hyperacetylation in rat cardiovascular tissues," *PLoS ONE*, vol. 10, no. 6, Article ID e0129091, 2015.

[13] M. K. Yadav, Y. Y. Go, S. H. Kim, S. Chae, and J. Song, "Antimicrobial and Antibiofilm Effects of Human Amniotic/Chorionic Membrane Extract on Streptococcus pneumoniae," *Frontiers in Microbiology*, vol. 8, 2017.

[14] Y.-M. Chun, S.-K. Moon, D. E. Brackmann et al., "Immortalization of normal adult human middle ear epithelial cells using a retrovirus containing the E6/E7 genes of human papillomavirus type 16," *Annals of Otology, Rhinology & Laryngology*, vol. 111, no. 6, pp. 507–517, 2002.

[15] H. Y. Lee, Y. I. Kim, J. W. Lee, J. Y. Byun, M. S. Park, and S. G. Yeo, "Decreased expression of TLR-9 and cytokines in the presence of bacteria in patients with otitis media with effusion," *Clinical and Experimental Otorhinolaryngology*, vol. 6, no. 4, pp. 195–200, 2013.

[16] J. E. Kerschner, "Mucin gene expression in human middle ear epithelium," *The Laryngoscope*, vol. 117, no. 9, pp. 1666–1676, 2007.

[17] E. J. Son, S. H. Kim, H. Y. Park et al., "Activation of epithelial sodium channel in human middle ear epithelial cells by dexamethasone," *European Journal of Pharmacology*, vol. 602, no. 2-3, pp. 383–387, 2009.

[18] L. M. Morris, J. M. DeGagne, J. B. Kempton, F. Hausman, and D. R. Trune, "Mouse middle ear ion homeostasis channels and intercellular junctions," *PLoS ONE*, vol. 7, no. 6, Article ID e39004, 2012.

[19] U. Manuelpillai, Y. Moodley, C. V. Borlongan, and O. Parolini, "Amniotic membrane and amniotic cells: Potential therapeutic tools to combat tissue inflammation and fibrosis?" *Placenta*, vol. 32, no. 4, pp. S320–S325, 2011.

[20] K. Kalia and S. J. S. Flora, "Strategies for safe and effective therapeutic measures for chronic arsenic and lead poisoning," *Journal of Occupational Health*, vol. 47, no. 1, pp. 1–21, 2005.

[21] World Health Organization, "Environmental health criteria 165: Inorganic lead," in *Proceedings of the International Program on Chemical Safety*, Geneva, Switzerland, 1995.

[22] P. Mushak, "Perspective. Defining lead as the premiere environmental health issue for children in America: Criteria and their quantitative application," *Environmental Research*, vol. 59, no. 2, pp. 281–309, 1992.

[23] S. Tong and A. J. McMichael, "The magnitude, persistence and public health significance of cognitive effects of environmental lead exposure in childhood," *Journal of Environmental Medicine*, vol. 1, no. 2, pp. 103–110, 1999.

[24] K. R. Mahaffey, J. L. Annest, J. Roberts, and R. S. Murphy, "National estimates of blood lead levels: United States, 1976-1980. Association with selected demographic and socioeconomic factors," *The New England Journal of Medicine*, vol. 307, no. 10, pp. 573–579, 1982.

[25] J. L. Pirkle, R. B. Kaufmann, D. J. Brody, T. Hickman, E. W. Gunter, and D. C. Paschal, "Exposure of the US population to lead, 1991-1994," *Environmental Health Perspectives*, vol. 106, no. 11, pp. 745–750, 1998.

[26] World Health Organization, "Childhood lead poisoning," Geneva, Switzerland, 2010.

[27] P. Mushak, *Lead and Public Health: Science, Risk and Regulation*, Elsevier, 1st edition, 2011.

[28] D. Preciado, E. Kuo, S. Ashktorab, P. Manes, and M. Rose, "Cigarette smoke activates NFκB-mediated Tnf-α release from mouse middle ear cells," *The Laryngoscope*, vol. 120, no. 12, pp. 2508–2515, 2010.

[29] J.-J. Song, J. D. Lee, B. D. Lee, S. W. Chae, and M. K. Park, "Effect of diesel exhaust particles on human middle ear epithelial cells," *International Journal of Pediatric Otorhinolaryngology*, vol. 76, no. 3, pp. 334–338, 2012.

[30] J. J. Song, J. Y. Kim, A. S. Jang et al., "Effect of cadmium on human middle ear epithelial cells," *The Journal of International Advanced Otology*, vol. 11, no. 3, pp. 183–187, 2015.

[31] J. Chang, Y. Go, M. K. Park, S.-W. Chae, S.-H. Lee, and J.-J. Song, "Asian sand dust enhances the inflammatory response and mucin gene expression in the middle ear," *Clinical and Experimental Otorhinolaryngology*, vol. 9, no. 3, pp. 198–205, 2016.

[32] A. Gupta, S. D. Kedige, and K. Jain, "Amnion and chorion membranes: potential stem cell reservoir with wide applications in periodontics," *International Journal of Biomaterials*, vol. 2015, Article ID 274082, 9 pages, 2015.

[33] C. M. Zelen, R. J. Snyder, T. E. Serena, and W. W. Li, "The use of human amnion/chorion membrane in the clinical setting for

lower extremity repair: a review," *Clinics in Podiatric Medicine and Surgery*, vol. 32, no. 1, pp. 135–146, 2015.

[34] F. S. Magaña-Guerrero, A. Domínguez-López, P. Martínez-Aboytes, B. Buentello-Volante, and Y. Garfias, "Human Amniotic Membrane Mesenchymal Stem Cells inhibit Neutrophil Extracellular Traps through TSG-6," *Scientific Reports*, vol. 7, no. 1, Article ID 12426, 2017.

[35] H.-N. Lee, R. Bernardo, G.-Y. Han et al., "Human amniotic membrane extracts have anti-inflammatory effects on damaged human corneal epithelial cells in vitro," *Journal of Hard Tissue Biology*, vol. 25, no. 3, pp. 282–287, 2016.

[36] H. Yoshio, M. Tollin, G. H. Gudmundsson et al., "Antimicrobial polypeptides of human vernix caseosa and amniotic fluid: Implications for newborn innate defense," *Pediatric Research*, vol. 53, no. 2, pp. 211–216, 2003.

[37] H. He, W. Li, S. Chen et al., "Suppression of activation and induction of apoptosis in RAW264.7 cells by amniotic membrane extract," *Investigative Ophthalmology and Visual Science*, vol. 49, pp. 4468–4475, 2008.

[38] P. Bonci, P. Bonci, and A. Lia, "Suspension made with amniotic membrane: Clinical trial," *European Journal of Ophthalmology*, vol. 15, no. 4, pp. 441–445, 2005.

Hindawi
BioMed Research International
Volume 2018, Article ID 9158187, 10 pages
https://doi.org/10.1155/2018/9158187

Research Article

Secondary Degeneration of Auditory Neurons after Topical Aminoglycoside Administration in a Gerbil Model

Jae-Hun Lee,[1,2] Min Young Lee,[1,3] Phil-Sang Chung,[1,2,3] and Jae Yun Jung[1,2,3]

[1]*College of Medicine, Dankook University, Beckman Laser Institute Korea, Cheonan, Republic of Korea*
[2]*Department of Otolaryngology-Head & Neck Surgery, College of Medicine, Dankook University, Cheonan, Republic of Korea*
[3]*Dankook University Hospital, Cheonan, Republic of Korea*

Correspondence should be addressed to Jae Yun Jung; jjkingy2k@gmail.com

Received 13 October 2017; Revised 29 December 2017; Accepted 9 January 2018; Published 1 March 2018

Academic Editor: Yong-Ho Park

Hair cells in the cochlea can be damaged by various causes. Damaged hair cells can lead to additional destruction of parts of the auditory afferent pathway sequentially, which is called secondary degeneration. Recently, researches regarding cochlear implants have been actively carried out for clinical purposes; secondary degeneration in animals is a much more practical model for identifying the prognosis of cochlear implants. However, an appropriate model for this research is not established yet. Thus, we developed a secondary degeneration model using an ototoxic drug. 35 gerbils were separated into four different groups and kanamycin was applied via various approaches. ABR was measured several times after drug administration. SGCs were also counted to identify any secondary degeneration. The results showed that outer and inner HCs were damaged in all kanamycin-treated groups. Twelve weeks after kanamycin treatment, the round window membrane injection group showed severe subject differences in hair cells and SGC damage, whereas the gelfoam group showed consistent and severe damage in hair cells and SGCs. In this study, we successfully induced secondary degeneration in hair cells in a gerbil model. This model can be used for various purposes in the hearing research area either for treatment or for preservation.

1. Introduction

Social impacts of hearing loss have increased in many aspects more than ever, since the prevalence of hearing loss surges in accordance with the aging process of our modern society. Noise, ototoxic drugs, infections, aging, and other diseases are responsible for cochlear end organ damage during our lifetimes. In many cases, the loss of cochlear hair cells is the main contributor to loss of sound perception. Cochlear hair cell damage can subsequently progress towards the proximal part of the auditory pathway including the nerve fiber, spiral ganglion cells (SGCs), and cochlear nucleus, which is also known as secondary degeneration [1]. This secondary degeneration shows various features in terms of the degree and rate of degeneration depending on etiologies of hair cell damage and species [2–6].

Specifically, this degeneration had been considered to be highly dependent on the status of the inner hair cell (IHC) [2, 7, 8]. Supporting cells, which are located under the inner hair cell, were also considered as an important factor that can contribute to the degree and time of secondary degeneration in both animals and humans [9, 10], and this was further supported by a study with transgenic mice [11].

Even after severe hearing loss, the degree of secondary degeneration on the remaining SGCs is very critical for hearing rehabilitation in the area of cochlear implant which is a cutting-edge modality for profound sensorineural hearing loss patients nowadays [12, 13]. Currently, cochlear implants rely on SGCs for electrical stimulation for coding of the processed acoustic sound, which means a higher hearing performance can be expected with a higher number of SGCs [14]. This urges the clinical modality to prevent or retard the secondary degeneration of SGCs while waiting for a cochlear implant surgery.

Aminoglycoside is a widely used class of antibiotics which also has ototoxicity that can induce permanent damage to the organ of Corti (OC) [15]. Particularly, kanamycin is more cochlear-toxic rather than vestibulotoxic [16] and has

been used in animal research for deafening [17, 18]. Several studies tracked the histological feature of the auditory afferent pathway after kanamycin deafening [19], especially when administered with furosemide [20] that also has a potential of causing hearing loss [21]. Kanamycin can be accumulated mainly in the mitochondria of HCs [22] which can result in SGC loss by affecting the neurotrophic factors [23–25].

As described above, delaying and attenuating the timing of secondary degeneration are important for hearing rehabilitation. To investigate the therapeutic methods which can delay or prevent secondary degeneration, a stable and consistent secondary degeneration model is essentially needed. For this reason, the purpose of this study is to establish a consistent secondary degeneration model by approaching different drug treatments of kanamycin.

2. Methods

2.1. Animals. Female Mongolian gerbils (40–45 g) at 6–8 weeks of age were included in the experiment and were divided into four different groups: kanamycin via percutaneous injection (KP, $N = 12$), kanamycin at round window niche soaked in gelfoam (KG, $N = 12$), kanamycin injection through the round window membrane (RWM) (KI, $N = 12$), and control ($N = 6$). For the drug administration and hearing measurements, gerbils were anesthetized with zolazepam (Zoletil, Virbac, Carros Cedex, France) and xylazine (Rompun, Bayer, Leverkusen, Germany). All procedures were approved by the Institutional Animal Care and Use Committee of Dankook University (DKU-15-006).

2.2. Drug Administration. Kanamycin (KM) sulphate was diluted in normal saline (150 mg/ml) and administered in three different ways (Figure 1). For the KP group, 50 ul of the drug solution was delivered by injection with an insulin syringe (Ultrafine Insulin Syringe, Becton Dickinson, USA) to the bulla. To improve the absorption to the RWM, the animal was laid on its contralateral side, injected, and sustained for half an hour. For both KG and KI groups, the bulla was exposed through a retroauricular skin incision. After anesthetization, furs near the bulla were removed and the skin was also incised. A small hole was made on the bulla and the RWM was exposed. A small gelfoam was placed on the RWM and 4 microliters of kanamycin solution was injected with a Hamilton syringe (Hamilton Company, Nevada, USA) for the KG group. In the case of the KI group, a small hole was made on the bulla and the tip of a cannula connected with the Hamilton syringe was fitted into the RWM after the endolymph liquid was drained. Then, 4 microliters of the KM solution was gently and slowly injected. Animals in both groups were also laid on their contralateral side for surgery for stable absorption of the drug.

2.3. Hearing Measurement. Auditory brainstem responses (ABRs) were measured to investigate the changes of hearing threshold before and after drug administration. The evoked response signal-processing system (System III; Rucker Davis Technologies, Alachua, Florida) was adopted for ABR measurement. Animals were anesthetized with zolazepam (Zoletil, Virbac, Carros Cedex, France) and xylazine (Rompun, Bayer, Leverkusen, Germany) and were placed in a soundproof chamber. Then, needle electrodes were inserted to the vertex (as response) and ventrolateral sides of both pinnae (as reference and ground). Tone stimuli with 4, 8, 12, 16, and 32 kHz were generated from 90 dB to 10 dB in 5 dB steps and average waveforms were generated from 1024 responses. Hearing thresholds were measured before and 1, 4, and 12 weeks after drug administration.

2.4. Histological Analysis and Quantification. Animals were sacrificed after 4 and 12 weeks of drug administration for the histological analysis. Cochleae were harvested and fixed in 4% paraformaldehyde for 24 hours at 4°C. After fixation, the samples were decalcified with 0.5 M ethylenediaminetetraacetic acid (EDTA) for a week. Cochleae from 6 gerbils in each group were embedded in paraffin and sectioned from the apex to the basal turn to quantify the number of SGCs at 4 and 12 weeks after drug administration. Four micrometers of sectioned samples was stained with hematoxylin and eosin (H&E).

The number of SGCs was counted using ImageJ software (http://rsb.info.nih.gov/ij/). Samples were sectioned as midmodiolar plan to represent the overall place of the cochlea. SGCs in 10000 square micrometers at four different parts of the cochlea (high middle, low middle, high basal, and low basal) were counted and compared with the control group. Three or more sectioned images at each part with a 50 um interval were averaged and examined by polarizing microscopy using a BX51-P microscope (Olympus, Tokyo, Japan).

Three cochleae at each group after 12 weeks of drug administration were prepared as whole mounts and were immunostained with anti-neurofilament heavy (anti-chicken, Millipore, 1:1000) and MyosinVIIa (anti-rabbit, Millipore, 1:200). After mounting on a slide, images were taken with a confocal microscope (FV-3000, Olympus, Tokyo, Japan). 40x magnification was used and z-stacks were generated.

2.5. Statistical Analysis. Statistical analysis was performed using the Statistical Package for the Social Sciences (SPSS, Chicago, USA) software. Two-way analysis of variance (ANOVA) with Bonferroni post hoc test was adopted and significant differences were determined when the p value was $<.05$.

3. Results

3.1. Serial Changes of ABR Thresholds. We tested different delivery techniques (single application) to induce hearing loss and evaluated the hearing outcome. ABR was measured at three time points in all groups, one, four, and twelve weeks after the drug administration. Hearing threshold shifts were observed in all groups at any given time points (Figure 2). At the one-week time point, hearing thresholds of all kanamycin injected groups were statistically different from the control (two-way ANOVA, df = 3, $F = 193.1$, $p < .0001$). In the KP group, post hoc t-test revealed that statistical significance exists at 12, 16, and 32 kHz (12 kHz: $p < .001$, 16 kHz: $p < .001$,

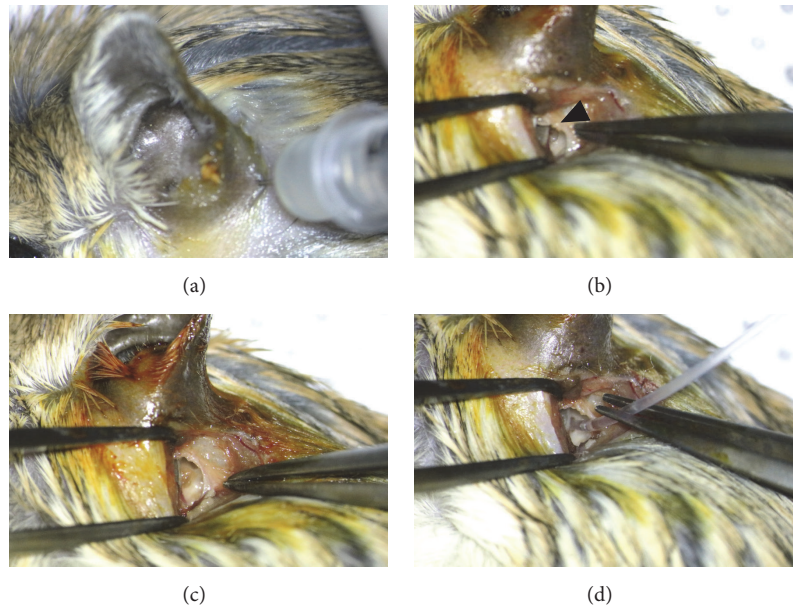

Figure 1: Drug delivery via different methods. The KM solution was injected by a syringe to the KP group (a). A small hole on the bulla was made and the RWM (black arrowhead) was exposed (b). A gelfoam with KM was placed on the RWM for the KG group (c). The tip of a cannula was inserted in the RWM niche for the KI group (d).

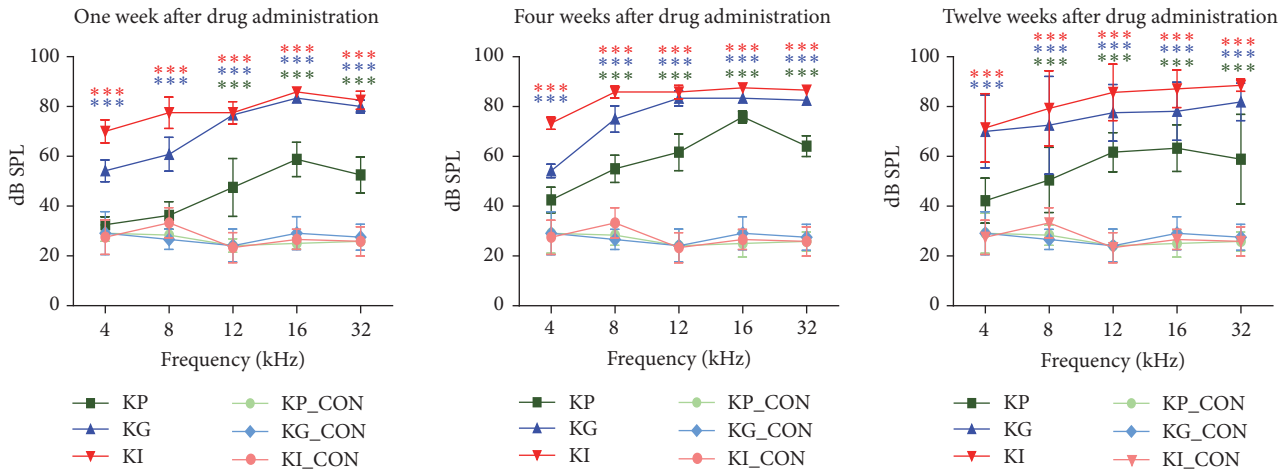

Figure 2: Serial changes of the hearing threshold after drug administration. Hearing thresholds at multiple frequencies were measured at three different time points (1 week, 4 weeks, and 12 weeks) for kanamycin percutaneous (KP), kanamycin gelfoam (KG), and kanamycin RW injection (KI) groups. See Methods for more descriptions. In the KP group, hearing thresholds increased at high frequency regions (12, 16, and 32 kHz) at four weeks after drug administration and these increased thresholds remained until 12 weeks after drug administration. KG group showed a more severe hearing threshold change at all time points. KI group showed the worst hearing thresholds change at all tested frequencies and all test points ($^{***}p < 0.001$).

32 kHz: $p < .001$). As with the KG group, hearing thresholds were significantly elevated at all test frequencies (p values of post hoc test: 4 kHz < .001, 8 kHz < .001, 12 kHz < .001, 16 kHz < .001, and 32 kHz < .001). Similarly, the KI group showed a significant difference at all test frequencies (p values of post hoc test: 4 kHz < .001, 8 kHz < .001, 12 kHz < .001, 16 kHz < .001, and 32 kHz < .001) (Figure 2).

According to the results of this part, using the local delivery techniques to induce a substantial hearing threshold shift with a single application was possible. Threshold changes of the KG and KP groups showed increased hearing threshold shifts at higher frequencies due to the closer location to the round window where the drug is presumably delivered. In the KI group, most of the deterioration in the hearing threshold was observed; however, the invasiveness of the delivery technique cannot be disregarded.

At the 4-week time point, hearing thresholds of all kanamycin injected groups were statistically different from the control (two-way ANOVA, $F < 326.9$, df < 3, $p < .0001$). Post hoc t-test revealed that all three groups showed

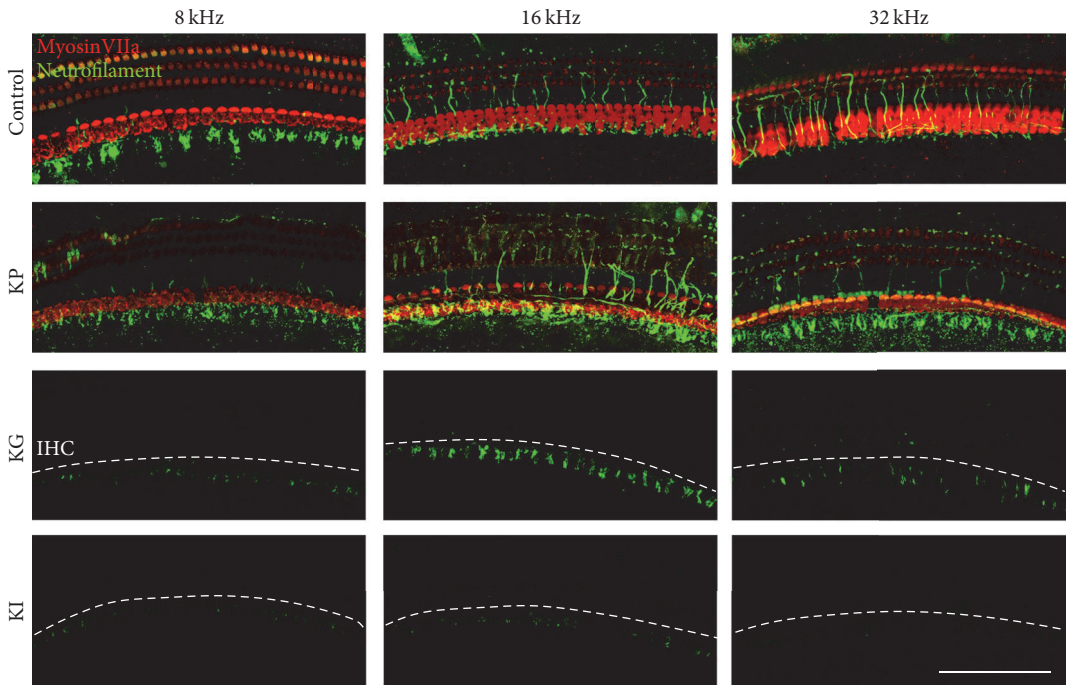

Figure 3: Epifluorescence analysis of the OC at 12 weeks after drug administration. Hair cells (MyosinVIIa, red) and the peripheral auditory nerve (Neurofilament, green) were observed at three parts of the cochlea that are tonotopically responsible for 8, 16, and 32 kHz of hearing. The control group showed intact hair cells and nerve fibers. KP group showed intact IHCs and a few defects of OHCs at three different parts. Nerve fiber connections from hair cells to SGCs were disrupted in the KP group. In the KG and KI groups, IHCs and OHCs completely disappeared and only fragments of nerve fibers were observed. The three groups were kanamycin percutaneous (KP), kanamycin gelfoam (KG), and kanamycin RW injection (KI). The white dotted lines represent the IHC place. Scale bar is 100 um.

statistically significant threshold shifts at all the tested frequencies (KP group: 4 kHz < .001, 8 kHz < .001, 12 kHz < .001, 16 kHz < .001, and 32 kHz < .001; KG group: 4 kHz < .001, 8 kHz < .001, 12 kHz < .001, 16 kHz < .001, and 32 kHz < .001; KI group: 4 kHz < .001, 8 kHz < .001, 12 kHz < .001, 16 kHz < .001, and 32 kHz < .001). These threshold shifts were constant until 12 weeks after the drug administration while the KP group showed a little recovery at 4 kHz ($p < .01$).

With a single application using a different delivery technique, hearing threshold change was maintained until the 12-week time point. This result suggests that the hearing deterioration observed at the 1-week time point is not transient but is permanent, possibly due to the irreversible loss and not the temporary damage of the hair cells.

3.2. Hair Cells and Neurofilaments Damage Was Variable Depending on the Drug Administration Methods. A decrement in hearing threshold after drug administration would be highly related to the status of the OC, especially hair cells (HCs) and nerve fibers connected to them. Thus, we investigated the status of the HC and nerve fibers by immunostaining with whole mount preparation. The status of HCs and nerve fibers at the apex, middle, and base parts of the cochlea, which represents 8, 16, and 32 kHz, was identified. After twelve weeks of drug administration, the KG and KI groups showed a total loss of HCs and a partial loss of nerve fibers at three selected parts of the cochlea. In the case of the KP group, we found that the status of the nerve fiber and HCs was preserved (Figure 3). These results suggest that the HC and nerve fiber can be severely damaged by a single application of kanamycin depending on the delivery method, and such damage would cause a permanent threshold shift in the KG and KI groups. In the case of the KP group, a threshold shift was maintained for 12 weeks without anatomical change in the HCs and nerve fibers.

3.3. OC Was Damaged over Time after Drug Administration. According to the immunostaining results, kanamycin causes damage not only to the HCs in the OC, but also to the auditory nerve fibers. To investigate the degree of degeneration in the OC and the possibility of additional degeneration of the auditory ascending pathway, the status of the OC within the sectioned images was identified. Four locations in the cochlea were selected as representative areas (Figures 4 and 5). After four weeks of drug administration, the OC was intact at the four selected locations in the control and KP groups. In the KG group, the OC was damaged and showed a flat epithelium at both high and low basal parts of the cochlea. In the case of the KI group, the OC was also damaged and showed a flat epithelium throughout the cochlea (Figure 4). This result confirmed that a single administration of kanamycin can cause damage to HCs at 4 weeks after the treatment depending on the administration method.

After twelve weeks of drug administration, still, the status of the OC was intact at all locations in the control and KP groups. In the KG group, damage to the OC was extended

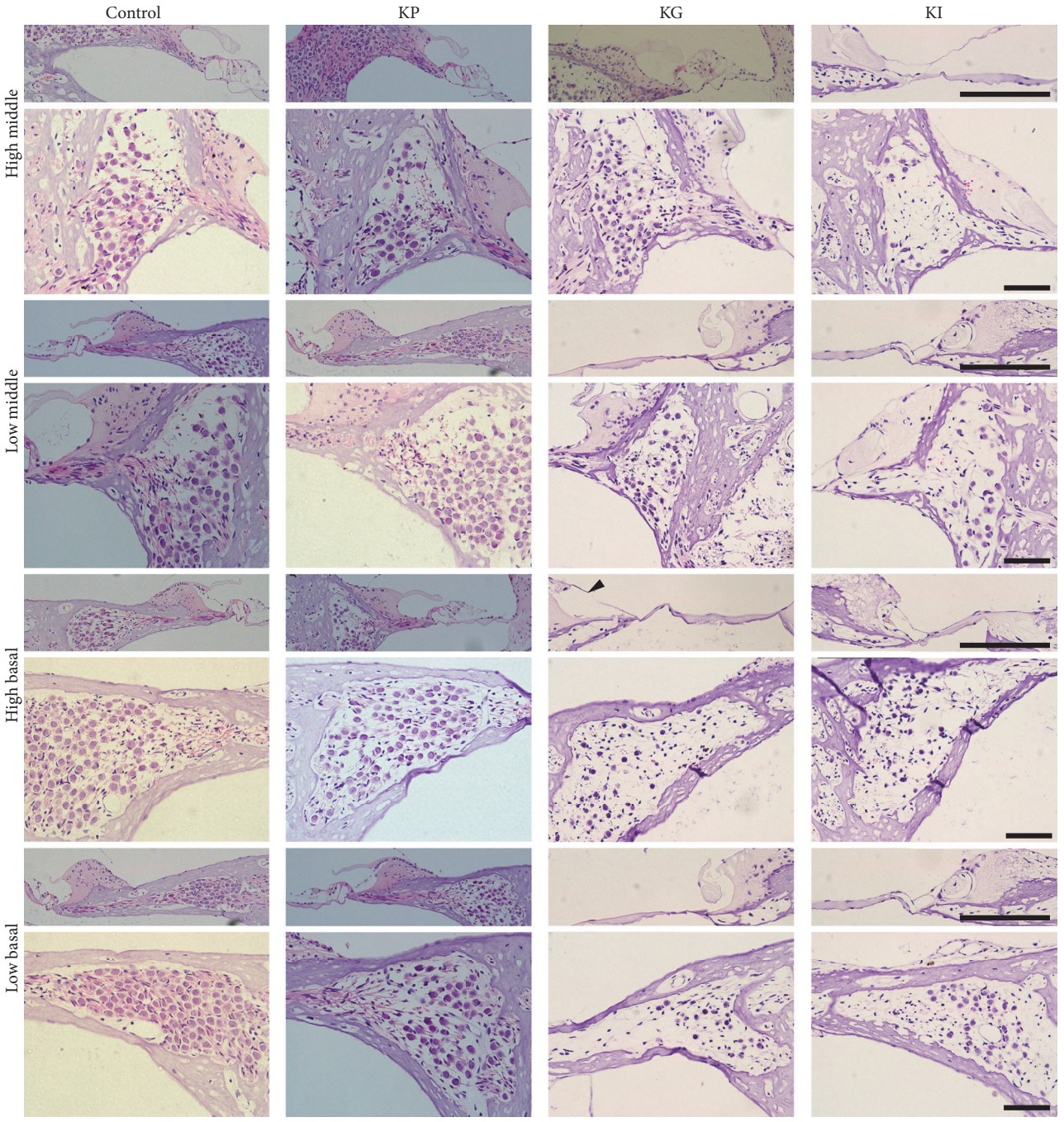

Figure 4: Histologic analysis of the OC and SGCs at four different parts of the cochlea at 4 weeks after drug administration. At 4 weeks after drug administration, OC was intact in both KP and KG groups, but the KG group showed a flat epithelium without any sensory cells at all parts except the high middle part. In the KG group, a damaged spiral limbus (black arrowhead) was found at the high basal part. The KI group also showed severely damaged OC at all parts of the cochlea. The KG group showed no reduction of SGC density, showing a similar result to the control group. The KG group showed sparse SGCs at low middle, high basal, and low basal parts of the cochlea. The KI group showed sparse SGCs at all parts of the cochlea. The three groups were kanamycin percutaneous (KP), kanamycin gelfoam (KG), and kanamycin RW injection (KI). Scale bar represents 100 um.

to the upper parts of the cochlea, but the high middle part of the OC was undamaged. In the KI group, the status of the OC was varied depending on the subject. One subject showed a total loss of the OC at all the selected parts, whereas two subjects showed an intact status of the OC. These results suggest that the kanamycin solution injected through the RWM would have leaked out if the perilymph was not well flushed.

3.4. SGCs Were Damaged following Hair Cell Loss. The status of SGC was also observed for identifying additional damage in the auditory pathway. Similar to the OC, SGCs

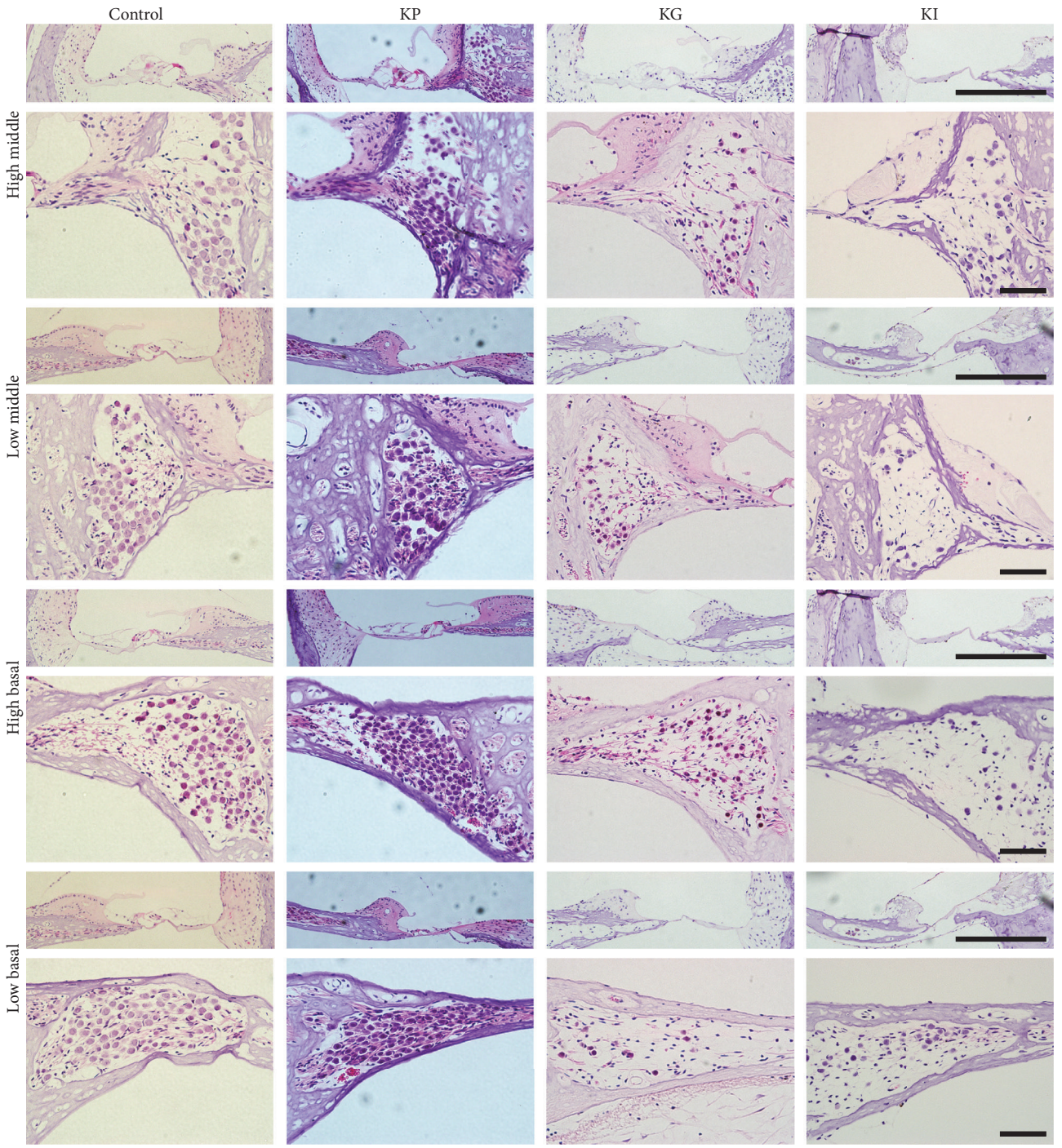

Figure 5: Histologic analysis of the OC and SGCs at four different parts of the cochlea at 12 weeks after drug administration. At 12 weeks after drug administration, the OC was intact in the KP group, but the KG group showed a flat epithelium without any sensory cells at all parts except the high middle part. The KI group showed a disrupted OC at all parts of the cochlea. The KP group showed no reduction of SGC density, showing a similar result to the control group. However, the KG group showed sparse SGCs at all parts of the cochlea, which is more severe than 4 weeks after drug administration. For the KI group, more severe depletion of SGCs was found at all parts of the cochlea. The three groups were kanamycin percutaneous (KP), kanamycin gelfoam (KG), and kanamycin RW injection (KI). Scale bar represents 100 um.

at four locations were counted and compared with the control group (Figures 3 and 4). In the KP group, there were no difference in the density of the SGC at four and twelve weeks after drug administration (Figure 6). However, the number of SGCs in the KG group was significantly decreased compared with the control group at four weeks after drug administration (Figure 6(a)), and these decrements were increased at twelve weeks after drug administration (Figure 6(b)). In the KI group, the number of SGCs was significantly decreased in all selected locations at four weeks

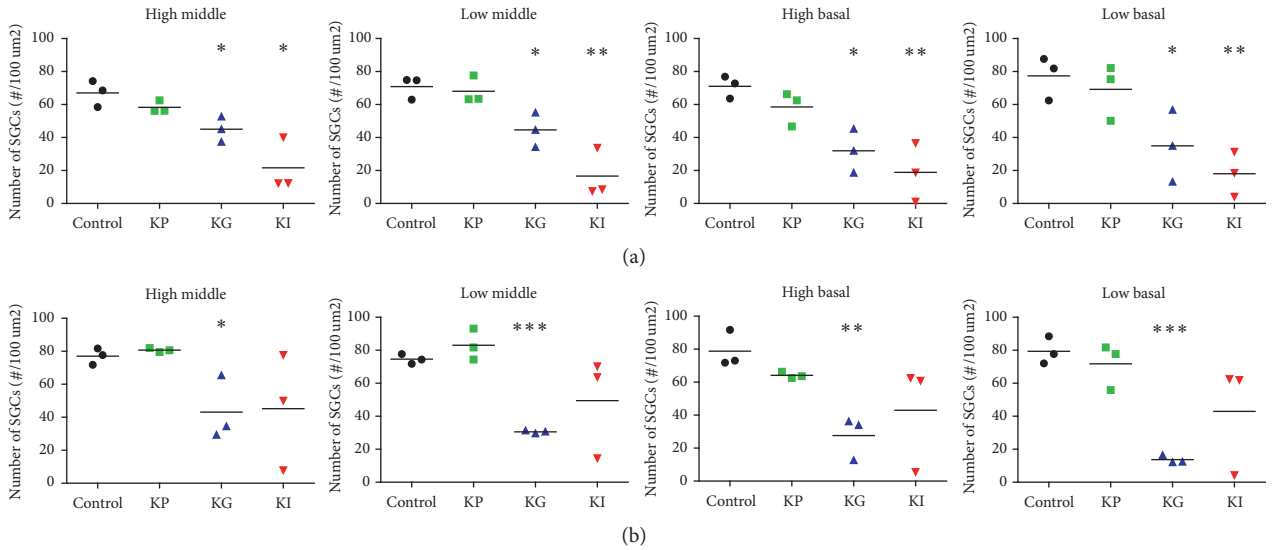

Figure 6: SGC densities at four different parts of the cochlea at 4 (a) and 12 weeks (b) after drug administration. The KP group showed no significant decrease in SGC densities compared to the control at both 4 and 12 weeks. The KG group showed a significant SGC density decrease at all locations at both time points. The KI group showed a significant SGC density decrease at all locations at the 4-week time point but did not show a significant decrease at the 12-week time point. All units in the plot (black dot: control; green square: KP; blue triangle: KG; red inverted triangle: KI) represent individual subjects. The three groups were kanamycin percutaneous (KP), kanamycin gelfoam (KG), and kanamycin RW injection (KI). The asterisk (∗) indicates a p value lower than .05, the double asterisk (∗∗) indicates a p value lower than .01, and the triple asterisk (∗ ∗ ∗) indicates a p value lower than .001.

after drug administration (Figure 6(a)). However, after twelve weeks of drug administration, the number of SGCs was not consistent between subjects and a huge subject difference existed and was not significantly different from the control group (Figure 6(b)). These results suggest that a single treatment of kanamycin can damage HCs and this HC loss causes deterioration at the upper part of the auditory pathway.

4. Discussions

4.1. KM Ototoxicity. Kanamycin is a well-known ototoxic agent, and it is a widely used model to mimic human sensorineural hearing loss with various delivery methods in an animal model [20, 26–29]. However, to induce substantial hearing loss in a rodent model, multiple injections or other drug combinations are required. Several previous researches used kanamycin as an ototoxic drug combined with other agents for achieving total loss of HC which is incomplete with kanamycin alone [5, 30]. In particular, furosemide, which can manipulate the blood labyrinth barrier, has been used as a combination agent and showed better ototoxic damage compared to kanamycin alone. However, this agent is a diuretic and can systemically affect the whole body. This untargeted effect would cause changes inside the cochlea, resulting in ambiguous toxic or inflammatory damage. It was reported that furosemide may itself cause a hearing loss by inducing transient malfunction in the stria vascularis [31, 32]. Therefore, we used a very high concentration of kanamycin and applied it directly to the round window membrane with a gelfoam and acquired severe SGN loss at 4 weeks after drug administration. This high concentration of kanamycin was two or three times higher than in previous studies [5, 30] and causes total loss of both hair cells and SGCs at 12 weeks after a single treatment.

The ototoxicity of kanamycin is a well-known issue throughout the clinical and animal research. It is reported that kanamycin induces production of reactive oxygen species and these attack the cochlear hair cells, which is an irreversible injury, resulting in a hearing disorder (Jiang et al., 2005). We did not explore the mechanism of kanamycin toxicity at the HC and SGC in this study. Nevertheless, we might expect that the same ototoxic mechanism would be involved in this study.

4.2. Gerbil as a Proper Hearing Research Model. The Mongolian gerbil is a well-established animal model for hearing research [33]. Since the range of audible frequency is more similar to that of humans than other rodents such as mice, rats, or guinea pigs [34], gerbils have been considered as a suitable model in hearing research including aminoglycoside toxicity [5]. Furthermore, the larger bulla and thin skull enable a surgical approach to the cochlea. In our study, we applied various approaches to treat with aminoglycosides and acquired consistent results after surgery with the aforementioned reasons except with the RWM injection group. Additionally, due to the location of the stapedial artery that is not blocking the round window, gerbils have been widely used as an animal model for CI studies. Moreover, the high reproduction rate and easier breeding and handling make gerbils more appropriate for animal studies. Their characteristics (i.e., they were born deaf and have a late onset of hearing [35]) boost the versatility for various approaches that are possible with this animal model. All in all, we suggest

that gerbils can serve as a proper animal model in various hearing research areas.

4.3. Drug Delivery Agent. We applied various ways of drug administration to find the most appropriate way that can induce secondary degeneration. According to our results, the RWM injection showed a more dramatic change in the OC within a short time than the gelfoam group. The number of SGCs was severely decreased at four selected parts of the cochlea at 4 weeks after kanamycin treatment through the RWM injection. However, a prominent subject difference also existed with this approach. During treatment, the KM solution could not disperse well because of the pressure inside the scala tympani, and it also leaked out right after injection using a cannula. Together with these, we considered that KM RWM injection is not an appropriate way to create a secondary degeneration model (Figure 6). Otherwise, KM application with gelfoam showed very consistent and effective results within subjects compared to any of the other methods (Figure 6).

Drug delivery agents have been studied in the otology research area for ototoxic or therapeutic purposes. It has been reported that gelfoam increases the effect of a drug itself by allowing the drug to be retained longer at the target area. Abbas and Rivolta (2015) used aminoglycosides with a gelatin sponge and reported a more significant change in the hearing threshold after 2 weeks of treatment than with KM alone [5]. However, when they applied gentamycin to the RWM with a gelatin sponge, which is also a well-known ototoxic drug, it did not cause hearing loss. They explained that this is due to the polar nature of the gelatin sponge which blocked the penetration of gentamycin into the RWM [5]. Poloxamer 407 has also been used as a delivery agent, including nanoparticles and an ototoxic drug, which can provide sustained release at the target area [36, 37]. Together with these, we thought that kanamycin treatment with poloxamer 407 would also be a proper way to create a secondary degeneration model in gerbils.

4.4. Secondary Degeneration Modeling and Possible Treatment. For generating a secondary degeneration model for diverse purposes, various methods would be applicable in animal research. A recent study that investigated KM toxicity reported that KM did not damage adult spiral ganglion neurons [4]. In this study, hair cells and ganglion neurons in postnatal day 3 rat cochlear organ culture were damaged by KM, whereas there was no toxicity in adult rat ganglion cells in an organotypic culture model. This result supports the notion that the degeneration of SGCs in our study was damaged not by KM itself but influenced from the loss of HC as secondary damage. It also supports the fact that our reproducible secondary degeneration model with the gelfoam approach is suitable for a secondary degeneration model.

As seen in Figure 3, the KP group showed an intact histological structure of HCs and neurofilaments, even with a hearing threshold decrement 12 weeks after drug administration. This result suggests the possibility that secondary degeneration could be initiated at the upper level of the HC. It was reported that a low dose of aminoglycoside causes synaptic changes without HC loss [38]. If the secondary degeneration starts from the damage synapse level which is the most vulnerable factor in the cochlea, neurotrophin and photobiomodulation would be appropriate therapeutic approaches. Neurotrophin factor, especially NT-3, was reported as a very useful agent which can protect against synaptic loss due to noise exposure [36, 39]. Photobiomodulation with a low-level laser (LLL) has also been studied in hearing research areas, and it was reported that it has a protective effect against HC after noise exposure [40, 41]. Furthermore, it has a neuroprotective effect against Ouabain on SGC [42]. We will try to protect or delay the secondary degeneration with either neurotrophin or photobiomodulation in the near future.

5. Conclusion

We induced secondary degeneration of HCs in a gerbil model through diverse drug delivery approaches in this study. High concentrations of kanamycin application with gelfoam on the RWM caused severe HC loss and this extended to degeneration of the auditory nerve and SGCs. This model can be used for various purposes in the hearing research area either for treatment or for preservation. Furthermore, this model would be applicable for research regarding cochlear implants.

Disclosure

An earlier version of this work was presented as an abstract at ARO 2017.

Conflicts of Interest

The authors declare that they have no conflicts of interest.

Acknowledgments

The authors would like to thank Nathaniel Carpena from Beckman Laser Institute Korea for reviewing grammatical errors. This research was supported by Leading Foreign Research Institute Recruitment Program through the National Research Foundation of Korea (NRF) funded by the Ministry of Science and ICT (MSIT) (2012K1A4A3053142) and by a grant of the Korea Health Technology R&D Project through the Korea Health Industry Development Institute (KHIDI), funded by the Ministry of Health & Welfare, Republic of Korea (Grant no. HI15C1524).

References

[1] H. Spoendlin, "Factors inducing retrograde degeneration of the cochlear nerve," *Annals of Otology, Rhinology & Laryngology*, vol. 93, no. 4, pp. 76–82, 1984.

[2] P. A. Leake and G. T. Hradek, "Cochlear pathology of long term neomycin induced deafness in cats," *Hearing Research*, vol. 33, no. 1, pp. 11–33, 1988.

[3] S. Kroon, D. Ramekers, E. M. Smeets, F. G. J. Hendriksen, S. F. L. Klis, and H. Versnel, "Degeneration of auditory nerve fibers in guinea pigs with severe sensorineural hearing loss," *Hearing Research*, vol. 345, pp. 79–87, 2017.

[4] K. Gao, D. Ding, H. Sun, J. Roth, and R. Salvi, "Kanamycin Damages Early Postnatal, but Not Adult Spiral Ganglion Neurons," *Neurotoxicity Research*, vol. 32, no. 4, pp. 603–613, 2017.

[5] L. Abbas and M. N. Rivolta, "Aminoglycoside ototoxicity and hair cell ablation in the adult gerbil: A simple model to study hair cell loss and regeneration," *Hearing Research*, vol. 325, pp. 12–26, 2015.

[6] W. Y. Bae, L. S. Kim, D. Y. Hur, S. W. Jeong, and J. R. Kim, "Secondary apoptosis of spiral ganglion cells induced by aminoglycoside: Fas-Fas ligand signaling pathway," *The Laryngoscope*, vol. 118, no. 9, pp. 1659–1668, 2008.

[7] D. H. Johnson, *The response of single auditory-nerve fibers in the cat to single tones: synchrony and average discharge rate*, Massachusetts Institute of Technology, 1974.

[8] C. E. Zimmermann, B. J. Burgess, and J. B. Nadol Jr., "Patterns of degeneration in the human cochlear nerve," *Hearing Research*, vol. 90, no. 1-2, pp. 192–201, 1995.

[9] Y. Suzuka and H. F. Schuknecht, "Retrograde cochlear neuronal degeneration in human subjects," *Acta Oto-Laryngologica*, vol. 105, no. 450, pp. 1–20, 1988.

[10] M. Sugawara, G. Corfas, and M. C. Liberman, "Influence of supporting cells on neuronal degeneration after hair cell loss," *Journal of the Association for Research in Otolaryngology*, vol. 6, no. 2, pp. 136–147, 2005.

[11] C. Rio, P. Dikkes, M. C. Liberman, and G. Corfas, "Glial fibrillary acidic protein expression and promoter activity in the inner ear of developing and adult mice," *Journal of Comparative Neurology*, vol. 442, no. 2, pp. 156–162, 2002.

[12] J. B. Nadol Jr., Y.-S. Young, and R. J. Glynn, "Survival of spiral ganglion cells in profound sensorineural hearing loss: implications for cochlear implantation," *Annals of Otology, Rhinology & Laryngology*, vol. 98, no. 6, pp. 411–416, 1989.

[13] J. B. Nadol, "Patterns of neural degeneration in the human cochlea and auditory nerve: implications for cochlear implantation," *Otolaryngology—Head and Neck Surgery*, vol. 117, no. 3, pp. 220–228, 1997.

[14] A. Incesulu and J. B. Nadol Jr., "Correlation of acoustic threshold measures and spiral ganglion cell survival in severe to profound sensorineural hearing loss: implications for cochlear implantation," *Annals of Otology, Rhinology & Laryngology*, vol. 107, no. 11, part 1, pp. 906–911, 1998.

[15] G. J. Greenwood, "Neomycin Ototoxicity: Report of a Case," *A.M.A. Archives of Otolaryngology*, vol. 69, no. 4, pp. 390–397, 1959.

[16] G. J. Matz, "Aminoglycoside ototoxicity," *American Journal of Otolaryngology - Head and Neck Medicine and Surgery*, vol. 7, no. 2, pp. 117–119, 1986.

[17] A. L. Miller, "Effects of chronic stimulation on auditory nerve survival in ototoxically deafened animals," *Hearing Research*, vol. 151, no. 1-2, pp. 1–14, 2001.

[18] T. Stöver, M. Yagi, and Y. Raphael, "Cochlear gene transfer: Round window versus cochleostomy inoculation," *Hearing Research*, vol. 136, no. 1-2, pp. 124–130, 1999.

[19] R. K. Shepherd, J. Matsushima, R. L. Martin, and G. M. Clark, "Cochlear pathology following chronic electrical stimulation of the auditory nerve: II deafened kittens," *Hearing Research*, vol. 81, no. 1-2, pp. 150–166, 1994.

[20] H. Versnel, M. J. H. Agterberg, J. C. M. J. de Groot, G. F. Smoorenburg, and S. F. L. Klis, "Time course of cochlear electrophysiology and morphology after combined administration of kanamycin and furosemide," *Hearing Research*, vol. 231, no. 1-2, pp. 1–12, 2007.

[21] C. Whitworth, C. Morris, V. Scott, and L. P. Rybak, "Dose-response relationships for furosemide ototoxicity in rat," *Hearing Research*, vol. 71, no. 1-2, pp. 202–207, 1993.

[22] D. Ding, X. Jin, and J. Zhao, "Accumulation sites of kanamycin in cochlear basal membrane cells," *Zhonghua Er Bi Yan Hou Tou Jing Wai Ke Za Zhi*, vol. 30, no. 6, pp. 323–325, 1995.

[23] A. A. Gerencser, J. Doczi, B. Töröcsik, E. Bossy-Wetzel, and V. Adam-Vizi, "Mitochondrial swelling measurement in situ by optimized spatial filtering: Astrocyte-neuron differences," *Biophysical Journal*, vol. 95, no. 5, pp. 2583–2598, 2008.

[24] N. J. Solenski, C. G. DiPierro, P. A. Trimmer, A. Kwan, and G. A. Helms, "Ultrastructural changes of neuronal mitochondria after transient and permanent cerebral ischemia," *Stroke*, vol. 33, no. 3, pp. 816–824, 2002.

[25] W. J. Kong, Z. D. Yin, G. R. Fan, D. Li, and X. Huang, "Time sequence of auditory nerve and spiral ganglion cell degeneration following chronic kanamycin-induced deafness in the guinea pig," *Brain Research*, vol. 1331, pp. 28–38, 2010.

[26] J. J. Brown, R. E. Brummett, K. E. Fox, and T. W. Bendrick, "Combined Effects of Noise and Kanamycin: Cochlear Pathology and Pharmacology," *JAMA Otolaryngology–Head & Neck Surgery*, vol. 106, no. 12, pp. 744–750, 1980.

[27] S.-A. Xu, R. K. Shepherd, Y. Chen, and G. M. Clark, "Profound hearing loss in the cat following the single co-administration of kanamycin and ethacrynic acid," *Hearing Research*, vol. 70, no. 2, pp. 205–215, 1993.

[28] R. E. Brummett, J. Traynor, R. Brown, and D. Himes, "Cochlear damage resulting from kanamycin and furosemide," *Acta Oto-Laryngologica*, vol. 80, no. 1-6, pp. 86–92, 1975.

[29] N. J. Russell, K. E. Fox, and R. E. Brummett, "Ototoxic effects of the interaction between kanamycin and ethacrynic acid: Cochlear infrastructure correlated with cochlear potentials and kanamycin levels," *Acta Oto-Laryngologica*, vol. 88, no. 1-6, pp. 369–381, 1979.

[30] K. Hirose and E. Sato, "Comparative analysis of combination kanamycin-furosemide versus kanamycin alone in the mouse cochlea," *Hearing Research*, vol. 272, no. 1-2, pp. 108–116, 2011.

[31] R. H. Mathog and W. J. Klein Jr., "Ototoxicity of ethacrynic acid and aminoglycoside antibiotics in uremia.," *The New England Journal of Medicine*, vol. 280, no. 22, pp. 1223-1224, 1969.

[32] L. P. Rybak, "Ototoxicity of loop diuretics," *Otolaryngologic Clinics of North America*, vol. 26, no. 5, pp. 829–844, 1993.

[33] A. Wiegner, C. G. Wright, and M. Vollmer, "Multichannel cochlear implant for selective neuronal activation and chronic use in the free-moving Mongolian gerbil," *Journal of Neuroscience Methods*, vol. 273, pp. 40–54, 2016.

[34] G. Otto and S. Jürgen, "The Mongolian gerbil as a model for the analysis of peripheral and central age-dependent hearing loss," in *Hearing Loss*, InTech, 2012.

[35] M.-L. Barrenäs and A. Axelsson, "The development of melanin in the stria vascularis of the gerbil," *Acta Oto-Laryngologica*, vol. 112, no. 1, pp. 50–58, 1992.

[36] J. Suzuki, G. Corfas, and M. C. Liberman, "Round-window delivery of neurotrophin 3 regenerates cochlear synapses after acoustic overexposure," *Scientific Reports*, vol. 6, Article ID 24907, 2016.

[37] X. Wen, S. Ding, H. Cai et al., "Nanomedicine strategy for optimizing delivery to outer hair cells by surface-modified poly(lactic/glycolic acid) nanoparticles with hydrophilic molecules," *International Journal of Nanomedicine*, vol. 11, pp. 5959–5969, 2016.

[38] L. Chen, S. Xiong, Y. Liu, and X. Shang, "Effect of different gentamicin dose on the plasticity of the ribbon synapses in cochlear inner hair cells of C57BL/6J mice," *Molecular Neurobiology*, vol. 46, no. 2, pp. 487–494, 2012.

[39] G. Wan, M. E. Gómez-Casati, A. R. Gigliello, M. Charles Liberman, and G. Corfas, "Neurotrophin-3 regulates ribbon synapse density in the cochlea and induces synapse regeneration after acoustic trauma," *eLife*, vol. 3, Article ID e03564, 2014.

[40] C.-K. Rhee, C. W. Bahk, S. H. Kim et al., "Effect of low-level laser treatment on cochlea hair-cell recovery after acute acoustic trauma," *Journal of Biomedical Optics*, vol. 17, no. 6, pp. 0680021–0680026, 2012.

[41] J.-H. Lee, S.-Y. Chang, W. J. Moy et al., "Simultaneous bilateral laser therapy accelerates recovery after noise-induced hearing loss in a rat model," *PeerJ*, vol. 2016, no. 7, Article ID e2252, 2016.

[42] M. Y. Lee, S.-H. Bae, S.-Y. Chang et al., "Photobiomodulation by laser therapy rescued auditory neuropathy induced by ouabain," *Neuroscience Letters*, vol. 633, pp. 165–173, 2016.

Hindawi
BioMed Research International
Volume 2018, Article ID 6280969, 12 pages
https://doi.org/10.1155/2018/6280969

Research Article

Transient Abnormalities in Masking Tuning Curve in Early Progressive Hearing Loss Mouse Model

Marion Souchal,[1] **Ludimila Labanca**,[1] **Sirley Alves da Silva Carvalho**,[2] **Luciana Macedo de Resende**,[2] **Christelle Blavignac**,[3] **Paul Avan**,[1] **and Fabrice Giraudet**[1]

[1]*Neurosensory Biophysics, INSERM UMR 1107, Clermont Auvergne University, Clermont-Ferrand, France*
[2]*Speech Therapy and Audiology Department, Federal University of Minas Gerais, Belo Horizonte, MG, Brazil*
[3]*Cellular Health Imaging Center, Clermont Auvergne University, Clermont-Ferrand, France*

Correspondence should be addressed to Fabrice Giraudet; fabrice.giraudet@uca.fr

Received 10 October 2017; Accepted 26 December 2017; Published 13 February 2018

Academic Editor: Jeong-Han Lee

Damage to cochlear outer hair cells (OHCs) usually affects frequency selectivity in proportion to hearing threshold increase. However, the current clinical heuristics that attributes poor hearing performance despite near-normal auditory sensitivity to auditory neuropathy or "hidden" synaptopathy overlooks possible underlying OHC impairment. Here, we document the part played by OHCs in influencing suprathreshold auditory performance in the presence of noise in a mouse model of progressive hair cell degeneration, the CD1 strain, at postnatal day 18–30 stages when high-frequency auditory thresholds remained near-normal. Nonetheless, total loss of high-frequency distortion product otoacoustic emissions pointed to nonfunctioning basal OHCs. This "discordant profile" came with a huge low-frequency shift of masking tuning curves that plot the level of interfering sound necessary to mask the response to a probe tone, against interfering frequency. Histology revealed intense OHC hair bundle abnormalities in the basal cochlea uncharacteristically associated with OHC survival and preserved coupling with the tectorial membrane. This pattern dismisses the superficial diagnosis of "hidden" neuropathy while underpinning a disorganization of cochlear frequency mapping with optimistic high-frequency auditory thresholds perhaps because responses to high frequencies are apically shifted. The audiometric advantage of frequency transposition is offset by enhanced masking by low-frequency sounds, a finding essential for guiding rehabilitation.

1. Introduction

Sensorineural hearing losses (SNHL) stem from a wide spectrum of diseases affecting the sensory receptors, outer hair cells (OHCs), inner hair cells (IHCs), or auditory neurons (afferent and even efferent fibers) [1–5]. Pure-tone audiometry is the routine clinical audiological test used for measuring hearing sensitivity, and the audiometric classification of hearing impairments is the main basis upon which audiologists determine their rehabilitation choice. Even though it cannot provide any fine-grained reflection of the mechanism of SNHL and may not delineate individual needs, it works in a large majority of cases because it is the damage to OHCs that usually accounts for the hearing impairment, particularly frequency selectivity that, in simple cases, is affected in proportion to the increase in hearing thresholds [6]. However, it is acknowledged that there are "discordant patterns," that is, subjects with near-normal audiometric thresholds yet difficulties in speech intelligibility, especially in noisy environments [7], Their investigation has led to the discovery of auditory disorders that widely differ from the typical OHC-related SNHL, namely, auditory neuropathies and synaptopathies [8, 9]. Auditory neuropathies are revealed by abnormal auditory-evoked potentials although a recent picture has been substantiated in animal models of short overexposure to intense sounds, which develop noise-induced synaptopathies

with no detectable auditory-evoked-potential abnormality [10–12]. In these conditions, pure-tone audiometry is obviously inadequate for predicting suprathreshold auditory perception tasks [13], as discrepancies among metrics of auditory performance are expected when SNHL arises, not from micromechanical stages but from transduction and action-potential generation or conduction. But pure-tone audiometry may also fail to provide a coherent picture of auditory performance in the case of pure OHC dysfunction, as shown by a mutation in the Nherf1 gene expressed only in OHCs at mature stages [14]. The mild ABR hearing threshold elevation of *Nherf1*$^{-/-}$ mice at high frequencies is contradicted by an absence of high-frequency DPOAEs and by an inordinate sensitivity of mid/high frequencies to low-frequency maskers. This nonconventional functional pattern comes with peculiar OHC hair bundle shape anomalies in the basal part of the cochlea. Thus, the finding of inconsistencies between auditory thresholds and suprathreshold auditory performance, for example, frequency selectivity, cannot guarantee that these inconsistencies point to auditory neuropathy, a diagnosis that, even when neuropathy is "hidden," might prompt clinicians to the prescription of auditory-neuropathy-specific intervention. Along the same line, recent papers stress the importance of OHC function as a determinant of speech-in-noise performance, highlighted by its decrease with decreased OAEs in a sample of subjects with audiometric thresholds within the normal range [15, 16]. All these studies warn against considering that hidden hearing loss excludes OHCs as a potential contributor.

Therefore, the goal of the present work is to better document the part played by OHCs in influencing suprathreshold auditory function. To bridge the gap between transgenic or knockout mouse models with precisely targeted deficits and human data in subjects for whom the causes of SNHL are difficult to track with unknown combinations of genetics, aging, and exposure to environmental factors, we sought to investigate a rapidly progressive sensorineural auditory impairment in a strain of noninbred mice, CD1 mice. These mice are known to exhibit early onset of hearing loss due to hair cell degeneration and to offer, between around 3 and 8 weeks after birth, a broad range of frequency intervals of hearing loss and proportion of damaged OHCs [17–19].

We performed a longitudinal functional study in CD1 mice at the first 30 postnatal days and observed progressive hearing loss, yet with a discrepancy between high-frequency audiometric thresholds, close to normal, and absence of DPOAE, akin to that described by Kamiya et al. [14] yet likely much more widespread as it results from generic OHC hair bundle abnormalities, not dependent on a very rare gene mutation. Masking tuning curves were built to test basal OHC functionality and scanning electron microscopy, to study OHC hair bundle shape anomalies in the basal cochlea. Observations suggested a transient disorganization of the cochlear frequency mapping.

2. Material and Methods

2.1. Animals. Male CD1 mice ($n = 15$) from Janvier Labs were included in this study at 18 days of age. The animals were maintained in temperature and humidity-controlled facilities. Ambient sound pressure levels inside the cages were below 40 dB SPL. For all hearing test experiments, mice were anesthetized with ketamine (100 mg/kg, i.p.) and xylazine (20 mg/kg, i.p.). Body temperature was maintained at 37°C (Microprobe Thermometer, BAT-12, WPI) with an isothermal pad (Homeothermic Blanket System, Harvard Apparatus). Prior to testing and to exclude middle ear damage, an otoscopic examination (using a binocular operating microscope) was performed on each mouse. Cochlear function was assessed via ABR and DPOAE at postnatal days 18, 21, 25, and 30 (i.e., P18, P21, P25, and P30). All the auditory tests were performed in a sound attenuated and electrically shielded recording chamber. After the final auditory test, animals were sacrificed for histological processing and scanning electron microscopy analyses of hair cell stereocilia. All procedures were approved by the Regional Ethics Committee for animal experiments in France (Comité d'Éthique pour l'Expérimentation Animale Auvergne; EC 92-12).

2.2. DPOAE Recording. All testing was conducted using a stimulation and acquisition chain (EPL Cochlear Function Test Suite, Eaton-Peabody Laboratories, Harvard Medical School) controlled by a computer (NI PXI-1031, National Instrument). A miniaturized acoustic system (consisting of two speakers and one microphone) was gently sealed into the ear canal. Using a dedicated software (EPL Cochlear Function Test Suite-Eaton, Peabody Laboratories, Harvard Medical School), the parameters used for the stimulation were $f2/f1 = 1.20$ with $L1 = L2$. DPOAEs were measured for $f2 = 10, 15, 22$, and 32 kHz, with $L1$ and $L2$ from 10 dB to 80 dB in steps of 5 dB. DPOAE threshold was defined as the lowest sound level producing a DPOAE with an amplitude of at least 7 dB above the noise floor. Absence of instrumental DPOAE was verified in dead mice from the same batch at each frequency.

2.3. ABR Thresholds. Responses were recorded with needle electrodes (stainless steel, diameter: 0.4 mm, Medtronic Xomed Inc.) inserted through the skin at the vertex (active electrode) and ipsilateral mastoid (negative electrode) and in the neck region (ground). All electrode impedances were similar and <5 kΩ at the start of the test. The responses from the electrodes were amplified (×100,000), filtered (100–3,000 Hz), digitally converted, and averaged (300 sweeps) by a two-channel recording system (Neuropack μ®-MEB 9104, Nihon Kohden). The acoustic stimulus was generated by an arbitrary waveform generator (TG4001, Thurlby Thandar Instruments) which produced tone-bursts at 5, 10, 15, 22, 27, and 32 kHz. The envelope of the tone-burst was built using the Blackman-Harris formula (with the whole stimulus window containing 60 periods of the tone), in order to remove the artefact impulse sound produced when an earphone receives a too steeply rising signal. The acoustic stimulus intensity was controlled by an attenuator (PA4/SM3/HB6/XB1, Tucker Davis Technologies); then it was sent to the high-frequency earphone in the external ear canal (Number 40–137 8 Ω 70 W 8A4, Radio Shack Japan). The intensity at which an ABR waveform was still

visually detected above noise floor was defined as the ABR threshold.

2.4. Masking Tuning Curve (MTC). The probe stimulus was the same for the measurement of ABR, emitted 10 dB above the ABR threshold, at the target frequencies of 10, 22, and 32 kHz. The masking sound was a pure tone generated by a second generator (TG4001, Thurlby Thandar Instruments) and sent by a separate electronic and acoustic track to avoid electric distortion. The intensity of the masking sound considered effective induced a reduction of 50% of the ABR wave I amplitude generated in response to the target stimulus. It was determined for different masking frequencies swept above and below the target frequency.

2.5. Electron Microscopy. The mice were deeply anesthetized with pentobarbital (50 mg/kg) and sacrificed by transcardiac perfusion with freshly prepared 4% PFA in 0.1 M PBS. The cochleas were removed from the temporal bones under a binocular microscope in PHEM buffer (Pipes, Hepes, EGTA, and Magnesium) and fixed in 2.5% glutaraldehyde overnight at 4°C. The next day, samples were dehydrated in a series of alcohol baths from 25° to 100° and then HMDS (Hexamethyldisilazane) and metalized to be visualized with a scanning electron microscope with a field emission gun (FEG) (JSM-6060LV, JEOL). A count of normal, altered, and missing OHC stereocilia bundles in the apical (corresponding to the place coding frequencies around 10 kHz), middle (place coding frequencies around 20 kHz), and basal regions (place coding frequencies around 32 kHz) at each postnatal age was achieved. Hair bundles were considered altered when they had asymmetrical, linear, or hooked shapes.

2.6. Data Analysis. Graphs represent either individual plots or means ± standard error of the mean (sem). Statistical analysis was performed using Shapiro-Wilk test (Sigmaplot®, Systat Software Inc.). Differences were considered statistically significant when $P < 0.05$.

3. Results

3.1. Progressive Age-Related Hearing Loss of CD1 Mice

3.1.1. ABR Threshold Changes with Age. We first assessed the hearing sensitivity in the 5 to 32 kHz frequency range. The changes in ABR hearing thresholds (mean ± sem) over time are illustrated in Figure 1. Hearing loss in CD1 mice was significant and progressive. A few days after the onset of hearing, on P18, mean ABR hearing thresholds are consistent with a normal hearing sensitivity at frequencies from 10 to 27 kHz but not at 32 kHz (41 ± 2 dB SPL). Three days later, the hearing loss had progressed substantially at 22 and 27 kHz, from normal hearing to mild hearing loss (increase of between 20 and 22 dB in average compared to P18). At P25, the hearing impairment was more pronounced for high frequencies from 22 to 32 kHz with ABR thresholds reaching 59 to 67 ± 2 dB SPL. For middle frequencies, the ABR hearing threshold increase was 35 dB for 15 kHz, 29 dB for 10 kHz, and 15 dB for 5 kHz. At 1 month, the ABR audiogram was flat at all frequencies tested with near 50 dB hearing loss.

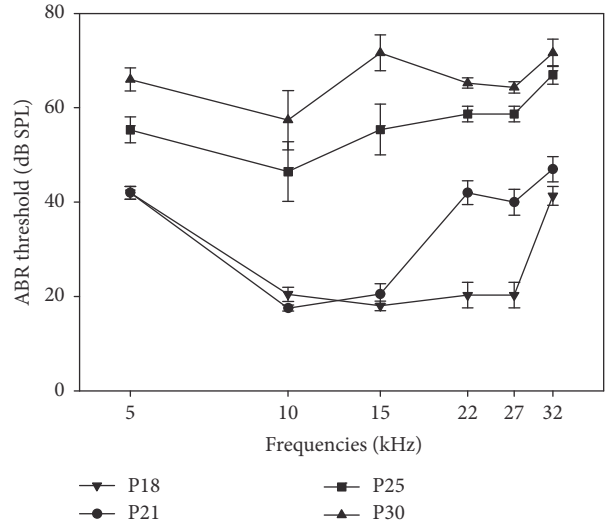

Figure 1: *ABR hearing thresholds of the CD1 mouse as a function of age*. Mean ABR hearing thresholds (±sem) measured for P18, P21, P25, and P30 CD1 mice ($n = 15$) with tone-bursts at 5, 10, 15, 22, 27, and 32 kHz.

So, there was a progressive elevation of the hearing threshold extending from high to low frequencies with a clear deterioration between P18 and P25. Between P25 and P30, the elevation of ABR thresholds slowed down.

3.1.2. Progressive Impairment of DPOAE Growth Functions. The mean DPOAE amplitudes as a function of the $f2$ primary level, that is, its growth functions, are shown in Figure 2 for 4 frequencies 10, 15, 22, and 32 kHz at P18, P21, P25, and P30. Except for the higher frequency (32 kHz) at P18, the general shape of the growth functions was characterized by a monotonically increasing DPOAE amplitude. At 32 kHz frequency, only P18 mice had detectable DPOAEs with very small amplitudes, with a signal-to-noise ratio of 7 (±5) for $L2 = 60$ dB. At all other frequencies, the growth functions shifted to the right more or less rapidly with increasing age. At P21 and lower frequencies 10 and 15 kHz, growth functions showed no significant change and only a little more than 10 dB downward shift at P25 and an additional 5 to 10 dB decrease at P30. Higher frequencies showed faster changes, −5 to −15 dB changes as soon as P21 at 22 kHz, while DPOAEs hardly emerged above noise at the highest stimulus levels after P25.

Relative to P18, ABR thresholds only increased by 30 to 40 dB at P25, suggesting the persistence of some degree of amplification by the cochlear amplifier, thought to normally have a 60 dB gain [20–23]. If OHCs are still functional enough to produce some gain, one might expect DPOAEs to persist at higher levels at least at high stimulus intensities. We therefore decided to look at individual cases assessed with the ABR and DPOAE in order to highlight the possible discrepancies between these two techniques.

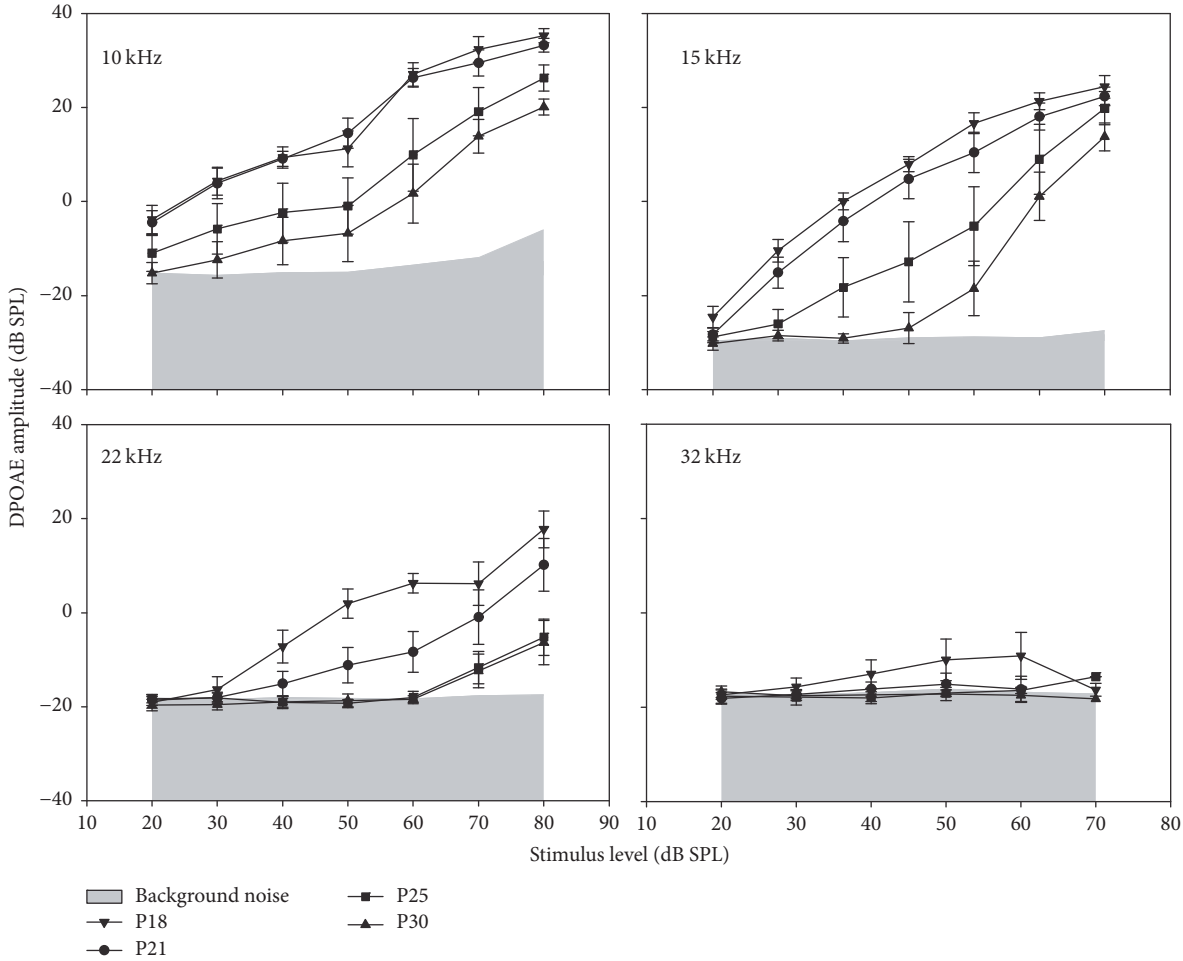

Figure 2: *DPOAE growth functions illustrating mean DPOAE amplitudes* (±sem) for primary levels ranging from 20 to 80 dB SPL in P18, P21, P25, and P30 CD1 mice at 10, 15, 22, and 32 kHz.

3.2. Slight Increase in ABR Hearing Thresholds Contrasts with Defective Responses of the OHCs at the Base and Shifted Tips of Masking Tuning Curves. The scatterplot of DPOAE thresholds at 32 kHz as a function of ABR thresholds and individual MTCs for a 32 kHz probe are represented in Figures 3(a) and 3(c), respectively. In some ears, the thresholds measured with these two techniques seemed well correlated, approximately along the diagonal line of the plot (Figure 3(a), dashed line). In view of these cases, a surprising discrepancy appears, with ears showing mild ABR threshold elevations yet no DPOAE (Figure 3(a), "discordant" points in red). The MTCs plotted in these cases at 32 kHz (Figure 3(c), red lines) contrast with the MTCs built in animals with a good correspondence between ABR and DPOAE thresholds (Figure 3(c), black lines) and with all MTCs built at 10 kHz, a frequency at which the animals kept normal thresholds between P18 and P25 (Figure 3(b)). More precisely, MTCs in black display a V-shaped profile with a deep tip at a frequency slightly above the probe frequency, corresponding to the most efficient frequency at which the masker interferes with the probe. At tip frequency, probe and masker levels are very close to each other. MTCs in red, in contrast, have no identifiable tip around the probe frequency, and the most efficient masker has a much lower frequency often lying around 12 kHz but sometimes between 16 and 32 kHz. A possible reading of these MTCs is that they only display a hypersensitive tail while the tip has become too shallow to be visible. The discordant profile, already observed at P18 (3 cases) occurred more frequently at P21 (10 cases) but almost vanished at P25 (one case, with most MTCs showing a blunt and elevated tip at the probe frequency).

The distributions of ABR and DPOAE thresholds as a function of age at 10 and 32 kHz differ in the following manner (Figure 4). At 10 kHz, DPOAE and ABR thresholds tended to covary. They were normal (≤40 dB SPL) and not much scattered at P18 and P21. At P25 and P30, both thresholds were more scattered and tended to increase by similar degrees, from 20 up to 75 dB SPL. This is not what happened at 32 kHz. At P18, despite ABR thresholds not exceeding 55 dB SPL, 6 mice already had lost their DPOAEs. The difference between ABR and DPOAE thresholds (when DPOAEs were still present) could reach 40 dB. At increasing ages, the ABR thresholds gradually shifted upwards. The discrepancy between ABRs and DPOAEs was still present

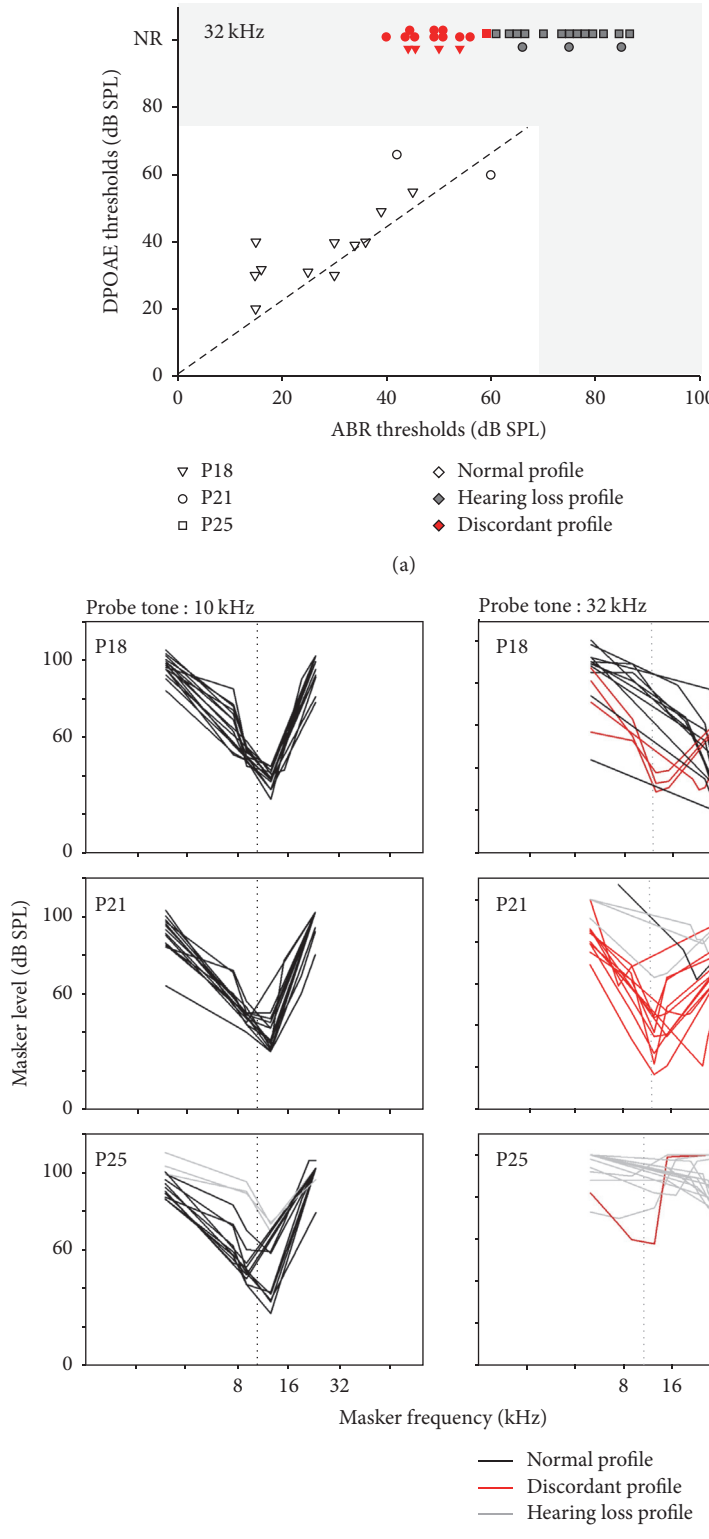

Figure 3: *Relationships between ABR and DPOAE thresholds and MTC at high frequencies*. Scatterplots of the individual DPOAE thresholds as a function of ABR thresholds at 32 kHz (a). Diagonal line: DPOAE and ABR thresholds are equal. Red symbols and red MTC correspond to individual with only slight increase in ABR thresholds (≤35 dB) but increase of DPOAE thresholds ≥40 dB or nonrecordable DPOAE (NR). The shaded areas correspond to the thresholds for which it is thought that OHCs have lost their function as they do not either generate gain, hence a 60 dB ABR threshold elevation, or emit distortion products. Individual masking tuning curves are presented for a probe tone at 10 kHz (b) and 32 kHz (c). Different symbols for different ages (see keys in (a)). Different lines for different MTC profiles (see keys in (c)).

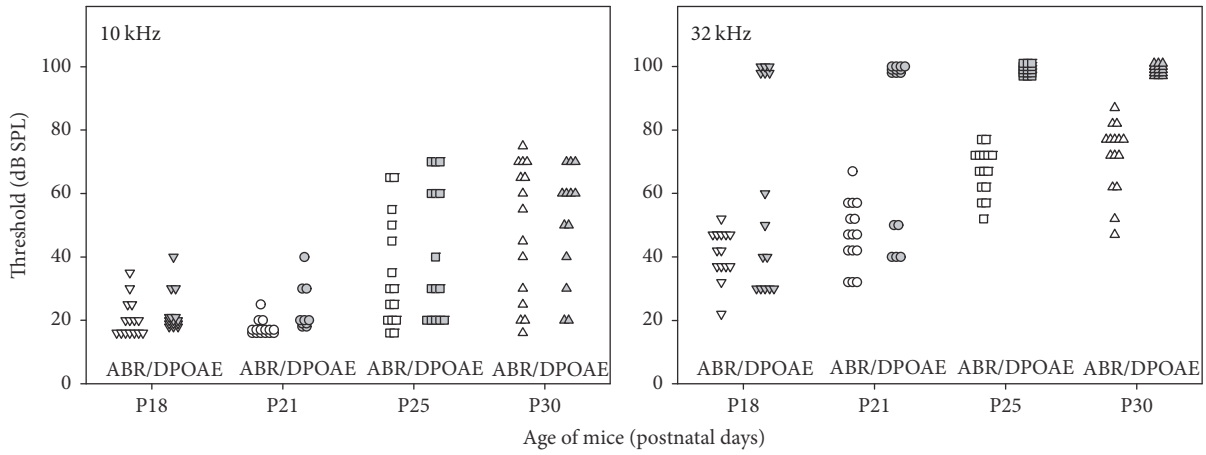

Figure 4: *ABR thresholds and DPOAE thresholds as a function of age*. Individual ABR hearing thresholds and individual DPOAE thresholds measured for P18, P21, P25, and P30 CD1 mice ($n = 15$, different symbols at different ages) at 10 and 32 kHz.

with no DPOAE in 10 mice at P21 and no DPOAE in all mice at P25 and P30.

At the intermediate frequency 22 kHz, ABR thresholds and DPOAE thresholds were still similar at P18 with corresponding MTC tips near the probe frequency (Figures 5(a) and 5(b)). At P21, 5 mice had no DPOAE despite only mildly elevated ABR thresholds, <40 dB SPL for some individuals (normal around 20 dB SPL). For those mice, the most efficient masking shifted towards lower frequencies (Figure 5(b), red curves). At P25, 8 mice presented a discordant profile similar to that previously described at 32 kHz and in 6 mice no MTC tip or tail could be identified (Figures 5(a) and 5(b)). Among the mice with discordant profile, some animals still had residual DPOAEs yet with a threshold near 70 dB SPL.

In all mice, ABR wave I latencies in response to a 10 kHz probe were around 1.5 ms for a stimulus at 40 dB SPL. At 22 and 32 kHz, for normal mice, they were, respectively, 0.85 and 1 ms (Figure 6). The difference in ABR wave I latencies at this sound level between 10 kHz and 22 and 32 kHz was consistent with the base-to-apex cochlea frequency map. In mice with discordant profiles, wave I latency at 22 and 32 kHz was near 1.5 ms, thus in the same range for 10 kHz tone-bursts.

3.3. Morphological Features Observed with Scanning Electron Microscope (SEM). We next looked at the OHC hair bundle aspect in different regions of the cochlea in CD1 mice (Figures 7 and 8). SEM analysis of the middle and basal regions of the cochlea showed hair bundle anomalies in OHCs but not IHCs (Figures 7(a)–7(g)). Some OHC hair bundles in this region displayed altered, asymmetrical, linear, or hooked shapes (Figures 7(a)–7(f)). In the basal region, OHC hair bundles remained anchored in the tectorial membrane (TM) by their taller raw of stereocilia even when bundles had abnormal shapes (Figures 7(h) and 7(i)).

A count of normal, altered, and missing OHC stereocilia bundles for each group of mice in the apical, middle, and basal region of the cochlea was achieved, and the results are shown in Figure 9. CD1-related OHC abnormalities are most evident in the basal region, with abnormal hair bundles in about 20% of cells from the earliest stage (Figure 8, red stars; Figure 9(c)). After P21, the main defect is the large percentage of missing OHCs, up to 62% (Figure 8, yellow stars). In the middle region, the progression of OHC abnormalities is qualitatively similar yet milder, with about 10% abnormally shaped hair bundles, stable during the period of interest, and only 23% missing OHCs at P25 (Figure 8; Figure 9(b)). The apical part of the CD1 cochlea is almost immune from defects at P18 and P21 (Figures 8(a), 8(b), and 8(c); Figure 9(a)), and, only at P25, 5 and 6% of OHCs show disorganized bundles or are absent.

4. Discussion

In CD1 mice, progressive hearing loss, already present at high frequencies at P18, rapidly extends to lower frequencies by P25 as already reported [17–19]. The prominent contribution of OHCs to this hearing loss was documented using microscopy, whereas the well-acknowledged damage to afferent neurons coexisting with that affecting hair cells was not the focus of this study. The variability in the degrees and progression of respective damage to these structures, also well-accepted, is viewed as supporting the CD1 model as a suitable though accelerated model for human presbycusis that shares similar characteristics [24].

In some mice, hearing loss combined an increase in ABR thresholds with a concomitant increase in DPOAE detection thresholds at the same frequencies, accompanied by a gradual loss of OHCs. However, a subgroup of mice displayed discrepancies, at high frequencies, between elevated DPOAE thresholds and less affected ABR thresholds. When DPOAEs become undetectable (i.e., thresholds well above 70 dB SPL), this indicates a loss of OHC function in the basal cochlea, which is not consistent with the small elevation (≤35 dB) of ABR thresholds from 22 kHz up. The OHCs, a key element of the cochlear amplifier, are thought to increase cochlear sensitivity by 50–60 dB [20–23]. Complete loss of OHC function signaled by complete loss of DPOAEs should therefore lead to an increase in hearing levels well

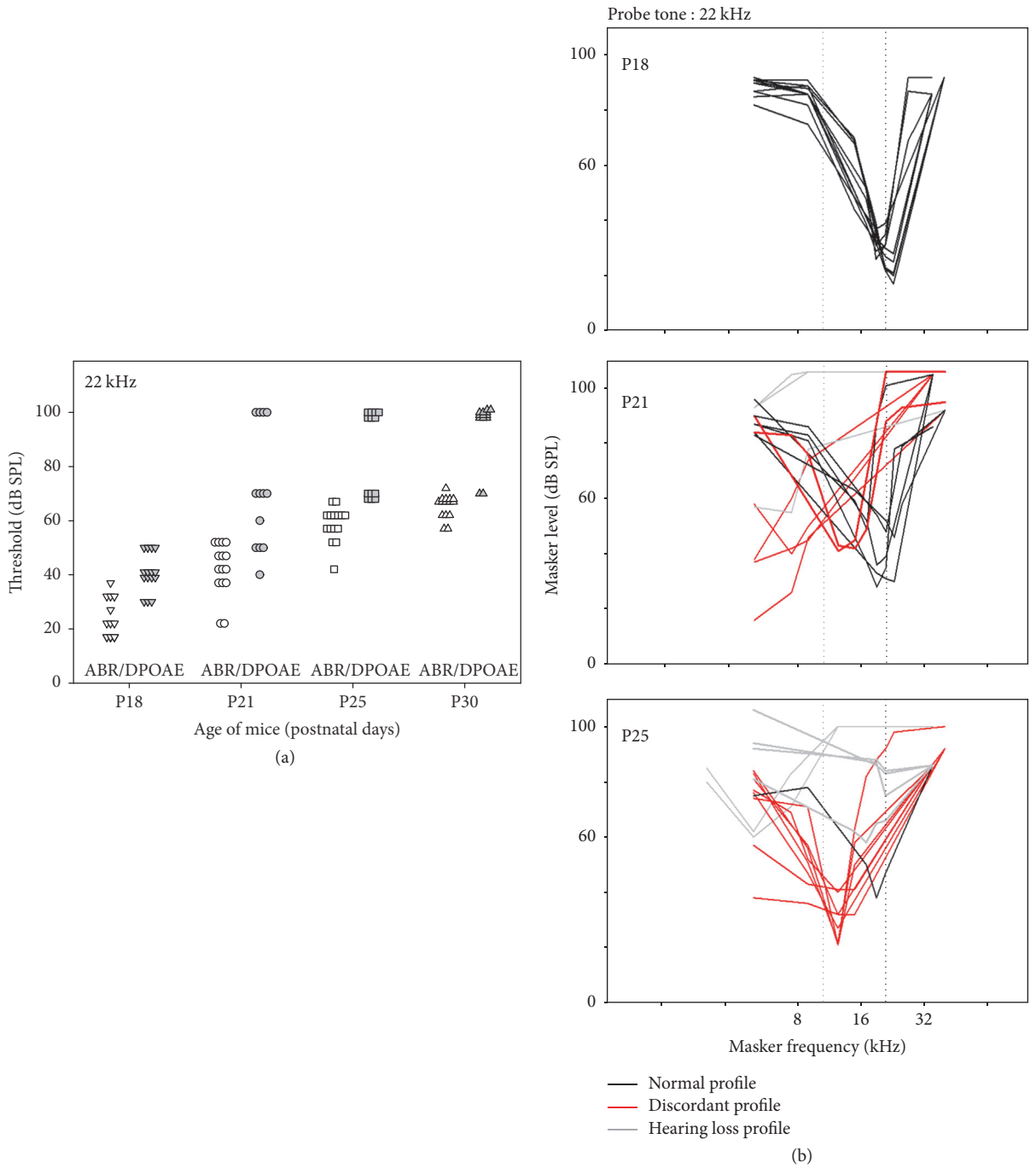

Figure 5: *Distribution of ABR hearing thresholds and DPOAE thresholds and MTC at 22 kHz.* Individual ABR hearing thresholds and individual DPOAE thresholds measured for P18, P21, P25, and P30 CD1 mice (n = 15, different symbols at different ages) at 22 kHz (a). Individual masking tuning curves for a probe tone at 22 kHz (b).

above 35 dB, which is not the case in the "discordant profile" presented by these CD1 mice.

This profile is associated with a tonotopic disorder, revealed by a large shift in the best masking frequency of MTC towards the low frequencies when the probe tone-burst is set within the interval with discordant DPOAE versus ABR thresholds. A possible pitfall of the MTC technique relates to the presence of a transient low-frequency artefact sound in addition to the high-frequency stimulus, which if intense enough would produce a spurious ABR response from the still normally sensitive apical part of the cochlea. However, the envelope of the probe tone-burst was a Blackman-Harris window that optimally softens the rising and falling transients driving the earphone. Although tone-bursts at and above 20 kHz did present a secondary low-frequency artefact around 10–12 kHz, its amplitude was more than 45 dB below

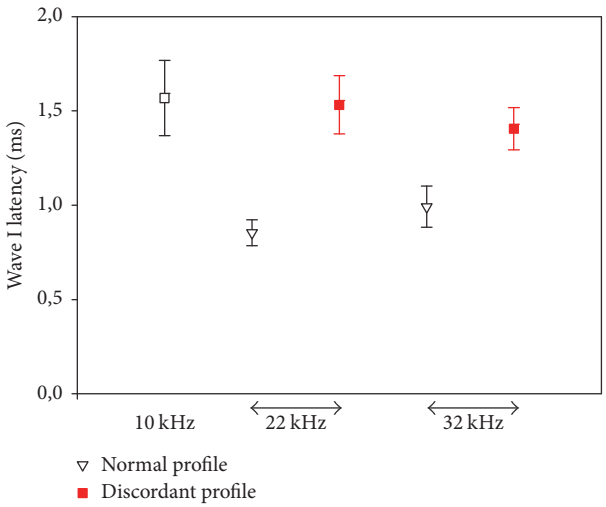

FIGURE 6: *ABR wave I latency* at 10, 22, and 32 kHz for a stimulus sound level of 40 dB SPL in mice presenting normal and discordant profiles.

the main stimulus peak. Thus, with a high-frequency probe level <65 dB SPL for plotting a MTC, this artefact is too low for the apical cochlea, even when still normally sensitive, to respond.

A normal masking curve is made of two parts, a sharp tip centered on the probe frequency at which masking is obtained for the lowest masker level and a broad tail at lower frequencies, at which maskers about 40–50 dB above probe level can still exert efficient masking. Masking occurs when action potentials produced by a probe tone just above its detection threshold, which activates only the auditory neurons most sensitive to it, are swamped by the activity produced in the same neurons by a masker sound at another frequency. In a masking experiment, the ability to respond to the probe or masker sounds is not an intrinsic property of the neurons, but of the inner hair cells to which the responding neurons are connected. Ultimately, inner hair cell responses passively reflect the local cochlear micromechanics chiefly determined by OHCs (e.g., [25]) and so does masking. Caveats to this rule, discussed later, are that in the presence of either of the regions with dead neurons or of leaking propagation channels that would bypass the basilar membrane [14], masking may be determined, not by OHC status at the place tuned to the probe tone, but rather, at the off-resonance place where neuronal responses to the probe are generated. Hence, the fact that a fraction of CD1 cochlear neurons may have suffered damage at the tested stage could only influence the size of neuronal responses to probe or masker tones, not the frequency dependence of the masking phenomenon itself.

Hypersensitive tails of a masking curve, one possible description of the shifted masking curves observed here, have received first explanation from the study of Liberman and Dodds [25] where single unit tuning curves presenting a hypersensitive low-frequency region were reported, particularly from neurons coming from cochlear places with OHCs disconnected from the TM. A systematic description of the phenomenon on the single unit level was performed in noise exposed guinea pigs [26]. While the loss of the tip reflects the loss of active resonance of the cochlear amplifier, when OHCs no longer exert amplification, increased sensitivity to masking at low frequencies is attributed to the increased mobility of the TM, due to loss of coupling with the organ of Corti in absence of OHC [27] that confers to the cochlear base an increased sensitivity to low-frequency maskers. In less severe circumstance, where OHCs are damaged but present, the MTC tip is located at the characteristic frequency and an increase in tail sensitivity is also visible [26].

The "discordant profile" of CD1 mice does not correspond to already described models of hypersensitive masking tail, in that the masking of high-frequency probes by low-frequency maskers is greater with MTCs forming a marked drop, down to levels near the probe level (Figure 3(c)). In MTC with standard "hypersensitivity of the tail," the masking effect occurs at a level only about 20 dB lower than in a normal MTC. The "discordant profile" is thus more reminiscent of "dead regions," where the neuronal response to stimuli at frequencies corresponding to these zones in which inner hair cells or neurons are totally lost is shifted to functional adjacent areas [28]. Thus, the MTCs obtained in this case have their tip at a frequency corresponding to the nearest functional region, as it is from this region that neuronal responses to the probe come. The stimulus must be of sufficient intensity for the vibration to propagate to the functional area. In the case of the CD1 "discordant profile," it seems difficult, however, to assume that a probe stimulus at 32 kHz and at about 65 dB SPL would be sufficient to produce a response of the place tuned to the MTC tip, around 12 kHz. The "discordant profile" of CD1 seems correlated with a presence of basal OHC whose stereociliary bundles sometimes exhibit abnormal conformations, as it tends to disappear once significant OHC losses appear (Figure 3(c) at P25). A coupling persists between these disorganized stereociliary bundles and the overhanging TM, as evidenced by the imprints found on its inferior side (Figure 7(h)). This profile resembles the recently reported *Nherf1*$^{-/-}$ mice profile, which present shifted MTC tips and extant yet totally nonfunctional basal OHCs with deeply altered hair bundles. The hypothesis formulated in the study of *Nherf1*$^{-/-}$ mice was that the tip of MTCs revealed that the responses to high-frequency probes actually came from more apical places than allowed by the normal tonotopy. Propagation of sound waves along the basilar membrane, as what happens in the case of basal dead regions, would have been too attenuated to allow deep tips to be observed and it was proposed that propagation occurred along the TM in relation to its persistent coupling with nonfunctional OHCs, able to leak vibrations without filtering them. Whereas the *Nherf1*$^{-/-}$ profile is caused by the genetic lack of one molecule of the hair bundle, resulting in targeted alterations of the OHC stereocilia, the "discordant profiles" found in the outbred strain CD1 do not occur in all mice, whose degrees of hearing loss and patterns of stereocilia defects are highly variable and occur in variable degrees (Figures 3(a) and 3(c)). Indeed, from P25 to 32 kHz, this profile is replaced by a more traditional sensorineural hearing loss. Of course, one cannot exclude the fact that the

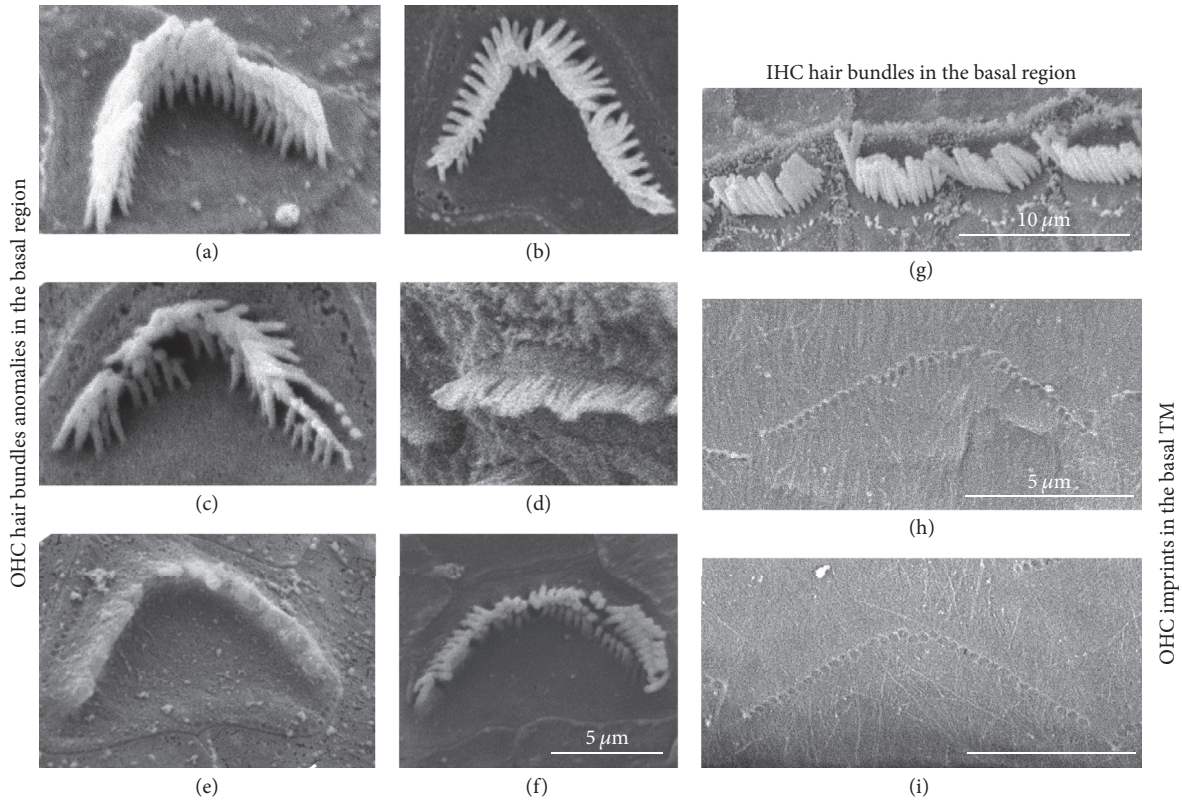

Figure 7: *Abnormal hair bundle shapes observed in the basal cochlear region*. SEM pictures of organ of Corti sections ((a)–(g)) and of tectorial membrane (TM) ((h), (i)) from CD1 mice. (a) Normal OHC hair bundle. (b) Asymmetrical hair bundle. (c) OHC with damaged stereocilia. (d) Linear OHC hair bundles. (e) OHC with fused stereocilia. (f) Hook-shaped OHC hair bundle. (g) Normal appearance of IHCs. ((h), (i)) Imprints left by abnormal (h) and normal (i) OHC stereocilia bundles in the TM in the basal region of cochlea.

"discordant profiles" of CD1 mice represent a form of extreme "hypersensitivity of the tail," with the place responding to high-frequency probe tones being still at its normal tonotopic place. The unusual intensity with which distorted modes of vibration occur in response to lower frequency maskers would be due to the abnormal basal mechanics produced by a peculiar coupling between the TM and abnormal OHCs.

Some CD1 mice presented a less pure "discordant profile" than *Nherf1*$^{-/-}$ mice with the presence of residual DPOAE at 22 kHz (Figure 5). A persistent ability to generate small DPOAEs, absent in *Nherf1*$^{-/-}$ mice and in CD1 mice at 32 kHz, does not preclude that coupling with the TM might be at the origin of a perturbed tonotopy as hypothesized above.

Irrespective of the explanatory mechanics, the expected perceptive consequences of a "discordant" functional pattern as described here are a rather better sensitivity to high frequencies than the one predicted with totally nonfunctional OHCs, allowing a sort of off-frequency listening to occur. As a counterpart, the "better than expected" ability to detect high frequencies, with an optimistic pure-tone audiogram that does not attract the clinician's attention, comes with no guarantee that suprathreshold behavior is normal, with the additional penalty of increased sensitivity to low-frequency masking. In clinical studies, it has been reported that minimal losses on high frequencies (≤30 dB), observed in some subjects, have deleterious effects on speech perception, normally associated with low or medium frequencies [15]. This decrease in intelligibility could result from suprathreshold deficiencies caused by OHC damage. Recently, another study found a correlation between loss of OHC function and reduced speech-in-noise performance, in subjects with minimal high-frequency hearing loss [16]. The "discordant profile" presented by some CD1 mice may therefore correspond to a reality in some patients, complaining of impaired intelligibility, but with normal audiometric thresholds and no neural alteration.

In conclusion, although it has been rightly emphasized that a clinical pattern with difficulties in the presence of noise out of proportion with the pure-tone audiogram should raise the possible diagnosis of auditory-neuropathy spectrum disorder [11], such difficulties may also be the hallmark of abnormal OHC function, when atypical OHC lesions occur [17], which the present work confirms, moreover, in an animal model that is thought to be a good model of the most frequent cause for sensorineural hearing loss, presbycusis [24]. An easy means for separating the two frameworks lies beyond pure-tone audiometry, with a contrast between extant OAEs and distorted ABRs in the case of neuropathy and absent OAEs and normal ABRs, in the case of "discordant profile."

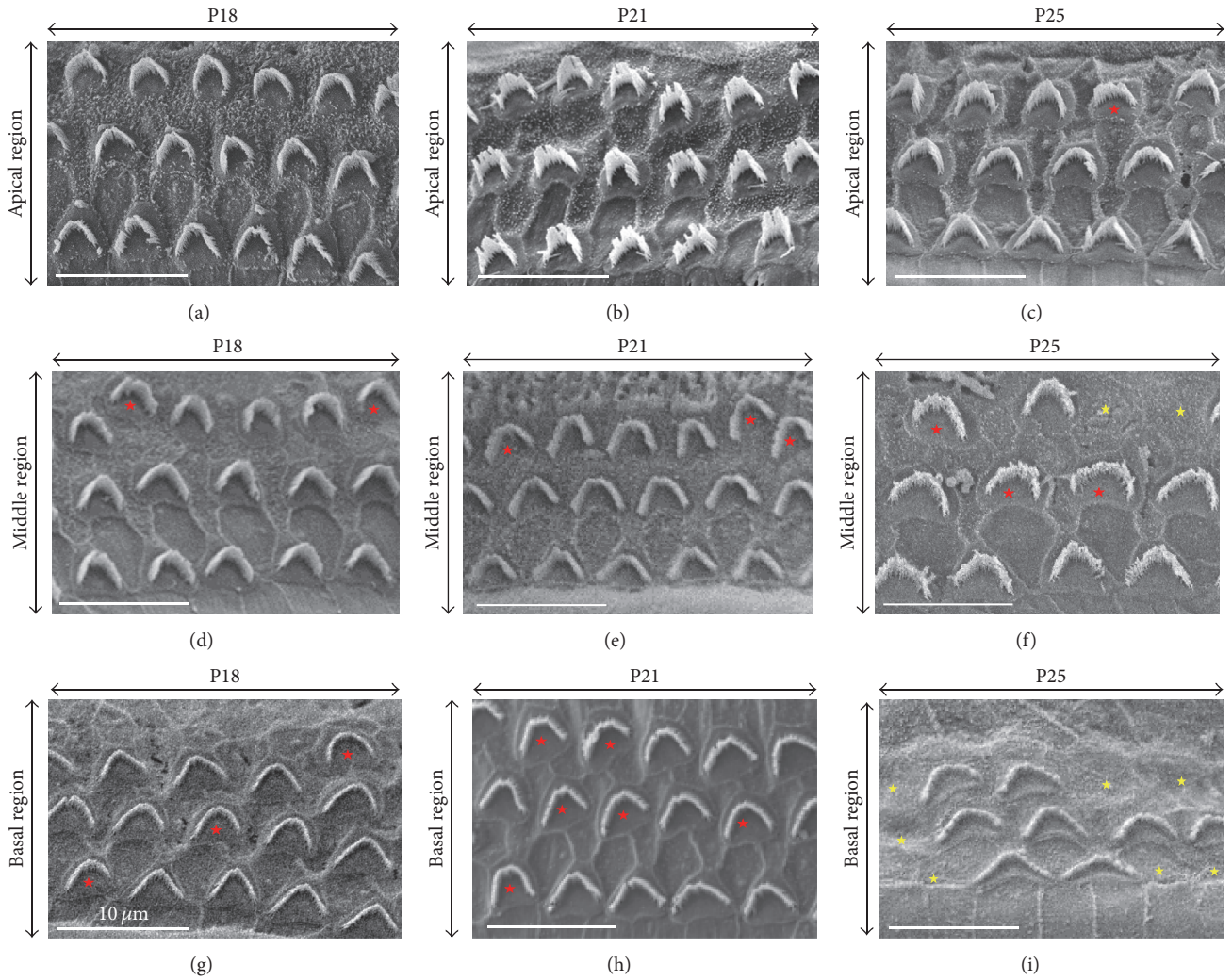

Figure 8: *Abnormal OHC hair bundle shapes observed at the cochlear base in CD1 mice.* SEM pictures of organ of Corti sections from CD1 mice at P18 ((a), (d), and (g)), P21 ((b), (e), and (h)), and P25 ((c), (f), and (i)). ((a), (b)) In the apical region, the OHC stereocilia bundles are normal at P18 and P21. (c) This apical section contains one OHC with an abnormal linear shape (red star). ((d), (e), and (f)) In the middle region at P18, P21, and P25, abnormal stereocilia bundles are found (asymmetric, linear, or hook-shaped) (red stars), and a few OHCs are missing at P25 (yellow stars). ((g), (h), and (i)) In the basal region, abnormal stereocilia bundles are observed at P18 and P21 (red stars, (g), (h)) and OHC losses are seen at P25 (yellow stars, (i)).

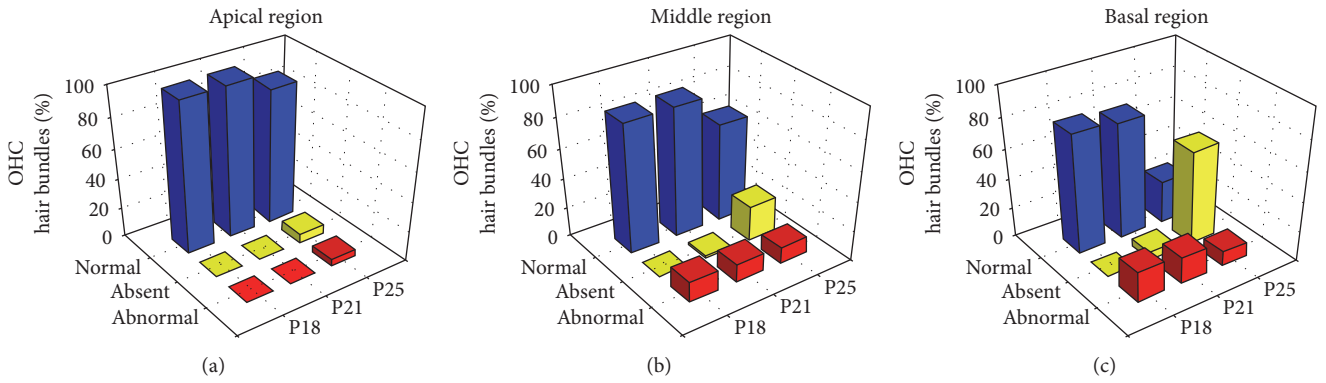

Figure 9: *The percentage of abnormal stereocilia bundles is greater at the base of the CD1 cochlea.* Amount of normal, abnormal, and absent OHC stereocilia bundles for P18 ($N = 4$), P21 ($N = 6$), and P25 ($N = 4$) CD1 mice in the apical, middle, and basal region.

Abbreviations

ABR: Auditory brainstem response
CM: Cochlear microphonic
DPOAE: Distortion product otoacoustic emission
ENT: Ear, nose, and throat
FEG: Field emission gun
HL: Hearing loss
HMDS: Hexamethyldisilazane
IHC: Inner hair cell
MTC: Masking tuning curve
OAE: Otoacoustic emission
OHC: Outer hair cell
PBS: Phosphate buffer saline
PFA: Paraformaldehyde
PHEM: Pipes, Hepes, Egtazic acid, and Magnesium
SNHL: Sensorineural hearing loss
SPL: Sound pressure level
TM: Tectorial membrane.

Additional Points

Highlights. (i) In CD1 mice, abnormal OHC function can come with near-normal auditory thresholds. (ii) The discrepancy occurs where hair cell to tectorial-membrane connections are abnormal. (iii) Low frequency masking of the high frequencies is excessive in CD1. (iv) Performance at threshold hides suprathreshold auditory impairment.

Conflicts of Interest

The authors declare that they have no conflicts of interest.

Acknowledgments

The research was initiated with the support of Fondation des Gueules Cassées (Grant 20-2013) and Capes-Cofecub (no. Me861/15 DANPE). One of the authors (Marion Souchal) received a grant from Groupe Entendre (GIPA2).

References

[1] H. F. Schuknecht, R. S. Kimura, and P. M. Naufal, "The pathology of sudden deafness," *Acta Oto-Laryngologica*, vol. 76, no. 1-6, pp. 75–97, 1973.

[2] T. Yamasoba, F. R. Lin, S. Someya, A. Kashio, T. Sakamoto, and K. Kondo, "Current concepts in age-related hearing loss: epidemiology and mechanistic pathways," *Hearing Research*, vol. 303, pp. 30–38, 2013.

[3] A. C. Y. Wong and A. F. Ryan, "Mechanisms of sensorineural cell damage, death and survival in the cochlea," *Frontiers in Aging Neuroscience*, vol. 7, article 58, 2015.

[4] B. C. J. Moore, *Cochlear Hearing Loss: Physiological, Psychological, and Technical Issues*, Wiley, Chichester, UK, 2nd edition, 2007.

[5] S. Kim, D. R. Frisina, and R. D. Frisina, "Effects of age on contralateral suppression of distortion product otoacoustic emissions in human listeners with normal hearing," *Audiology and Neurotology*, vol. 7, no. 6, pp. 348–357, 2002.

[6] B. C. J. Moore, "Frequency selectivity and temporal resolution in normal and hearing-impaired listeners," *British Journal of Audiology*, vol. 19, no. 3, pp. 189–201, 1985.

[7] C. J. Plack, D. Barker, and G. Prendergast, "Perceptual consequences of 'hidden' hearing loss," *Trends in Hearing*, vol. 18, 2014.

[8] A. Starr, T. W. Picton, Y. Sininger, L. J. Hood, and C. I. Berlin, "Auditory neuropathy," *Brain*, vol. 119, no. 3, pp. 741–753, 1996.

[9] S. G. Kujawa and M. C. Liberman, "Synaptopathy in the noise-exposed and aging cochlea: primary neural degeneration in acquired sensorineural hearing loss," *Hearing Research*, vol. 330, pp. 191–199, 2015.

[10] M. C. Liberman and S. G. Kujawa, "Cochlear synaptopathy in acquired sensorineural hearing loss: Manifestations and mechanisms," *Hearing Research*, vol. 349, pp. 138–147, 2017.

[11] M. C. Liberman, M. J. Epstein, S. S. Cleveland, H. Wang, and S. F. Maison, "Toward a differential diagnosis of hidden hearing loss in humans," *PLoS ONE*, vol. 11, no. 9, Article ID e0162726, 2016.

[12] A. J. Oxenham, "Predicting the Perceptual Consequences of Hidden Hearing Loss," *Trends in Hearing*, vol. 20, 2016.

[13] S. N. Merchant and J. B. Nadol, *Schuknechts Pathology of the Ear*, Peoples Medical Publishing House, Shelton Shelton, 3rd edition, 2010.

[14] K. Kamiya, V. Michel, F. Giraudet et al., "An unusually powerful mode of low-frequency sound interference due to defective hair bundles of the auditory outer hair cells," *Proceedings of the National Acadamy of Sciences of the United States of America*, vol. 111, no. 25, pp. 9307–9312, 2014.

[15] A. C. Léger, B. C. J. Moore, and C. Lorenzi, "Abnormal speech processing in frequency regions where absolute thresholds are normal for listeners with high-frequency hearing loss," *Hearing Research*, vol. 294, no. 1-2, pp. 95–103, 2012.

[16] R. Hoben, G. Easow, S. Pevzner, and M. A. Parker, "Outer hair cell and auditory nerve function in speech recognition in quiet and in background noise," *Frontiers in Neuroscience*, vol. 11, article no. 157, 2017.

[17] S. Le Calvez, P. Avan, L. Gilain, and R. Romand, "CD1 hearing-impaired mice. I: Distortion product otoacoustic emission levels, cochlear function and morphology," *Hearing Research*, vol. 120, no. 1-2, pp. 37–50, 1998.

[18] S. Le Calvez, A. Guilhaume, R. Romand, J. M. Aran, and P. Avan, "CD1 hearing-impaired mice. II: Group latencies and optimal f2/f1 ratios of distortion product otoacoustic emissions, and scanning electron microscopy," *Hearing Research*, vol. 120, no. 1-2, pp. 51–61, 1998.

[19] G. Shone, Y. Raphael, and J. M. Miller, "Hereditary deafness occurring in cd/1 mice," *Hearing Research*, vol. 57, no. 1, pp. 153–156, 1991.

[20] P. Dallos, "Cochlear amplification, outer hair cells and prestin," *Current Opinion in Neurobiology*, vol. 18, no. 4, pp. 370–376, 2008.

[21] A. J. Hudspeth, "Making an Effort to Listen: Mechanical Amplification in the Ear," *Neuron*, vol. 59, no. 4, pp. 530–545, 2008.

[22] A. J. Hudspeth, "Mechanical amplification of stimuli by hair cells," *Current Opinion in Neurobiology*, vol. 7, no. 4, pp. 480–486, 1997.

[23] L. Robles and M. A. Ruggero, "Mechanics of the mammalian cochlea," *Physiological Reviews*, vol. 81, no. 3, pp. 1305–1352, 2001.

[24] S. Mahendrasingam, J. A. Macdonald, and D. N. Furness, "Relative time course of degeneration of different cochlear structures in the CD/1 mouse model of accelerated aging.," *Journal of the Association for Research in Otolaryngology : JARO*, vol. 12, no. 4, pp. 437–453, 2011.

[25] M. C. Liberman and L. W. Dodds, "Single-neuron labeling and chronic cochlear pathology. III. Stereocilia damage and alterations of threshold tuning curves," *Hearing Research*, vol. 16, no. 1, pp. 55–74, 1984.

[26] H. Versnel, V. F. Prijs, and R. Schoonhoven, "Auditory-nerve fiber responses to clicks in guinea pigs with a damaged cochlea," *The Journal of the Acoustical Society of America*, vol. 101, no. 2, pp. 993–1009, 1997.

[27] J. J. Guinan Jr., "How are inner hair cells stimulated? Evidence for multiple mechanical drives," *Hearing Research*, vol. 292, no. 1-2, pp. 35–50, 2012.

[28] B. C. J. Moore and J. I. Alcántara, "The use of psychophysical tuning curves to explore dead regions in the Cochlea," *Ear and Hearing*, vol. 22, no. 4, pp. 268–278, 2001.

Hindawi
BioMed Research International
Volume 2018, Article ID 7601232, 9 pages
https://doi.org/10.1155/2018/7601232

Research Article

Susceptibility of Diabetic Mice to Noise Trauma

Wook Kyoung Han,[1] Eung Hyub Kim,[1] Sun-Ae Shin,[1,2] Dong-Sik Shin,[3] Bong Jik Kim,[1] Ah-Ra Lyu ,[1,2] and Yong-Ho Park [1,4]

[1] *Department of Otolaryngology-Head and Neck Surgery, College of Medicine, Chungnam National University, Daejeon, Republic of Korea*
[2] *Department of Medical Science, College of Medicine, Chungnam National University, Daejeon, Republic of Korea*
[3] *Biomedical Convergence Research Center, Chungnam National University Hospital, Daejeon, Republic of Korea*
[4] *Brain Research Institute, College of Medicine, Chungnam National University, Daejeon, Republic of Korea*

Correspondence should be addressed to Ah-Ra Lyu; ahmilove@naver.com and Yong-Ho Park; parkyh@cnu.ac.kr

Received 29 October 2017; Revised 26 December 2017; Accepted 17 January 2018; Published 12 February 2018

Academic Editor: Yoshifumi Saisho

Diabetes can lead to many end-organ complications. However, the association between diabetes and hearing loss is not well understood. Here, we investigated the effect of noise exposure on diabetic mice compared with wild-type mice. Hearing threshold shifts, histopathologic changes in the cochlea, and inflammatory responses were evaluated over time. After noise exposure, more severe hearing threshold shifts, auditory hair cell loss, and synaptopathies were notable in diabetic mice compared with wild-type mice. Moreover, increased inflammatory responses and reactive oxygen species production were observed in the ears of diabetic mice. The results demonstrated that diabetic mice are more susceptible to noise trauma.

1. Introduction

Diabetes is a representative metabolic disease that results in many complications [1–3]. In general, patients with diabetes are prone to inflammatory diseases and increased inflammatory responses in many organs [4–11] and are more vulnerable to trauma and tissue injuries in end organs [1, 3, 12–14]. Diabetes per se is regarded as a risk factor of many inflammatory diseases and trauma due to disrupted homeostasis and immune responses [4–6, 9, 11].

Hearing loss is a highly heterogeneous disorder, with multifactorial causes including infections, genetic etiologies, and physical or noise traumas to the inner ear. Hearing loss could occur congenitally or gradually reaching about a half in prevalence for those older than 75 (https://www.nidcd.nih.gov/health/statistics/quick-statistics-hearing). Hearing loss can be divided into sensorineural hearing loss, conductive hearing loss, mixed hearing loss, or neural hearing loss according to the mechanism of hearing loss. Specifically, noise-induced hearing loss is the second most frequent form of sensorineural hearing impairment and noise trauma is a well-studied universal trigger for hearing loss throughout the life with its main pathophysiologic mechanism based on mechanical destruction and metabolic decompensation, resulting in pathologies in ribbon synapses and organ of Corti [15–18]. Given that diabetes is a systemic metabolic disease affecting almost all parts of human body, it would be worth investigating the hearing loss in relation to diabetes.

Although there have been many reports on optic and peripheral neuropathies in diabetes, the association between diabetes and hearing loss is not well understood. Recently, meta-analysis and cohort studies showed that hearing impairment is associated with diabetes and insulin resistance [19–22], putting diabetic patients on an increased risk of future hearing loss.

Thus, we speculated that the cochlea of diabetic mice also responds differently to injuries and trauma such as noise compared with that of wild-type mice, and sensorineural hearing loss may be a delayed complication of diabetes. In this study, we aimed to evaluate the effect of noise trauma as well as the inflammatory responses in diabetic mice compared with wild-type mice via functional and morphologic studies.

2. Materials and Methods

2.1. Animals and Noise Exposure. All animal experiments were approved by the Chungnam National University Animal Experiment Committee (CNU00859). For this study, 30 C57BL/6J db/db ($^{++}$) mice and 30 age-matched wild-type mice at 7 weeks of age were used. In each group, 25 mice were exposed to noise, and the remaining five were not exposed to noise, serving as controls. The mice were exposed to broadband noise (250 to 8 kHz) at 116 dB SPL for 1 h in an acoustically insulated reverberation chamber. The noise signals were routed through a computer and amplifier (INTER-M R300 Plus power amplifier, Canford Audio PLC, Washington, UK) to a loudspeaker (ElectroVoice DH1A-WP, Sonic Electronix Inc., Sylmar, CA, USA). The noise level was measured using a sound level meter (B&K type 2250, Brüel & Kjaer, Naerum, Denmark), sound calibrator (B&K type 4231, Brüel & Kjaer), and a condenser microphone (B&K type 4189, Brüel & Kjaer).

2.2. Auditory Brainstem Response (ABR). Auditory brainstem response (ABR) was measured as previously reported [23]. The ABRs were recorded prior to, just after, and at 1 day, 1 week, and 2 weeks after noise exposure. Threshold shift was defined as the difference between the before- and after-noise exposure values. A positive threshold shift indicated an elevation of the auditory threshold.

2.3. Tissue Preparation and Immunohistochemistry. Animals were sacrificed, and cochlear tissues were obtained to assess survival of hair cells, nerve fibers, and the synaptic ribbon. Tissue preparations were performed as previously reported [23]. Auditory hair cells, nerve fibers, and the ribbon synapse were evaluated by incubating the tissues with rabbit anti-myosin VIIA (Proteus BioSciences, Inc., Ramona, CA, USA), mouse anti-NF200 (Novus Biologicals, Littleton, CO, USA), and mouse anti-C-terminal binding protein 2 primary antibodies (BD Biosciences, San Jose, CA, USA), respectively, diluted 1 : 200 in blocking solution overnight at 4°C. After rinsing in PBS for 10 min, the tissues were incubated with an Alexa Fluor 594-conjugated goat anti-rabbit secondary antibody (Molecular Probes, Eugene, OR, USA) or Alexa Fluor 488-conjugated goat anti-mouse secondary antibody (Molecular Probes) diluted 1 : 200 in PBS for 30 min. After another rinse in PBS for 10 min, the specimens were further dissected to separate individual cochlear turns and mounted on glass slides using Crystal Mount (Biomeda, Foster City, CA, USA). The specimens were observed under an epifluorescence microscope (Zeiss Axio Scope A1; Zeiss, Oberkochen, Germany) with a digital camera, and the number of stained hair cells per 100 μm of tissue was counted.

2.4. Quantitative Reverse-Transcription Polymerase Chain Reaction (qRT-PCR). To compare the inflammatory responses and production of reactive oxygen species (ROS) between groups, 5 diabetic and 5 wild-type animals were sacrificed at each time point after noise exposure. qRT-PCR was conducted to measure the expression of interleukin-1β (IL-1β), IL-6, nitric oxide synthase 2 (NOS2), tumor necrosis factor-α (TNF-α), and cyclooxygenase 2 (COX2), as indicators of the inflammatory response. Heme oxygenase-1 (HO-1), superoxide dismutase 1 (SOD1), catalase, and nuclear respiratory factor 1 (NRF1), as oxidative stress and ROS markers, were also measured. qRT-PCR was performed as previously reported [23]. The primers used are presented in Table 1. The time lines for all experiments are shown in Figure 1.

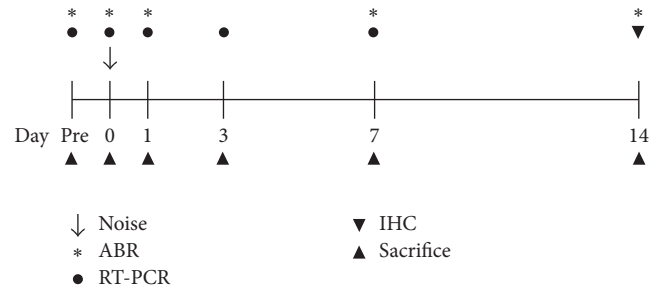

Figure 1: Schematic time course of the experiments. Auditory brainstem response (ABR) thresholds were measured prior to; immediately after; and at 1 day, 1 week, and 2 weeks after noise exposure. Reactive oxygen species and inflammatory responses were evaluated by quantitative reverse-transcription polymerase chain reaction (qRT-PCR) prior to; immediately after; and at 1 day, 3 days, and 1 week after noise exposure. The numbers of hair cells and inner hair cell synapses were assessed at 2 weeks after noise exposure. Five diabetic and 5 wild-type animals were used for each time point.

2.5. Image Processing and Statistical Analysis. Adjustment of image contrast, image superimposition, and colorization of monochrome fluorescence images were performed using Adobe Photoshop (version 7.0). Statistical analysis was performed using GraphPad Prism (version 3.02, San Diego, CA, USA) and SPSS (version 16.0, SPSS Inc., Chicago, IL, USA). ABR threshold shifts and the levels of ROS and inflammatory cytokines measured in each group were compared before and after noise exposure using one-way repeated measures analysis of variance (ANOVA), and the differences between groups at each time point were compared using one-way ANOVA. The numbers of surviving hair cells and synapses between groups were compared using the Kruskal–Wallis test. p values < 0.05 were considered significant.

3. Results

3.1. ABR Threshold Shifts. The ABRs were recorded prior to; immediately after; and at 1 day, 1 week, and 2 weeks after noise exposure. While the ABR threshold shifts recovered partially with time in wild-type mice, they did not recover in db/db mice until 2 weeks after noise exposure. ABR threshold shifts were significantly greater at 1 and 2 weeks after noise exposure in db/db mice compared with wild-type mice ($p < 0.05$) (Figure 2). These results suggested that db/db mice ears were more damaged and susceptible by noise exposure compared to wild-type mice.

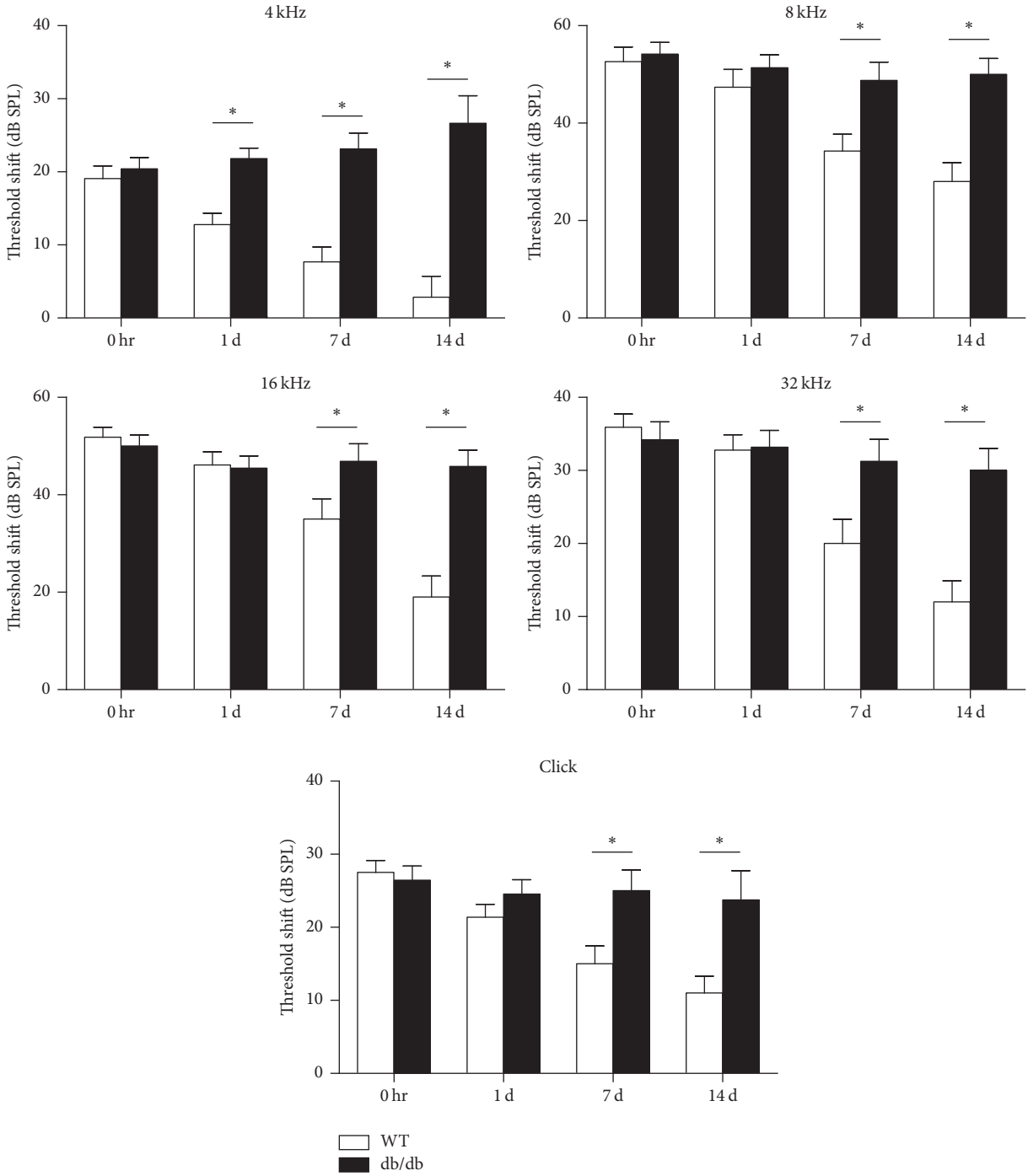

Figure 2: ABR threshold shifts immediately after noise exposure. ABR threshold shifts were greater in db/db mice compared with wild-type mice at 1 and 2 weeks after noise exposure at all frequencies evaluated. $^{*}P < 0.05$.

3.2. Loss of Auditory Hair Cells. Two weeks after noise exposure, almost all outer hair cells in the basal turn were destroyed in both db/db (Figure 3(B3)) and wild-type (Figure 3(A3)) mice, but greater preservation of the inner hair cells was evident in wild-type mice (Figure 3(A3)) compared with db/db mice (Figure 3(B3)). In the middle turn, greater preservation of the outer hair cells was observed in wild-type mice (Figure 3(A2)) compared with db/db mice (Figure 3(B2)). The number of surviving hair cells was also significantly higher in wild-type mice (Figure 4), suggesting that the auditory hair cells in db/db mice were more vulnerable to noise trauma.

3.3. Loss of Synapses in Inner Hair Cells. Two weeks after noise exposure, synapse loss in the middle turn of the cochlea was significantly more severe in db/db mice compared with wild-type mice (Figures 5(a), 5(b), and 5(c)). This suggested that, even in surviving inner hair cells, synaptopathies were

Table 1: The primer sequences used for quantitative reverse-transcription polymerase chain reaction.

	Forward	Reverse
GAPDH	TGTGTCCGTCGTGGATCTGA	CCTGCTTCACCACCTTCTTGAT
HO-1	CCCACCAAGTTCAAACAGTCT	AGGAAGGGGGTCTTAGCCTC
SOD1	GTATGGGGACAATACACAAGGC	GGCCACCATGTTTCTTAGAGTG
Catalase	TCA GGA TGT GGT TTT CAC TG	GTG TAA AAT TTC ACT GCA AAC
NRF1	GCT GCT GCG TGG CAA CAG	TTG GGT TTG GAG GGT GAG AT
IL-1β	TCTTTGAAGTTGACGGACCC	TGAGTGATACTGCCTGCCTG
IL-6	TCGTGGAAATGAGAAAAGAGTTG	AGTGCATCATCGTTGTTCATACA
TNF-α	CTGAGGTCAATCTGCCCAAGTAC	CTTCACAGAGCAATGACT CCAAAG
NOS2	GGCAGCCTGTGAGACCTTTG	GCATTGGAAGTGAAGCGTTTC
COX2	GGGTTAAACTTCCAAAGGAGACATC	CAGCCTGGCAAGTCTTTAACCT

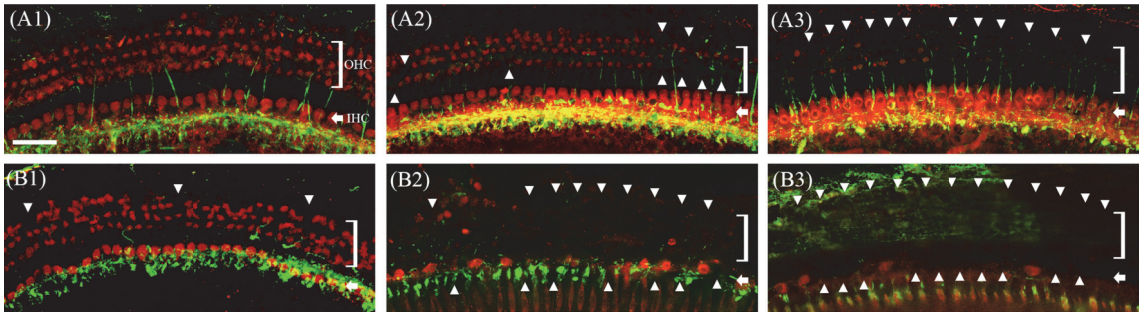

Figure 3: Whole mounts of the auditory epithelium from wild-type (A1, A2, and A3) and db/db mice (B1, B2, and B3) at 2 weeks after noise exposure. Tissues were stained for myosin VIIa (red) to identify the hair cells and for NF200 (green) to identify nerve fibers and then observed by epifluorescence microscopy. Hair cell loss was more severe in the middle (B2) and basal turns (B3) of the db/db compared with wild-type mice (A2 and A3). (A1) and (B1): apical turn; (A2) and (B2): middle turn; A3 and B3: basal turn; OHC: outer hair cell; IHC: inner hair cell; scale bar = 30 μm.

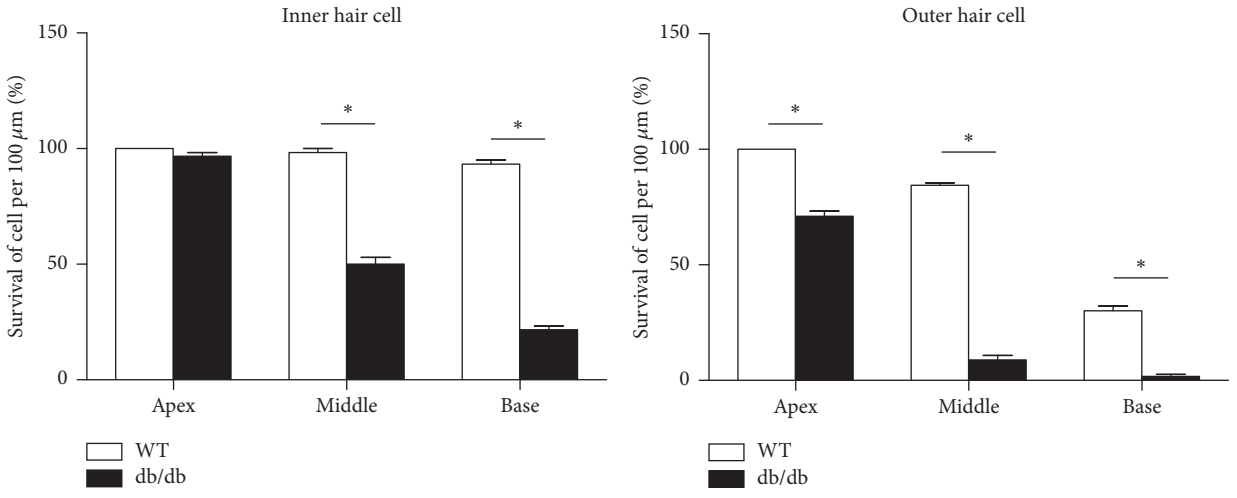

Figure 4: Surviving hair cell counts after surgery. Greater preservation of the outer hair cells was observed in all cochlear turns and of the inner hair cells in the middle and basal turns of wild-type mice compared with db/db mice. $^{*}p < 0.05$.

more severe in db/db mice than in wild-type mice after noise exposure. Synaptopathies in basal turn was not evaluable because almost all hair cells including inner hair cells were lost in the basal turn.

3.4. Changes in Markers of Oxidative Stress and ROS. After noise exposure, HO-1 and catalase levels were increased at 3 and 7 days, and SOD1 and NRF1 levels were increased at 7 days in db/db mice compared with wild-type mice. The mild increases in HO-1 and NRF1 levels observed in wild-type mice immediately after noise exposure returned to normal levels with time. These results suggested that ROS production after noise exposure was greater in db/db mice compared with wild-type mice (Figure 6).

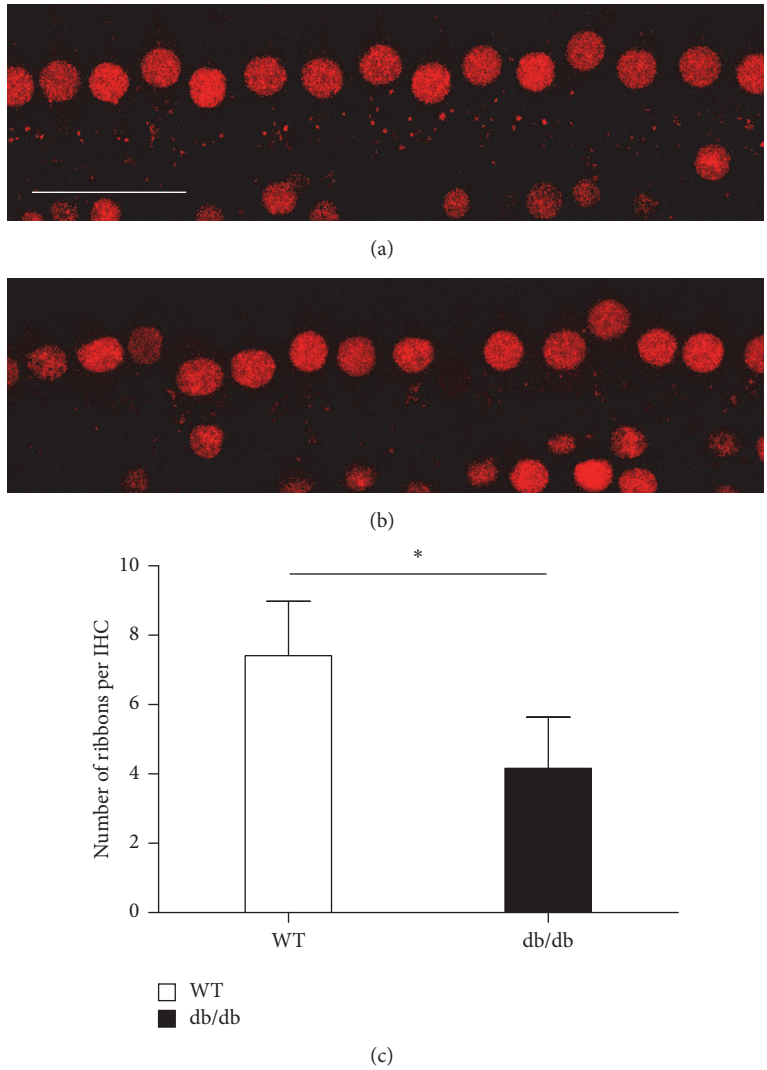

Figure 5: Inner hair cells and their afferent synapses in the middle turn after noise exposure. Tissues were stained for C-terminal binding protein 2 (red) to identify the presynaptic ribbons and then imaged using confocal microscopy. Loss of synapses was more severe in db/db mice (b) compared with wild-type mice (a, c). $^{*}p < 0.05$.

3.5. Changes in Inflammatory Cytokines. IL-1β, IL-6, and TNF-α levels were significantly increased at 3 and 7 days, NOS2 levels at 1 and 3 days, and COX2 levels at 1, 3, and 7 days after noise exposure in db/db mice compared with wild-type mice. The mild increases in IL-6 and COX2 observed in the wild-type mice immediately after noise exposure returned to normal levels with time (Figure 7). These results suggested that inflammatory responses in the cochlea were more severe in db/db mice than in wild-type mice.

4. Discussion

Diabetes can cause many organic complications as a result of neuropathies and angiopathies [1–3, 12]. The association between hearing loss and diabetes is not well known; however, several reports have shown that diabetes is associated with, and a potential risk factor for, hearing loss. Recently, large population studies have revealed that diabetes is an independent risk factor for hearing loss [19, 22, 24]. Kim et al. showed that diabetes was associated with the development of bilateral hearing loss in prospective cohort study [19] and there were reports that showed the association of hearing loss with both type 1 [20] and type 2 diabetes [21]. Furthermore diabetes is also associated with a poor prognosis in terms of recovery of sudden hearing loss [25–30]; Lin et al. revealed that the incidence of sudden hearing loss was 1.54-fold higher in the diabetic group compared with that in the nondiabetic group [27] and sudden hearing loss may be an initial symptom or complication of diabetes [31, 32]. Although the precise etiologies of these associations are not well known, they may involve histopathological changes in the cochlea including hair cells, spiral ganglion neurons (SGNs), and the lateral wall, according to studies in animal models of diabetes [24, 33, 34] and human temporal bone [35–39].

Noise is a common trauma imposed on the ear, and it can induce transient or permanent threshold shifts according

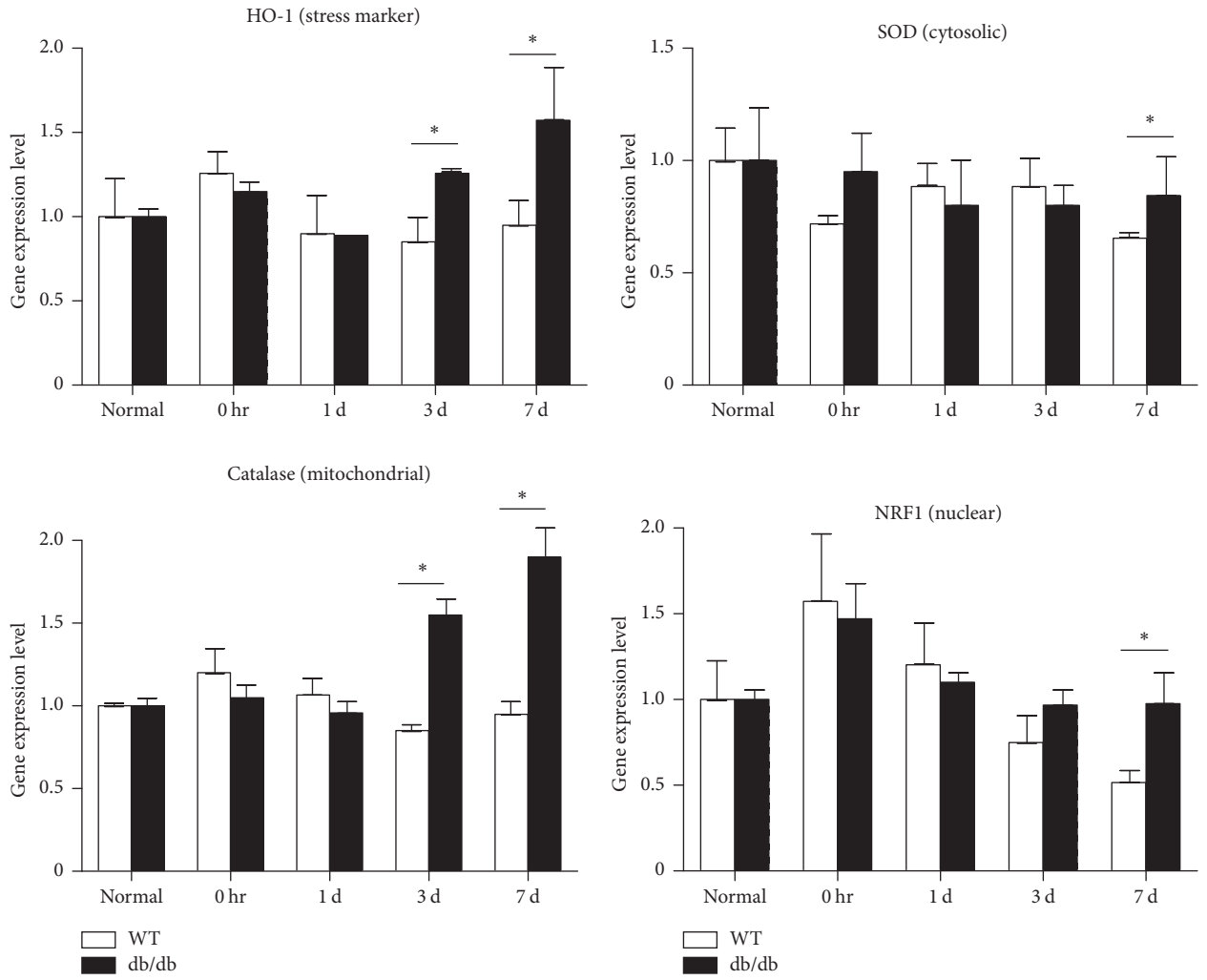

Figure 6: qRT-PCR analysis of reactive oxygen species after noise exposure. HO-1 and catalase levels were significantly increased in db/db compared with wild-type mice at 3 days and sustained until 7 days, after noise exposure. Superoxide dismutase 1 (SOD1) and nuclear respiratory factor 1 (NRF1) levels were significantly increased in db/db mice at 7 days after noise exposure. $^{*}p < 0.05$.

to the level and timing of the noise exposure. In this study, we compared the effect of noise on hearing threshold shifts between diabetic and wild-type mice. The results indicated that hearing loss was more severe in diabetic mice compared with wild-type mice. Although we used a transient hearing threshold shift model, the hearing threshold shift did not recover in diabetic mice compared with wild-type mice until 2 weeks after noise exposure and resulted in loss of hair cells and synaptopathies, especially in the middle and basal turns of the cochlea. This coincided well with other reports that streptozocin-induced diabetic mice exhibited greater susceptibility to noise trauma, decreased cochlear blood flow, SGN loss, and failed recovery of ABR threshold shifts and distortion product otoacoustic emissions [13]. In addition, another report showed no recovery of hearing threshold after noise-induced temporary hearing loss in diabetic mice [14].

Noise can induce inflammatory responses in the cochlea, as well as tissue injury and hearing loss [40, 41]. Tan et al. showed that acute and chronic noise exposure could induce the expression of proinflammatory mediators in the cochlea and mediate the recruitment and extravasation of inflammatory cells into the cochlea. As a result, they postulated that cochlear inflammatory response could be induced by noise exposure [40]. Besides, Liu et al. reported the increased level of inducible and endothelial NOS in diabetic rat cochleae, which might be involved in the cochlear functional loss [42]. Thus, in this study, we compared the inflammatory response in the cochlea after noise exposure between diabetic and wild-type mice. As a result, oxidative stress and ROS markers were increased in both diabetic and wild-type mice during the early stage following noise exposure; however, the increased HO-1 level was sustained until 7 days after noise exposure in the diabetic mice, suggesting that ROS production is increased for longer in diabetic compared with wild-type mice.

The inflammatory cytokines IL-1β, IL-6, NOS2, TNF-α, and COX2 were also significantly increased in diabetic

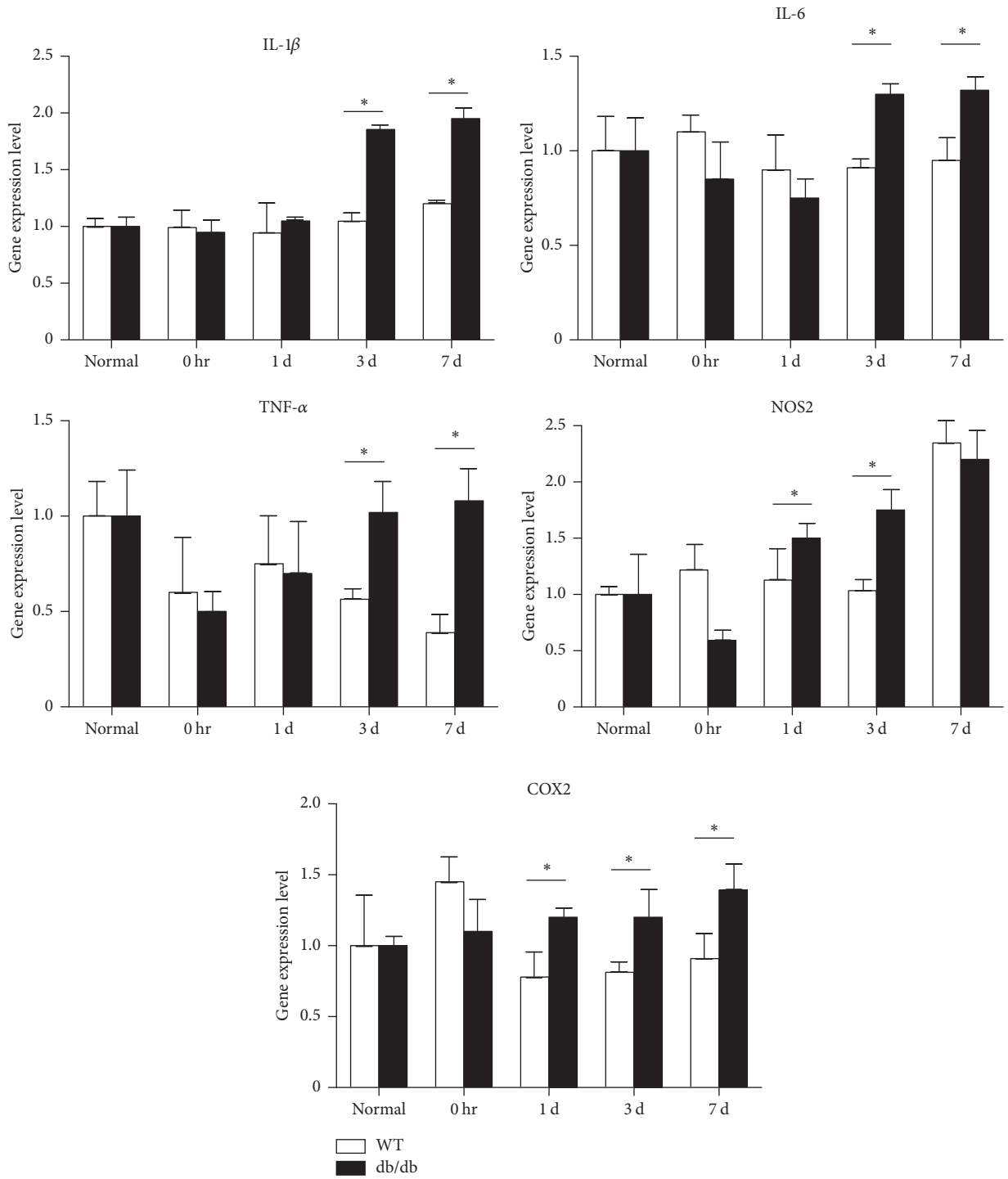

Figure 7: qRT-PCR analysis of inflammatory markers after noise exposure. Significantly increased expression was seen for cyclooxygenase 2 (COX2) at 1, 3, and 7 days, for IL-1β, IL-6, and TNF-α at 3 days and 1 week, and for nitric oxide synthase 2 (NOS2) at 3 days after noise exposure in db/db compared with wild-type mice. $^{*}p < 0.05$.

mice compared with wild-type mice. These results indicate an elevated inflammatory response in diabetic mice, which may induce greater oxidative stress and ROS production and, thereby, tissue damage such as hair cell loss and synaptopathies. This result was supported by previous report showing that N-acetylcysteine, a powerful antioxidant, attenuated the degree of noise-induced permanent hearing loss in diabetic rats [43].

In this study, we investigated the effect of noise exposure on diabetic mice compared with wild-type mice. Diabetic mice showed a more severe hearing threshold shift, hair cell loss, and synaptopathies compared with wild-type mice.

Increased inflammatory responses and ROS production are possible reasons for these effects in diabetic mice. So we thought that ROS scavengers or anti-inflammatory reagents would be applicable for the prevention of diabetes associated hearing loss.

5. Conclusion

Taken together, our study suggests that diabetic mice seem to be more susceptible to noise trauma than wild-type mice. This might lead to more robust hearing loss in diabetic mice, as evidenced by more severe hair cell damage and synaptopathy due to increased inflammatory responses and ROS production in diabetic mice.

Additional Points

The English in this document has been checked by at least two professional editors, both native speakers of English. For a certificate, please see the following: http://www.textcheck.com/certificate/gLdxYL.

Conflicts of Interest

The authors declare that there are no conflicts of interest regarding the publication of this paper.

Authors' Contributions

Wook Kyoung Han and Eung Hyub Kim contributed equally to this work.

Acknowledgments

This work was supported by a Chungnam National University Hospital Research Fund 2014 and the Basic Science Research Program through the National Research Foundation of Korea (NRF), funded by the Ministry of Education (NRF-2015R1D1A3A01018881 to Yong-Ho Park).

References

[1] J. M. Forbes and A. K. Fotheringham, "Vascular complications in diabetes: old messages, new thoughts," *Diabetologia*, vol. 60, no. 11, pp. 2129–2138, 2017.

[2] M. A. Bodman and S. C. Dulebohn, *Neuropathy, Diabetic. StatPearls. Treasure Island (FL)*, StatPearls Publishing StatPearls Publishing LLC, 2017.

[3] S. Giatti, R. Mastrangelo, M. D'Antonio et al., "Neuroactive steroids and diabetic complications in the nervous system," *Frontiers in Neuroendocrinology*, 2017.

[4] S. R. Ramirez and M. R. K. Dasu, "Toll-like receptors and diabetes complications: Recent advances," *Current Diabetes Reviews*, vol. 8, no. 6, pp. 480–488, 2012.

[5] N. Esser, S. Legrand-Poels, J. Piette, A. J. Scheen, and N. Paquot, "Inflammation as a link between obesity, metabolic syndrome and type 2 diabetes," *Diabetes Research and Clinical Practice*, vol. 105, pp. 141–150, 2014.

[6] S. K. Sonnenschein and J. Meyle, "Local inflammatory reactions in patients with diabetes and periodontitis," *Periodontology 2000*, vol. 69, no. 1, pp. 221–254, 2015.

[7] H. S. Herlitz-Cifuentes, P. C. F. Garcés, L. I. L. Fernández, and E. A. Guzmán-Gutiérrez, "Effect of systemic inflammation on the function of insulin and glucose metabolism in rheumatoid arthritis," *Current Diabetes Reviews*, vol. 12, no. 2, pp. 156–162, 2016.

[8] A. J. Scheen, N. Esser, and N. Paquot, "Antidiabetic agents: potential anti-inflammatory activity beyond glucose control," *Diabetes & Metabolism*, vol. 41, no. 3, pp. 183–194, 2015.

[9] R. Pop-Busui, L. Ang, C. Holmes, K. Gallagher, and E. L. Feldman, "Inflammation as a Therapeutic Target for Diabetic Neuropathies," *Current Diabetes Reports*, vol. 16, no. 3, article no. 29, pp. 1–10, 2016.

[10] K. C. Shih, K. S. Lam, and L. Tong, "A systematic review on the impact of diabetes mellitus on the ocular surface," *Nutrition & Diabetes*, vol. 7, no. 3, p. e251, 2017.

[11] H. Tilg, A. R. Moschen, and M. Roden, "NAFLD and diabetes mellitus," *Nature Reviews Gastroenterology & Hepatology*, vol. 14, no. 1, pp. 32–42, 2017.

[12] T. Wu, S. Qiao, C. Shi, S. Wang, and G. Ji, "Metabolomics window into diabetic complications," *Journal of Diabetes Investigation*, 2017.

[13] T. Fujita, D. Yamashita, S. Katsunuma, S. Hasegawa, H. Tanimoto, and K.-I. Nibu, "Increased inner ear susceptibility to noise injury in mice with streptozotocin-induced diabetes," *Diabetes*, vol. 61, no. 11, pp. 2980–2986, 2012.

[14] H.-P. Wu, T.-J. Cheng, C.-T. Tan, Y. L. Guo, and C.-J. Hsu, "Diabetes impairs recovery from noise-induced temporary hearing loss," *The Laryngoscope*, vol. 119, no. 6, pp. 1190–1194, 2009.

[15] E. Borg, B. Canlon, and B. Engstrom, "Noise-induced hearing loss: Literature review and experiments in rabbits: Morphological and electrophysiological features, exposure parameters and temporal factors, variability and interactions," *Scandinavian Audiology Supplementum*, vol. 24, no. 40, pp. 1–147, 1995.

[16] L. Shi, Y. Chang, X. Li, S. Aiken, L. Liu, and J. Wang, "Cochlear Synaptopathy and Noise-Induced Hidden Hearing Loss," *Neural Plasticity*, vol. 2016, Article ID 6143164, 9 pages, 2016.

[17] K. Hirose and M. C. Liberman, "Lateral wall histopathology and endocochlear potential in the noise-damaged mouse cochlea," *Journal of the Association for Research in Otolaryngology*, vol. 4, no. 3, pp. 339–352, 2003.

[18] S. G. Kujawa and M. C. Liberman, "Adding insult to injury: Cochlear nerve degeneration after "temporary" noise-induced hearing loss," *The Journal of Neuroscience*, vol. 29, no. 45, pp. 14077–14085, 2009.

[19] M. Kim, Y. Zhang, Y. Chang et al., "Diabetes mellitus and the incidence of hearing loss: a cohort study," *International Journal of Epidemiology*, 2016.

[20] Z.-P. Teng, R. Tian, F.-L. Xing et al., "An association of type 1 diabetes mellitus with auditory dysfunction: A systematic review and meta-analysis," *The Laryngoscope*, vol. 127, no. 7, pp. 1689–1697, 2017.

[21] E. P. U. Helzner and K. J. Contrera, "Type 2 Diabetes and Hearing Impairment," *Current Diabetes Reports*, vol. 16, no. 1, p. 3, 2016.

[22] H. J. Park, M. H. Yoo, S.-Y. Woo, S. W. Kim, and Y.-S. Cho, "Prevalence of hearing loss and associated factors in subjects

with normal otoscopy: a national cross-sectional study," *International Journal of Audiology*, pp. 1–7, 2017.

[23] K. A. Ryu, A.-R. Lyu, H. Park, J. W. Choi, G. M. Hur, and Y.-H. Park, "Intracochlear bleeding enhances cochlear fibrosis and ossification: An animal study," *PLoS ONE*, vol. 10, no. 8, Article ID e0136617, 2015.

[24] O. V. Akinpelu, F. Ibrahim, S. Waissbluth, and S. J. Daniel, "Histopathologic changes in the cochlea associated with diabetes mellitus - A review," *Otology & Neurotology*, vol. 35, no. 5, pp. 764–774, 2014.

[25] S. Orita, K. Fukushima, Y. Orita, and K. Nishizaki, "Sudden hearing impairment combined with diabetes mellitus or hyperlipidemia," *European Archives of Oto-Rhino-Laryngology*, vol. 264, no. 4, pp. 359–362, 2007.

[26] C. Aimoni, C. Bianchini, M. Borin et al., "Diabetes, cardiovascular risk factors and idiopathic sudden sensorineural hearing loss: a case-control study," *Audiology & Neurotology*, vol. 15, no. 2, pp. 111–115, 2010.

[27] S. W. Lin, Y. S. Lin, S. F. Weng, and C. W. Chou, "Risk of developing sudden sensorineural hearing loss in diabetic patients: a population-based cohort study," *Otology & Neurotology: Official Publication of The American Otological Society, American Neurotology Society and European Academy of Otology and Neurotology*, vol. 33, no. 9, pp. 1482–1488, 2012.

[28] O. H. Ryu, M. G. Choi, C. H. Park, D.-K. Kim, J. S. Lee, and J. H. Lee, "Hyperglycemia as a potential prognostic factor of idiopathic sudden sensorineural hearing loss," *Otolaryngology - Head and Neck Surgery (United States)*, vol. 150, no. 5, pp. 853–858, 2014.

[29] C.-Y. Chien, S.-Y. Tai, L.-F. Wang et al., "Metabolic syndrome increases the risk of sudden sensorineural hearing loss in Taiwan: A case-control study," *Otolaryngology - Head and Neck Surgery (United States)*, vol. 153, no. 1, pp. 105–111, 2015.

[30] C.-F. Lin, K.-J. Lee, S.-S. Yu, and Y.-S. Lin, "Effect of comorbid diabetes and hypercholesterolemia on the prognosis of idiopathic sudden sensorineural hearing loss," *The Laryngoscope*, vol. 126, no. 1, pp. 142–149, 2016.

[31] D. Assimakopoulos, V. Danielides, N. Kontogianis, A. Skevas, and A. Tsatsoulis, "Sudden hearing loss as the presenting symptom of diabetes mellitus," *Diabetes Research and Clinical Practice*, vol. 53, no. 3, pp. 201–203, 2001.

[32] W. Gawron, L. Pospiech, A. Noczynska, and E. Koziorowska, "Sudden hearing loss as a first complication of long-standing Type 1 diabetes mellitus: A case report," *Diabetic Medicine*, vol. 21, no. 1, pp. 96–98, 2004.

[33] M. Balslevjorgensen, "Changes of aging in the inner ear, and the inner ear in diabetes mellitus. histological studies," *Acta Oto-Laryngologica, Supplement*, vol. 188, Supplement 188:25+, 1964.

[34] B. Nageris, T. Hadar, M. Feinmesser, and J. Elidan, "Cochlear histopathologic analysis in diabetic rats," *Otology & Neurotology*, vol. 19, no. 1, pp. 63–65, 1998.

[35] P. A. Wackym and F. H. Linthicum Jr., "Diabetes mellitus and hearing loss: clinical and histopathologic relationships," *Otology & Neurotology*, vol. 7, no. 3, pp. 176–182, 1986.

[36] H. Fukushima, S. Cureoglu, P. A. Schachern et al., "Cochlear changes in patients with type 1 diabetes mellitus," *Otolaryngology—Head and Neck Surgery*, vol. 133, no. 1, pp. 100–106, 2005.

[37] H. Fukushima, S. Cureoglu, P. A. Schachern, M. M. Paparella, T. Harada, and M. F. Oktay, "Effects of type 2 diabetes mellitus on cochlear structure in humans," *Archives of Otolaryngology—Head and Neck Surgery*, vol. 132, no. 9, pp. 934–938, 2006.

[38] S. Kariya, S. Cureoglu, H. Fukushima et al., "Comparing the cochlear spiral modiolar artery in type-1 and type-2 diabetes mellitus: A human temporal bone study," *Acta Medica Okayama*, vol. 64, no. 6, pp. 375–383, 2010.

[39] G. Rance, D. Chisari, F. O'Hare et al., "Auditory neuropathy in individuals with Type 1 diabetes," *Journal of Neurology*, vol. 261, no. 8, pp. 1531–1536, 2014.

[40] W. J. T. Tan, P. R. Thorne, and S. M. Vlajkovic, "Characterisation of cochlear inflammation in mice following acute and chronic noise exposure," *Histochemistry and Cell Biology*, vol. 146, no. 2, pp. 219–230, 2016.

[41] G. M. Kalinec, G. Lomberk, R. A. Urrutia, and F. Kalinec, "Resolution of cochlear inflammation: Novel target for preventing or ameliorating drug-, noise- and age-related hearing Losss," *Frontiers in Cellular Neuroscience*, vol. 11, article no. 192, 2017.

[42] F. Liu, M. Xia, and A. Xu, "Expression of VEGF, iNOS, and eNOS is increased in cochlea of diabetic rat," *Acta Oto-Laryngologica*, vol. 128, no. 11, pp. 1178–1186, 2008.

[43] H.-P. Wu, C.-J. Hsu, T.-J. Cheng, and Y. L. Guo, "N-acetylcysteine attenuates noise-induced permanent hearing loss in diabetic rats," *Hearing Research*, vol. 267, no. 1-2, pp. 71–77, 2010.

Hindawi
BioMed Research International
Volume 2018, Article ID 6795397, 7 pages
https://doi.org/10.1155/2018/6795397

Research Article

Evaluation of Cerebral White Matter in Prelingually Deaf Children Using Diffusion Tensor Imaging

Kye Hoon Park,[1] Won-Ho Chung,[2] Hunki Kwon,[3] and Jong-Min Lee[4]

[1]*Department of Otorhinolaryngology-Head and Neck Surgery, Soonchunhyang University College of Medicine, Cheonan, Republic of Korea*
[2]*Department of Otorhinolaryngology-Head and Neck Surgery, Samsung Medical Center, Sungkyunkwan University School of Medicine, Seoul, Republic of Korea*
[3]*Department of Neurology, Yale University School of Medicine, New Haven, CT, USA*
[4]*Department of Biomedical Engineering, Hanyang University, Seoul, Republic of Korea*

Correspondence should be addressed to Won-Ho Chung; whchung@skku.edu

Received 14 November 2017; Accepted 9 January 2018; Published 4 February 2018

Academic Editor: Yong-Ho Park

This study compared white matter development in prelingually deaf and normal-hearing children using a tract-based spatial statistics (TBSS) method. Diffusion tensor imaging (DTI) was performed in 21 prelingually deaf (DEAF group) and 20 normal-hearing (HEAR group) subjects aged from 1.7 to 7.7 years. Using TBSS, we evaluated the regions of significant difference in fractional anisotropy (FA) between the groups. Correlations between FA values and age in each group were also analyzed using voxel-wise correlation analyses on the TBSS skeleton. Lower FA values of the white matter tract of Heschl's gyrus, the inferior frontooccipital fasciculus, the uncinate fasciculus, the superior longitudinal fasciculus, and the forceps major were evident in the DEAF group compared with those in the HEAR group below 4 years of age, while the difference was not significant in older subjects. We also found that age-related development of the white matter tracts may continue until 8 years of age in deaf children. These results imply that development of the cerebral white matter tracts is delayed in prelingually deaf children.

1. Introduction

Cochlear implantation (CI) is the only rehabilitative method that restores auditory sensation in profoundly deaf subjects, but improvements in hearing and speech following successful CI are inconsistent, especially in prelingually deaf subjects [1]. Many researchers have reported on the critical factors that determine the success of auditory language rehabilitation following CI, and the results suggest that the younger deaf children are at the time of CI, the better the outcome is. Consequently, CI surgery is more likely to be successful when performed on younger deaf children than on older ones [2]. However, several traditional demographic factors, including age at implantation, duration of deafness, number of inserted electrodes, and mode of communication, explained less than 50% of the observed variance in outcomes among implanted children [3]. Biological factors have also been investigated, such as the relationship between residual spiral ganglion cell populations in the temporal bones of CI patients and their speech perception ability during life [4]. However, an unexpected negative correlation suggested that certain processes in the central nervous system (CNS) are at least as important as peripheral factors.

A great deal of evidence supports the development of plastic changes in the brains of congenitally deaf subjects [5]. In a signing deaf subject, some processing of visual information is performed in the auditory cortex [6], indicating that the brain copes, to some extent, with alterations in sensory input. This is one reason why hearing after CI seems to be poor in prelingually signing deaf adults [1]. One study using positron emission tomography (PET) reported that the under-used auditory cortices of prelingually deaf individuals gradually changed over time, being initially hypometabolic and later normal or hyperactive [7]. An association was

also evident between better perception after CI and more pronounced presurgical hypometabolism in the superior temporal regions. Removal of sensory receptors in young animals exerted profound effects on the maturation of brain stem neuronal structures [8]. One example of such changes is sensory deprivation-induced cell death, evident in a variety of models when afferent activity is interrupted during development [9, 10]. The poorly understood phenomenon of deprivation-induced cell death and other experience-induced changes in neural structure and function, that is, alterations in normal activity patterns during finite periods early in life, dramatically change the CNS, whereas identical manipulations later in life exert little or no effect [11]. We hypothesized that a similar phenomenon might occur in congenitally deaf children, associated with a delay in development or myelination of cerebral white matter. However, white matter development has not yet been evaluated in prelingually deaf children. Our purpose here was to explore differences in cerebral white matter development in prelingually deaf children compared with that in normal children via diffusion tensor imaging (DTI).

2. Materials and Methods

2.1. Subjects. Twenty-one profoundly hearing-impaired children (8 boys and 13 girls; mean age: 3.9 (range: 1.7–7.7) years; DEAF group) were included. DTI was performed when conventional MRI was taken as a presurgical evaluation for CI. The control group included 20 normal-hearing children (12 boys and 8 girls; mean age: 4.7 (range: 2.0–7.6) years; HEAR group). Cerebral anatomy, as depicted by conventional MRI, was normal; none of the 41 children had any clinical history of neurological disease or developmental abnormality. The study was approved by our institutional review board. Written informed consent was obtained from all parents. All children were sedated with chloral hydrate administered by a radiologist prior to MRI.

2.2. Image Acquisition. All scans were acquired using a Philips 3.0 T scanner (Philips Achieva, Philips Medical System; Best, Netherlands). DTI was obtained via single-shot echo-planar acquisition from 45 noncollinear, noncoplanar diffusion-encoded gradient directions with the following parameters: b-value = 1000 s/mm^2, TR/TE = 3700 ms/80 ms, matrix = 128 × 128, slice thickness = 3 mm, and FOV = 180 × 180 mm^2. Two images with no diffusion weighting (b-value = 0 s/mm^2) and diffusion weighting (b-value = 1000 s/mm^2) were acquired for each slice and each gradient direction.

2.3. DTI Preprocessing. DTI data were processed using FMRIB Software Library (FSL) (http://www.fmrib.ox.ac.uk/fsl). Motion artifacts and eddy current distortions were corrected by normalizing each directional volume to the non-diffusion-weighted image ($b0$) using the FMRIB Linear Image Registration Tool (FLIRT) with 6 degrees of freedom. After correcting motion artifacts and eddy current distortions, the diffusion tensor was calculated, normally using a simple least squares fit of the tensor model to the diffusion data to calculate the three eigenvalues (λi, $i = 1, 2, 3$) and eigenvectors (εi, $i = 1, 2, 3$). Then, the fractional anisotropy (FA), an index of directional selectivity of water diffusion, and the mean diffusivity (MD) were determined for every voxel according to standard methods using the program DTIFIT in FSL.

2.4. Tract-Based Spatial Statistics (TBSS) Analysis. The fractional anisotropy (FA) images of the DTI preprocessing result were used in the TBSS analysis [12, 13]. In adult studies, all FA images are aligned onto a standard FMRIB58 FA template provided with FSL using a nonlinear registration algorithm implemented in the TBSS package. However, this approach is not appropriate for children's data. A new target image was selected: the one with the minimum mean displacement score from all other subjects in the group using TBSS option (tbss_2_reg -n) [12]. The original FA images were transformed to the new target image using linear and nonlinear registration methods. The transformed FA maps were averaged to make a group-specific template, which was inserted in the standard TBSS protocol. All of the original FA images were aligned onto the group-specific template using linear and nonlinear registration methods. To create a skeletonized mean FA image, the FA images that aligned on the group-specific template were averaged. Each subject's (aligned) FA image projects onto the skeleton by filling the skeleton with the highest FA values from the nearest relevant center of fiber tracts. A threshold FA value of 0.2 was chosen to exclude voxels of adjacent grey matter or cerebrospinal fluid.

2.5. Statistical Analysis. Voxel-wise statistical analyses were performed across subjects on the skeleton-space FA images. Voxel-wise statistical analysis of individual skeleton images was performed in the randomise package (v2.9) using a nonparametric permutation test. To assess differences between the DEAF and HEAR groups, a null distribution was built up over 5000 permutations on the skeleton mask of projected FA values. The same test was applied after stratification by the age of 4 years. Correlations between FA values and age in each group were also shown on the skeleton mask. To correct for multiple comparisons, we used threshold-free cluster enhancement (TFCE) with the "2D" parameter setting [14]. The significance level was set at $P < 0.05$. We evaluated differences in the mean FA values of each tract of interest, including the superior longitudinal fasciculus (SLF), uncinate fasciculus (UF), inferior frontooccipital fasciculus (IFOF), forceps major (FM), and the white matter tract leading to Heschl's gyrus (HG). The JHU White Matter Tractography Atlas of the FSL atlas tool (http://www.fmrib.ox.ac.uk/fsl/fslview/atlas.html) was applied to the common FA skeleton mask (Figure 1). Individual FA values were extracted by aligning the specific tractography to the FA skeleton mask, and the mean FA values were obtained. The Mann–Whitney U test in SPSS ver. 16.0 (SPSS, Chicago, IL, USA) was used to compare between-group differences in the mean FA values for each tract.

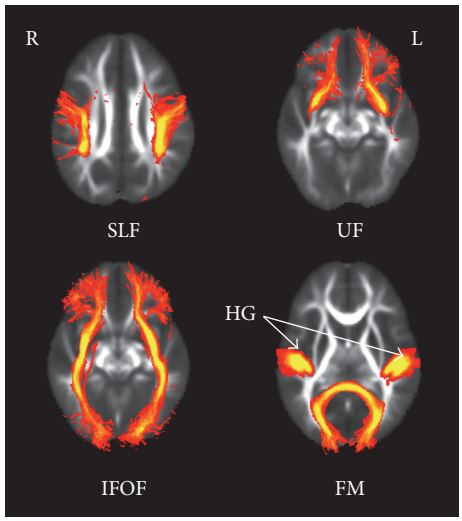

Figure 1: The tracts of interest of the FSL JHU White Matter Tractography Atlas Tool. SLF, superior longitudinal fasciculus; UF, uncinate fasciculus; IFOF, inferior frontooccipital fasciculus; FM, forceps major; HG, Heschl's gyrus.

3. Results

Voxel-wise between-group statistical analyses were performed using skeleton-space fractional anisotropy (FA) images. No significant differences were observed in the FA values within the whole-brain TBSS skeleton between the DEAF and HEAR groups.

To evaluate correlations between FA values and the ages of each group, we performed voxel-wise correlation analyses of the TBSS skeletons. These revealed a few regions in which the FA values were positively correlated with age in the HEAR group. However, significant positive correlations were evident between FA values and age for almost all white matter tracts in the DEAF group (Figure 2(a)). To further evaluate FA differences between groups, all subjects were stratified by age (cutoff: 4 years). We performed between-group comparisons in subjects younger than 4 years and found significantly lower FA values for many regions of the TBSS skeleton in the DEAF4− group ($n = 12$) compared with the HEAR4− group ($n = 10$) (Figure 2(b)). In subjects older than 4 years, no significant differences were found between groups within the TBSS skeleton.

We explored differences between the mean FA values of each tract of interest, including the superior longitudinal fasciculus (SLF), uncinate fasciculus (UF), inferior frontooccipital fasciculus (IFOF), forceps major (FM), and the white matter tracts leading to Heschl's gyrus (HG). In the DEAF group, subjects aged <4 years (the DEAF4− group) exhibited significantly lower FA values for each tract compared with the values of those aged >4 years (DEAF4+ group). However, in the HEAR group, we found no significant difference between subjects aged <4 (HEAR 4−) and >4 (HEAR4+) years in any tract of interest, with the exception of the right UF. In subjects aged <4 years, the DEAF4− group exhibited significantly lower FA values in all tracts of interest (except the UF) compared with the HEAR4− group. However, in subjects aged >4 years, no significant differences were evident between the DEAF4+ and HEAR4+ groups (Figure 3).

4. Discussion

Recent advances in MRI have facilitated in vivo studies of CNS microstructure [15]. Diffusion tensor imaging (DTI), a form of MRI, reveals the orientation of white matter tracts in vivo and yields a measure of microstructural integrity by quantifying the directionality of water diffusion. In the time since DTI was introduced, many studies have sought correlations between the connectivities of white matter tracts and the pathophysiologies of CNS diseases including multiple sclerosis, Alzheimer's disease, and epilepsy [16].

In the DTI technique, voxel-based morphometry (VBM) and tract-based spatial statistics (TBSS) analysis of diffusion data are the two main methods used to localize white matter changes in a whole-brain manner. VBM is a useful exploratory method and is widely used in anisotropy analysis to detect the changes in white matter which occur in many brain diseases. All of the steps in this method were performed automatically with greater reproducibility than region-of-interest and tractography-based methods. However, the normalization algorithm available in Statistical Parametric Mapping (SPM) software was not designed to handle highly heterogeneous FA images such as children's developing brains, so there is a risk of false-positive results [13]. Another limitation of the VBM method is the arbitrary choice of smoothing kernels. In this study, we used the TBSS technique to overcome the drawbacks of VBM, such as alignment and smoothing issues, because the subjects were young children with developing brains. Additionally, to evaluate differences in the subjects' white matter in the standard brain space, a new target image was chosen: the one with the minimum mean displacement score from all other subjects instead of the standard FMRIB58 FA template used in adult brain studies.

A few studies have used whole-brain DTI analyses to explore white matter changes in prelingually deaf adults and adolescents [17–20]. Kim et al. [17] found that, in deaf patients, FA values were reduced in the internal capsule, the white matter tract lying close to the superior temporal gyrus, the superior longitudinal fasciculus, and the inferior frontooccipital fasciculus. Such changes were interpreted in terms of both disuse-driven atrophy and compensatory plasticity. Recently, Li et al. [19] compared the white matter structures of congenitally deaf individuals, those with acquired deafness, and controls. Deaf individuals exhibited significantly reduced FA values of both superior temporal cortices and the splenium of the corpus callosum compared to hearing-positive controls. A DTI study on prelingually deaf adolescents found that the FA values of the superior temporal gyrus and Heschl's gyrus were lower than normal, consistent with changes reported in adults [20]. Also, deaf adolescents exhibited a significantly reduced auditory brain area volume and/or increased gray matter/WM ratio in Heschl's gyrus and other auditory-related brain areas [18]. However, no whole-brain

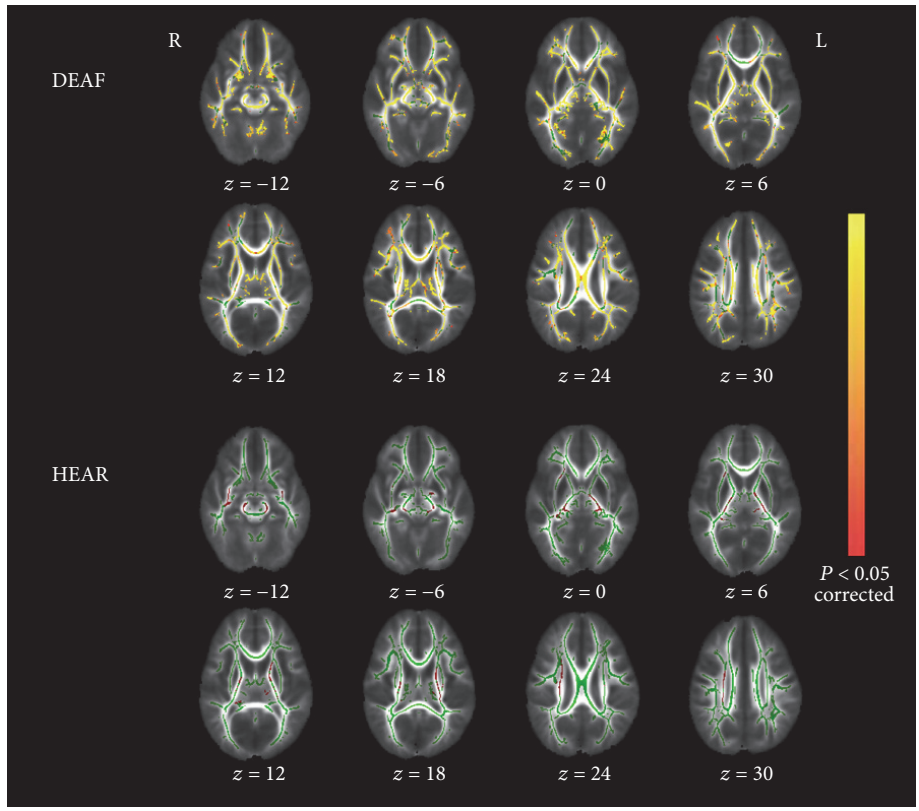

(a)

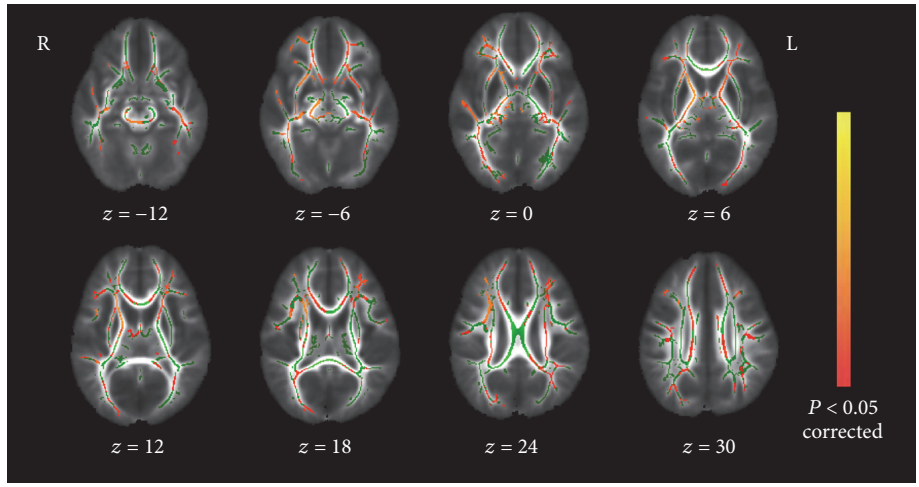

(b)

Figure 2: Voxel-wise statistical analyses of skeleton-space FA images. (a) Effects of age on regional FA in both groups. White matter tracts in red-yellow reveal a significant age-related increase in FA. In the DEAF group, significant correlations with age appear for nearly every white matter tract. (b) White matter structures exhibiting significantly lower FAs in the DEAF4 group ($P < 0.05$, corrected for multiple comparisons). The background image is a group-specific brain template. Green voxels are the FA white matter skeleton. Red to yellow voxels show regions of lower FA values in the DEAF4− group compared with the HEAR4− group. Axial sections with z-values ranging from −12 to 30 (the MNI coordinates) are shown.

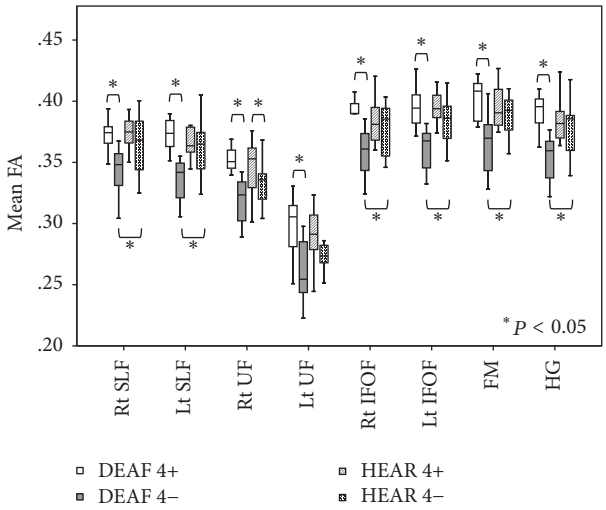

Figure 3: The mean FA values in tracts of interest [the superior longitudinal fasciculus (SLF); the uncinate fasciculus (UF); the inferior frontooccipital fasciculus (IFOF); the forceps major (FM); and the white matter tracts leading to Heschl's gyrus (HG)]. In the DEAF group, DEAF4– subjects (compared with DEAF4+ subjects) exhibited significantly lower FA values in each tract of interest. However, in the HEAR group, no significant difference was apparent between HEAR 4– and HEAR4+ subjects except in the right UF. Of subjects aged <4 years, those in the DEAF4– group exhibited significantly lower FA values in all tracts of interest (except the UF) than did HEAR4– subjects. However, in subjects aged >4 years, no significant difference was apparent between the DEAF4+ and HEAR4+ groups.

DTI analyses have yet been performed on prelingually deaf children.

In a DTI study of white matter maturation in early childhood, FA at major neuronal tracts of the brain increased rapidly during the first 12 months but plateaued after 24 months [21]. This increase in FA before 24 months was explained as the influence of the myelination process. Most of the subjects in our study were older than 24 months; we observed a strong correlation between age and FA at almost all white matter tracts in the DEAF group, whereas no correlation appeared for most tracts in the HEAR group. We also observed increased FA with age at several tracts in the DEAF group, based on the extracted regional DTI data. This finding implies that the development of white matter tracts continues until a specific age in deaf children, while it appears to be stable after 2 years of age in normal-hearing children.

Researchers have postulated that the younger deaf children are at the time of CI, the better the outcome of CI is likely to be. Govaerts et al. [22] reported that children who underwent CI before the age of 4 years were likely to score at least 7 on the Categories of Auditory Performance (CAP) scale. Researchers studying the auditory cortex have reported that peak synaptic density is attained at 2–4 years of age in children with normal hearing. After this time, the synaptic counts decrease, and unused synapses are eliminated, reflecting the brain's need to specialize to accommodate prevailing conditions [23]. In congenitally deaf cats, overall synaptic activity was developmentally delayed, with exaggerated synaptic overshoot and increased elimination of synaptic function [24]. Therefore, we performed between-group comparisons after stratification using an age cutoff of 4 years.

In the DEAF4– group, the FA values of many white matter tracts were lower than those in the HEAR4– group. Reduced values of white matter tract FAs in the temporal lobe may be associated with delayed development of such tracts because of loss of auditory input. In contrast, no significant between-group difference was evident in subjects >4 years of age. Moreover, the FA values of the white matter tracts of Heschl's gyrus were significantly correlated with age in the DEAF group, perhaps reflecting cross-modal plasticity, consistent with PET data indicating that under-use of the auditory cortex in prelingually deaf individuals gradually changes over time from a hypometabolic state to a normal or hyperactive presentation [7]. However, our findings do not agree with the results of Miao et al. [20] who studied adolescents. It is difficult to explain the discrepancy, but it is possible that cerebral white matter tract development continues to a certain age in deaf children, and at adolescence, white matter tracts in the temporal lobe may be affected by clinical factors such as learning sign language, visual experiences, and intelligence.

Human language function involves not only the gray matter of circumscribed brain regions in the frontal and temporal cortices but also the white matter fiber tracts connecting these regions [25]. The SLF and UF are white matter tracts connecting Broca's and Wernicke's areas. The SLF is a dorsal pathway from the posterior portion of Broca's area to the superior temporal region and is important in terms of higher-order functionality. The IFOF connects the frontal and occipital lobes and the frontal, posterior parietal, and temporal lobes, and it links the auditory and visual cortices with the prefrontal cortex controlling working memory and executive function [26]. Lee et al. [27] found that deaf children with better executive and visuospatial functions delivered by the prefrontal and parietal cortices were auditorily successful when learning a language after CI. In our present study, the correlations between FA and age in terms of functionality of these white matter tracts were stronger in the DEAF group, reflecting the development of these tracts, which, in turn, affected speech outcomes after CI.

One previous PET study [28] reported that prelingually deaf children aged 5–7 years at CI exhibited the widest variation in individual outcomes, and the child with the broadest hypometabolic area had the best speech perception. They concluded that the extent of hypometabolism as assessed by PET was one of the major predictors of the outcome of CI. We found that the FA values of many white matter tracts were lower in the DEAF4– group than in the HEAR4– group, while no significant differences appeared between groups in older subjects. CI is intended to promote auditory development in children who are deaf; this development will be restricted if cross-modal changes cannot be reversed and normal corticocortical and corticofugal activity is not restored. Therefore, CI should be performed as early as

possible to limit the potential for the auditory brain to reorganize. In other words, the auditory brain must be used in early life to ensure that it is not lost to other modalities [29].

5. Conclusions

In this study, we used TBSS analysis to investigate WM development in prelingually deaf children. The FA values at many WM tracts were lower in the DEAF group than in the HEAR group younger than 4 years, while no significant differences appeared in older subjects. We also found that the age-related development of WM tracts might continue until 8 years of age in prelingually deaf children. These results are the first to imply the delayed development of cerebral WM tracts in prelingually deaf children, constituting circumstantial evidence that CI should be performed as early as possible to avoid reorganization of the auditory brain.

Disclosure

Some results reported in this paper were previously published in the doctoral thesis of the first author (Kye Hoon Park), presented to Soonchunhyang University in 2013.

Conflicts of Interest

The authors declare that they have no conflicts of interest.

Acknowledgments

This study was supported by the Samsung Medical Center Clinical Research Development Program (CRDP) (Grant no. CRS106-19-1) and the Soonchunhyang University Research Fund.

References

[1] R. Campbell, M. Macsweeney, and B. Woll, "Cochlear implantation (CI) for prelingual deafness: the relevance of studies of brain organization and the role of first language acquisition in considering outcome success," *Frontiers in Human Neuroscience*, vol. 8, article no. 834, 2014.

[2] J. G. Nicholas and A. E. Geers, "Spoken language benefits of extending cochlear implant candidacy below 12 months of age," *Otology & Neurotology*, vol. 34, no. 3, pp. 532–538, 2013.

[3] G. M. O'Donoghue, T. P. Nikolopoulos, and S. M. Archbold, "Determinants of speech perception in children after cochlear implantation," *The Lancet*, vol. 356, no. 9228, pp. 466–468, 2000.

[4] J. B. J. R. Nadol, J. Y. Shiao, B. J. Burgess et al., "Histopathology of cochlear implants in humans," *Ann Otol Rhinol Laryngol*, vol. 110, no. 9, pp. 883–891, 2001.

[5] E. Striem-Amit, J. Almeida, M. Belledonne et al., "Topographical functional connectivity patterns exist in the congenitally, prelingually deaf," *Scientific Reports*, vol. 6, Article ID 29375, 2016.

[6] H. Nishimura, K. Hashikawa, K. Doi et al., "Sign language 'heard' in the auditory cortex," *Nature*, vol. 397, no. 6715, p. 116, 1999.

[7] D. S. Lee, J. S. Lee, S. H. Oh et al., "Cross-modal plasticity and cochlear implants," *Nature*, vol. 409, no. 6817, pp. 149-150, 2001.

[8] S. P. Mostafapour, N. M. Del Puerto, and E. W. Rubel, "Bcl-2 overexpression eliminates deprivation-induced cell death of brainstem auditory neurons," *The Journal of Neuroscience*, vol. 22, no. 11, pp. 4670–4674, 2002.

[9] A. Baldi, E. Calia, A. Ciampini et al., "Deafferentation-induced apoptosis of neurons in thalamic somatosensory nuclei of the newborn rat: Critical period and rescue from cell death by peripherally applied neurotrophins," *European Journal of Neuroscience*, vol. 12, no. 7, pp. 2281–2290, 2000.

[10] R. M. Sherrard and A. J. Bower, "Role of afferents in the development and cell survival of the vertebrate nervous system," *Clinical and Experimental Pharmacology and Physiology*, vol. 25, no. 7-8, pp. 487–495, 1998.

[11] N. Berardi, T. Pizzorusso, and L. Maffei, "Critical periods during sensory development," *Current Opinion in Neurobiology*, vol. 10, no. 1, pp. 138–145, 2000.

[12] G. Ball, S. J. Counsell, M. Anjari et al., "An optimised tract-based spatial statistics protocol for neonates: applications to prematurity and chronic lung disease," *NeuroImage*, vol. 53, no. 1, pp. 94–102, 2010.

[13] S. M. Smith, M. Jenkinson, H. Johansen-Berg et al., "Tract-based spatial statistics: voxelwise analysis of multi-subject diffusion data," *NeuroImage*, vol. 31, no. 4, pp. 1487–1505, 2006.

[14] S. M. Smith and T. E. Nichols, "Threshold-free cluster enhancement: addressing problems of smoothing, threshold dependence and localisation in cluster inference," *NeuroImage*, vol. 44, no. 1, pp. 83–98, 2009.

[15] D. Le Bihan, J.-F. Mangin, C. Poupon et al., "Diffusion tensor imaging: concepts and applications," *Journal of Magnetic Resonance Imaging*, vol. 13, no. 4, pp. 534–546, 2001.

[16] E. R. Melhem, S. Mori, G. Mukundan, M. A. Kraut, M. G. Pomper, and P. C. M. Van Zijl, "Diffusion tensor MR imaging of the brain and white matter tractography," *American Journal of Roentgenology*, vol. 178, no. 1, pp. 3–16, 2002.

[17] D.-J. Kim, S.-Y. Park, J. Kim, D. H. Lee, and H.-J. Park, "Alterations of white matter diffusion anisotropy in early deafness," *NeuroReport*, vol. 20, no. 11, pp. 1032–1036, 2009.

[18] J. Li, W. Li, J. Xian et al., "Cortical thickness analysis and optimized voxel-based morphometry in children and adolescents with prelingually profound sensorineural hearing loss," *Brain Research*, vol. 1430, pp. 35–42, 2012.

[19] Y. Li, G. Ding, J. R. Booth et al., "Sensitive period for white-matter connectivity of superior temporal cortex in deaf people," *Human Brain Mapping*, vol. 33, no. 2, pp. 349–359, 2012.

[20] W. Miao, J. Li, M. Tang et al., "Altered white matter integrity in adolescents with prelingual deafness: a high-resolution tract-based spatial statistics imaging study," *American Journal of Neuroradiology*, vol. 34, no. 6, pp. 1264–1270, 2013.

[21] L. Hermoye, C. Saint-Martin, G. Cosnard et al., "Pediatric diffusion tensor imaging: normal database and observation of the white matter maturation in early childhood," *NeuroImage*, vol. 29, no. 2, pp. 493–504, 2006.

[22] P. J. Govaerts, C. De Beukelaer, K. Daemers et al., "Outcome of cochlear implantation at different ages from 0 to 6 years," *Otology & Neurotology*, vol. 23, no. 6, pp. 885–890, 2002.

[23] A. Kral and G. M. O'Donoghue, "Profound deafness in childhood," *The New England Journal of Medicine*, vol. 363, no. 15, pp. 1438–1450, 2010.

[24] A. Kral, J. Tillein, S. Heid, R. Hartmann, and R. Klinke, "Postnatal cortical development in congenital auditory deprivation," *Cerebral Cortex*, vol. 15, no. 5, pp. 552–562, 2005.

[25] A. D. Friederici, "Pathways to language: fiber tracts in the human brain," *Trends in Cognitive Sciences*, vol. 13, no. 4, pp. 175–181, 2009.

[26] T. Kammer, M. E. Bellemann, F. Gückel et al., "Functional MR imaging of the prefrontal cortex: specific activation in a working memory task," *Magnetic Resonance Imaging*, vol. 15, no. 8, pp. 879–889, 1997.

[27] H. J. Lee, E. Kang, and S.-H. Oh, "Preoperative differences of cerebral metabolism relate to the outcome of cochlear implants in congenitally deaf children," *Hearing Research*, vol. 203, no. 1-2, pp. 2–9, 2005.

[28] S.-H. Oh, C.-S. Kim, E. J. Kang et al., "Speech perception after cochlear implantation over a 4-year time period," *Acta Oto-Laryngologica*, vol. 123, no. 2, pp. 148–153, 2003.

[29] K. A. Gordon, D. D. E. Wong, J. Valero, S. F. Jewell, P. Yoo, and B. C. Papsin, "Use it or lose it? lessons learned from the developing brains of children who are deaf and use cochlear implants to hear," *Brain Topography*, vol. 24, no. 3-4, pp. 204–219, 2011.

Hindawi
BioMed Research International
Volume 2017, Article ID 4630241, 9 pages
https://doi.org/10.1155/2017/4630241

Research Article

A Simple Model for Inducing Optimal Increase of *SDF-1* with Aminoglycoside Ototoxicity

Hyun Mi Ju,[1,2] Sun Hee Lee,[1,2] Jin Sil Choi,[1,2] and Young Joon Seo[1,2]

[1]*Laboratory of Smile Snail, Yonsei University Wonju College of Medicine, Wonju, Republic of Korea*
[2]*Department of Otorhinolaryngology, Yonsei University Wonju College of Medicine, Wonju, Republic of Korea*

Correspondence should be addressed to Young Joon Seo; okas2000@hanmail.net

Received 28 June 2017; Revised 29 August 2017; Accepted 17 September 2017; Published 21 December 2017

Academic Editor: Yong-Ho Park

Objectives. As a homing factor of stem cell, stromal derived factor-1 *(SDF-1)* is important for the regenerative research in ototoxicity. Mice models with aminoglycoside ototoxicity have been widely used to study the regeneration capacity of MSCs in repair of cochlear injury. We developed a mouse model with maximal increase in *SDF-1* levels in the inner ear, according to the "one-shot" doses of kanamycin and furosemide. *Methods*. C57BL/6 mice had kanamycin (420, 550, and 600 mg/kg) dissolved in PBS, followed by an intraperitoneal injection of furosemide (130 mg/kg). The injuries of inner ear were measured with hearing thresholds, histology, and outer hair cell counts at 0, 3, 5, 7, 10, and 14 days before the sacrifice. The levels of *SDF-1* in the inner ear were tested by real-time RT-PCR and immunohistochemistry. *Results*. There were a significant reduction in hearing thresholds and a maximal increase of *SDF-1* levels in the furosemide 130 mg/kg + kanamycin 550 mg/kg group, but severe hearing deterioration over time was observed in the furosemide 130 mg/kg + kanamycin 600 mg/kg group and four mice were dead. *SDF-1* was detected mostly in the stria vascularis and organ of Corti showing the highest increase in expression. *Conclusion*. We observed optimal induction of the stem cell homing factor in the newly generated aminoglycoside-induced ototoxicity mouse model using a "one-shot" protocol. This study regarding high *SDF-1* levels in our mouse model of ototoxicity would play a major role in the development of therapeutic agents using MSC homing.

1. Introduction

Stromal derived factor-1 *(SDF-1)* is a cytokine for stimulating the homing of stem cells into injured organs. The expression of *SDF-1* in injured tissue correlates with recruitment of stem cells and tissue regeneration. Recent studies have shown that homing of mesenchymal stem cells (MSCs) across the blood-brain barrier (BBB) occurred in ischemic brain tissue. Myocardial protection by homing of stem cells was also shown in myocardial infarction via mobilization of the stem cells into the injured myocardial tissue and increase in local angiogenesis after myocardial infarction.

Mice models with aminoglycoside ototoxicity have been widely used to study the regeneration capacity of MSCs in repair of cochlear injury. Several studies showed that mice can be used as models for aminoglycoside-induced hearing loss using a "one-shot" protocol, in which a single dose of kanamycin is accompanied by a dose of the loop diuretic furosemide [1, 2].

In the case of cochlear homing, Tan et al. [3] demonstrated that upregulation of *SDF-1* in the spiral ligament after acoustic deafening could promote the homing capability of bone marrow-derived cells to an injured cochlea. Another study showed that efficient invasion of MSCs to the inner tissue occurred when MSCs, which had enhanced expression of the *SDF-1* receptor and the C-X-C chemokine receptor type 4 (CXCR4), were transplanted in the lateral semicircular canal [4].

In the field of ear research, researches are being actively carried out to bring about the regeneration of hair cells using stem cell homing [4]. To prove that this ototoxicity mice model, in which *SDF-1* is markedly increased, could be the appropriate model to study homing, we confirmed

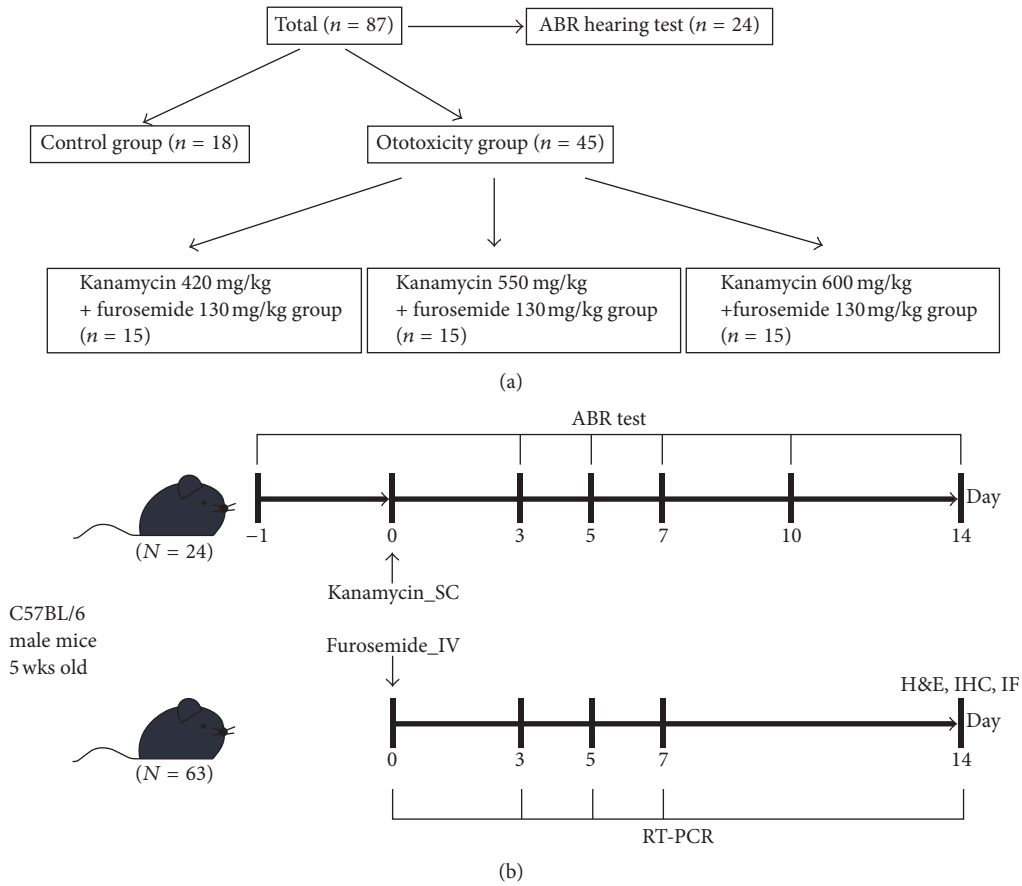

Figure 1: The study design for the mice model showing optimal increase of *SDF-1* with aminoglycoside ototoxicity. (a) Total population involving 63 male C57BL/6 mice (including 18 control mice). Mice were treated according to the following protocol: to record auditory brainstem responses (ABRs) 24 h after the second LPS injection, mice were injected with kanamycin (420, 550, and 600 mg/kg) and, 30 min later, with furosemide (130 mg/kg). (b) Auditory brainstem responses (ABRs) were tested on days 3, 5, 7, and 14 after kanamycin-furosemide administration. On the 14th day, fixative was perfused through the heart and cochleas were harvested for histologic analysis.

the changes in *SDF-1* levels with increasing hearing thresholds based on the various conditions of one-shot ototoxicity. Thereafter, we demonstrated an effective homing phenomenon in a mouse model with maximal increase in *SDF-1* levels in the inner ear.

2. Method

2.1. Animals. 87 male C57BL/6 mice, including 24 mice for the changes of hearing thresholds after the ototoxicity drugs, were allowed free access to water and regular mouse diet and were kept at room temperature under a standard 12 h light/dark cycle for 1 week of acclimatization before the experiments. The animals were 5 weeks old and weighed approximately 18–25 g. The mice were anaesthetized by intraperitoneal injection of 30 mg/kg tiletamine-zolazepam (Zoletil, 500 mg/vial; Virbac, Carros, France) and 10 mg/kg xylazine (Rompun; Bayer Korea, Ansan, Korea) and sacrificed by decapitation. The animals underwent cardiac perfusion with phosphate-buffered saline (PBS: Dulbecco's formula modified, ICN Biochemicals, England) before tissue harvest. The temporal bones were dissected, and the bony shells of the cochlea and vestibule were removed in chloride-free physiological saline. The animal experiments were conducted in accordance with the guidelines of the Institutional Animal Care and Use Committee of Yonsei University, Korea (YWC-150728-1, YWC-160826-1).

2.2. Ototoxic Drug Administration. The first injection for each mouse was given at the beginning of the daily light cycle. The three subgroups ($n = 15$ for each group) in the ototoxicity group received subcutaneous injection of kanamycin (420, 550, and 600 mg/kg; Sigma-Aldrich Oakville, ON, Canada) dissolved in PBS, followed by an intraperitoneal injection of furosemide (130 mg/kg; Sigma-Aldrich, Oakville, ON, Canada) via the tail vein after 30 min [5]. The mice in the sham control group received a subcutaneous injection of saline, followed by another tail vein injection of saline 30 min later. Mice showing signs of severe dehydration or other significant illness were sacrificed. All animals were monitored by trained animal care technologists supervised by a veterinarian. All animals survived the drug administration (Figure 1).

2.3. Testing of Hearing Ability. Pretest auditory brainstem response (ABR) thresholds were measured in the 24 mice (6 mice/each group) 24 h prior to the first drug administration. Each animal was gently anaesthetized with an intraperitoneal injection of ketamine (100 mg/kg; Yuhan Corporation, Seoul, Korea) and xylazine (1 mg/kg; Rompun, Korea Bayer, Ansan, Korea) and kept warm using a heating pad. Subdermal needle electrodes were placed at the scalp vertex (inverting), posterior bulla (noninverting), and lower back (ground) for recording ABR in anaesthetized mice. The test stimuli were clicks generated using the BioSigRP (Tucker-Davis Technologies, Inc.). The stimulus intensity decreased gradually in 5-dB (decibel) steps until a visually discernible ABR waveform disappeared, and the lowest sound level that caused this waveform was defined as the "threshold." Scanning time was 10 ms, and 1024 sweeps were averaged with 300–3000 Hz filtering band-width. Threshold shifts are reported as the difference between the pre- and posttest ABR thresholds. Posttest ABR thresholds after kanamycin and furosemide administration were measured at 3, 5, 7, 10, and 14 days without any scarification to observe the changes of hearing threshold after the ototoxicity drugs.

2.4. Histological Assessment and Immunohistochemistry. Normal and ototoxic drug-administrated mice were sacrificed after 14 days of treatment. The temporal bones were removed, and the apex of the cochlea, the round window, and the oval window were punctured. A fixative was perfused on right side cochleas of three animals in each group through the cochlear apex with 4% paraformaldehyde (Biosesang, Seongnam, Korea), and the sample was immersed in fixative for 24 h at 4°C. Cochleas were decalcified by immersion in Calci-Clear Rapid (National Diagnostics, Atlanta, GA, USA) for 24 h, dehydrated in 30% sucrose (Sigma-Aldrich, Gillingham, UK) for 24 h, embedded in the optimal cutting temperature (OCT) compound (Leica, Bensheim, Germany), and sectioned from 2 to 10 μm thickness using a cryostat (Leica CM1850 Cryostat; Leica, Wetzlar, German). A standard hematoxylin and eosin (H & E) staining protocol was followed, with a 1–3 min incubation in hematoxylin and 30–60 s staining with eosin, before mounting the samples.

Immunohistochemistry for *SDF-1* was performed on the cryosections of the cochlea in each group. The slide samples were incubated with appropriate primary antibodies as follows. Antibody against *SDF-1* 1 (Abcam, Inc., Cat #ab18919) was used. Sections were incubated with the primary antibody overnight at 4°C. After washing thrice with 0.1 M PBS, the sections were incubated with an appropriate biotin-tagged secondary antibody at room temperature for 1 h. Thereafter, the sections were incubated in an avidin-biotin-peroxidase complex solution (Vector Laboratories, Inc., Burlingame, CA, USA) and developed with diaminobenzidine substrate kit (Vector Laboratories, Inc.) after washing thrice with 0.1 M PBS. Then, the sections were dehydrated, mounted, and visualized with a BX50 microscope (Olympus, Tokyo, Japan), and digital images were captured.

2.5. Immunofluorescent Microscopy. The temporal bones of the left side in three mice of each group that were sacrificed for the histology were fixed and decalcified as described above. Subsequently, the basilar membrane was dissected under a dissecting microscope, and the stria vascularis and the tectorial membrane were removed. To identify F-actin and cell nucleus in the sensory epithelium, phalloidin-FITC (Sigma-Aldrich, Chemie BV, Zwijndrecht, the Netherlands) was applied for 40 min at room temperature in a dark room. The fluorescent signals were visualized using a BX50 microscope (Olympus, Tokyo, Japan) and digital images were captured. The outer hair cells in the sensory epithelium were counted from a minimum of 10 captures per cochlea, including the apical, mid, and basal turns.

2.6. Real-Time Reverse Transcription-Polymerase Chain Reaction (RT-PCR) Analysis. Total RNA was isolated with the TRIzol Reagent (Invitrogen, Carlsbad, CA) from the sensory epithelium of right cochlea of three mice in each group, which were sacrificed 3, 5, 7, and 14 days after the treatment. On day 0 before the ototoxicity, the results were replaced by those from the control group ($n = 6$). Total RNA was subjected to reverse transcription using the SYBR® Select master mix (Applied Biosystems, CA, USA) following the manufacturer's protocol. Real-time RT-PCR was performed using Applied Biosystems sequence detection system 7900 to quantify *SDF-1* levels. The following primers were used for sequencing: *SDF-1*, forward: 5′-CGC CAG AGC CAA CGT CAA GC-3′ and reverse: 5′-TTT GGG TCA ATG CAC ACT TG-3′; β-actin, forward: 5′-CGT GCG TGA CAT CCA AGA GAA-3′ and reverse: 5′-TGG ATG CCA CAG GAT TCC AT-3′. To exclude the possibility of genomic DNA amplification during PCR, no-template controls were performed and accepted when the Ct value was at least nine cycles greater than the template run. Measurements were performed in duplicate and accepted if the difference in Ct values between the duplicates was less than 1. The real-time PCR data were normalized to the level of β-actin, and the relative quantity of mRNA was determined using the comparative cycle threshold method.

2.7. Statistical Analysis. Statistical analysis was performed using the SPSS statistical package version 17.0 (SPSS, Chicago, IL, USA). Descriptive results of continuous variables are expressed as mean ± standard deviation (SD) for normal distribution variables. Means were compared by the 2-way analysis of variance (ANOVA) for ABR tests and Mann–Whitney test for counts of hair cells and *SDF-1*. The level of statistical significance was set at 0.05.

3. Results

3.1. Changes in the Hearing Thresholds of the Kanamycin/Furosemide-Induced Mouse Model of Ototoxicity. ABR evaluations were performed at 0, 3, 5, 7, 10, and 14 days after drug administration to test whether the combined effect of kanamycin/furosemide is able to induce hearing loss in mice. We compared the average ABR thresholds for the four groups, which was measured with click sounds (Figure 2(a)). The ABR thresholds were significantly elevated in the groups receiving both drugs, namely, furosemide 130 mg/kg + kanamycin 420 mg/kg, furosemide

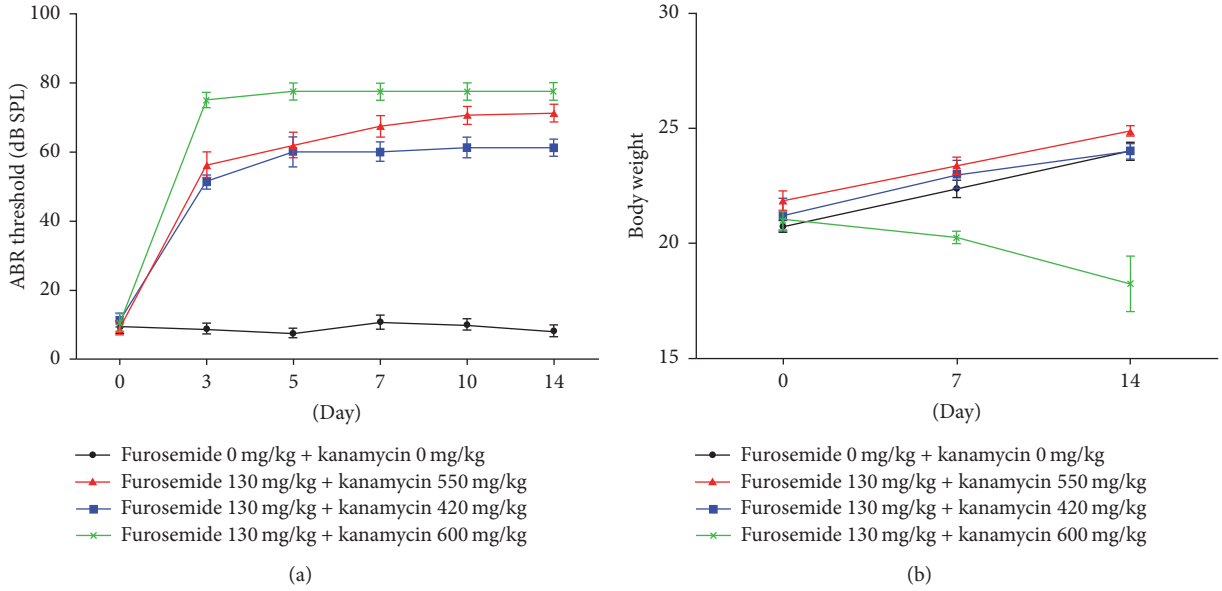

FIGURE 2: The shifts of auditory brainstem response (ABR) thresholds in the mouse model of ototoxicity were measured after injections with different doses of furosemide and kanamycin. In the groups receiving furosemide 130 mg/kg + kanamycin 420 mg/kg, furosemide 130 mg/kg + kanamycin 550 mg/kg, and furosemide 130 mg/kg + kanamycin 600 mg/kg, the ABR thresholds were significantly increased compared to that of the control group at all tested frequencies ($P < 0.01$). The data are expressed as the mean ± SD of 5 mice in each group and were analyzed using Student's t-test.

130 mg/kg + kanamycin 550 mg/kg, and furosemide 130 mg/kg + kanamycin 600 mg/kg, compared to that of the control group at each frequency ($P < 0.01$). Abrupt changes in threshold in the ototoxicity groups occurred after 3 days of drug administration. High doses of kanamycin caused more severe hearing impairment in the third to the fourteenth day posttreatment, as seen by an increase in the ABR threshold in the furosemide 130 mg/kg + kanamycin 600 mg/kg group than in the furosemide 130 mg/kg + kanamycin 420 and 550 mg/kg groups. Final hearing levels worsened with administration of different concentrations of kanamycin; however, there were no significant differences among them. Despite definite changes in the hearing threshold, the body weights of mice treated with kanamycin 600 mg/kg decreased, and 4 among 15 mice died of urinary insufficiency within 7 days (Figure 2(b)). However, no such problem occurred in mice treated with the other doses of kanamycin.

3.2. Cochlear Histopathology of Kanamycin/Furosemide-Treated Mice. To examine the ototoxic effects of furosemide and kanamycin, structural changes in the inner ear were examined by H & E staining of cochlear sections 14 days after the drug administration. We observed a loss of inner and outer hair cells in mice treated with a combination of kanamycin and furosemide, which caused damage of the organ of Corti (Figure 3). The loss of outer hair cells in the organ of Corti was higher in the cochlea exposed to kanamycin/furosemide than in the normal cochlea. At the same time, there was a reduction in the number of spiral ganglia cells and thinning of the stria vascularis in the groups receiving both the drugs. High doses of kanamycin (550 and 600 mg/kg) caused more severe structural changes.

3.3. Hair Cell Counts in Kanamycin/Furosemide-Treated Mice. The process of degeneration in the organ of Corti 14 days after drug administration was examined by the structure analysis using immunofluorescence microscopy (Figure 4). Cochleas from furosemide 130 mg/kg + kanamycin 550 mg/kg and furosemide 130 mg/kg + kanamycin 600 mg/kg treated mice were analyzed. The alignment of outer hair cells (OHCs), indicated by their V-shaped bundles, indicated that the organization of the organ of Corti and the stereocilia bundle integrity were well-maintained at this stage. In contrast, damage to the stereocilia was observed in the furosemide 130 mg/kg + kanamycin 550 mg/kg treated mice, which was more evident in mice treated with furosemide 130 mg/kg + kanamycin 600 mg/kg, particularly at the top of their V-shaped bundles. In addition, the hair cells presented an increasingly disorderly rearrangement, and some OHC stereocilia and the cuticular plate were absent. To quantify bundle damage caused by furosemide and kanamycin sulfate, the total number of bundles of the three-layered outer hair cells was counted. Combined injection of furosemide and kanamycin sulfate caused a significant reduction in the number of bundles of the inner and outer hair cells in the furosemide 130 mg/kg + kanamycin 550 mg/kg and furosemide 130 mg/kg + kanamycin 600 mg/kg groups compared to that of the control group ($P < 0.01$).

3.4. Changes in SDF-1 Level in the Kanamycin/Furosemide-Treated Mice. SDF-1 is an important chemokine required for the homing of mesenchyme-derived stem cells. We observed that the mRNA levels of *SDF-1* increased with concentration of kanamycin (Figure 5), reaching maxima in the furosemide 130 mg/kg + kanamycin 550 mg/kg group.

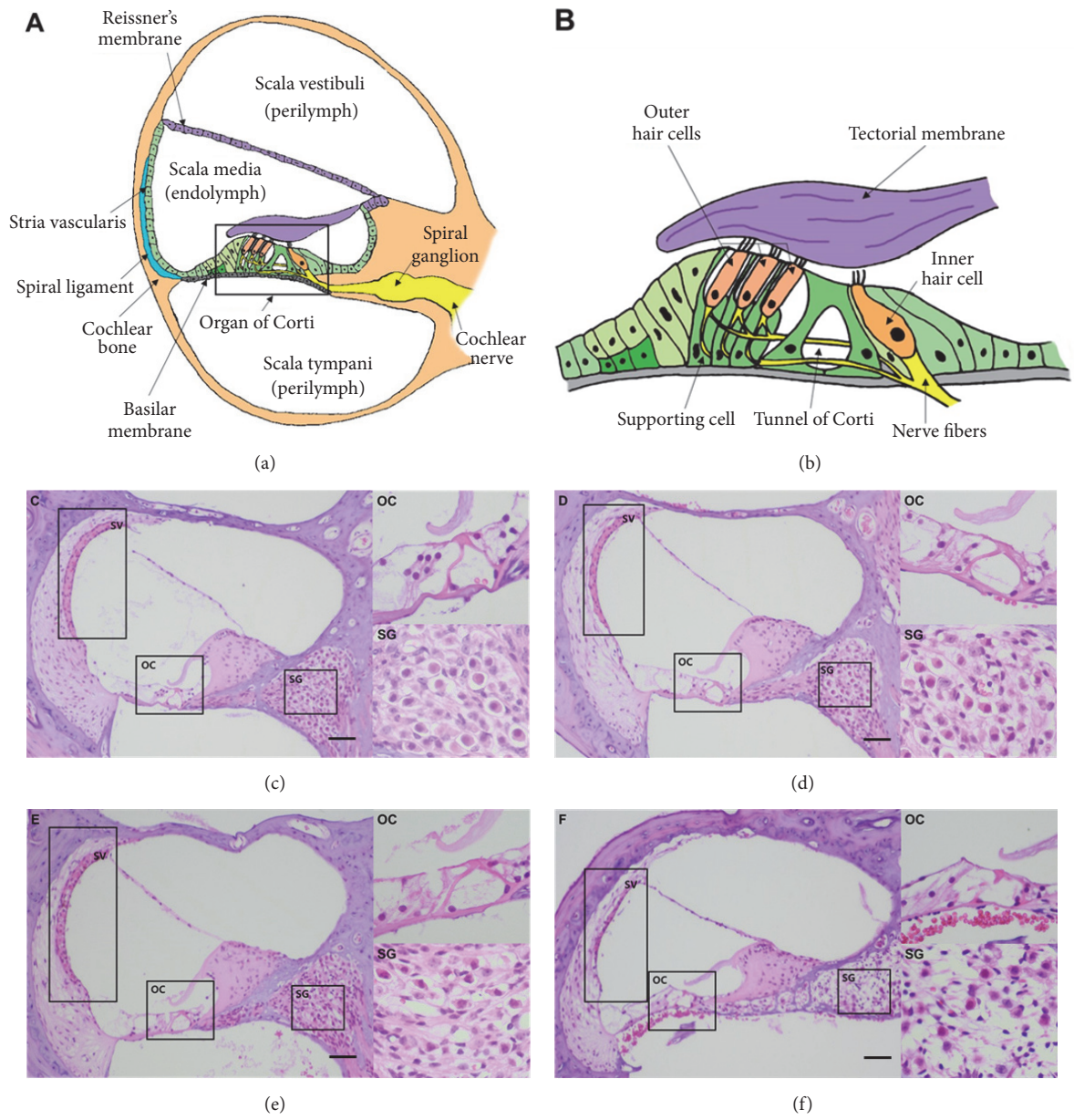

Figure 3: The cochlear morphology in the mouse model of ototoxicity analyzed after furosemide and kanamycin treatments showed cochlear degeneration. (a) and (b) show the normal microstructures of cochlea, especially of the organ of Corti and the spinal ganglion. We compared the hematoxylin and eosin staining in the cryosections from (c) normal mice and mice treated with furosemide, (d) 130 mg/kg + kanamycin 420 mg/kg, (e) furosemide 130 mg/kg + kanamycin 550 mg/kg, and (f) furosemide 130 mg/kg + kanamycin 600 mg/kg. SV: scala vestibuli; SM: scala media; ST: scala tympani; RM: Reissner's membrane; TM: tectorial membrane; BM: basilar membrane; SG: spiral ganglion; OHC: outer hair cells; IHC: inner hair cells. Scale bars: 20 μm.

However, the levels decreased in the furosemide 130 mg/kg + kanamycin 600 mg/kg group. Next, we measured the change in *SDF-1* with time using 550 mg/kg kanamycin. The hearing thresholds dropped suddenly on the third day. In contrast, the mRNA levels of *SDF-1* were highest on the 7th day and decreased afterwards. Next, we investigated the extent and timing of the increase in the protein levels of *SDF-1* (Figure 6). *SDF-1* was detected in the stria vascularis, Reissner's membrane, organ of Corti, and the spinal ganglion, confirming that *SDF-1* was expressed mostly in the damaged area as ototoxicity progressed in the second week. Furthermore, the stria vascularis and organ of Corti showed the highest increase in expression. Both outer and inner hair cells also showed increased expression.

4. Discussion

Stem cell homing via circulation to the bone marrow is the first critical step in regenerative medicine [6, 7]. Stem cell homing is one of the crucial mechanisms that has to be

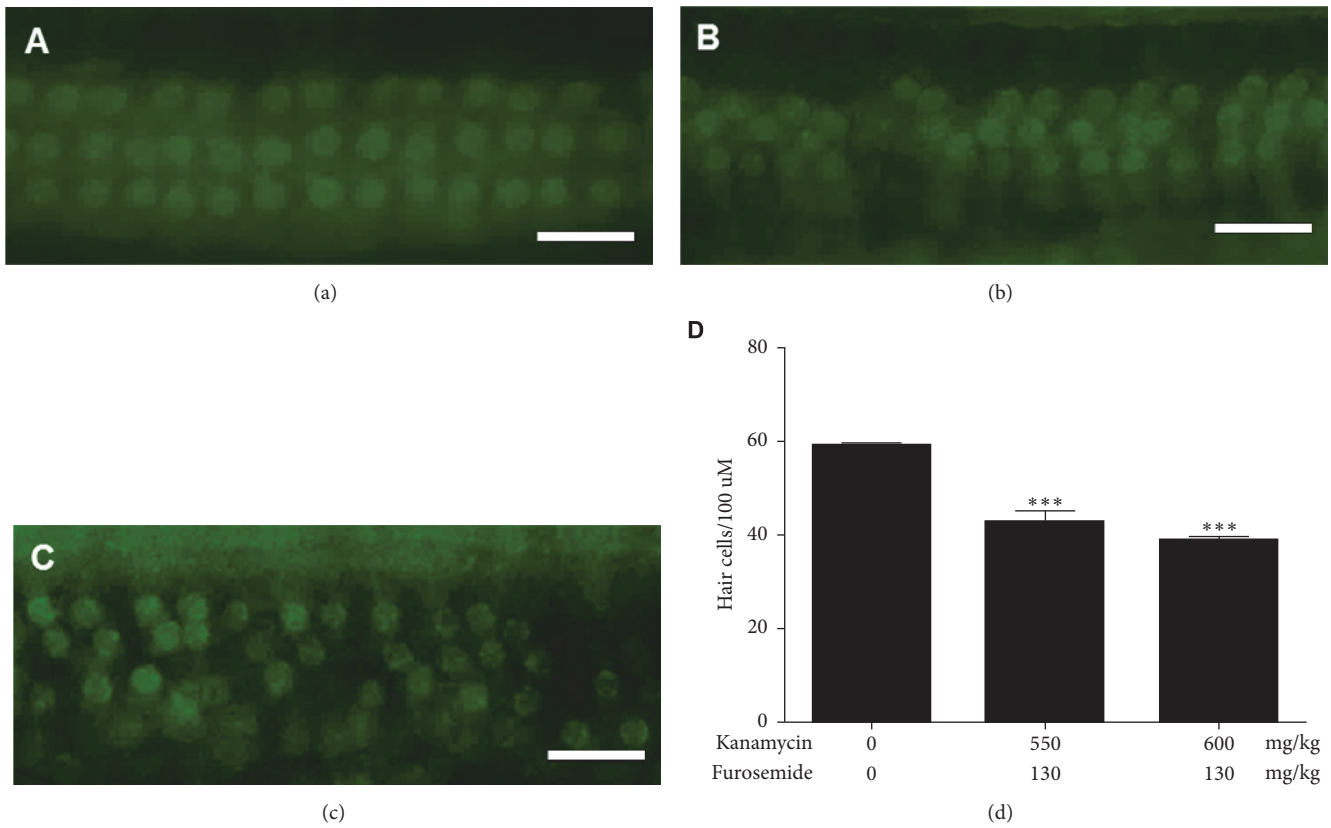

Figure 4: Phalloidin-FITC immunofluorescence shows loss of outer hair cells. Immunofluorescence in sections from mice treated with (a) furosemide 130 mg/kg + kanamycin 420 mg/kg, (b) furosemide 130 mg/kg + kanamycin 550 mg/kg, and (c) furosemide 130 mg/kg + kanamycin 600 mg/kg. The outer hair cells in the three layers show dysmorphic, out of line cells and deletion of cells. (d) There were significant differences for counts of outer hair cells in the kanamycin 550 mg/kg and 600 mg/kg treated groups than in the sham control group.

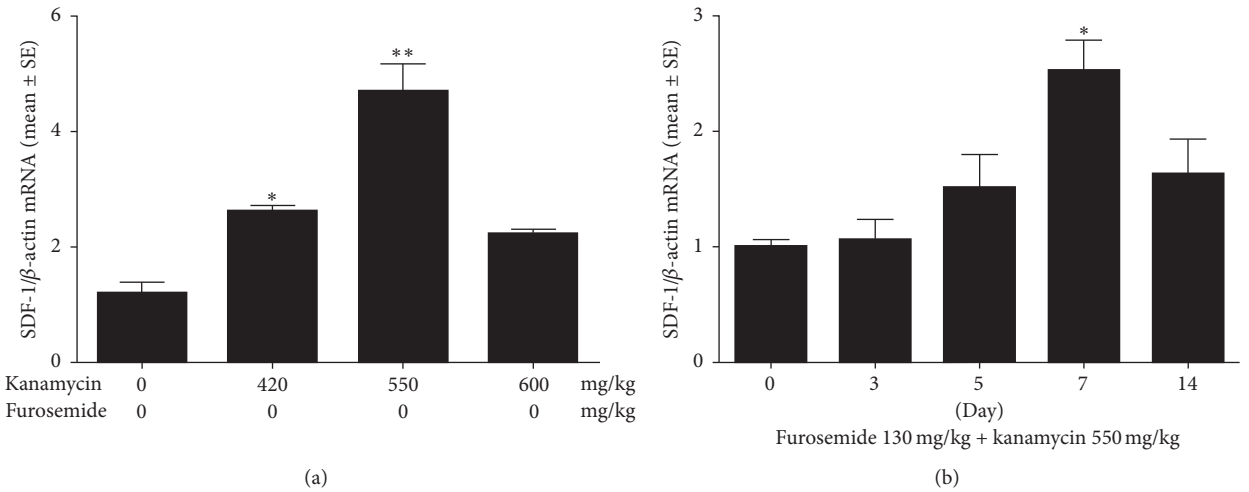

Figure 5: The changes in *SDF-1* mRNA levels in the sensory epithelium of inner ear after dose and time-dependent treatment with furosemide and kanamycin were assessed by real-time RT-PCR. (a) The maximal increase in *SDF-1* occurred at the dose of furosemide 130 mg/kg + kanamycin 550 mg/kg. (b) *SDF-1* levels increased significantly (more than 2.5-fold) on the 7th day after treatment with furosemide 130 mg/kg + kanamycin 550 compared with that of the control ($P < 0.01$).

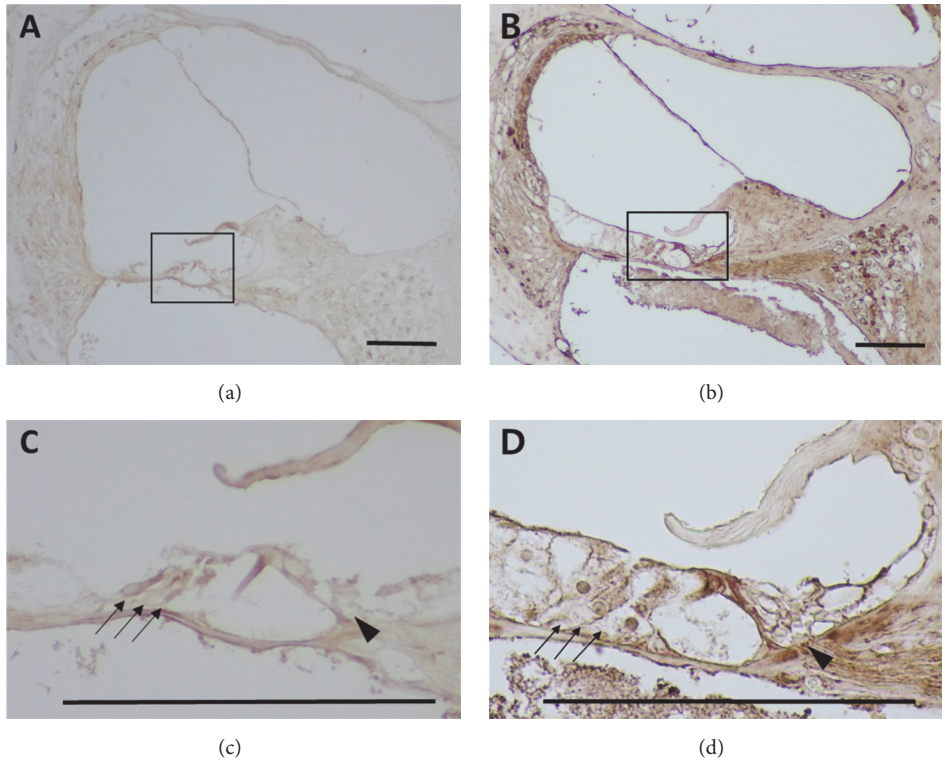

Figure 6: The distribution of *SDF-1* in the cochlea after treatment with furosemide 130 mg/kg + kanamycin 550 mg/kg was assessed by immunohistochemistry. *SDF-1* was detected in the stria vascularis, Reissner's membrane, organ of Corti, and spinal ganglion. (a) ×200 magnified image of the cochlea of normal control mice. (b) ×200 magnified image of the cochlea of the treated mice with furosemide 130 mg/kg + kanamycin 550 mg/kg. Furthermore, the organ of Corti showed the highest increase (d) in expression, compared to the control (c). Both outer and inner hair cells showed increased levels of *SDF-1*. Scale bars: 50 μm.

activated for efficient cell delivery to the inner ear [4]. Sensory hair cells of the inner ear are responsible for conducting auditory stimulation. The hair cells in the inner ear are never replaced and are regenerated after injury. Injection of neural stem cells for homing to the injured cochlea is required to induce regeneration via the supporting cells in the organ of Corti following inner ear trauma [8]. However, there are only few animal models for an increasing number of homing factors, showing an obvious dearth of appropriate study models. Tan et al. [3] studied the homing capability of bone marrow-derived stem cells to the deafened cochlea in the rat model 3 months after acoustic deafening. Here, we attempted to develop a mouse model with an optimal increase of *SDF-1* for homing studies. This would be a useful tool to evaluate the efficacy of stem cell therapy for other related researchers.

SDF-1 (CXCL12), a member of the C-X-C family of chemokines, plays an important role in cell migration at the injured site [9]. CXCR4 on the circulating stem cells are trapped by *SDF-1*, which represent high-affinity cell surface integrins. In the presence of the *SDF-1-CXCR4* combination, the cells stop rolling, disseminate, and migrate through the vascular endothelium towards the chemokine gradient [10, 11]. Kamiya [4] transplanted MSCs in the cochlea after the induction of *SDF-1* in *CX26*-deficient mice, which was used as a model of hereditary hearing loss [12]. We observed optimal induction of the stem cell homing factor in the newly generated aminoglycoside-induced ototoxicity mouse model using a "one-shot" protocol. There was a significant reduction in hearing thresholds and a maximal increase of *SDF-1* levels when furosemide 130 mg/kg + kanamycin 550 mg/kg was used to treat the mice. Severe ototoxicity was observed in the furosemide 130 mg/kg + kanamycin 600 mg/kg group, which was accompanied by distorted structures in the organ of Corti, cell death, and weight loss among the population with urinary insufficiency. Since high doses of aminoglycoside cause drug-induced nephrotoxicity [13, 14], the nephrotoxicity induced by kanamycin 600 mg/kg, which manifested as a reduction in urine volume, was considered as a case of renal failure. There were no such symptoms in the other groups, which were treated with doses of kanamycin less than 550 mg/kg. The hearing thresholds decreased abruptly on the 3rd day and plateaued on the 5th day after the ototoxicity injury. We consider the 7th day posttreatment as the optimal day for the homing mouse model with aminoglycoside ototoxicity, because *SDF-1* levels peaked on the 7th day after the drug treatment.

Immunohistochemistry performed on the 7th day post-treatment showed that *SDF-1* was distributed diffusely in the stria vascularis, Reissner's membrane, organ of Corti, and spinal ganglion. This observation corroborates the results obtained with kanamycin-mediated injury. Extensive

destruction of the outer hair cells in the triple-layer arrays and decreased count and vacuolization of the spiral ganglion cells were typical initial characteristics of cochlea exposed to ototoxicity [15]. However, dominant staining with the *SDF-1* antibody in the scala vascularis represented the possibility of increasing the homing effect of the stem cells, because scala vascularis consists of condensed vascular structures.

The "one-shot" injection with combinations of kanamycin and furosemide in the mouse model of ototoxicity is a novel technique for inducing local inner ear injury [16–18]. Abbas and Rivolta [1] showed the efficiency of the "one-shot" approach. A single dose regimen might be a reliable model for ototoxicity-mediated hearing loss with kanamycin and adequate for inducing rapid and profound hearing impairment. Furthermore, it reduces the risks associated with chronic treatment of aminoglycoside and is thus preferred for animal welfare. Although Abbas et al. [1] used 400–500 mg/kg kanamycin, followed by an intraperitoneal injection of furosemide 100 mg/kg after 20–30 mins in gerbils, we used various doses of kanamycin (420–600 mg/kg) with 130 mg/kg furosemide in C57BL/6 mice. We observed that ototoxicity-mediated hearing impairment occurred upon using kanamycin doses equal to or greater than 420 mg/kg. However, we conclude that the optimal dose of kanamycin for the homing mice model of ototoxicity is 550 mg/kg. In the future, we will use this animal model to study the MSC homing in the ototoxicity mice after the injection of MSCs intratympanically or intravenously, which have increased potency of *CXCR4* with hypoxic conditions.

Investigation regarding the mechanism of ototoxicity induced by the combination of kanamycin-furosemide is important for understanding stem cell homing in the inner ear [19–21]. In future, we would use the *SDF-1/CXCR4* axis to induce MSC homing in the injured cochlear site in this mice model through the administration of MSC with elevated *CXCR4* expression. Eventually, studies regarding high *SDF-1* levels in our mouse model of ototoxicity would play a major role in the development of therapeutic agents using MSC homing.

Conflicts of Interest

The authors declare that they have no conflicts of interest.

Acknowledgments

This research was supported by Basic Science Research Program through the National Research Foundation of Korea (NRF) funded by the Ministry of Education (2016R1A6A3A11933471), by the Gangwon Institute for Regional Program Evaluation grant funded by the Korean government (Ministry of Trade, Industry and Energy) (no. R0005797), and by Industrial Core Technology Development Program of Biomedical Devices funded by the Ministry of Trade, industry and Energy (MI, Korea) (10051518).

References

[1] L. Abbas and M. N. Rivolta, "Aminoglycoside ototoxicity and hair cell ablation in the adult gerbil: A simple model to study hair cell loss and regeneration," *Hearing Research*, vol. 325, pp. 12–26, 2015.

[2] S. Murillo-Cuesta, J. Contreras, R. Cediel, and I. Varela-Nieto, "Comparison of different aminoglycoside antibiotic treatments to refine ototoxicity studies in adult mice," *Laboratory Animals*, vol. 44, no. 2, pp. 124–131, 2010.

[3] B. T. G. Tan, M. M. G. Lee, and R. Ruan, "Bone marrow-derived cells that home to acoustic deafened cochlea preserved their hematopoietic identity," *Journal of Comparative Neurology*, vol. 509, no. 2, pp. 167–179, 2008.

[4] K. Kamiya, "Inner ear cell therapy targeting hereditary deafness by activation of stem cell homing factors," *Frontiers in Pharmacology*, vol. 6, article no. 02, 2015.

[5] H. M. Schmitz, S. B. Johnson, and P. A. Santi, "Kanamycin-furosemide ototoxicity in the mouse cochlea: A 3-dimensional analysis," *Otolaryngology - Head and Neck Surgery (United States)*, vol. 150, no. 4, pp. 666–672, 2014.

[6] J. P. Chute, "Stem cell homing," *Current Opinion in Hematology*, vol. 13, no. 6, pp. 399–406, 2006.

[7] F. Belema-Bedada, S. Uchida, A. Martire, S. Kostin, and T. Braun, "Efficient homing of multipotent adult mesenchymal stem cells depends on FROUNT-mediated clustering of CCR2," *Cell Stem Cell*, vol. 2, no. 6, pp. 566–575, 2008.

[8] T. Okano and M. W. Kelley, "Stem Cell Therapy for the Inner Ear: Recent Advances and Future Directions," *Trends in Hearing*, vol. 16, no. 1, pp. 4–18, 2012.

[9] C. Yellowley, "CXCL12/CXCR4 signaling and other recruitment and homing pathways in fracture repair," *BoneKEy Reports*, vol. 2, no. 3, 2013.

[10] P. Kolar, K. Schmidt-Bleek, H. Schell et al., "The early fracture hematoma and its potential role in fracture healing," *Tissue Engineering—Part B: Reviews*, vol. 16, no. 4, pp. 427–434, 2010.

[11] J. M. Fox, G. Chamberlain, B. A. Ashton, and J. Middleton, "Recent advances into the understanding of mesenchymal stem cell trafficking," *British Journal of Haematology*, vol. 137, no. 6, pp. 491–502, 2007.

[12] K. Kamiya, S. W. Yum, N. Kurebayashi et al., "Assembly of the cochlear gap junction macromolecular complex requires connexin 26," *The Journal of Clinical Investigation*, vol. 124, no. 4, pp. 1598–1607, 2014.

[13] F. Van Bambeke, P. M. Tulkens, R. Brasseur, and M.-P. Mingeot-Leclercq, "Aminoglycoside antibiotics induce aggregation but not fusion of negatively-charged liposomes," *European Journal of Pharmacology: Molecular Pharmacology*, vol. 289, no. 2, pp. 321–333, 1995.

[14] Pharmacologic the Chinchilla1, 1. 2005:1-6.

[15] P. A. Leake, A. L. Kuntz, C. M. Moore, and P. L. Chambers, "Cochlear pathology induced by amimoglycoside ototoxicity during postnatal maturation in cats," *Hearing Research*, vol. 113, no. 1-2, pp. 117–132, 1997.

[16] T. Nakagawa, T. S. Kim, N. Murai et al., "A novel technique for inducing local inner ear damage," *Hearing Research*, vol. 176, no. 1-2, pp. 122–127, 2003.

[17] Y. Quan, L. Xia, J. Shao et al., "Adjudin protects rodent cochlear hair cells against gentamicin ototoxicity via the SIRT3-ROS pathway," *Scientific Reports*, vol. 5, p. 8181, 2015.

[18] Q. Ruan, H. Ao, J. He et al., "Topographic and quantitative evaluation of gentamicin-induced damage to peripheral innervation of mouse cochleae," *NeuroToxicology*, vol. 40, pp. 86–96, 2014.

[19] K. Kamiya, Y. Fujinami, N. Hoya et al., "Mesenchymal stem cell transplantation accelerates hearing recovery through the repair of injured cochlear fibrocytes," *The American Journal of Pathology*, vol. 171, no. 1, pp. 214–226, 2007.

[20] H. M. Ju, S. H. Lee, T. H. Kong, S. Kwon, J. S. Choi, and Y. J. Seo, "Usefulness of intravital multiphoton microscopy in visualizing study of mouse cochlea and volume changes in the scala media," *Frontiers in Neurology*, vol. 8, 2017.

[21] J. S. Hwang, K. H. Kim, and J. H. Lee, "Factors affecting sentence-in-noise recognition for normal hearing listeners and listeners with hearing loss," *Journal of Audiology and Otology*, vol. 21, no. 2, pp. 81–87, 2017.

Hindawi
BioMed Research International
Volume 2017, Article ID 3098230, 6 pages
https://doi.org/10.1155/2017/3098230

Review Article

Nanomedicine for Inner Ear Diseases: A Review of Recent *In Vivo* Studies

Dong-Kee Kim

Department of Otolaryngology-Head and Neck Surgery, Daejeon St. Mary's Hospital, College of Medicine, The Catholic University of Korea, Daejeon, Republic of Korea

Correspondence should be addressed to Dong-Kee Kim; cider12@catholic.ac.kr

Received 18 July 2017; Accepted 30 August 2017; Published 10 October 2017

Academic Editor: Kenneth H. Lee

Nanoparticles are promising therapeutic options for inner ear disease. In this report, we review *in vivo* animal studies in the otologic field using nanoparticles over the past 5 years. Many studies have used nanoparticles to deliver drugs, genes, and growth factors, and functional and morphological changes have been observed. The constituents of nanoparticles are also diversifying into various biocompatible materials, including poly(lactic-co-glycolic acid) (PLGA). The safe and effective delivery of drugs or genes in the inner ear will be a breakthrough for the treatment of inner ear diseases, including age-related hearing loss.

1. Introduction

Hearing loss is a common feature of many inner ear conditions, including presbycusis, sudden sensorineural hearing loss (SSNHL), genetic diseases, noise-induced hearing loss, ototoxic hearing loss, and autoimmune inner ear disease. The prevalence of hearing loss due to these inner ear diseases is increasing because of an increase in life expectancy, exposure to noise, and the use of medicines such as anticancer drugs.

These inner ear diseases remain intractable, and treatment results are poor. One of several reasons for their intractability is that the drug does not readily reach the inner ear. When a drug is administered systemically, it must cross the blood labyrinth barrier (BLB) to reach the inner ear [1]. However, only a small amount of the drug crosses the BLB and reaches the inner ear. Therefore, high doses of medication must be administered to achieve the appropriate drug concentration in the inner ear and have a therapeutic effect. However, systemic administration of high drug concentrations, particularly steroids, has numerous side effects.

Intratympanic drug injection has been used to address these problems and has become the standard treatment for Meniere's disease and sudden deafness [2, 3]. In some ways, the inner ear is well suited to local delivery of drugs. Local delivery bypasses the BLB, allowing drugs to reach their intended target at a lower dose. Thus, higher drug concentrations can be achieved while systemic effects are minimized. However, the drug concentration in the inner ear obtained through intratympanic drug injection remains low.

Several methods have been proposed to improve the efficiency of intratympanic drug injection, such as use of the Silverstein Microwick (Micromedics, St. Paul, MN), microcatheter implantation, hydrogels, and nanoparticles [4]. In this report, we focus on *in vivo* studies in the otologic field using nanoparticles within the past 5 years. In theory, nanoparticle-based drug delivery can enhance the efficiency of delivery to the inner ear and release drugs in a sustained manner [5]. Nanoparticles also provide physical protection *in vivo* for delicate drug structures [6].

2. Challenges with Inner Ear Drug Delivery

The first challenge is ensuring the safety of the drug carrier in the middle or inner ear [7]. Nanoparticles have been used extensively in cancer therapy where cell viability is not an important issue; however, safety is an absolute requirement for nanoparticle applications for the treatment of deafness. To increase permeability into cells or to perform gene transfer, a positively charged moiety such as a cell-penetrating peptide can be attached to the nanoparticle [8, 9]. However, because positively charged nanoparticles can be ototoxic through limited biodegradability of the particle, the production of

intracellular reactive oxygen species, and damage of cell membranes, their application to hearing loss is limited [10]. In addition, it must be determined whether the constituent materials of the nanoparticles will accumulate in the inner ear and be cleared or remain in the inner ear and whether these materials are toxic to hair cells.

When a drug is administered to the middle ear through intratympanic drug injection, it must pass the round window membrane (RWM) or the annular ligament of the oval window (OW) to reach the inner ear. It remains unclear whether these two windows are crossed through diffusion or endocytosis [11]. However, the drug must remain in the middle ear cavity for a sufficient amount of time and remain in contact with these two windows to be delivered to the inner ear. Unfortunately, drugs that enter the middle ear cavity do not remain and are quickly discharged to the Eustachian tube through mucociliary flow of the middle ear [12]. In response to this, gels have been studied in many animal studies. Other studies have used thermosensitive gels, which exist in a liquid state at room temperature and a gel state at body temperature [13].

Another challenge with intratympanic drug delivery is the low permeability of the RWM and annular ligament of the OW. Although the dominant entry route for the inner ear remains unknown, the RWM seems to be the dominant route. Salt et al. [14] reported distribution of an ionic marker, trimethylphenylammonium (TMPA), in the cochlea after intracochlear injection or application to the round window niche based on direct monitoring using a TMPA selective electrode or sequential collection of perilymph. A total of 65% of TMPA entered through the RWM while 35% entered the vestibule in the vicinity of the stapes. However, in clinical situations, RWM may be blocked by fat or fiber tissue; fat or fiber tissue can interfere with drug delivery through the RWM [15]. Factors such as size, configuration, concentration, liposolubility, electrical charge, and membrane thickness influence permeability [16]. Smaller agents are transported more readily through the RWM. Zou et al. [17] explored size-dependent nanoparticle transport. Three sizes of liposome nanoparticles (95, 130, and 240 nm) were manufactured, and their distribution was measured after transtympanic injection in rats. The 95 nm particles were transported most easily whereas the 240 nm particles were transported least easily. With regard to charge, in rodents cationic ferritin readily passes through the normal RWM, whereas anionic ferritin does not [16, 18].

3. Studies Investigating the Uptake or Toxicity of Nanoparticles in the Inner Ear

Wen et al. [19] explored several surface-modified PLGA nanoparticles for inner ear drug delivery, of which poloxamer 407-PLGA nanoparticles showed the greatest cellular uptake and strongest fluorescence based on cochlear imaging. It is possible to analyze quantitatively the amount of nanoparticle entering the cochlea using a near-infrared fluorescence imaging system after cochlea harvest (Table 1). However, a more physiological and accurate method would be to analyze quantitatively the cochlea in a live state. This may be accomplished by isolating the perilymph and determining the concentration of the drug using HPLC. However, it is difficult to quantify drug absorbed in cells of the inner ear (not the perilymph) using this method.

In addition, inner ear drug delivery studies using superparamagnetic nanoparticles and chitosan hydrogel-based nanoparticles have recently been published, and both showed good safety and drug delivery efficiency [20, 21] (Table 1).

4. Studies Attempting to Deliver Actual Drugs to the Inner Ear Using Nanoparticles

In recent years, rather than simply investigating the permeation of nanoparticles into the inner ear, a growing number of reports have loaded a drug onto the nanoparticle and transferred it to the inner ear to observe functional changes (Table 2).

Drug delivery using polyethylene glycol-coated polylactic acid (PEG-PLA) nanoparticles has been attempted twice by the same group [22, 23]. This group used cisplatin to deafen guinea pigs after pretreatment systemically or intratympanically with dexamethasone-loaded nanoparticles. In both studies, administration of dexamethasone-loaded nanoparticles protected hearing in the 4 kHz and 8 kHz frequencies. In another study in which 6α-methylprednisolone was loaded onto nanoparticles using alpha-tocopherol derivatives, cisplatin-induced hearing loss was protected at 10, 14, and 16 kHz [24].

Other reports (excluding the aforementioned studies) have not evaluated changes in hearing after the administration of nanoparticles but instead have analyzed quantitatively the concentration of drug delivered to the inner ear based on high-performance liquid chromatography (HPLC) or fluorescence spectrophotometry [25–28]. One interesting study proposed intratympanic drug injection as a potential brain drug delivery route by analyzing the drug concentration in brain tissue and cerebrospinal fluid (CSF) after intratympanic drug administration [26]. Multiple agent-loaded nanoparticles following intratympanic injection in guinea pigs significantly improved drug distribution within the inner ear, CSF, and brain tissues and protected the brain from cerebral ischemia reperfusion injury.

5. Studies Attempting to Deliver Growth Factors to the Inner Ear Using Nanoparticles

The delivery of macromolecules including growth factors to the inner ear may be more clinically useful than simple drug delivery. This is because in individuals with chronic hearing loss, hair cells cannot be regenerated through drug delivery, although they may be facilitated by the delivery of growth factors or genes. Brain-derived neurotrophic factor (BDNF) has been investigated in many animal studies and can preserve the population of spiral ganglion neurons after hair cell loss [37, 38]. It is also considered a candidate growth factor for reversing hearing loss [39].

Table 1: Studies investigating the uptake or toxicity of nanoparticles in the inner ear.

Nanoparticle	Size of nanoparticle	Animal	Administration route	Loaded drug or gene	Evaluation time	Evaluation of nanoparticle uptake
Poloxamer 407-PLGA NP [19]	181.5 nm	Guinea pigs	Intratympanic	DiR	At 24 h	Near-infrared fluorescence imaging system, confocal microscope
Superparamagnetic NP [20]	100, 200, and 500 nm (three kinds)	Guinea pigs	Intracochlear	None	At 7 days	Toxicity evaluation by ABR
Chitosan-hydrogel-based NP [21]	160 nm	C57BL/6J mice	Intratympanic	Fluorescent dye	At 24 h	Fluorescent microscopy

PLGA: poly(lactic-co-glycolic acid); NP: nanoparticle; DiR: 1,1′-dioctadecyl-3,3,3′,3-tetramethylindotricarbocyanine iodide; ABR: auditory brainstem response.

Table 2: Studies attempting to deliver actual drugs to the inner ear using nanoparticles.

Nanoparticle	Size of nanoparticle	Animal	Administration route	Loaded drug or gene	Evaluation time	Evaluation of nanoparticle uptake
PEG-PLA NP [22]	Not described	Guinea pig, deafened with cisplatin	Intraperitoneal	Dexamethasone	At 3 days	ABR and morphology
PEG-PLA NP [23]	130 ± 4.78 nm	Guinea pig, deafened with cisplatin	Intratympanic	Dexamethasone	At 3 days	ABR and morphology
Multimicellar NP [24]	120.8~159.9 nm	Wistar rats, deafened with cisplatin	Intratympanic	6α-methylprednisolone	At 3 days	ASSR
PLGA NP [25]	135 nm with a PDI of 0.17	Guinea pigs	Intratympanic	Salvianolic acid B, tanshinone IIA, and total panax notoginsenoside	At several predetermined time points within 96 h	HPLC of perilymph
PLGA NP [26]	154 nm with PDI 0.007	Guinea pigs	Intratympanic	Salvianolic acid B, tanshinone IIA, and total panax notoginsenoside	At several predetermined time points within 36 h	HPLC of blood, perilymph, CSF, and brain tissue
PLGA-magnetite-NP [27]	482.8 ± 158 nm	Guinea pigs	Intratympanic	Dexamethasone acetate	At 30 min	HPLC of perilymph, RWM, and inner ear tissue
Cubic liquid crystalline NP [28]	138.6~210.9 nm	Guinea pigs	Intratympanic	Earthworm fibrinolytic enzyme	At several predetermined time points within 24 h	Fluorescence microscope and spectrophotometer

NP: nanoparticle; ABR: auditory brainstem response; PEG-PLA: polyethylene glycol-coated polylactic acid; ASSR: auditory steady-state responses; RWM: round window membrane.

Recently, several studies have explored the ability of BDNF and NGF to deliver growth factors to the inner ear; however, many of these studies used intracochlear delivery [29–32] (Table 3). Because intracochlear delivery requires surgery and can lead to the loss of remnant hearing by opening the cochlea, it can only be attempted in completely deaf patients, such as for cochlear implant surgery. Intratympanic delivery is more useful because of easy clinical access. However, delivering a large macromolecule such as a growth factor remains challenging.

6. Studies Attempting to Deliver Genes to the Inner Ear Using Nanoparticles

A safe and useful nonviral gene delivery system has very high clinical value and can be used to deliver genes to patients with congenital or chronic hearing loss. For example, genes such as Atoh1 can potentially regenerate hair cells in patients with chronic hearing loss, such as presbycusis.

Two recent studies have attempted gene transfer using GFP fluorescence as a positive transfer marker [8, 33]

Table 3: Studies attempting to deliver growth factors to the inner ear using nanoparticles.

Nanoparticle	Size of nanoparticle	Animal	Administration route	Loaded drug or gene	Evaluation time	Evaluation of nanoparticle uptake
Silica supraparticle [29, 30]	500 μm (porous structure)	Deafened guinea pigs	Intracochlear	BDNF	At 4 weeks	Survival of SGNs
Phytantriol lipid-based crystalline NP [31]	215.6~227.2 nm	Guinea pigs, deafened with cisplatin	Intratympanic	NGF	At several predetermined time points within 24 h	ELISA assay of cochlear fluid
Nanoporous PGA NP [32]	1.8–3.2 μm	Guinea pig, deafened with aminoglycoside	Intracochlear	BDNF	At 20 days	Morphology

BDNF: brain-derived neurotrophic factor; SGN: spiral ganglion neurons; NP: nanoparticle; NGF: nerve growth factor; PGA: poly(L-glutamic acid).

Table 4: Studies attempting to deliver genes to the inner ear using nanoparticles.

Nanoparticle	Size of nanoparticle	Animal	Administration route	Loaded drug or gene	Evaluation time	Evaluation of nanoparticle uptake
PHEA NP [16]	103.1 nm	C57/BL6 mice	Intratympanic	GFP plasmid DNA and fluorescent dye	At 48 h	Confocal microscope
Dendrimer-based NP [33]	132 ± 20 nm	Sprague Dawley rats	Intratympanic	Atoh1-EGFP plasmid	At 7 days	Confocal microscope, RT-PCR, and Western blot

NP: nanoparticle; PHEA: poly(2-hydroxyethyl L-aspartamide).

(Table 4). However, it remains difficult to analyze quantitatively the amount of gene delivered to the inner ear using this method because of autofluorescence of the inner ear and the vulnerability of fluorescence intensity to the laser of a confocal microscope. In one of these studies, pRK5-Atoh1-EGFP plasmids were transferred and gene transfer was analyzed quantitatively based on RT-PCR and Western blot, which appeared to be a reliable approach [33]. Although this report did not assess structural or functional changes after *atoh1* delivery, these results demonstrate the possibility of the possibility of nonviral gene delivery through nanoparticles.

Several challenges with gene delivery using nanoparticles must be addressed before it can be applied clinically, such as decreasing the particle size while stably integrating the gene into the particle; administering a gene and nanoparticle complex to the body; protecting the gene from degrading enzymes such as endonuclease; and ensuring that the gene enters the cytoplasm, escapes the endosome, and enters the nucleus.

7. Inner Ear Drug Delivery Studies with Imaging Modalities

Direct observation of drugs or nanoparticles in the inner ear with micro-CT or MRI can be used for quantitative analysis of the amount or distribution of a drug delivered to the cochlea. Zou et al. [34] recently injected silver nanoparticles (Ag NPs) intratympanically and observed the distribution of Ag NPs in the middle and inner ear using micro-CT, showing a gradient concentration from the middle ear to the inner ear (Table 5).

It is possible to detect the distribution of nanoparticles within the inner ear using MRI if the nanoparticles contain paramagnetic agents such as gadolinium chelate [40]. In a recent study, gadolinium chelate was encapsulated in a liposome nanocarrier and the distribution of nanoparticles in the inner ear after intratympanic injection was observed using MRI [35]. In addition to nanoparticles containing gadolinium, superparamagnetic iron oxide nanoparticles (SPION) or ceric ammonium nitrate oxidant-stabilized gamma-maghemite nanoparticles were identified in the inner ear using MRI after intratympanic or intracochlear administration [36, 41].

8. Conclusion

The use of nanoparticles is a promising therapy for inner ear disease. The ideal nanocarrier should be able to permeate the RWM or the annular ligament on the OW, be capable of specific targeting, provide controlled release of the loaded materials, and be safe in the inner ear. Many studies have attempted to deliver drugs, genes, and growth factors to the inner ear *in vivo*, and promising results have been reported. The safe and effective delivery of drugs or genes will be an important advancement for the treatment of many inner

Table 5: Inner ear drug delivery studies with imaging modalities.

Nanoparticle	Size of nanoparticle	Animal	Administration route	Loaded drug or gene	Evaluation time	Evaluation of nanoparticle uptake
Silver NP [34]	21 ± 8 nm	Sprague Dawley rats	Intratympanic	None	At 4, 7, and 24 h and at 7 days	Micro-CT
Liposome nanocarrier [35]	115 ± 10 nm	Sprague Dawley rats	Intratympanic	Gd-DOTA	At several predetermined time points within 7 days	MRI, ABR, and inflammatory biological markers
Ceric ammonium nitrate oxidant-stabilized gamma-maghemite NP [36]	50–60 nm	Sprague Dawley rats	Intratympanic	None	At several predetermined time points within 14 days	MRI

NP: nanoparticle; Gd-DOTA: gadolinium-tetra-azacyclo-dodecane-tetra-acetic acid; ABR: auditory brainstem response.

ear diseases, including age-related hearing loss, which is currently a refractory disease.

Disclosure

The English in this document has been checked by at least two professional editors, both native speakers of English. For a certificate, please see http://www.textcheck.com/certificate/lbQYk7.

Conflicts of Interest

The author declares that there are no conflicts of interest regarding the publication of this paper.

Acknowledgments

This research was supported by the Basic Science Research Program through the National Research Foundation of Korea (NRF) and funded by the Ministry of Education (NRF-2017R1D1A1B03027894) and the Catholic Medical Center Research Foundation in program year 2017.

References

[1] S. K. Juhn, L. P. Rybak, and W. L. Fowlks, "Transport characteristics of the blood-Perilymph barrier," *American Journal of Otolaryngology—Head and Neck Medicine and Surgery*, vol. 3, no. 6, pp. 392–396, 1982.

[2] H. Sajjadi and M. M. Paparella, "Meniere's disease," *The Lancet*, vol. 372, no. 9636, pp. 406–414, 2008.

[3] W. H. Slattery, L. M. Fisher, Z. Iqbal, R. A. Friedman, and N. Liu, "Intratympanic steroid injection for treatment of idiopathic sudden hearing loss," *Otolaryngology - Head and Neck Surgery*, vol. 133, no. 2, pp. 251–259, 2005.

[4] A. A. McCall, E. E. L. Swan, J. T. Borenstein, W. F. Sewell, S. G. Kujawa, and M. J. McKenna, "Drug delivery for treatment of inner ear disease: current state of knowledge," *Ear and Hearing*, vol. 31, no. 2, pp. 156–165, 2010.

[5] I. Pyykko, J. Zou, W. Zhang, and Y. Zhang, "Nanoparticle-based delivery for the treatment of inner ear disorders," *Current Opinion in Otolaryngology & Head and Neck Surgery*, vol. 19, no. 5, pp. 388–396, 2011.

[6] M. Yokoyama, M. Miyauchi, N. Yamada et al., "Characterization and Anticancer Activity of the Micelle-forming Polymeric Anticancer Drug Adriamycin-conjugated Poly(ethylene glycol)-Poly(aspartic acid) Block Copolymer," *Cancer Research*, vol. 50, no. 6, pp. 1693–1700, 1990.

[7] J. Zou, H. Feng, M. Mannerström, T. Heinonen, and I. Pyykkö, "Toxicity of silver nanoparticle in rat ear and BALB/c 3T3 cell line," *Journal of Nanobiotechnology*, vol. 12, no. 1, article no. 52, 2014.

[8] J. Y. Yoon, K.-J. Yang, D. E. Kim et al., "Intratympanic delivery of oligoarginine-conjugated nanoparticles as a gene (or drug) carrier to the inner ear," *Biomaterials*, vol. 73, pp. 243–253, 2015.

[9] R. Y. Seung, B. K. Seung, C. O. Joe, and J.-D. Kim, "Intracellular delivery enhancement of poly(amino acid) drug carriers by oligoarginine conjugation," *Journal of Biomedical Materials Research - Part A*, vol. 86, no. 1, pp. 137–148, 2008.

[10] H. Zhou, X. Ma, Y. Liu et al., "Linear polyethylenimine-plasmid DNA nanoparticles are ototoxic to the cultured sensory epithelium of neonatal mice," *Molecular Medicine Reports*, vol. 11, no. 6, pp. 4381–4388, 2015.

[11] M. V. Goycoolea, "Clinical aspects of round window membrane permeability under normal and pathological conditions," *Acta Oto-Laryngologica*, vol. 121, no. 4, pp. 437–447, 2001.

[12] J. Sadé, "Mucociliary flow in the middle ear," *Annals of Otology, Rhinology & Laryngology*, vol. 80, no. 3, pp. 336–341, 1971.

[13] A. N. Salt, J. Hartsock, S. Plontke, C. LeBel, and F. Piu, "Distribution of dexamethasone and preservation of inner ear function following intratympanic delivery of a gel-based formulation," *Audiology & Neuro-otology*, vol. 16, no. 5, pp. 323–335, 2011.

[14] A. N. Salt, E. B. King, J. J. Hartsock, R. M. Gill, and S. J. O'Leary, "Marker entry into vestibular perilymph via the stapes following applications to the round window niche of guinea pigs," *Hearing Research*, vol. 283, no. 1-2, pp. 14–23, 2012.

[15] K. S. Alzamil and F. H. Linthicum Jr., "Extraneous round window membranes and plugs: Possible effect on intratympanic therapy," *Annals of Otology, Rhinology and Laryngology*, vol. 109, no. 1, pp. 30–32, 2000.

[16] M. V. Goycoolea, D. Muchow, and P. Schachern, "Experimental studies on round window structure: Function and permeability," *The Laryngoscope*, vol. 98, no. S44, pp. 1–20, 1988.

[17] J. Zou, R. Sood, S. Ranjan et al., "Size-dependent passage of liposome nanocarriers with preserved posttransport integrity across the middle-inner ear barriers in rats. Otology Neurotology: Official Publication of the American Otological Society," *Otology & Neurotology: Official Publication of the American Otological Society, American Neurotology Society [and] European Academy of Otology and Neurotology*, vol. 33, no. 4, pp. 666–673, 2012.

[18] Y. Nomura, "Otological significance of the round window," *Advances in oto-rhino-laryngology*, vol. 33, pp. 1–162, 1984.

[19] X. Wen, S. Ding, H. Cai et al., "Nanomedicine strategy for optimizing delivery to outer hair cells by surface-modified poly(lactic/glycolic acid) nanoparticles with hydrophilic molecules," *International Journal of Nanomedicine*, vol. 11, pp. 5959–5969, 2016.

[20] Y. Nguyen, C. Celerier, R. Pszczolinski et al., "Superparamagnetic nanoparticles as vectors for inner ear treatments: Driving and toxicity evaluation," *Acta Oto-Laryngologica*, vol. 136, no. 4, pp. 402–408, 2016.

[21] S. A. Lajud, D. A. Nagda, P. Qiao et al., "A novel chitosan-hydrogel-based nanoparticle delivery system for local inner ear application," *Otology & Neurotology: Official Publication of the American Otological Society, American Neurotology Society [and] European Academy of Otology and Neurotology*, vol. 36, no. 2, pp. 341–347, 2015.

[22] C. Sun, X. Wang, D. Chen, X. Lin, D. Yu, and H. Wu, "Dexamethasone loaded nanoparticles exert protective effects against Cisplatin-induced hearing loss by systemic administration," *Neuroscience Letters*, vol. 619, pp. 142–148, 2016.

[23] C. Sun, X. Wang, Z. Zheng et al., "A single dose of dexamethasone encapsulated in polyethylene glycol-coated polylactic acid nanoparticles attenuates cisplatin-induced hearing loss following round window membrane administration," *International Journal of Nanomedicine*, vol. 10, pp. 3567–3579, 2015.

[24] S. Martín-Saldaña, R. Palao-Suay, A. Trinidad, M. R. Aguilar, R. Ramírez-Camacho, and J. San Román, "Otoprotective properties of 6α-methylprednisolone-loaded nanoparticles against cisplatin: In vitro and in vivo correlation," *Nanomedicine: Nanotechnology, Biology, and Medicine*, vol. 12, no. 4, pp. 965–976, 2016.

[25] H. Cai, X. Wen, L. Wen et al., "Enhanced local bioavailability of single or compound drugs delivery to the inner ear through application of PLGA nanoparticles via round window administration," *International Journal of Nanomedicine*, p. 5591.

[26] X. Zhang, G. Chen, and L. Wen, "Novel multiple agents loaded PLGA nanoparticles for brain delivery via inner ear administration: *in vitro* and *in vivo* evaluation," *European Journal of Pharmaceutical Sciences*, vol. 48, no. 4-5, pp. 595–603, 2013.

[27] X. Du, K. Chen, S. Kuriyavar et al., "Magnetic targeted delivery of dexamethasone acetate across the round window membrane in guinea pigs," *Otology & Neurotology: Official Publication of the American Otological Society, American Neurotology Society [and] European Academy of Otology and Neurotology*, vol. 34, no. 1, pp. 41–47, 2013.

[28] H. Liu, Y. Wang, Q. Wang et al., "Protein-bearing cubosomes prepared by liquid precursor dilution: Inner ear delivery and pharmacokinetic study following intratympanic administration," *Journal of Biomedical Nanotechnology*, vol. 9, no. 10, pp. 1784–1793, 2013.

[29] A. K. Wise, J. Tan, Y. Wang, F. Caruso, and R. K. Shepherd, "Improved auditory nerve survival with nanoengineered supraparticles for neurotrophin delivery into the deafened cochlea," *PLoS ONE*, vol. 11, no. 10, Article ID e0164867, 2016.

[30] Y. Wang, A. K. Wise, J. Tan, J. W. Maina, R. K. Shepherd, and F. Caruso, "Mesoporous silica supraparticles for sustained inner-ear drug delivery," *Small*, vol. 10, no. 21, pp. 4244–4248, 2014.

[31] M. Bu, J. Tang, Y. Wei et al., "Enhanced bioavailability of nerve growth factor with phytantriol lipid-based crystalline nanoparticles in cochlea," *International Journal of Nanomedicine*, vol. 10, pp. 6879–6889, 2015.

[32] J. Tan, Y. Wang, X. Yip, F. Glynn, R. K. Shepherd, and F. Caruso, "Nanoporous peptide particles for encapsulating and releasing neurotrophic factors in an animal model of neurodegeneration," *Advanced Materials*, vol. 24, no. 25, pp. 3362–3366, 2012.

[33] N. Wu, M. Li, Z.-T. Chen et al., "In vivo delivery of Atoh1 gene to rat cochlea using a dendrimer-based nanocarrier," *Journal of Biomedical Nanotechnology*, vol. 9, no. 10, pp. 1736–1745, 2013.

[34] J. Zou, M. Hannula, S. Misra et al., "Micro CT visualization of silver nanoparticles in the middle and inner ear of rat and transportation pathway after transtympanic injection," *Journal of Nanobiotechnology*, vol. 13, no. 1, article no. 5, 2015.

[35] J. Zou, H. Feng, R. Sood, P. K. Kinnunen, and I. Pyykko, "Biocompatibility of Liposome Nanocarriers in the Rat Inner Ear After Intratympanic Administration," *Nanoscale Research Letters*, vol. 12, no. 1, 2017.

[36] J. Zou, S. Ostrovsky, L. L. Israel et al., "Efficient penetration of ceric ammonium nitrate oxidant-stabilized gamma-maghemite nanoparticles through the oval and round windows into the rat inner ear as demonstrated by MRI," *Journal of Biomedical Materials Research - Part B Applied Biomaterials*, 2016.

[37] R. T. Richardson, A. K. Wise, B. C. Thompson et al., "Polypyrrole-coated electrodes for the delivery of charge and neurotrophins to cochlear neurons," *Biomaterials*, vol. 30, no. 13, pp. 2614–2624, 2009.

[38] D. Ramekers, H. Versnel, S. B. Strahl, S. F. L. Klis, and W. Grolman, "Temporary neurotrophin treatment prevents deafness-induced auditory nerve degeneration and preserves function," *Journal of Neuroscience*, vol. 35, no. 36, pp. 12331–12345, 2015.

[39] I. Khalin, R. Alyautdin, G. Kocherga, and M. A. Bakar, "Targeted delivery of brain-derived neurotrophic factor for the treatment of blindness and deafness," *International Journal of Nanomedicine*, vol. 10, pp. 3245–3267, 2015.

[40] I. Pyykkö, J. Zou, A. Schrott-Fischer, R. Glueckert, and P. Kinnunen, "An overview of nanoparticle based delivery for treatment of inner ear disorders," *Methods in Molecular Biology*, vol. 1427, pp. 363–415, 2016.

[41] J. Zou, W. Zhang, D. Poe et al., "MRI manifestation of novel superparamagnetic iron oxide nanoparticles in the rat inner ear," *Nanomedicine*, vol. 5, no. 5, pp. 739–754, 2010.